Application of comprehensive gas chromatography (GC×GC) to measurements of volatile organic species in ambient air

Dissertation
zur Erlangung des Grades
"Doktor der Naturwissenschaften"

am Fachbereich Chemie, Pharmazie und Geowissenschaften
der Johannes Gutenberg-Universität in Mainz

vorgelegt von

Sandra Bartenbach
geb. in Heilbronn/Neckar

Mainz, 2005

Tag der mündlichen Prüfung: 20.12.2005
D77-Mainzer Dissertation

頑張って

Abstract

The focus of this thesis was the in-situ application of the new analytical technique „GC×GC“ in both the marine and continental boundary layer, as well as in the free troposphere. Biogenic and anthropogenic VOCs were analysed and used to characterise local chemistry at the individual measurement sites.
The first part of the thesis work was the characterisation of a new set of columns that was to be used later in the field. To simplify the identification, a time-of-flight mass spectrometer (TOF-MS) detector was coupled to the GC×GC. In the field the TOF-MS was substituted by a more robust and tractable flame ionisation detector (FID), which is more suitable for quantitative measurements. During the process, a variety of volatile organic compounds could be assigned to different environmental sources, e.g. plankton sources, eucalyptus forest or urban centers.
In-situ measurements of biogenic and anthropogenic VOCs were conducted at the Meteorological Observatory Hohenpeissenberg (MOHP), Germany, applying a thermodesorption-GC×GC-FID system. The measured VOCs were compared to GC-MS measurements routinely conducted at the MOHP as well as to PTR-MS measurements. Furthermore, a compressed ambient air standard was measured from three different gas chromatographic instruments and the results were compared. With few exceptions, the in-situ, as well as the standard measurements, revealed good agreement between the individual instruments. Diurnal cycles were observed, with differing patterns for the biogenic and the anthropogenic compounds. The variability-lifetime relationship of compounds with atmospheric lifetimes from a few hours to a few days in presence of O_3 and OH was examined. It revealed a weak but significant influence of chemistry on these short-lived VOCs at the site. The relationship was also used to estimate the average OH radical concentration during the campaign, which was compared to in-situ OH measurements for the first time. The OH concentration ranging from 3.5 to 6.5×10^5 molecules cm^{-3} (0.015 to 0.027 ppt) obtained with this method represents an approximation of the average OH concentration influencing the discussed VOCs from emission to measurement. Based on these findings, the average concentration of the nighttime NO_3 radicals was estimated using the same approach and found to range from 2.2 to 5.0×10^8 molecules cm^{-3} (9.2 to 21.0 ppt).
During the MINATROC field campaign, in-situ ambient air measurements with the GC×GC-FID were conducted at Tenerife, Spain. Although the station is mainly situated in the free troposphere, local influences of anthropogenic and biogenic VOCs were observed. Due to a strong dust event originating from Western Africa it was possible to compare the mixing ratios during normal and elevated dust loading in the atmosphere. The mixing ratios during the dust event were found to be lower. However, this could not be attributed to heterogeneous reactions as there was a change in the wind direction from northwesterly to southeasterly during the dust event.

Zusammenfassung

Der Fokus dieser Arbeit lag auf der in-situ Anwendung der neuen „GC×GC“ Technik in der marinen und kontinentalen Grenzschicht sowie der freien Troposphäre. Biogene und anthropogene flüchtige organische Verbindungen (VOCs) wurden analysiert und zur Charakterisierung der lokal vorherrschenden Chemie an den jeweiligen Orten herangezogen. Im ersten Teil der Arbeit wurde eine neue Säulenkombination für spätere Messkampagnen charakterisiert. Ein Time-of-Flight Massenspektrometer (TOF-MS) wurde zur einfacheren Qualifizierung als Detektor an das GC×GC verwendet, für die Quantifizierung im Feld wurde dieser gegen einen robusteren Flammenionisationsdetektor (FID) ausgetauscht. Während des Identifikationsprozesses konnte eine Vielzahl von VOCs verschiedenen Quellen zugeordnet werden, z.B. Plankton, Eukalyptuswald oder städtischen Gebieten.
Mit einem GC×GC-FID wurden in-situ Messungen von biogenen und anthropogenen VOCs am Meteorologischen Observatorium Hohenpeissenberg (MOHP), Deutschland, durchgeführt. Die analysierten VOCs wurden mit routinemässigen GC-MS Messungen am MOHP und PTR-MS Messungen verglichen. Des weiteren wurde ein Standard mit komprimierter Umgebungsluft mit Hilfe von drei verschiedenen gas chromatographischen Instrumenten gemessen und die Werte verglichen. Mit wenigen Ausnahmen stimmten die Ergebnisse der Feld- und Standard-Messungen der einzelnen Instrumenten überein. Unterschiedlich strukturierte Tagesgänge wurden für biogene und anthropogene Verbindungen beobachtet. Die Variabilitäts-Lebensdauer-Beziehung von VOCs mit atmosphärischen Lebenszeiten von wenigen Stunden bis wenige Tage in Gegenwart von O_3 und OH wurde untersucht. Es ergab einen schwachen, aber signifikanten Einfluss der Chemie auf diese kurzlebigen VOCs am Messort. Diese Beziehung wurde auch benutzt um die durchschnittliche OH Radikal Konzentration während der Kampagne zu berechnen, das Ergebnis konnte das erste Mal mit in-situ OH Messungen verglichen werden. Die berechneten optimalen OH Konzentrationen zwischen 3.5 und 6.5×10^5 Moleküle cm^{-3} (0.015 - 0.027 ppt) repräsentieren hierbei die durchschnittliche OH Konzentration, die auf die VOCs von Emission bis zur Messung einwirkt. Basierend auf diesem Ergebnis wurde die durchschnittliche Konzentration der nächtlichen NO_3 Radikale mit der gleichen Herangehensweise auf zwischen 2.2 und 5.0×10^8 Moleküle cm^{-3} (9.2 - 21.0 ppt) geschätzt.
Während der MINATROC Kampagne wurden in-situ Messungen mit GC×GC-FID auf Teneriffa, Spanien, durchgeführt. Obwohl sich die Station meistens in der freien Troposphäre befindet, wurden Einflüsse lokaler anthropogener und biogener VOCs beobachtet. Aufgrund eines starken Staubsturms, entstanden im westlichen Afrika, war es möglich, die VOC Mischverhältnisse während normaler und erhöhter Staubladung in der Atmosphäre zu vergleichen. Obwohl die Konzentrationen während des Staubsturms niedriger waren, konnte dies nicht auf heterogene Reaktionen zurückgeführt werden, da sich die Windrichtung während des Staubsturms von nordwestlich zu südöstlich gedreht hatte.

CONTENTS

LIST OF FIGURES

LIST OF TABLES

ABBREVIATIONS

α	Selectivity factor
a.s.l.	above sea level
amu	atomic mass unit
b	Basewidth of peak
BL	Boundary Layer
CFC	Chlorofluorocarbon
CI	Chemical Ionisation
CO_2	Carbon dioxide
d	Distance
DMS	Dimethylsulfide
DOAS	Differential Optical Absorption Spectrometry
DWD	Deutscher Wetterdienst
ECD	Electron Capture Detector
ECN	Effective Carbon Number
FT	Free Troposphere
FTIR	Fourier Transform Infrared Spectroscopy
GC×GC-FID	Two-dimensional Gas Chromatograph - Flame Ionisation Detector
GC-MS	Gas Chromatograph-Mass Spectrometer
H_2O	Water
HCHO	Formaldehyde
IAC	Instituto de Astrofísica de Canarias
INM	Instituto Nacional de Meteorología
IR	Infrared
K	Kelvin
k'	Retention factor
LMCS	Longitudinally Modulated Cryogenic System
MBL	Marine Boundary Layer
MOHP	Meteorological Observatory Hohenpeissenberg
MPI-C	Max-Planck-Institute for Chemistry
MSD	Mass Spectrometer Detector
N_2	Nitrogen
nm	nanometer
NO_3	Nitrate radical
O_3	Ozone
OH	Hydroxyl radical
PAN	Peroxyacetylnitrate
PCB	Polychlorinated Biphenyls
PFA	Perfluoroalkoxy

ppb	parts per billion
ppt	parts per trillion
PTFE	Polytetrafluorethene
PTR-MS	Proton-Transfer-Reaction-Mass Spectrometer
R_S	Resolution
REMPI	Resonance-Enhanced Multiphoton Ionisation
RH	Relative Humidity
RI	Retention Index
S/N	Signal to noise
SPI	Single Photon Ionisation
t_M	Retention time of the mobile phase
t_R	Retention time of the analyte
TCD	Thermal Conductivity Detector
TDLAS	Tunable Diode Laser Absorption Spectrometry
TDM	Thermal Desorption Modulator
Tg	Teragram
TOF-MS	Time-of-flight-Mass Spectrometer
UV	Ultraviolet
VOC	Volatile Organic Compound

CHAPTER 1

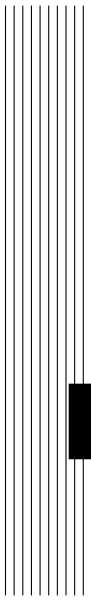

Introduction

1.1 Structure of the atmosphere

The Earth is surrounded by an envelope of gas, which we call the atmosphere. Although it makes up a negligible fraction of the Earth's mass, the atmosphere is essential for many forms of life. The main constituents of the atmosphere are nitrogen and oxygen, making up 99% of the total volume, yet many other species are present in trace amounts. Despite being present at mixing ratios of less then parts per million, these trace gases have a significant impact on the chemistry and physics of the atmosphere, making it a complex and fascinating system. The incoming solar radiation plays an important role in determining the structure of the atmosphere. It can be absorbed in the atmosphere or backscattered into space, but a fraction reaches the Earths surface, warming the ground, water, the adjoining air masses and providing energy for the vegetation. Some energy is re-emitted from the surface as infrared radiation, which can be absorbed by certain atmospheric components like H_2O, CO_2, O_3 and aerosols. The resultant energy fluxes induce distinct vertical temperature gradients in the Earths atmosphere. Based on these gradients the atmosphere has been nominally divided into the specific layers troposphere, stratosphere, mesosphere and thermosphere, see Fig. 1.1 [1].

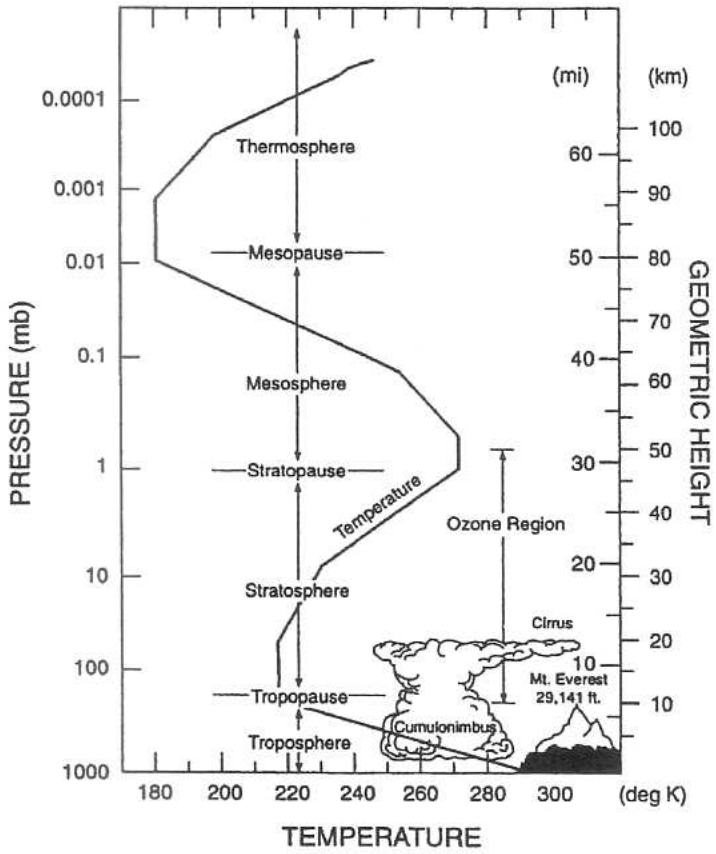

Fig. 1.1: Vertical temperature profile in the atmosphere

The troposphere extends from the Earths surface to an average altitude of 11 km and can be subdivided into the boundary layer (BL, 0-2 km) and the free troposphere (FT, 2-11 km). The BL as the lowest part of the troposphere is directly influenced by the activities at the Earths surface and anthropogenic and biogenic emissions are accumulated in this layer. The BL thickness is variable and can range from 100 m to 3 km. It is dynamically segregated from the free troposphere by a temperature inversion at approximately 3 km over land and 1 km over ocean. This inversion isolates the free troposphere and slows the transport of VOCs from the BL [1]. The BL is also the most turbulent region of the atmosphere and responds to surface forcings like friction, evaporation and transpiration, solar heating, or terrain induced flow modification at a timescale of a few hours or less [2]. At sunrise, the heating at the surface activates the turbulence and mixing processes [3]. In contrast, the nocturnal BL is more stable and generally only a few hundred meters thick. Horizontal transport of air in the BL is created by surface pressure gradients that induce high and low pressure systems. Further tropospheric mixing is effected by cold and warm fronts moving horizontally over the surface, especially at temperate latitudes. Transport of air masses and pollution from the BL to the FT can occur via vertical transport such as convection. These convection events can be in isolated towers, particularly in the Tropics, or embedded in synoptic scale features such as warm and cold fronts, particularly in temperate latitudes [1, 2]. The free troposphere is separated from the stratosphere by a further temperature inversion, called the tropopause. At this upper boundary of the troposphere convective processes cease to be important, since in the stratosphere the temperature increases with height. The height of the tropopause depends strongly on the geographic position: as convection at the equator is enhanced by higher surface temperatures, stronger vertical motions ensue, thus the tropopause is situated at about 18 km at the equator and between 6-8 km at the poles. Complete mixing of air masses within the boundary layer is typically achieved in a period of one day, whereas the exchange between the troposphere and the tropopause can take two to four weeks. Tropospheric mixing within one hemisphere is on the order of months and about one year on an interhemispheric scale [1].
The stratosphere contains about 90% of the atmospheric ozone. In this layer, the short wavelength solar ultraviolet radiation is absorbed by ozone leading to diabatic heating and an increasing temperature with increasing altitude. This inversion gives stability against vertical motion and hinders exchange of air masses between the stratosphere and the troposphere. The approximate time required to exchange the mass of the entire troposphere with the stratosphere is about two years. Above the stratosphere lies the mesosphere where the temperature decreases again with increasing altitude, as heating by radiation is lower than cooling. Above the mesosphere lies the thermosphere distinguished by a very low gas density. The absorption of far-UV wavelength radiation by gaseous oxygen and nitrogen molecules can heat the few molecules in the thermosphere up to an equivalent 2000 K, depending on solar activity [1, 4].

1.2 Volatile organic compounds - Emissions

Volatile organic compounds (VOCs) play an important role in tropospheric air chemistry and are emitted to the atmosphere from a variety of anthropogenic and biogenic sources. These compounds can have an impact on health and the environment either directly, or indirectly after undergoing a complex series of atmospheric reaction cycles resulting in secondary organic pollutants such as O_3.
Photochemistry initiated by actinic radiation plays a vital role in the degradation of VOCs in the troposphere. The oxidation of VOCs in the presence of NO_x (NO and NO_2) leads to the formation of ozone. This chemistry was first elucidated by the biochemist Haagen-Smits in the 1950's when he analysed the Los Angeles smog. He also studied the effects of ozone on plants in laboratory based chambers and realised, that these exhibit the same symptoms of damage as plants in outdoor smog [3]. The oxidation of the simplest of all VOCs, methane, is the basis for tropospheric photochemistry. Although methane is the most abundant hydrocarbon in the global atmosphere at 1.8 ppm, other, non-methane, organic compounds are far more reactive and can similarly influence the composition of the atmosphere despite being at much lower mixing ratios. The atmospheric lifetime of the VOCs can vary from a few minutes or hours, to several months, methane can even persist in the atmosphere for years [1].
Volatile organic compounds can be released to the atmosphere from human activities ('anthropogenic') as well as from terrestrial and marine vegetation ('biogenic'). The emissions of biogenic organic species are estimated to be about an order of magnitude greater on a global scale than anthropogenic hydrocarbons, which on the other hand dominate in populated and industrialised areas. From the global perspective, biogenic compounds are mostly emitted in the Tropics, whereas anthropogenic compounds are predominately emitted in the temperate zones of the northern hemisphere between the 40° and 50° latitude.
Since the beginning of the industrial revolution, human activities have played an ever increasing role as a source of VOCs in the atmosphere. The most significant anthropogenic source of VOCs on global scale is road traffic, followed by combustion of fossil fuel, wood or crop residue. Solvent use, liquid fuel production and distribution, waste disposal, as well as industrial processing of chemicals, also all play a role in the estimated 130 Tg carbon, 10^{12} g(C), emitted annually [4, 5]. Another emission inventory estimated an emission of 110 Tg(C) per year, with 45% of the emissions being alkanes, 35% alkenes and 17% aromatic compounds [6]. Aromatic hydrocarbons such as benzene, toluene, xylenes and ethylbenzene (known collectively as BTEX), as well as acyclic alkanes, alkenes and halogenated compounds, for example chlorofluorocarbons (CFCs) are mainly emitted to the atmosphere from anthropogenic sources. Some example anthropogenic compounds are depicted in Fig. 1.2.
An estimated 1150 Tg(C) biogenic VOCs are emitted each year to the atmosphere from vegetation or via microbial production [7]. Emission rates are highly variable, being strongly dependant on temperature and light intensity, as well as stress induced by injuries, parasites or atmospheric pollutants such as O_3. Typical volume mixing ratios range from between a few parts per trillion by volume (pptv=pmol/mol) to

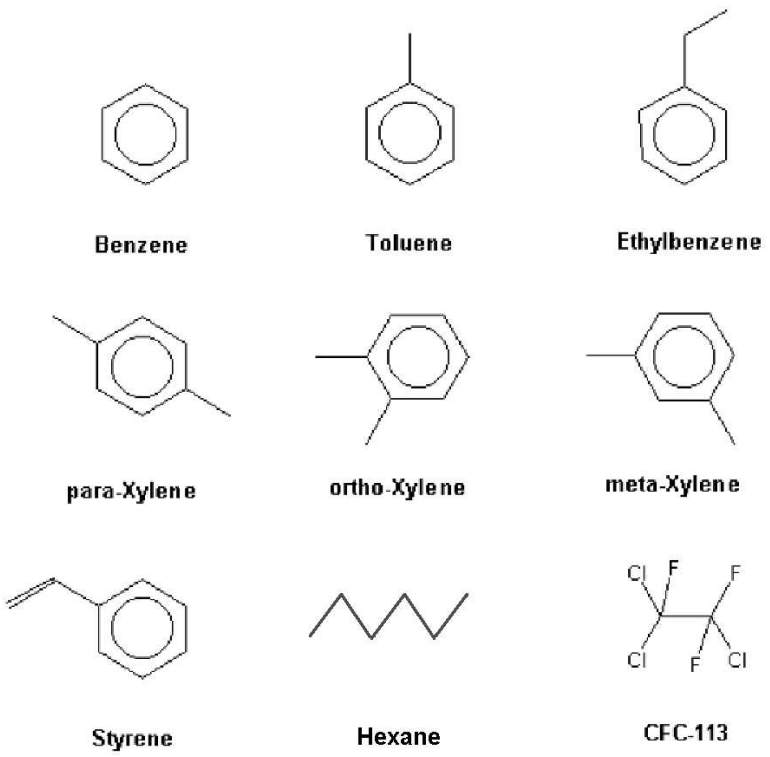

Fig. 1.2: Chemical structures of selected anthropogenic VOCs

several parts of tens per billion by volume (ppbv = nmol/mol) [8]. Vegetation emits large amounts of VOCs in reduced form such as hemiterpenes (e.g. isoprene C_5H_8, or methylbutenol $C_5H_{10}O$), monoterpenes ($C_{10}H_{16}$ compounds, such as α-pinene, β-pinene, eucalyptol), sesquiterpenes ($C_{15}H_{24}$ compounds such as β-caryophyllene) and other oxygenated volatile organic compounds (e.g. methanol, 2-methyl-3-buten-2-ol or 6-methyl-5-hepten-2-one) [9]. The structures of some selected biogenic compounds are shown in Fig. 1.3 [10]. It is a considerable analytical challenge to separate and quantify atmospheric compounds like the monoterpenes. Since they possess the same molecular formula $C_{10}H_{16}$, powerful separation techniques must be employed (as was used in this study) to effect reliable measurements.
Large uncertainties remain in the estimates of biogenic VOC (BVOCs) emissions worldwide. Recent estimates suggest a total biogenic emission of about 84 Tg(C) annually for North America, with 30% being isoprene, 25% terpenoid compounds and 40% non-terpenoid VOCs [11]. The emission of the terpenes is not only depending on temperature, recent studies showed an additional dependency on the light intensity [8, 10, 12, 13, 14, 15]. Many of these organic compounds are highly reactive in the troposphere, with calculated lifetimes of a few hours or even less, depending on the oxidant. Some of the studied BVOCs, e.g. α-terpinene, β-caryophyllene

and α-humulene, react extremely rapidly with ozone and are present at very low atmospheric concentrations, despite having significant fluxes.
The oceans have proven to be a source of some atmospheric biogenic VOCs like alkanes and alkenes, but also trace gases containing sulfur and organohalogens. Characteristic compounds are dimethylsulfide (DMS), methyl chloride and methyl iodide. The estimated annual emission of marine hydrocarbons ranges from 2.5 to 6 Tg(C) [4, 16, 17].
The photooxidation chemistry of both anthropogenic and biogenic VOCs is discussed in detail in the following section 1.3.

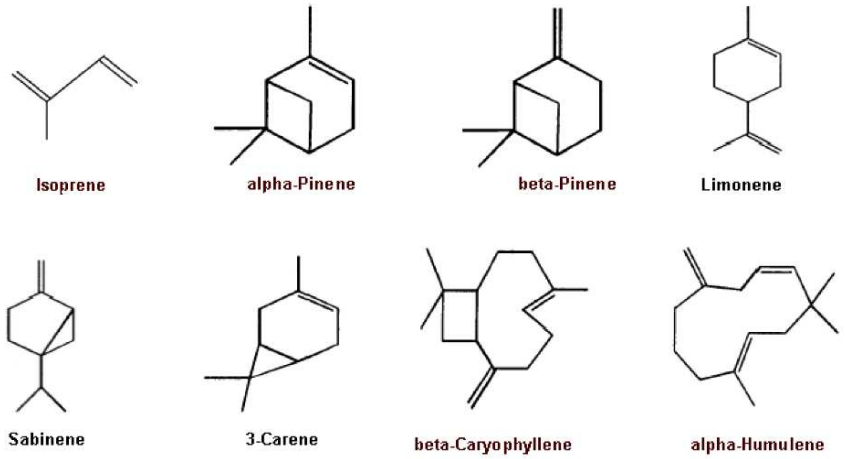

Fig. 1.3: Chemical structures of selected biogenic terpenes

1.3 Chemistry of VOCs in the atmosphere

As discussed in the previous section, VOCs are emitted to the atmosphere from a variety of sources. Since their concentrations do not all rise with time, there must also be an effective removal mechanism. Oxidative degradation of VOCs in the atmosphere is initiated by the reaction with OH radicals, NO_3 radicals, O_3, or direct photolysis, depending on the structure of the organic species and the local conditions. Intermediate products resulting from these breakdown processes are partially oxidised organic species like aldehydes, ketones and organic peroxides. The ultimate end-products of this complex oxidation chemistry of VOCs are carbon dioxide and water [9, 18]. The OH catalysed oxidation of a saturated hydrocarbon RH (R = CH_3, C_2H_5 etc.) in the presence of NO_x and the resultant formation of O_3 is shown schematically in Fig. 1.4 [18]. Most atmospheric oxidation processes during the day are initiated by the reaction of the VOC with an OH radical generated by photolysis of O_3 in the near ultraviolet band ($\lambda < 310$ nm). The subsequent reaction of the resulting $O(^1D)$ with a water molecule leads to two OH-radicals:

$$O_3 + h\nu \rightarrow O_2 + O(^1D) \quad (1.1)$$

$$O(^1D) + H_2O \rightarrow 2OH \quad (1.2)$$

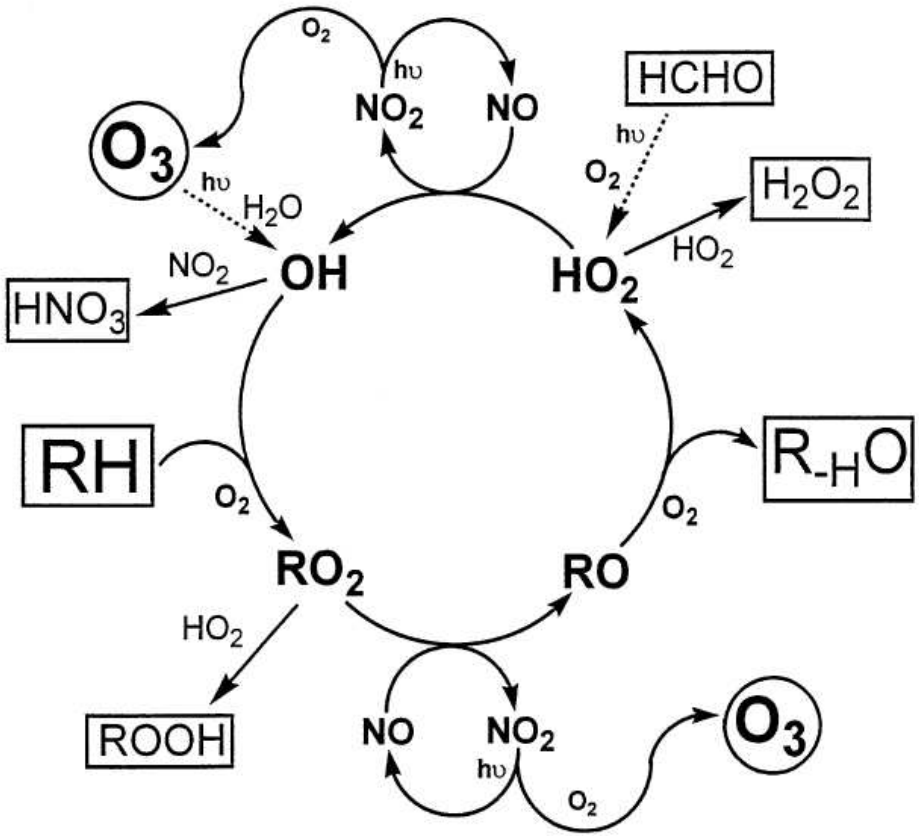

Fig. 1.4: Schematic representation of the oxidation of a saturated hydrocarbon RH to the oxidised product $R_{-H}O$ and the by-product O_3

The photolysis rate strongly depends on the atmospheric pathlength of the incident sunlight and therefore varies with latitude, altitude and season [18].
Other known sources of OH radicals include the photolysis of nitrous acid (HONO), formaldehyde (HCHO) or other carbonyls, and reactions of O_3 with alkenes [9].
In the initial step, the OH radical oxidises the hydrocarbon (RH) to the alkyl radical R, which reacts rapidly with an O_2 molecule to form the alkyl peroxy radical RO_2. This peroxy radical can then either react with HO_2 to form an organic hydroperoxide ROOH, or with NO when present to form an alkoxy radical RO. The subsequent reaction of the alkoxy radical with molecular oxygen leads to the abstraction of an H-atom and the formation of an oxygenated species such as a carbonyl as well as HO_2:

$$RH + OH \rightarrow R + H_2O \tag{1.3}$$
$$R + O_2 \rightarrow RO_2 + M \tag{1.4}$$
$$RO_2 + NO \rightarrow RO + NO_2 \tag{1.5}$$
$$RO + O_2 \rightarrow R_{-H}O + HO_2 \tag{1.6}$$

In the subsequent reaction steps the OH radical used in the initial reaction is regenerated through

$$HO_2 + NO \rightarrow NO_2 + OH \tag{1.7}$$

with the NO typically originating from natural emissions or anthropogenic fossil-fuel combustion.
A competing reaction is the chain termination reaction of the HO_2 with a second HO_2 or another peroxy radical RO_2, to form O_2 plus H_2O_2 and ROOH respectively, or the the formation of H_2O and O_2 with an OH radical.

During daytime, the NO_2 produced in reaction 1.5 and 1.7 above can photolyse in the troposphere at wavelengths $\lambda < 420$ nm to generate $O(^3P)$ radicals which react with O_2 to produce O_3:

$$NO_2 + h\nu \rightarrow NO + O(^3P)(\lambda < 420nm) \tag{1.8}$$
$$O(^3P) + O_2 + M \rightarrow O_3 + M(M = N_2) \tag{1.9}$$

The photolysis lifetime of NO_2 is about 5 s for overhead sun conditions, meaning that the NO_2 concentration is lower by day [9].
The following equation shows the net reaction of the VOC oxidation cycle, with NO_x and HO_x acting as catalysts:

$$RH + 4O_2 \rightarrow R_{-H}O + H_2O + 2O_3 \tag{1.10}$$

During the night, in the absence of OH, an important sink for the VOCs is the reaction with NO_3. The NO_3 radical itself is formed in a slow process by the reaction

$$NO_2 + O_3 \rightarrow NO_3 + O_2 \tag{1.11}$$

In sunlight conditions, this radical is photolysed in a few seconds to regenerate NO_2 and O, or reacts with NO to form NO_2. At night, however, the chemistry is entirely different. The main sink for NO_3 is to form N_2O_5 in the equilibrium reaction

$$NO_2 + NO_3\ (+M) \rightleftharpoons N_2O_5\ (+M) \tag{1.12}$$

which can subsequently react in the presence of water vapour to form HNO_3:

$$N_2O_5 + H_2O \rightarrow 2\ HNO_3 \tag{1.13}$$

A further removal pathway for the NO_3 radical at night is the reaction with VOCs. The abstraction reaction with saturated VOCs (RH) converts NO_3 to HNO_3

$$NO_3 + RH \rightarrow HNO_3 + R \tag{1.14}$$

whereas the addition mechanism with alkenes initiates the complex chemistry displayed in Fig. 1.5 at the example of 2-methylpropene.

The initial reaction of 2-methylpropene with NO_3 can start via two different channels:

$$NO_3 + H_2C = C(CH_3)_2 \rightarrow H_2C(ONO_2)C(CH_3)_2 \tag{1.15a}$$
$$\rightarrow H_2CC(ONO_2)(CH_3)_2 \tag{1.15b}$$

Equation 1.15a is the major reaction pathway, ultimately resulting in the generation of formaldehyde, a ketone and NO_2, whereas the minor reaction channel shown in equation 1.15b results in a bifunctional organic nitrate product (2-nitro-oxy-2-methylpropanal for the example of 2-methylpropene).
Table 1.1 shows calculated lifetimes for selected anthropogenic and biogenic compounds with respect to reaction with the OH radical, NO_3 radical and O_3 [9, 10]. It is apparent, that for aromatic compounds the reaction with OH radicals is dominant for tropospheric removal, whereas oxidation through the reaction with O_3 will not be significant. Reaction with OH radicals also dominate the tropospheric oxidation of alkanes and other saturated organic compounds and are often considered the driving force behind tropospheric chemistry [9]. Unsaturated organic compounds such as alkenes, dienes or monoterpenes, not only react with OH radicals like most other compounds, but are also reactive enough to be significantly oxidised by O_3 and NO_3. Ambient concentrations of OH radicals, NO_3 radicals and O_3 are highly variable. OH radical concentrations usually peak at around solar noon for clear sky conditions. Maximum concentrations measured at midlatitude Northern Hemisphere sites mounted to 2-10$\times10^6$ molecules cm^{-3} OH (0.08 - 0.42 ppt), a 12-hours daylight average of 2×10^6 molecules cm^{-3} is usually assumed for the calculation of tropospheric lifetimes. The concentration of NO_3 is low during daylight hours, but can increase over continental areas during nighttime to 1×10^{10} molecules cm^{-3} (430 ppt), a reasonable value for lifetime calculations also adopted in Table 1.1 is 5×10^8 molecules cm^{-3} (20 ppt). The estimated O_3 concentration on a 24-hours average is 7×10^{11} mol-

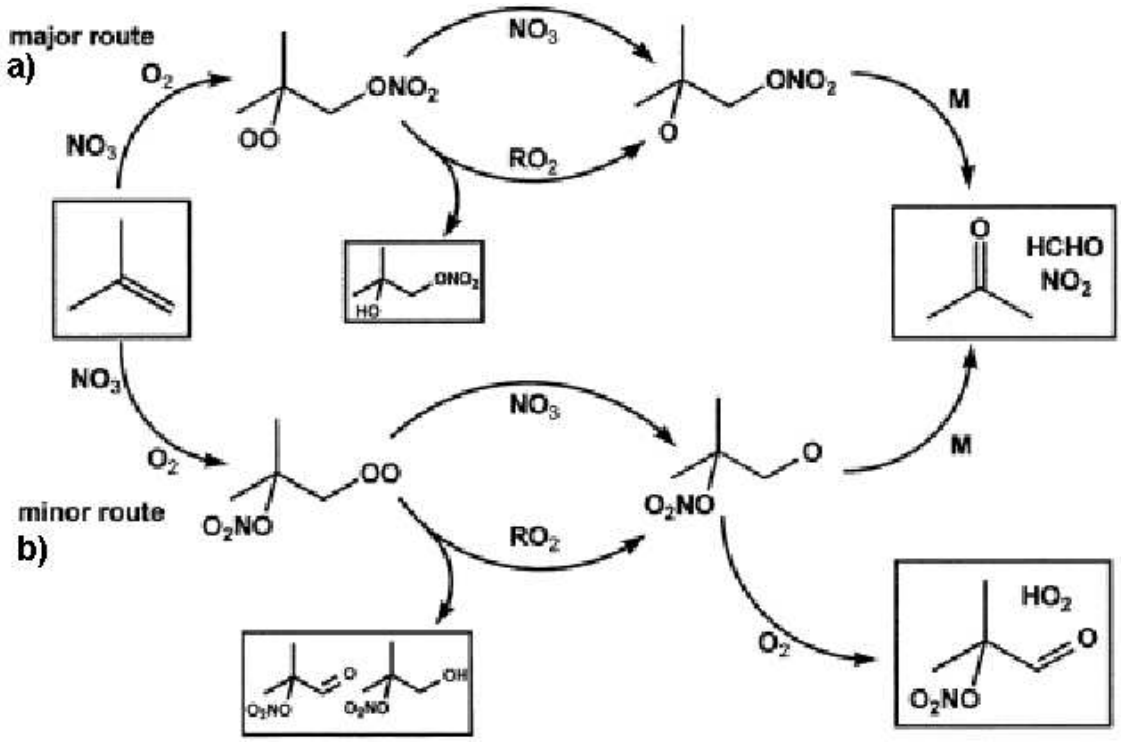

Fig. 1.5: Schematic diagram of the nocturnal NO_3 reaction with unsaturated VOCs (example 2-methylpropene)

ecules cm^{-3} (30 ppb), although concentrations from zero to several hundred ppbv have been measured in the troposphere. The residence time or lifetime of VOCs in the atmosphere depends on the concentration of OH, NO_3 and O_3.

Anthropogenic VOC	**OH**	**NO_3**	**O_3**
Ethane	29 d	91 yr	[a]
Propane	6.3 d	7.8 yr	[a]
Butane	2.9 d	2.7 yr	[a]
Ethene	20 h	7.3 mth	9.7 d
Propene	6.6 h	4.9 days	1.5 d
1-Butene	5.5 h	3.5 days	1.6 d
2-Butene	2.9 h	2.9 h	2.4 h
Benzene	9.4 d	$>$ 4 yr	[a]
Toluene	1.9 d	1.9 yr	[a]
Ethylbenzene	0.8 d	41 d	[a]
o-Xylene	12 h	4.1 mth	[a]
m-Xylene	5.9 h	200 d	[a]
p-Xylene	12 h	3.4 mth	[a]
1,2,4-Trimethylbenzene	4.3 h	26 d	[a]
Styrene	2.4 h	3.7 h	1.0 d
Biogenic VOC			
Isoprene	1.4 h	50 min	1.3 d
α-Pinene	2.6 h	5 min	4.6 h
β-Pinene	1.8 h	13 min	1.1 d
Camphene	2.6 h	50 min	18 d
Sabinene	1.2 h	3 min	4.6 h
3-Carene	1.6 h	4 min	11 h
Limonene	50 min	3 min	2.0 h
Eucalyptol	1 d	270 d	[a]
β-Caryophyllene	40 min	2 min	2 min
Methyl vinyl ketone	6.8 h	$>$ 1.0 yr	3.6 d
6-Methyl-5-heptene-2-one	50 min	4 min	1.0 h

[a] Rate coefficient for these reactions are less than 1×10^{-22} cm^3 $molecule^{-1}$ s^{-1} and therefore omitted

Tab. 1.1: Calculated tropospheric lifetimes of selected anthropogenic and biogenic VOCs for the gas-phase reaction with OH radicals, NO_3 radicals and O_3. Values are based on assumed concentrations of 2×10^6 molecules cm^{-3} OH (0.08 ppt, 12 hrs daytime average), 5×10^8 molecules cm^{-3} NO_3 (20 ppt, 12 hrs nighttime average), and 7×10^{11} molecules cm^{-3} O_3 (30 ppb, 24 hrs average)

1.4 Measurement techniques for volatile organic compounds (VOCs) in the atmosphere

To characterise the complex mixture of biogenically and anthropogenically emitted volatile organic compounds (VOC) in the atmosphere, a range of different measurement techniques has been devised and employed. The first measurements of VOCs were performed in the 1940s, when atmospheric CH_4 at parts per million levels was identified by Migeotte using infrared (IR) spectroscopy [19]. The first VOC to be measured at parts per billion was peroxy acetyl nitrate (PAN), also using IR spectroscopy [20, 21]. Optical techniques are important in the analysis of volatile organic compounds in air, although their sensitivity is rarely sufficient for concentrations in the ppt range and the specifity not suited to the complex VOC mixtures present. In the ultraviolet (UV) and visible wavelength regions, differential optical absorption spectrometry (DOAS) has been used to measure the aromatic compounds benzene, toluene and the xylenes in urban air [22, 23, 24]. Fourier transform infrared spectroscopy (FTIR) and tunable diode laser absorption spectrometry (TDLAS) can be applied for small compounds such as formaldehyde and ethyne, but the techniques are not capable of measuring the wider range of larger hydrocarbons at trace levels [25]. Satellite observations also use optical methods to probe the atmosphere and provide data for a small selection of trace gases with specific absorption structures like NO_2 and CH_4 on a global scale [1]. Complex VOC mixtures in the atmosphere, however, contain many species, in very low concentration with very similar absorption behaviour and in such cases in-situ techniques with better selectivity have to be applied.
One approach with greater selectivity is monitoring with mass spectrometry. Different ionisation techniques can be used, e.g. chemical ionisation (CI), electronic impact ionisation (EI), resonance-enhanced multiphoton ionisation (REMPI), or single photon ionisation (SPI) enabling a wide range of species to be detected. The proton transfer reaction mass spectrometer (PTR-MS) is a chemical ionisation method frequently applied in the analysis of air [26, 27, 28, 29]. It is a technique with excellent time response of a few seconds, a detection limit of 10-100 ppt depending on the analyte, but isomers, i.e. different species with a common mass, can not be separated and some masses can not be absolutely assigned to one compound [30, 31]. Traces of aromatic compounds can also be detected using the REMPI method [32], whereas the SPI coupled to a mass spectrometer has been shown to be suitable for aliphatic compounds [33]. These techniques have only recently been used for atmospheric gases and their detection limits are not yet good enough for measurements of very low background concentrations.
To achieve not only high sensitivity but also unequivocal identification of the target compounds in a mixture such as air, separation prior to detection is critical.
A suitable analytical technique is without doubt gas chromatography (GC), which can be coupled to a variety of detection methods (further details on chromatography in chapter 2). Gas chromatography combines a very high selectivity and resolution; good accuracy and precision; a wide dynamic concentration range; and a high sensitivity. This method is therefore well suited for analysis of air. Indeed, much of our

atmospheric chemistry knowledge to date has been deduced from the application of gas chromatography in all parts of the world.
Automated on-line GC-flame ionisation detector (GC-FID), and GC-mass selective detector (GC-MSD) systems have been used for both long-term and intensive short-term measurements of atmospheric hydrocarbons [34, 35, 36, 37, 38]. The gas chromatographic analysis can also be performed off-line, i.e. in a laboratory situated away from the sampling site, the air samples have to be collected by means of canisters or adsorbent cartridges and shipped back to the laboratory for analysis. This method is often applied in isolated areas [39, 40, 41], and with airborne [42, 43, 44] or ship-based measurements [45] where it is inconvenient or impossible to analyse in-situ.
Recently, a fast GC-MS system has been flown on an aircraft for the measurement of C_2 to C_4 VOCs and methanol [46]. A fast GC-ECD system for in-situ measurements of long-lived species like Chlorofluorocarbons (CFCs) and PAN in the upper troposphere and lower stratosphere has also been deployed on board an aircraft effectively [47]. The advantage hereby compared to canister or cartridge sampling is no limitation of samples through volume or weight restrictions, and additionally no possibility of changes in sample composition during storage.
Recently, a promising technique with a higher resolution than conventional gas chromatography has been developed and successfully applied in air analysis. Two-dimensional gas chromatography (2D-GC or GC×GC) is able to separate and classify several hundred chemical species of VOCs in ambient air when coupled to an appropriate detector. Concentrations of a few ppt can be measured and even the separation of isomers, e.g. monoterpenes, the aromatic C_2, C_3, C_4 and C_5 benzenes, can be achieved [48, 49, 50]. Section 2.2.1 gives a detailed description of the GC×GC technique.

1.5 Summary

It has been shown in the previous sections, that anthropogenically and biogenically emitted compounds play a significant role in the atmosphere. Although their mixing ratios are relatively low, they can profoundly influence tropospheric chemistry from the local to the global scale. Their contribution to tropospheric O_3 production or organic particle formation are, as well as the direct impact on living organisms, a major current research topic. To better understand tropospheric oxidation and the future atmosphere and climate it is increasingly important to quantify these volatile organic species.

CHAPTER 2

Gas Chromatography

- Experimental -

Technique and application of
gas chromatography and GC×GC

2.1 Basic principles of gas chromatography

Gas chromatography is an analytical technique that can be used to separate volatile organic compounds in a gaseous mixture and it can be used to measure such compounds qualitatively and quantitatively. Separation is achieved by selective retention of compounds in a separating bed as a function of their polarity, size or vapour pressure.
A mixture of gas phase species is normally separated inside a narrow tube, called the column. Within the column the individual components partition dynamically between two different phases, a mobile phase, and a stationary phase attached to the column. The gas sample is carried by the inert mobile phase (carrier gas, such as helium) through the column. Those components with a greater affinity for the stationary phase take longer to progress through the column, and gradually bands of individual species form. The separated species elute from the column and then trigger a response in a detecting device situated at the end. As the gas mixture moves through the column, the individual components of the gas mixture partition to the stationary phase to different extents, depending on the species and the temperature.

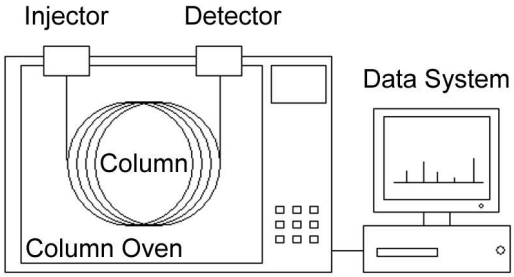

Fig. 2.1: Schematic set-up of a gas chromatograph system

The gas chromatographic system consists of: (1) an injector system, (2) a separation column containing a stationary phase with a large surface area and held at controlled temperature, and (3) the detector, see Fig. 2.1 [51]. These parts are described in detail below.

2.1.1 Injector

The injector serves to transfer the sample onto the column, and various different devices may be considered. For liquid as well as gaseous samples, the use of a syringe in combination with a self-sealing silicon-rubber septum and a flash vapouriser port at the head of the column is common. The column capacity expresses the maximum amount of solute that can be injected onto a column before significant peak distortion

occurs, i.e. the peaks appear asymmetric with a leading edge. Due to the relatively low capacity of capillary columns much smaller samples are needed than for packed ones, so usually a sample splitter system has to be added. The sample splitter sends a defined fraction of the sample into the GC and has the advantage of making the injection instantaneous and the resultant peak sharp.
Another common method of injection is sample introduction via a rotary valve. In this case the sample is flushed through a sampling loop valve, which is then rotated to inject the previously flushed volume to be swept into the GC by the mobile phase [52].
For the gas chromatographic measurement of volatile organic compounds in air, the very low ambient concentration of the compounds requires that a pre-concentration step be made before the sample can be injected. One possible technique is via solid phase micro-extraction (SPME), where the sample is concentrated onto a fiber coated with an adsorbent phase, simply by exposure to the surrounding air. After sampling, the SPME fiber is heated and the adsorbed sample desorbs directly onto the column. In the studies performed here, the pre-concentration step is done either by passing outside air through a small-volume adsorbent trap filled with Tenax TA and Carbograph I (on-line mode), or the samples are collected onto separate cartridges filled with particulate sorbents, then subsequently thermally desorbed and refocussed on the smaller trap (off-line mode). The second trap is introduced at this stage to enhance the chromatography, as the relatively large volume of elution gas required to desorb the cartridge would lead to poor analytical resolution and low sensitivity. The analytes are desorbed from the small volume trap by rapid heating and are directly injected onto the column, see chapter 2.6.3. The application of sorbents to concentrate the VOCs is particularly useful, as other gases like nitrogen, oxygen or carbon dioxide are flushed through without being retained. Adsorbents additionally allow focussing of the analytes at room temperature, unlike other methods like cryofocussing, which require temperatures down to -150°C or lower, and therefore must use expendable cryogens such as liquid nitrogen.

2.1.2 Columns

The first columns for chromatographic separation to be used were packed columns. These are typically made of metal, Teflon or glass, with an outside diameter of 1/4" (6.4 mm) or 1/8" (3.2 mm) filled tightly with finely divided packing material coated with a thin layer of the stationary liquid phase. Nowadays capillary columns are almost always preferred. These are more efficient and faster and therefore also used in this study. They comprise of polyimide coated fused silica tubing of 0.25 or 0.32 mm internal diameter. Instead of packing material, only a thin film of the liquid immobilised stationary phase covers the walls [51].
The ideal stationary phase should be thermally stable, chemically inert, and possess low volatility and solvent characteristics. The degree of retention and selectivity for a specific compound in a specific column is given by the retention factor k' and the selectivity factor α. k' describes the migration rate of an analyte A on a column and is defined as,

$$k'_A = (t_R - t_M)/t_M$$

where the retention time t_R denotes the time between injection and the analyte A reaching the detector and t_M the time taken for the mobile phase to pass through the column with no interaction with the stationary phase. The ideal retention factor for an analyte is between one and five, a k' below one indicates a very fast elution and a high k' means elution takes a long time.
The selectivity factor α describes the separation of two species A and B on the column,

$$\alpha = k'_B/k'_A$$

where A elutes faster than B and α is greater than one to guarantee separation. The stationary phase should therefore be chosen such that the compounds can be separated, but the elution time is within a reasonable timescale [52].

The key parameter for column selection is the resolution, R_S, which is used to express the degree of separation between two adjacent peaks. For chromatography it is defined as

$$R_S = \frac{2((t_R)_B - (t_R)_A)}{(w_b)_A + (w_b)_B} = \frac{2d}{(w_b)_A + (w_b)_B}$$

where d is the distance between the peak maxima for two solutes A and B and w_b the base width of the respective peak A or B. If R_S equals 1.5, the two peaks are considered resolved.

The ideal stationary phase is usually selected after the principle 'like dissolves like', where 'like' refers to the polarities of the solute and the stationary phase. It can generally be said that the polarity of the phase should match that of the sample components, i.e. non-polar stationary phases for non-polar hydrocarbons, polynuclear aromatics, polychlorinated biphenyls (PCBs) etc. and a more polar stationary phase for alcohols, esters, glycols etc. [52].
An important factor for selecting the proper column is the film thickness of the stationary phase. Thin films produce better resolved chromatograms, whereas thick films possess a higher capacity for larger sample quantities without overloading the column. A 0.25μm film is normally used for practical reasons, as the column bleed, i.e. the background signal of the stationary phase breaking down and eluting, is minimised and the flow rate of the carrier gas can be either fast for high speed analysis or slow for higher resolution. The ideal column is small in diameter to improve the speed. Commonly used columns have an inner diameter of 0.25 mm or 0.32 mm, which represents the best compromise between resolution, speed and sample capacity. The column length usually ranges between 25-30 m, as longer columns increase the analysis time and shorter columns lower the resolution of the peaks [51].
In this study, two columns with different properties were chosen. To separate the compounds according to their boiling points, the most widely used nonpolar columns were deployed (DB-1 and DB-5, 100% polydimethyl siloxane, and 95% polydimethyl siloxane plus 5% phenyl, respectively), whereas the polar columns selected for separating the compounds according to their polarity were Carbowax (polyethylene glycol) and BPX-50, with 50% phenyl polysilphenylene-siloxane. The nonpolar columns were 25-30 m long, with a stationary phase of 1μm for the DB-5 and 2μm for the DB-1,

the film thickness of both polar columns was 0.1μm with a length from 1 to 3 m, depending on the measurements conducted.

2.1.3 Detectors

The injected gas sample is carried by the mobile phase through the column, migrating between the stationary and the mobile phase until the separated components elute sequentially from the column and produce a signal by means of a detector. A variety of detectors is available to measure species separated in the column. These rely on various physical principles of detection and these ultimately determine which species can be measured.
The Thermal Conductivity Detector (TCD) is based upon changes in the thermal conductivity of the gas stream caused by analyte molecules; the Electron Capture Detector (ECD) is highly sensitive to molecules with high electron affinity and 'electron-capturing' functional groups. Increasingly the Mass Spectrometer Detector (MSD) is employed, which ionises the molecules and separates the fractions by their mass-to-charge ratio (m/z), by either magnetic or electrical fields. One of the most widely used is the Flame Ionisation Detector (FID), which pyrolyses the molecules in an oxy-hydrogen flame and measures the current produced by the resultant ions and electrons [51].
The FID was selected as means of detection in these studies. It is stable, easy to use and robust, which are all very important factors for the use of a chromatographic system in the field. It offers good reproducibility, linearity and a high sensitivity towards combustible substances in the air sample. As the two-dimensional gas chromatographic system operated in these studies generates narrow peaks, a very important aspect is the high measurement frequency provided by the FID, which can be operated at rates of 100 to 200 Hz. Quadrupole MS detectors are generally unsuitable for GC×GC as the measurement frequency is only 10 Hz. However, a fast time-of-flight MS (TOF-MS, 100-500 Hz) can be used for identification, see section 3. The drawback of the TOF-MS is, that it is very large and therefore less suitable for transport and field campaigns.
Additionally, as the signal is approximately proportional to the carbon content of the compound burned, it is not necessary to calibrate every compound individually, as is the case for an MSD. Holm et al. [53] showed, that the constant response to carbon atoms is caused by the conversion of these atoms contained in the solute to methane during the combustion process. With this, the so-called equal per carbon rule can be applied, and as all hydrocarbons should exhibit the same response per carbon atom (= number of carbon atoms × 1), it is therefore possible to calibrate for example methyl-hexane with heptane as a standard. However, the response decreases if heterogenic atoms such as nitrogen or oxygen are present. By using relative response values, obtainable in the literature for the most common analytes, it is possible to calculate the concentration of a known heterogenic compound not contained in the standard [51]. If response values are not available for heterogeneous molecules, the effective carbon number, ECN, can be calculated. The contribution of various types

of functional groups to the ECN has been listed in [54]. An oxygen in the molecule for example diminishes the ECN with 1.0 for an ether bond and 0.6 for a primary alcohol. The ECN for decanol would be calculated thus as follows: 10 carbon atoms, 1 oxygen as primary alcohol = 10 ×1 + 1 ×(-0.6) = 9.4.
The advantages of the gas chromatographic separation technique are quite clear: the analysis is efficient, provides high resolution and a large linear range, requires only small samples, and, depending on the detection technique, it is sensitive down into the ppt region. It is also reliable, relatively simple, inexpensive, and suitable to characterise complex mixtures of hydrocarbons in air.
Disadvantages of the gas chromatographic method with FID are: restriction to samples that can be volatilised or are thermally stable. It is also fairly difficult to identify unknown peaks and for this usually a GC-MSD is needed. The number of measurements that can be made in a given time is limited, because of the time required in the separation step, i.e. one per 30 to 60 minutes.

2.2 History of Chromatography – a short outline

Gas chromatography began at the start of the twentieth century, when the Russian botanist Mikhail Tswett performed the first chromatographic separations of plant pigments. He passed solutions of compounds containing chlorophylls and xanthophylls over glass columns filled with finely divided calcium carbonate and achieved their separation into coloured bands on the column. Based on these phenomena, he chose the name chromatography from the Greek words chroma, meaning 'colour' and graphein, meaning 'to write' [52]. Interestingly his Russian surname is identical with the Russian word for colour (ЦВЕТ) and one might speculate if he really meant 'colour writing' [55].
Unfortunately, the benefits of separating all components within a complex sample both from the matrix and from another did not immediately get the attention it deserved. The main goal for leading botanists at that time was to isolate and crystallise a single substance and only few scientists adopted the process proposed by Tswett. It was not until the 1930s, that chromatography was applied again in earnest [55, 56], leading to the invention of partition chromatography theory and the prediction and final realisation of gas chromatography in 1953 by A. J. P. Martin and R. L. M. Synge [55].
Over the past 50 years, there has been a huge number of chromatographic applications in all branches of science and industry indicating the acceptance and importance of gas chromatography, which has moved from packed columns at the beginning to capillary columns in the late Seventies [57].
Although an excellent technique, very complex samples are difficult to separate and the peak capacity (maximum number of components placeable side by side in the available separation space at the given resolution) in one dimension is limited, overlapping peaks being the result of it and thus a lot of information contained in the sample can be lost.

2.2.1 Conventional and comprehensive two-dimensional chromatography

Where conventional chromatography failed to separate the targeted analytes satisfactorily, increased separation was achieved through heart-cutting methods, also referred to as 'conventional multidimensional gas chromatography'. In this technique, only selected small fractions of the sample eluting from the first column are transferred to another column to undergo further separation. In Fig. 2.2, the schematic of heart-cutting gas chromatography is shown.

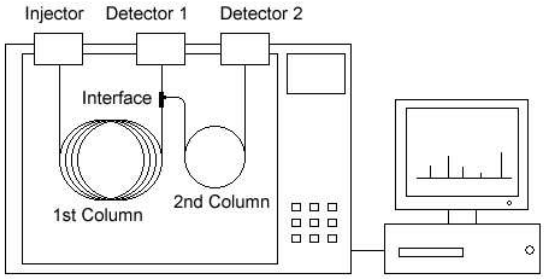

Fig. 2.2: Schematic of a conventional multidimensional gas chromatograph (heart-cut)

The analytes are separated on the first column and subsequently detected with detector 1. If part of the sample is of special interest to the analyst and a better resolution is required, it can be transferred to the second column for additional separation and detection with detector 2. During the analysis of the heart-cut fraction on the second column, the succeeding sample eluting from the first column is either further separated with less resolution on the first column or is discharged through an outlet. The transfer between first and second column is either achieved via a valve or a Deans' switch device [58] which uses valveless switching based on pressure balancing, so the effluent can be directed in either one of two possible directions [59]. To achieve a good resolution on the second column (second dimension) the sample must first be focussed on a cryotrap. This is a trapping device cooled to subambient temperatures with liquid nitrogen or CO_2 through which gases like nitrogen and oxygen can pass while the organic species are retained [60, 61].
An extensive application of heart-cutting chromatography was conducted by Gordon et al. [62], who separated hundreds of compounds in a flue-cured tobacco essential oil over a course of 48 hours, performing 23 heart-cuts during that time. A considerable time reduction was achieved seven years later by using multiple parallel working traps, switches and columns instead of just on single trap with one column [63].
Heart-cut chromatography is used in various fields. Some typical applications are separations of gasoline samples [64, 65, 66], separation of polychlorinated biphenyl (PCBs), polychlorinated dibenzo-dioxine (PCDDs) and dibenzo-difurane (PCDFs) isomers [67], analysis of essential oils [68], enantiomeric separations of chiral analytes in flavors and essential oils [69], gas analysis of pyrolytically decomposed polymers [70]

or, for example, the analysis of organic pollutants in environmental samples [71].
A disadvantage of the heart-cut method is that only the targeted part of the sample is subjected to further separation, whereas the following fraction is either lost through a vent or the separation continues on the first column with less resolution. In addition, the overall analysis time increases significantly by this method [72, 73].
Long analysis times, overlapping of peaks and thus loss of information justified the search for a new technique that could solve these analytical problems. And even though it was theoretically considered impossible to combine chromatographic techniques [74], the concept of separating an entire sample during one run on two columns with completely different properties via gas chromatographic methods was applied with success, and the new technique of comprehensive multidimensional gas chromatography was born.

2.3 Development of GC×GC

2.3.1 The GC×GC Modulator – Purpose and Evolution

The difference between comprehensive gas chromatography and heart-cutting gas chromatography described above is, that with GC×GC trapping time and column separation speed on the second column are fast enough to analyse many heart-cuts during the course of a first-column run without losing any information of the sample. The key element hereby is the modulator, which ensures complete transfer of the effluent from the first column to the second while simultaneously preserving the original separation. The first column is typically a long 30 m non-polar column, whereas the second column is typically a short 1 m polar column. A schematic of a two-dimensional set-up is shown in Fig. 2.3.
The function of the modulator is to allow: (1) a trapping or accumulation of small fractions of sample eluting from the first column during the first dimension separation process; (2) the injection of the focussed sub-fraction as a narrow pulse into the secondary column [75].

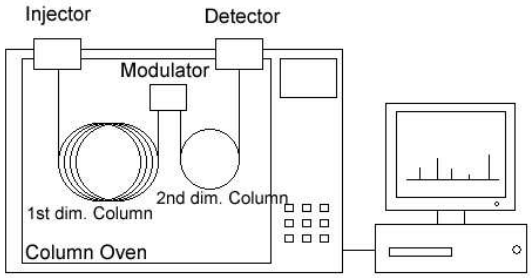

Fig. 2.3: Schematic of a GC×GC chromatographic system with modulator. The two columns are typically combined with a press-fit connector

Usually, the modulator works at a frequency of typically 0.1 – 1.0 Hz, focussing and injecting in time-intervals of a few seconds. It is key that the separation in the second dimension is finished before the next injection. Therefore a short, narrow column is required, giving second dimension chromatograms of 30 milliseconds and peaks three to four modulation periods in width [76].
To obtain well structured chromatograms and accurately quantifiable peaks, the setting of the modulation frequency is as important as the temperature used during trapping and release of the sample. The retention of a peak in the second dimension for a longer period than the modulation time results in so-called 'wrap-around peaks', which means the compound does not elute in the expected modulation cycle, but later. This primarily occurs, if the modulation time is too short, or, in other words, if the second column is too short for the selected modulation period. These wrap-around peaks lead to the loss of structure in the chromatogram and complicate identification. If the chosen modulation frequency is too long, the peaks are crowded in the lower chromatogram part of the second dimension, while the remaining space is empty. It can also result in an insufficient resolution.
For effective two-dimensional chromatography, the focussing and releasing temperatures of the modulator also play a vital role. If the trapping is effected by cooling and the temperature is very low, parts of the sample can be retained in the modulator, if the re-injecting hot jet does not pulse for long enough. If the trapping temperature is not cold enough, the sample can not effectively be retained in the modulator during increased oven temperatures and the components are constantly passing into the second column. Both cases lead to an underestimation of the measured concentration, the second case additionally produces an increasing background.

Many different types of modulators have been developed. One is the heated modulator, which uses thick-film modulation capillary columns to trap fractions which are subsequently desorbed by application of heat. The other type are cooled modulators, which trap the analytes via cryogenic focussing at the beginning of the second column, desorption is performed by either raising the surrounding oven temperature or by applying a stream of heated gas. A third alternative is the modulation via multiple valve-based means.

2.3.2 Thermal modulators

The first modulators successfully used were dual-stage thermal desorption modulators (TDMs), consisting of a thin conductive metal film applied to the exterior of a thick-film modulator column installed outside the oven. By passing electrical current pulses through this metal film at appropriate times, the heating and injection of the focussed sample was carried out. This set-up, however, was not ideal, as it was difficult to manufacture and not very robust, leading to unpredictable burnouts [77, 78, 79]. De Geus et al. [80] tried to overcome these problems by employing copper wire coiled around the column, but the thermal response proved to be too sluggish and slowed down the chromatographic analysis remarkably.
In one approach, the modulator was constructed of two adjacent sorbent traps

made of Silcosteel tubing filled with Tenax TA sorbent. Fast heating is attained by capacitive discharge power supply similar to the ones used in in-column pyrolysis. This assembly is mounted inside a cryochamber, where either ambient air or nitrogen is used to quickly cool the trap after the heating process [81].

A recently invented low cost multi-stage thermal modulator consists of an array of 10 successively heated segments, Fig. 2.4 [82]. A fused-silica modulator capillary without stationary phase is fitted into the heater made of stainless-steel tubing, glass-fiber insulated copper leads are soldered to connectors attached every 10 mm of the heater tube. To perform modulation, heat is applied via current pulses passing through the succeeding individual segments.

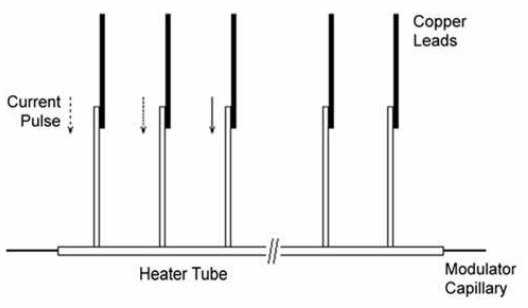

Fig. 2.4: Multi-stage thermal modulator

In 1996, Phillips et al. [83] developed a heating device where a heater element, termed 'the Sweeper', rotates over a small part of a thick-film capillary column. When rotating, this heater forms a hot spot traveling along the modulation column, forcing the compounds slowed down in the cooler area inside the oven to focus, accelerate and getting injected onto the second column (see Fig. 2.5). As the modulator moves off the first stage, the modulation part rapidly cools, thus accumulating the following eluting compounds again until the next modulation cycle [83, 84, 85]. To release the retained fraction, a temperature difference between the temperature surrounding the trapping capillary and the Sweeper of at least 100°C is necessary, thus the maximum operating temperature is determined by the stationary film in the trapping column itself.

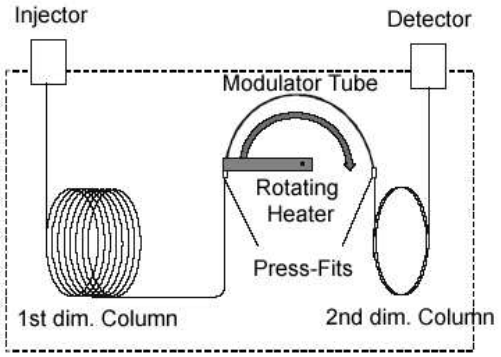

Fig. 2.5: Sweeper modulation system

2.3.3 Valve-based modulators

Differential flow modulation GC×GC is a modulation technique which involves a multiple-port diaphragm valve fitted with a sample loop to couple the primary and secondary column [86, 87, 88]. The sample loop fitted to the high-speed diaphragm valve is filled with sample eluting from the primary column and then flushed into a short transfer line leading to the secondary column.
The transfer is not 100% as with most of the thermal modulation techniques, but the authors consider it comprehensive as well, because the primary column efflu-

ent is modulated throughout a complete chromatographic run at a frequency high enough so the primary separation can be retained. Approximately 80% of the sample originally entering the primary column reaches the detector, the rest is lost through the column exhaust during injection of the sample from the sample loop on the secondary column [89]. In the aforementioned system the operating temperature of the chromatographic analysis was restricted by the maximum allowed temperature of the valve, a new design, however, has moved the temperature-restrictive part of the valves outside the oven, allowing temperatures up to 250°C [90].

2.3.4 Cryogenic modulators

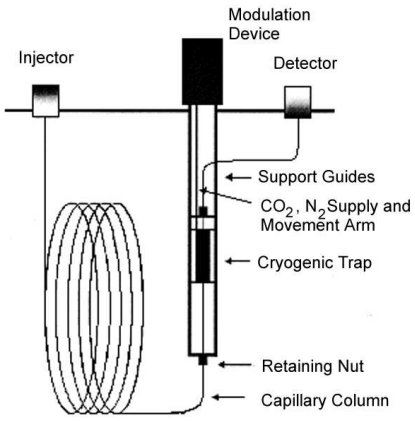

Fig. 2.6: Longitudinally Modulated Cryogenic System (LMCS)

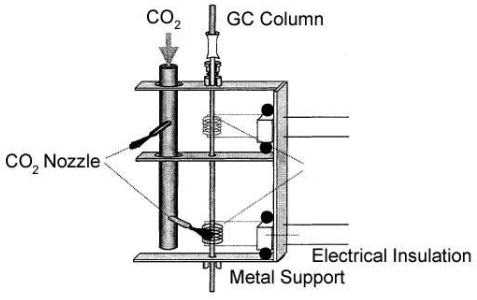

Fig. 2.7: Rotating modulator system with CO_2

Developed around the same time as the Sweeper mentioned earlier, a further method for GC×GC involves the trapping of the eluting compounds at subambient temperatures. The trapped eluent is subsequently released by moving the cooling trap away from the cold spot on the column to expose the cooled part to the oven temperature (LMCS, Longitudinally Modulated Cryogenic System, see Fig. 2.6). The cooling is achieved by a liquid CO_2 flow, the modulator is moved using a pneumatic system [91, 92]. Initial problems where the cryotrap froze to the column leading to breakage during the moving of the trap have since been resolved.

A different modulator type was constructed using two-step cryogenic trapping through a rotating device which directs liquid CO_2 onto the column. The thermal desorption is done by coiled wire resistors spiraling around the trapping part (see Fig. 2.7). A metal tube is turned with a magnetic actuator and the CO_2 is sprayed onto the column through two nozzles which are soldered to the tube in a 45° angle. During modulation, the liquid stream is first directed at the upper heating coil, then rotated towards the lower part of the capillary, while the upper heating wire is heated. The released sample gets trapped downstream in the second cold spot and is released again by turning the rotator to the original position [93].

During the past few years, efforts have been made to improve reproducibility and to reduce the risk of breaking columns by minimising the moving parts in the modulators and many different mechanisms have been developed. The solution was to use stationary cooling and heating jets. To prevent break-through of the trapped solute a pair of jets is used, see Fig. 2.8. A development based on this principle uses pressurised liquid CO_2 as modulation coolant, the cold spot is heated up by the surrounding oven temperature [94].

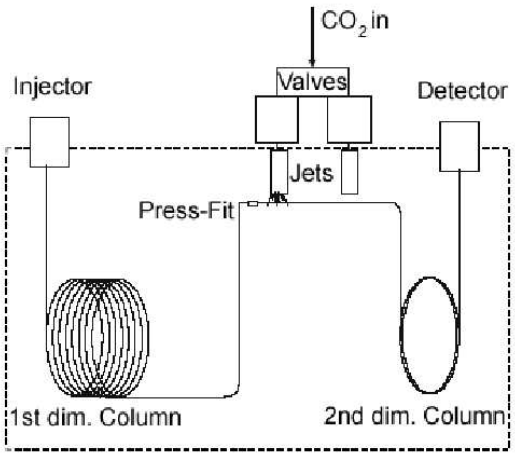

Fig. 2.8: Cryogenic modulation system with two jets

In Fig. 2.9, the modulation scheme for a jet-operated modulation system is depicted. The first cryojet upstream is turned on, trapping the sample eluting from the primary column in its cold spot, Fig. 2.9 A. When this cold spot is heated up, either by turning off the cryojet or using a hot jet, the focussed sample is released onto the second column. Meanwhile the second cryojet upstream is switched on to prevent interference of the material eluting from the first column with the re-injected fraction, Fig. 2.9 B. The first cryojet is then switched on again and the next modulation cycle starts, Fig. 2.9 C.

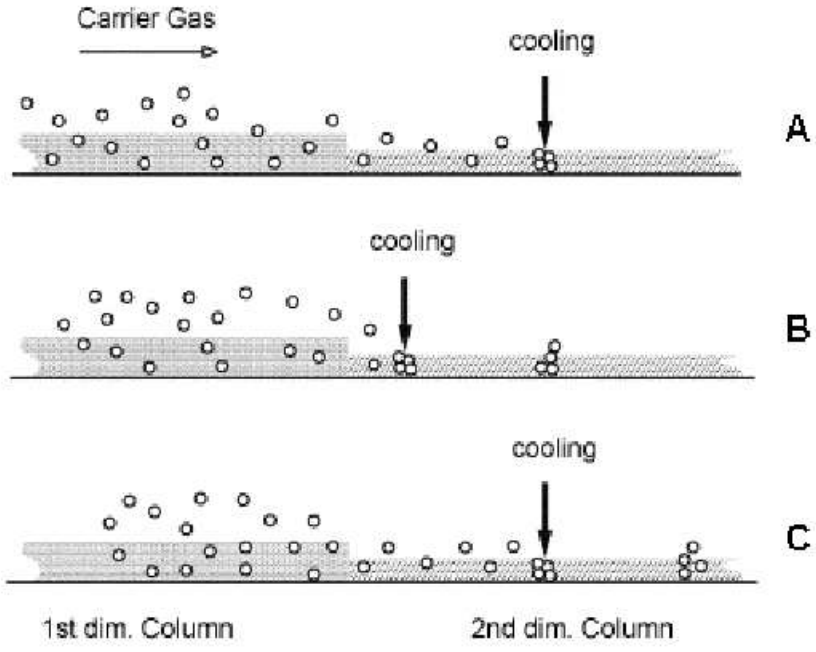

Fig. 2.9: Modulation cycle for cryogenic modulation with jets

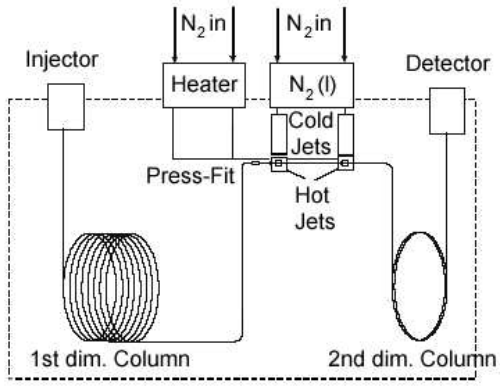

Fig. 2.10: Four-jet modulation design

The four-jet modulator, as used in this study, was first designed in 2000. The cold jets operate with gaseous N_2, cooled by heat exchange with liquid N_2. Hot jets are fixed orthogonally to the cold jets and operate with either gaseous nitrogen or pressurised air, see Fig. 2.10 and section 2.6.1 for further description [95, 96]. An additional improvement of this system is the direct use of liquid N_2 for the cold jets [97, 98]. However, by introducing liquid N_2 into the chromatographic oven, the temperature does not stay stable and removal of the increased amount of cool nitrogen gas is essential.

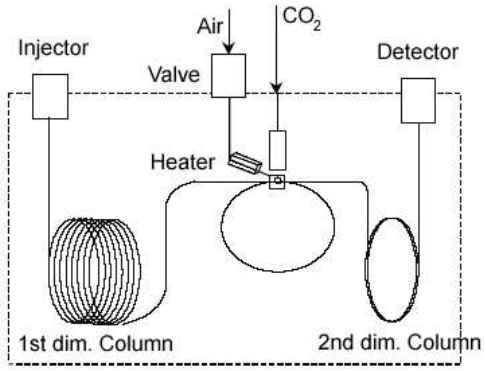

Fig. 2.11: Single loop modulator [96]

The latest development made in this area is the single-jet loop modulator, commercially available since 2004. This modulator consists of one cold and one hot jet, at 90 degrees to each other. Two-stage modulation is effected by looping a segment of the column or uncoated capillary twice through the path of the nozzles (see Fig. 2.11).
Two spots form approximately 0.6 m apart, depending on the size of the loop, and get cooled, or heated, respectively, at the same time with one jet operation. When the upstream cold spot is heated up for a few milliseconds, the material enters the delay loop and gets refocussed downstream as the loop passes the cold jet the second time. The next hot pulse releases the trapped material downstream into the second column, while the upstream released material enters the delay loop.
This reduces the consumption of the cooling gas to about half of that needed in quadruple-jet configuration, but can also bear the disadvantage of an additional press-fit connector if a modulation capillary is used as looping segment instead part of the analytical columns [98, 99].

2.4 3-D Chromatogram generation

From the description given above, it is clear that the detector will record a sequence of short chromatograms emerging from the second column. These individual chromatograms need to be arranged so that both dimensions of this separation can be

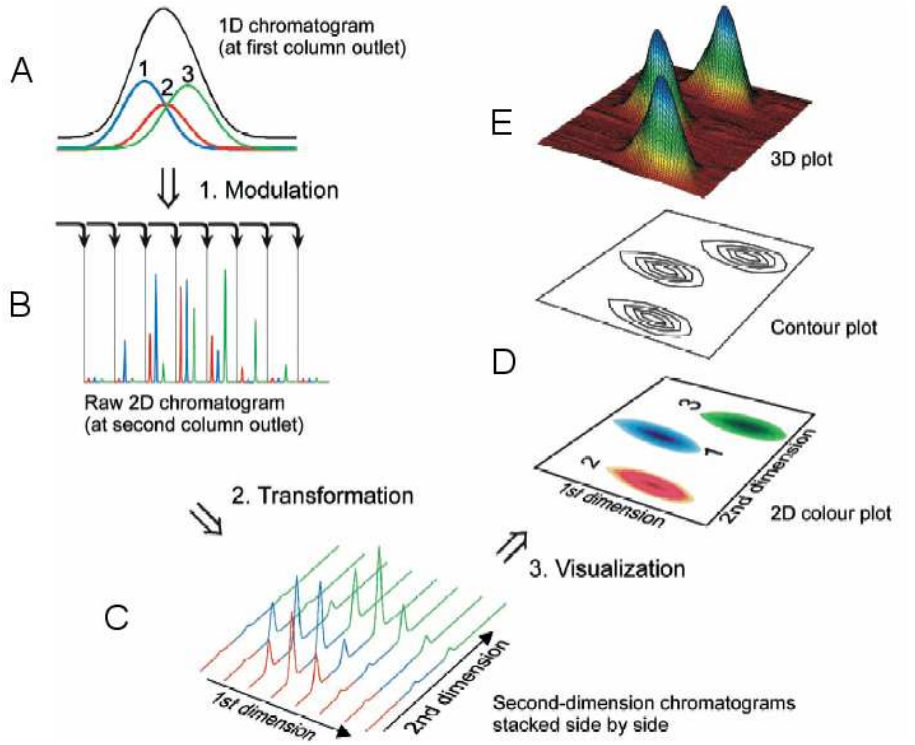

Fig. 2.12: Generation of a chromatogram. Taken from Dallüge et al. [75]

seen. The steps necessary for generating the final two-dimensional chromatogram from the raw signal output of the detector are shown in Fig. 2.12. Compounds eluting from the primary column at the same retention time are still contained in one peak and would be detected as such if a detector was connected to the outlet, see Fig. 2.12 A, this peak is then separated on the second column after the modulation. The data generated during a GC×GC run is seen at the detector as a linear signal and shows the retention time and signal amplitude as with any other one-dimensional chromatogram. But what is detected consists actually of a series of short second-dimension separations in the time-frame of the modulation performed plotted continuously, see Fig. 2.12 B. This raw data file has to be transformed from the linear form to a 2D-matrix array by cutting the signal output into slices of the individual second-dimension chromatograms, see Fig. 2.12 C. This has been done for the most part with custom written software and is usually performed by slicing the output signal according to the modulation period set. These mini-chromatograms are then aligned side by side with the primary retention plotted into the x-axis and the secondary retention into the y-axis direction. The visualisation of the third dimension is usually carried out by using colours, shadings or contour lines to indicate the signal intensity, Fig. 2.12 D. For clarity, a three-dimensional plot is shown in Fig. 2.12 E showing the signal intensity plotted into z-axis direction [75, 100].

An advantage of GC×GC over conventional gas chromatographyis a much higher peak capacity, which is usually seen in an improved separation of analytes in the sample from each other and from interfering matrix substances into the second di-

mension. A further advantage is the better detection limit and the sharper peaks. Also, if proper orthogonal conditions are used, i.e. the two columns provide independent separation mechanisms by different stationary phase coatings, the chemically related substances show ordered structures. This can facilitate group-type analysis and enable the tentative identification of unknowns. The grouping of the compound classes can be seen particularly in the sample of a light cycle oil (Fig. 2.13) [75]. Another main advantage can be found in the reproducibility of retention times in both directions, which is typical for every compound and usually changes only slightly if the analytical conditions remain constant [101]. An example for constant retention time and structure is depicted in Fig. 2.14, where the calibration gas shows the same structure as the air sample and the classification of already identified VOCs can be done easily. An intralaboratory study conducted with an LMCS modulator on the reproducibility of peak positions revealed a standard deviation of 0.2% in the first and 1% in the second dimension for the run-to-run repeatability. The day to day re-

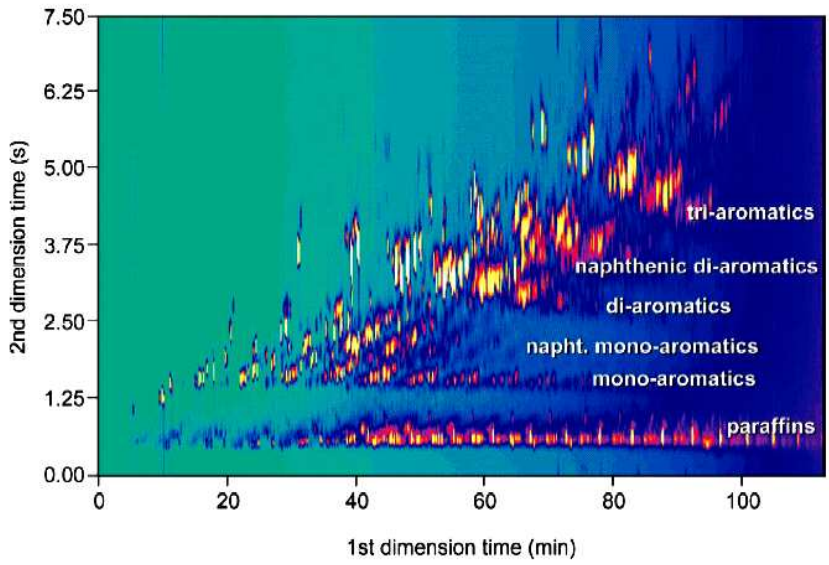

Fig. 2.13: Two-dimensional chromatogram of a light cycle oil [75]

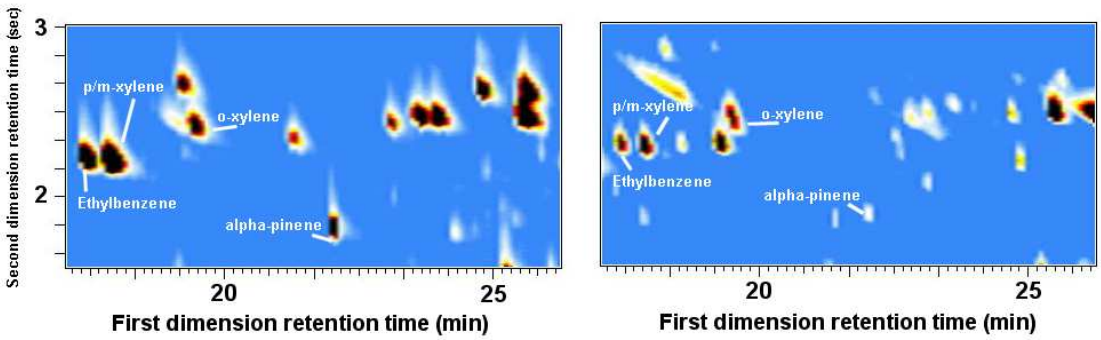

Fig. 2.14: Chromatograms of a standard (left) and a real air sample (right).

peatability showed that most components elute within plus or minus one modulation period in the first dimension [101]. It can be concluded that for a given column set highly reproducible results are possible, which can be confirmed in the work completed in this study with a four-jet cryogenic modulator.

2.5 Applications of GC×GC

Two-dimensional gas chromatography has, despite being only recently developed, already been applied in many fields. Without doubt, its major application has been in the field of petrochemistry, such as group-type characterisation [75, 84, 102, 103, 104, 105, 106, 107], biomarker identification [108] and target compound analysis [109, 110, 111].
The flavour and fragrance sector is also strongly involved in GC×GC research, mainly in the area of essential oil analysis [112, 113, 114, 115, 116, 117, 118, 119, 120, 121, 122], quality control development [123] or trace analysis of flavours in food [124]. The technique is very suitable for environmental investigations of the complex mixture of volatile organic compounds in air [48, 49, 50, 125, 126], oil spill source identification [102], polycyclic aromatic hydrocarbons and polychlorinated biphenyls in food, water, sediments etc. [75, 127, 128, 129, 130, 131, 132, 133], sterols in water [134], steroids in algae [75] and aerosol measurements [135, 136]. Pesticide analysis in different matrices is also profiting from the application of the system [79, 137, 138, 139]. Its high potential in unravelling complex mixtures of fatty acids in biological samples has also been demonstrated [140, 141].
Recently, comprehensive gas chromatography has been used for the characterisation of roasted coffee beans by Mondello et al. [142], cigarette smoke in general [143], as well as the acidic and basic fractions of cigarette smoke [144, 145]. Progress has also been made in the area of doping control and general drug screening [146, 147].

With the increasing popularity of two-dimensional gas chromatography, the recent emergence of commercially available two-dimensional gas chromatographs with different detectors like FID, ECD or TOF-MS (LECO, Mönchengladbach, Germany and Thermo Electron Corporation, Dreieich, Germany), the simplification for handling the hardware and the availability of intelligible software, the variety of applications can be expected to grow in the future and make its entry into routine laboratory work in the fields of research and industry.

2.6 GC×GC-FID system

The GC×GC-FID system applied during this study is described here. The system consists of a thermodesorption unit connected to a gas chromatograph configured to allow two dimensional separation via the four jet system described in chapter 2.3.4. The chromatograph is equipped with a Flame Ionisation Detector (FID) operated at 100 Hz. Two alternative sampling methods were used for trapping the volatile

organic compounds (VOCs): these were the thermodesorption unit directly (on-line) for ground-based campaigns and laboratory work or indirectly by cartridges that are desorbed later. A schematic drawing can be seen in Fig. 2.15, a picture of the system is shown in Fig. 2.16.

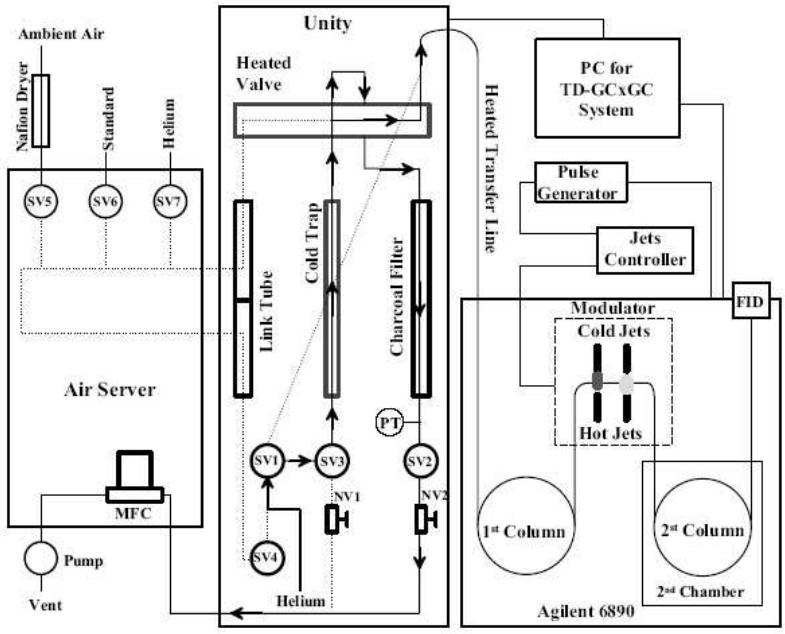

Fig. 2.15: Two-dimensional gas chromatograph with the thermodesorption system for on-line sampling

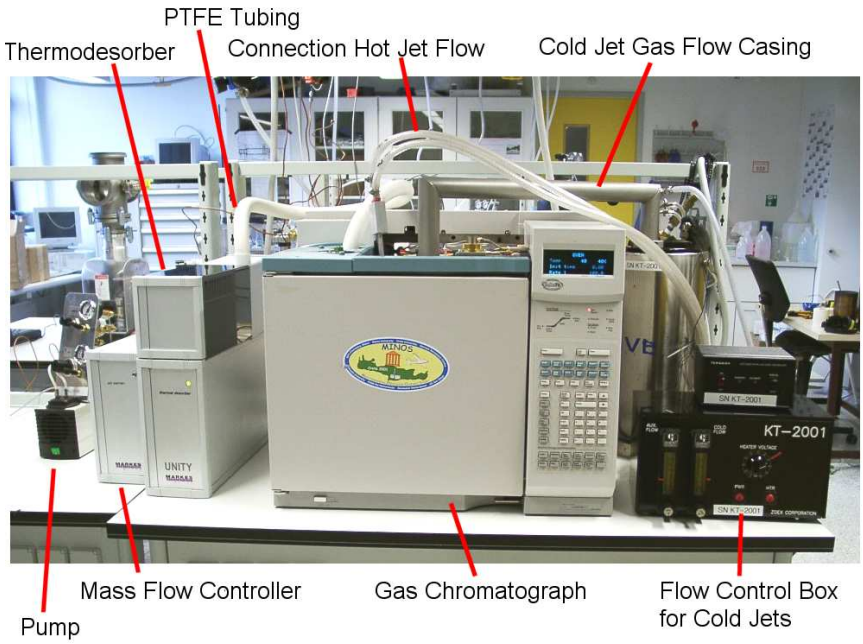

Fig. 2.16: Picture of the GC×GC system in the on-line sampling mode

2.6.1 Two-dimensional Gas Chromatograph (GC×GC)

The two-dimensional gas chromatographic (GC×GC) system used comprises of a gas-chromatograph GC6890 with a flame ionisation detector (FID) (Agilent, Wilmington, DE, USA) and quad jet modulator (Zoex, Lincoln, NE, USA).
The chromatographic system is controlled by the ChemStation software (Agilent, Wilmington, DE, USA), the GC×GC modulation is controlled and synchronised with the GC via the multipurpose process control module V25 made at the Max-Planck-Institute for Chemistry (Mainz, Germany). This pulse generator is linked with the GC to permit consistent synchronisation between the modulator, the thermodesorber and the start of the GC run without drift in the second dimension retention, which is critical to the reproducibility of chromatograms. Additionally, the controlling sequence provided by the V25 for the different jets is crucial to prevent breakthrough caused by the upstream hot jet pulsing too long or incomplete release of the trapped analytes with hot jets pulsing too short.
The starting signal is given by the software of the thermodesorbing system so both the acquisition of data from the flame ionisation detector (FID) and the start of the modulation are triggered with the beginning of the injection of the sample onto the column. The inside of the GC oven with the two-dimensional configuration is shown in Fig. 2.17. The four-jet type modulator used in these studies allows rapid cooling and heating of the column (Zoex, NE, USA). It comprises of two parallel cold jet tubes at a distance of 80 mm and two parallel hot-jet tubes at a distance of 110 mm placed orthogonally to the cold jets, see Fig. 2.18 and 2.19. The cold jets are operated with gaseous nitrogen at approximately -50°C, the temperature being reached via conductive cooling, i.e. gas passing through copper tubing bundled inside a dewar filled with liquid nitrogen. To keep the gas temperature as low as possible and to minimise condensation of ambient water vapour, it is transported to the jets in an evacuated outer casing. The hot jets operate with pressurised air at 2.5 bar, heated inside the GC oven directly at the tube outlet to temperatures > 200°C.
The modulation is performed on the second, polar column, about 10 cm from the connection with the first non-polar column. The columns are connected with a deactivated fused silica Press-Tight Connector sealed with polyimide glue (Restek GmbH, Bad Homburg, Germany).
The first segment of the short polar column, about 25 cm, is subjected to the GC oven temperature just as the primary column, whereas the main part of the second column is isolated inside a small second oven. This oven is insulated and its temperature can be regulated separately from the GC oven by the ChemStation software. At the end of each run this oven is cooled by gaseous nitrogen to the required starting temperature. An approximately 10 cm long end segment of the column is again exposed to the air of the main oven before it enters the FID.
The FID is set at a temperature of 300°C, with a carrier gas flow (helium 6.0, 99,9999%, Messer-Griesheim, Krefeld, Germany) of 30 ml min^{-1}, and a makeup gas flow (synthetic air, Messer Griesheim, Krefeld, Germany) of 400 ml min^{-1}. The combustible gas used is hydrogen 5.0 (99.999%, Messer-Griesheim, Krefeld, Germany) at a flow of 30 ml min^{-1}. The data acquisition rate is set at 100 Hz.

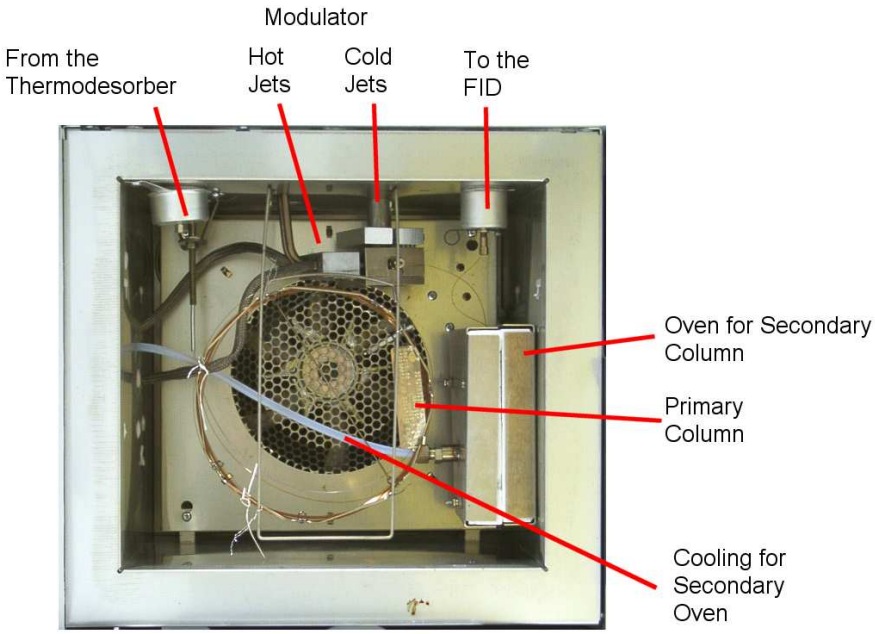

Fig. 2.17: View inside the gas chromatograph oven

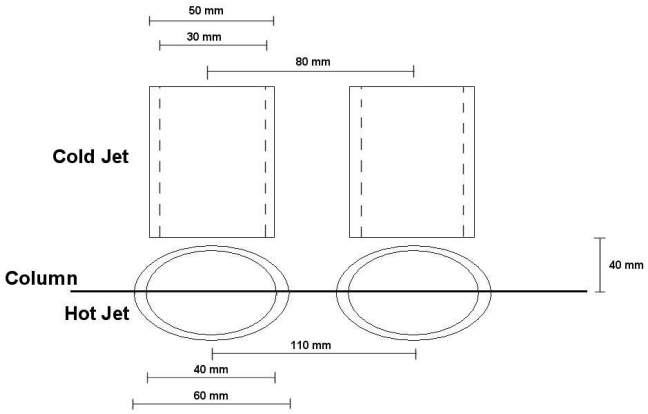

Fig. 2.18: Schematics of the jet design

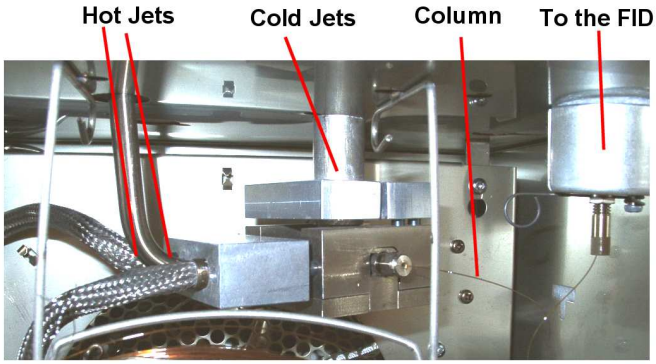

Fig. 2.19: Close-up view of the modulator

Modulation periods as well as column configuration and temperature programs are described in the individual sections of the experiments.

2.6.2 Thermodesorption System

Since concentrations of VOCs in the atmosphere are in low ppbV (10^{-9}) and pptV (10^{-12}) levels, a pre-concentration step is required in order to permit detection. This pre-concentration can be done either by cryogenic focussing with liquid nitrogen or CO_2, absorption in a liquid or by adsorbing the analytes on a suitable material.
Even though cryofocussing and absorption have the advantage of producing less artefacts, the adsorption and thermal desorption method was favoured as the sorbent is contained inside a small tube and can be easily transported and operated even at remote sites or in aircrafts. Additionally, the chosen adsorbent beds Tenax TA and Carbograph 1TD are suitable for the target compounds in the C_6 to C_{14} range. This region is of interest, as the chemical complexity is high and many isomeric compounds can be found.

2.6.3 Thermodesorber *Unity*

On-line mode

If the measurements are done on-line, the sampled air is drawn with a small membrane pump at a rate of 50 ml min^{-1} through the sample entrance and concentrated directly on the cold trap.

The main and most important feature of the thermodesorber '*Unity*' is the cold trap which concentrates and focusses the analytes in a low volume according to the preset conditions. The cold trap is a quartz tube filled with a 2 mm diameter × 60 mm long bed of sorbent, here Tenax TA and Carbograph I, supported by quartz wool. The sorbent bed can be cooled down with a 2-stage Peltier cell to -10°C in ambient temperatures of up to 30°C. In the on-line sampling mode the trap was set to higher temperatures (10°C at MINATROC, 25°C at HOHPEX) to prevent the freezing out of ambient water vapour in the trap and the subsequent interference during measurements. Test runs with a Nafion dryer were completed but found not to be suitable due to the loss of some compounds [50].
After concentrating the target analytes on the cold trap, the trap oven heats fast to the set desorption temperature. During the first critical stage of the desorption, the rate can reach heating rates in excess of 60°C sec^{-1}.
The trap is operated in backflush mode, meaning the sample gas enters and leaves the cold trap through the same narrow-bore end. It is possible to use a series of 2 or 3 sorbents with increasing strength in the trap to capture compounds of different ranges of volatility. In so doing, the high boiling compounds are retained by the first weak sorbent and quantitatively desorbed without ever getting into contact with the stronger sorbents for the lower boiling compounds behind.

Desorbing the sample from the cold trap can be done in the non-split or the split mode. With the non-split method, the whole sample is desorbed and injected onto the column. In the split mode, a fraction of the sample can be re-collected with another sample tube and analysed again, or the split air can be vented through a charcoal filter to the laboratory environment. To achieve good peak shapes without tailing and avoid overloading of the analytical column, the sample injection is usually carried out in split mode. A high sample split is helpful to transfer the trapped analytes efficiently from the trap without exceeding the column capacity.
The thermodesorber is connected to the gas chromatograph with the chromatographic column inserted into a PTFE flexible tube embedded in an insulating silicone foam transfer line, heated to a temperature of 140°C over its entire length with a distributed heater and heat conduction from the GC oven. At the beginning of this 1 m long transfer line, the column is connected with a push fit coupling to the heated valve of the thermodesorber, which itself functions as connecting unit between the cold trap and the column. The transfer line enters the GC oven via the unused back injector port.

Off-line mode

If the sampling is done off-line, i.e. onto cartridges which are analysed later, the analytes can be desorbed from the sampling tube using the two-stage thermal desorption method with the autosampler (see section Autosampler Accessory *Ultra*), or it can be inserted and desorbed in the thermodesorber itself. To extract the analytes of interest retained on the sorbent bed of the cartridge tube during the primary desorption step, the tube is heated and purged with an inert gas (helium 30 sccm) and the desorbed analytes are subsequently refocussed on the small volume cold trap described previously.
The tube is inserted directly into the sample tube desorption oven upstream of the cold trap and sealed with Viton O-rings into the sample flow path. Behind each O-ring a porous PTFE filter is placed to prevent contamination of the interior tubing with high boiling sample material or sorbent particles. The tube desorption oven can be used at any temperature desired, although it has to be kept in mind that the desorption temperature of the sample tube should be lower than the maximum recommended temperature of any sorbent used and should not exceed the highest temperature set during the chromatographic run.
The desorption oven heats up rapidly with approximately 100°C min^{-1} at the start of desorption to the required temperature and afterwards cools down from 300°C to 50°C within 10 minutes.

2.6.4 Air Server / Mass Flow Controller Accessory

An integrated mass flow controller accessory, named '*Air Server*', can be used for collecting whole air/gas samples, e.g. air sampled directly or from canisters and is controlled by the thermodesorber software. It contains an electronic mass flow controller, switching valves and link tubing to interface to the thermodesorber *Unity*.

The empty link tube is inserted into the sample oven of *Unity*. The on-line sampling unit has three inlet ports which can be used for standard, blank and on-line sampling or for three different sampling entrances.
During the sampling phase, air is pumped in and distributed from the *Air Server* directly into the cold trap from the thermodesorber. Stripped of the target VOCs, the gas exits the cold trap and re-enters the mass flow controller, where the exact flow is measured and thus the exact volume can be calculated.

2.6.5 Autosampler Accessory *UltrA*

An extension to the system described above is an autosampler (*UltrA*). This allows a sequence of analyses to be performed where the primary tube desorption process takes place starting from there. The capacity of the autosampler is 100 standard tubes, which can be desorbed with different temperature programs and sampling order as necessary.
The analytes are desorbed from the individual sample tube and swept in the carrier gas stream through heated and inert connection tubing directly onto the cold trap of *Unity*. The connection is created via an empty link tube, which is similar to the one used in the *Air Server/ Unity* configuration, except that the whole flow path from the cartridge to the cold trap is heated to guarantee no sample loss.

2.6.6 Sample cartridges

The thermodesorber applied in these studies can also be used with industry standard steel or glass sample tubes (89 mm × 6.4 mm O.D, 5 mm I.D).
For the identification process described in chapter 3, Markes Silcosteel SafeLok cartridges (Markes International, Pontyclun, UK) with two different sorbents were used. The sorbents are retained in the cartridge with stainless steel gauzes and diffusion locking inserts, which impede diffusion in and out of the tube during storage. The diffusion locking technology (see Fig. 2.20) consists of an insert with a thread cut on the outside to lengthen the migration path of gas to the sorbents. This significantly reduces risk of contamination due to poorly fitted or loose brass caps. Additionally there is no ingress of volatiles from lab air during capping and uncapping and furthermore it is possible to carry out long-term pumped sampling at flow rates lower than 1 ml min^{-1}.

The tubes were closed using brass caps with PTFE ferrules to further diminish the risk of migration from contaminants outside the cartridge during storage or after cleaning.
DiffLok caps (Markes International, Pontyclun, UK) with Viton O-rings have to be used during analysis with the autosampler system. These caps are designed to provide an effective tube seal until pressure is applied and the gas starts flowing, thus also limiting diffusion from or onto the sorbents to a minimum.

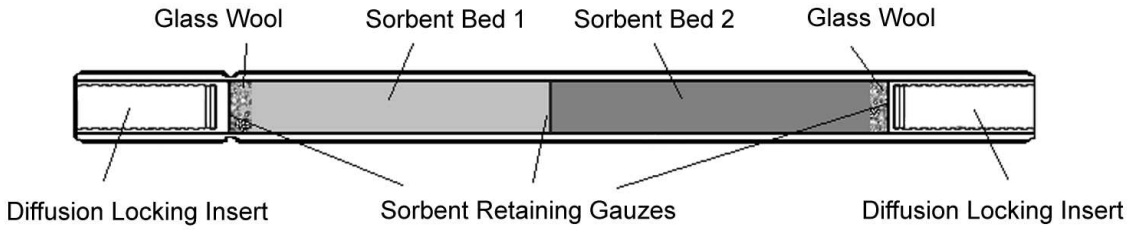

Fig. 2.20: Sample cartridge

The application and the results obtained with the described thermodesorption / GC×GC-FID system are shown in the following chapters 3 to 5.

CHAPTER 3

GC×GC/TOF-MS

Results of the identification process

Mapping the two-dimensional space with diverse samples

3.1 Introduction

From the GC×GC plots shown in Fig. 2.13 and 2.14 on page 30 it is clear that this powerful separation technique can reveal a multitude of peaks. The identification of unknown compounds from such a plot using solely an FID is very difficult, for although the first and second dimension provide information about boiling point and polarity, unequivocal compound identification can be only achieved by injection of each individual substance. This slow and labour-intensive process can be shortened with the aid of mass spectrometric detection, since the obtained mass spectra of unknown analytes can be compared to spectra already stored in a mass spectral database. However, once the peaks have been characterised, the same column set can be attached to the FID, which is easier to calibrate.
Quadrupole mass spectrometers can be applied for this identification, although their usefulness for GC×GC is limited by the detector frequency of ca. 10 Hz. This is an important aspect, since the peak widths generated by GC×GC chromatography are usually between only 100-600 ms at the base, and a scanning speed of approximately 0.5 s produces unsatisfactory results [117]. A time-of-flight mass spectrometer coupled to the GC×GC provides the fast acquisition rate needed, with scan speeds up to 500 full spectra per second it is ideally suited to identify peaks in GC×GC. Indeed it has been successfully used for the purpose [75, 109, 138, 143, 148, 149, 150]. In the order to improve on the separation provided by the original column set (DB-5 and Carbowax), a new set of columns (DB-1 and BPX-50) was characterised using a GC×GC-TOF/MS.
Samples from environments considered of interest for future study as well as standard mixtures were analysed to determine retention times of a wide range of compounds. Cartridge samples taken in Prague adjacent to a busy street were used to characterise urban anthropogenically influenced air, while samples taken from a eucalyptus plantation, pine and mixed forest, respectively, represented terrestrial biogenic emissions. Several plankton cultures with different ages were used to characterise emissions from the marine environment. The different samples types are listed in Table 3.3.

3.2 Experimental setup

The multi-dimensional gas chromatographic system used here for the identification of VOCs with a new column configuration consisted of the flow-controller *Air Server*, the multi-tube autosampler *UltrA* and the thermal desorption unit *Unity* (all three Markes International, Pontyclun, UK) described in section 2.6.2. They were connected to a gas-chromatograph (GC6890N, Agilent, Wilmington, DE, USA) equipped with modulator and secondary oven (Leco, St. Joseph, MI, USA). Detection was performed with a PEGASUS III time-of-flight mass spectrometer (Leco). The thermodesorption devices and the starting signal for the GC were controlled by the software provided by the manufacturer of the thermodesorber system (Markes). Both the gas chromatograph and mass spectrometer were

controlled by the software package ChromaTOF (Leco, St. Joseph, MI, USA) which enabled instrument control, data acquisition, processing and peak deconvolution. Modulation was conducted on the secondary column via a quad jet system similar to the one described in the section before, providing two liquid nitrogen cooled cold jets and two hot jets heated by resistively heated compressed air. The first and second columns were connected with a deactivated fused silica Press-Tight Connector sealed with polyimide glue (Restek GmbH, Bad Homburg, Germany). The secondary oven is constructed for easy installation of the short column and is controlled independently from the first oven by the software.

Desorbing Data	
Desorption	Prepurge: 4 min Desorption: 250°C, 5 min (Tenax TA/Carbograph I) Flow Path: 200°C
Analysis data	
First column	DB-1, 30 m, 0.32 mm I.D., 2μm film 35°C, hold 0.2 min, 4°/min to 250°C, hold 10 min
Second column	BPX-50, 1 m, 0.1 mm I.D., 0.1μm film 40°C, hold 0.20 min, 4°/min to 255°C, hold 10 min
Analysis time	60 min
Modulation	3 sec, four-jet system (Zoex, USA), nitrogen-cooled

Tab. 3.1: Sampling, desorption and analysis data for the GC×GC TOF-MS identification

Sample	**Location**		**Volume**
Phaeocystis gl. old	Lab/NL	Headspace growth flasks	1.0 L
Phaeocystis gl. young	Lab/NL	Headspace growth flasks	1.0 L
Pseudonitzschia sp.	Lab/NL	Perspex cuvette	1.0 L
Ectocarpus sp.	Lab/NL	Headspace growth flasks	0.4 L
Emiliania hux.	Lab/NL	Perspex cuvette	0.4 L
Room Air	Lab/NL	Laboratory	1.0 L
Prague Air	Czech Rep.	Ambient air	2.7 L
E. camaldulensis	Australia	Cuvette outlet	9.4 L
Mixed forest	Tenerife	Ambient air Eucalyptus, leaftrees	3.0 L
Pine forest	Tenerife	Ambient air Pine trees, shrub	3.0 L
Calibration gas		Apel-Riemer, CT, USA	0.5 L

Tab. 3.2: Sampling details of the cartridges analyses

The first dimension column used was a nonpolar 100% dimethylpolysiloxane DB-1 (30 m, 0.32 mm I.D., 2μm film, Agilent, Waldbronn, Germany), the second dimension column a polar 50% phenylpolysiloxan BPX-50 (1.5 m, 0.1 mm I.D., 0.1μm film, SGE Deutschland GmbH, Darmstadt, Germany). About 1 meter of the DB-1 column was

embedded in the heated transfer line from the thermodesorber to the gas chromatograph. Circa 20 centimeters of the second column connected the gas chromatograph with the mass spectrometer. The recorded masses ranged between 35 and 500 amu, the acquisition rate was 200 spectra per second, the detector voltage was set to 1800 Volts. The analysis time was 60 minutes.

Samples were taken using standard Silcosteel tubes (Markes International, Pontyclun, UK) packed with the sorbents Tenax TA and Carbograph 1TD. The tubes were closed by brass screw caps including PTFE ferrules during storage and with DiffLok caps during analysis.
In order to map the two dimensional separation space as extensively as possible, air samples were sampled from a wide range of environments. Marine biogenic emissions were represented by plankton culture samples, terrestrial biogenic emissions were inter alia taken from eucalyptus forests and Prague air was used as representative for urban anthropogenic air. Storing times for the pine and mixed forest sample taken on Tenerife were roughly 8 months, for the eucalyptus sample of Australia 3 to 4 weeks, for the plankton samples about 2 weeks in plastic bags, which were in an isolated box in the fridge. The samples of Prague air were analysed immediately after the sampling. Details about the sampling and analyses are given in Table 3.2 and Table 3.1, respectively. The measurements were recorded using the ChromaTOF software (Leco). This software uses a deconvolution algorithm to separate partially co-eluting peaks and then compares the mass spectra obtained to the NIST mass spectra library (National Institute of Standards and Technology, Gaithersburg, MD, USA). The reports given here include the name of the tentatively identified compound, formula, the similarity, retention times in both dimensions, signal to noise ratio (S/N), and probability. Several thousands of peaks were detected in each measurement and quality assurance for identification was achieved by selecting only peaks with a mass-spectral match higher than 900 (90%) and a S/N ratio higher than 1000. Each spectrum was checked, compared to the suggested spectrum of the library and then either discarded or approved.

Retention indices (RI) for the first dimension were calculated using the formula

$$RI_x = 100 \times \left(\frac{RT_x - RT_n}{RT_{n+1} - RT_n} + n \right)$$

with RI_x as retention index of the compound x, n as carbon number of the last n-alkane eluting before component x, RT_x, RT_n and RT_{n+1} are the retention times of component x, the preceding n-alkane with the carbon number n, and the next n-alkane with the carbon number n+1, respectively. Since octane could not be separated from the cyclotrisiloxane artefact produced by the column, the retention time of the artefact was used to calculate the RIs for compounds eluting before or after octane. A procedure to obtain second dimension retention indices employing polar fatty acid methyl esters (FAME) or alcohols has been reported recently [151, 152], but was not performed in this work.

3.3 Results and discussion

During the identification process, a multitude of peaks was discovered. Fig. 3.1 on page 47 shows a selection of the species identified in this study. Included are: the alkanes; 2-alkanones; biogenic compounds; a selection of compounds containing a heteroatom; and aromatic compounds. Close examination of the plot reveals, that compounds of the same chemical class or family are aligned in the chromatogram. This can aid the identification of peaks. Some (artefact) peaks are also present in every chromatogram again aiding orientation and identification, although in some cases these overlap with targeted species. In this configuration for example, octane overlaps with hexamethyl-trisiloxane, a degradation product of the primary column. The density of peaks revealed by the GC×GC separation emphasises the high probability of interferences during analysis with a one-dimensional GC. Either more selective detectors or more sophisticated separation methods such as GC×GC are clearly needed for the analysis of ambient air.

Urban anthropogenic emission samples	
Ambient Air	Prague/Czech Republic
Terrestrial biogenic emission samples	
Eucalyptus camaldulensis	Australia
Mixed forest (Eucalyptus, leaftrees)	Tenerife
Pine forest (Pine trees, shrub)	Tenerife
Marine biogenic emission samples[1]	
Phaeocystis globosa young[2]	Lab
Phaeocystis globosa old[3]	Lab
Pseudonitzschia sp.	Lab
Emiliania huxleyi	Lab
Ectocarpus sp.	Lab
Room Air	Lab
Standard	
Calibration gas	Apel-Riemer, CT, USA

[1] University of Groningen Culture Collection; courtesy J. Stefels
[2] cells growing
[3] cells mostly dead and decomposed

Tab. 3.3: Various samples used for the identification of VOCs

Table 3.4 lists a selection of the VOCs identified in the samples. The complete table with identified compounds is alphabetically listed in Appendix A.2. In addition to retention indices in the first dimension, retention times in both dimensions and the sample containing the species are given.
To be included in the table and to be considered 'identified' the mass spectra had to satisfy specific criteria. First of all, the mass-spectral match, i.e. the similarity between the mass spectra of the tentatively identified compound and the mass spectra of the NIST library, had to be higher than 800. Compounds with a lower similarity were discarded. A second criterion was the signal-to-noise ratio, which had to be

higher than 1000. To further eliminate the risk of false identification, the boiling points of all compounds were consulted and compared to their position in the chromatogram.
Several compounds could only be identified in the biogenic samples taken in the forests or directly from certain trees. A distinctive emission of eucalyptus trees is eucalyptol. Accordingly, this compound was identified in the *E. camaldulensis* sample, but also in the mixed forest containing a large number of eucalyptus trees. Interestingly, 2-coumaranone, an aldehyde of benzofuran, was found in all forest samples, whereas the terpene sabinene was only identified in the mixed forest sample. Many terpenoid species were not only found in the ambient forest, but also in the planktonic samples and in the freshly collected Prague air. The presence of α-pinene, verbenone, camphor, norinone, limonene and camphene in the urban sample was attributed to springtime emissions from trees within the city.
An unexpected finding was, that many of the plankton species emitted terpenes, with α-pinene, limonene and verbenone being the most prolific. *Ectocarpus sp.* seems to be the species producing the widest variety of terpenes, including β-pinene, which was also present in the mixed and pine forest samples; and cardene which was also found in *E. camaldulensis*.
6-methyl-5-hepten-2-one (6-MHO) and 6,6-dimethyl-5,9-un-decadien-2-one (geranyl acetone) are reported to be degradation products of an ozone/vegetation reaction [153]. However they were also detected in the plankton samples, which were grown in controlled chamber environments that are supposed to not contain ozone. 6-MHO also appears in the outdoor forest samples, while geranyl acetone was identified both in urban air and the eucalyptus tree sample.
Curiously, plankton have been shown here to emit many unusual heterogeneous VOCs containing nitrogen and oxygen including 2-furanmethanol, 2-butyl-furan, benzofuran, chloromethyl-oxirane and benzylnitrile, as well as unmethylated and methylated alkanenitriles. Emissions of the related compound acetonitrile might explain the highly variable acetonitrile fluxes measured in the Tropical Atlantic [154]. To date it has been supposed that oceans are predominantly a sink for acetonitrile [155]. Sulfur-containing species like DMS (Dimethyl sulfide) and DMSO (Dimethyl sulfoxide) were expected based on previous measurements [156] and also identified. Carbon disulfide, THF (tetrahydrofuran), other furans and pyrazine were not only determined in different plankton samples, but also in anthropogenically influenced urban air.
Dimethyl trisulfide was identified both in the plankton *E. huxleyi* and the Prague air sample, with a higher concentration in the former. This compound is associated with microbial growth [157] or aroma studies of foods [158, 159, 160, 161] and has not been reported before in environmental samples. The sulfuric compounds dimethyl sulfone and dimethyl sulfoxide, identified only in the plankton, was found in a recent study in Cheddar cheese [161].
Apart from the biogenically emitted terpenes and the aforementioned VOCs, the urban Prague air sample shows typical aromatic and aliphatic anthropogenically emitted compounds. Characteristic are benzene, toluene, ethylbenzene, dimethyl- and trimethylbenzenes, as well as alkanes from pentane to tetradecane [4]. These same compounds were also present in the biological samples albeit at very low concentra-

tions. For many VOCs it is therefore not possible to assign them uniquely to one emission type. The aromatic toluene for example, usually allocated to anthropogenic emissions, was unexpectedly found in some of the phytoplankton samples. Toluene originating from plants has been previously observed in a study on emissions from stressed sunflower and Scots pine [162]. Measurements of blank samples showed no indication of any of these species as a contaminant in the analytical system and emissions can be attributed to the stated sources. A further example is the family of heterogeneous compounds like benzonitrile, benzothiazole and furfural, which have not only been found in the plankton samples, but also in the urban and forest air.
An interesting group are the alkylated dihydro-2(3H)-furan-ones, which have been identified in the analysed urban air, plankton, and to some extent in the *E. camaldulensis* and pine forest samples. This homologous series of compounds has also been identified previously in the Algiers/Algeria city area [163].
Chlorinated compounds such as chloroform, methylene chloride, 1,2-dichloro-ethane and CFC-113 (1,1,2-trichloro-1,2,2-trifluoro-ethane) were found on occasions from plankton and urban air. Carbon tetrachloride and chlorobenzene were detected additionally in the mixed forest, and the eucalyptus sample, respectively.

The main objective of this study was to obtain retention times for a range of species interesting for future measurements of ambient air applying the GC×GC-FID. The range of compounds revealed during the identification process showed the potential of applying this analytical technique in various environments. The variety of emitted VOCs is largest in the plankton samples, although many of the species have also been detected in urban air. Many compounds thus far not associated with plankton emissions have been discovered in this study. Further work is however needed to quantify the compound fluxes to determine their impact on the marine environment. Although now identified, further work will be required to ascertain these biogenic emissions quantitatively.

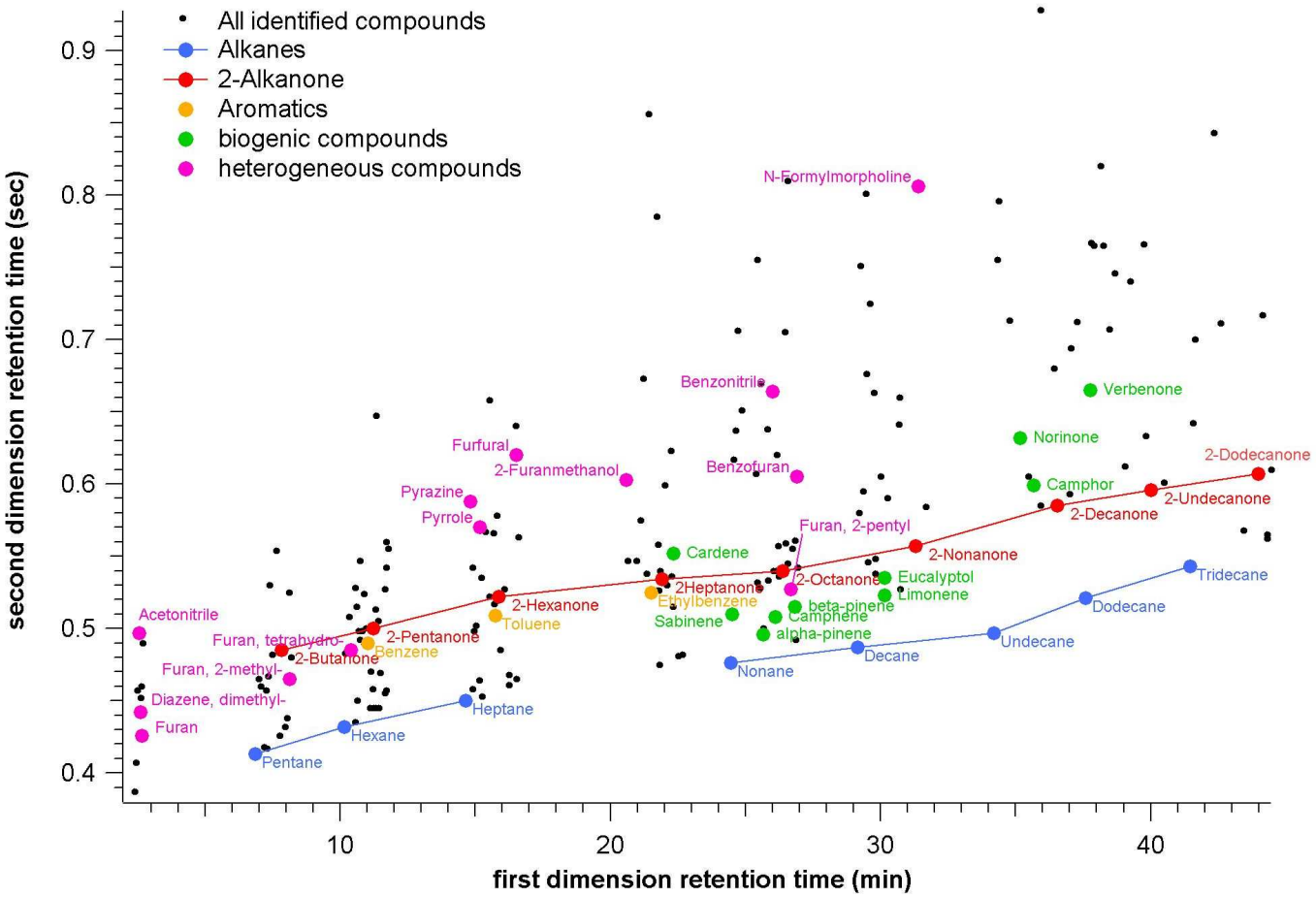

Fig. 3.1: Retention map of the identified compounds

Identified compound	RI	Ambient air	*Phaeocystis gl. old*	*Phaeocystis gl. young*	*Ectocarpus sp.*	*E. huxleyi*	*Pseudonitzschia sp.*	Laboratory air	*E. camaldulensis*	Mixed forest	Pine forest
Alkanes											
Pentane	500.0	•	•	•	•	•	•	•			
Hexane	600.0	•	•		•	•	•	•		•	
Heptane	700.0	•	•	•	•	•	•	•	•	•	
Nonane	900.0	•	•		•	•	•	•	•	•	•
Decane	1000.0	•	•		•	•	•	•	•	•	•
Undecane	1100.0	•					•			•	•
Dodecane	1200.0	•	•		•	•	•	•	•	•	•
Tridecane	1300.0	•	•				•	•	•		•
Tetradecane	1400.0	•				•					•
Aromatics											
Benzene	652.2	•	•	•	•	•	•	•	•	•	•
Toluene	752.3	•	•	•	•	•		•	•	•	•
Ethylbenzene	847.9	•		•	•	•	•	•	•	•	•
Benzene, 1,4-dimethyl-	856.3	•			•	•	•				
Benzene, 1,3-dimethyl-	859.2	•	•					•	•		•
Benzene, propyl-	950.7	•							•		
Benzene, 1-ethyl-3-methyl-	957.5	•	•						•		•
Benzene, 1-ethyl-4-methyl-	961.3		•								
Benzene, 1,3,5-trimethyl-	965.0	•	•	•				•	•		
Benzene, 1-ethyl-2-methyl-	977.3	•	•		•	•			•		•
Benzene, 1,2,4-trimethyl-	991.6	•			•		•	•	•		
Benzene, 1-methyl-2-(1-methylethyl)-	1022.4	•			•				•		•
Benzene, 1,2,3-trimethyl-	1022.0	•	•			•	•		•		
Benzene, 1-methyl-3-(1-methylethyl)-	1074.1				•				•		
Benzene, 1,3-bis(1-methylethenyl)-	1270.1					•	•	•			
Benzene, 1,4-bis(1-methylethenyl)-	1303.7					•	•				
Terpenes and biogenic compounds											
Cardene	879.9		•		•			•	•		
Sabinene	978.0									•	
α-Pinene	944.1	•	•	•	•	•	•	•		•	•
Camphene	960.4	•	•		•	•	•			•	•
β-Pinene	987.6				•					•	•
Limonene	1033.8	•	•		•	•	•	•	•	•	•
Eucalyptol	1035.5								•	•	
Norinone	1131.2	•			•		•			•	•

Identified compound	RI	Ambient air	*Phaeocystis gl. old*	*Phaeocystis gl. young*	*Ectocarpus sp.*	*E. huxleyi*	*Pseudonitzschia sp.*	Laboratory air	*E. camaldulensis*	Mixed forest	Pine forest
Camphor	1147.6	•	•			•	•		•	•	•
Verbenone	1205.4	•	•		•	•	•		•	•	•
5,9-Undecadien-2-one, 6,6-dimethyl- (geranyl acetone)	1424.7	•	•	•	•	•	•	•	•		
5-Hepten-2-one, 6-methyl- (6-MHO)	964.3		•		•		•			•	•
Nitrogen containing compounds											
Propanenitrile	538.8		•	•	•	•	•	•			
Propanenitrile, 2-methyl-	592.1		•	•	•	•					
Butanenitrile	634.4				•	•					
Butanenitrile, 2-methyl-	691.3			•	•	•					
Butanenitrile, 3-methyl-	696.2				•	•	•	•			
Pyrazine	708.7	•	•		•		•				
Pentanenitrile, 4-methyl-	792.7				•	•	•		•		
Hexanenitrile	832.1				•	•					
Benzonitrile	957.6	•	•		•	•	•	•	•	•	•
Benzyl nitrile	1102.9		•		•		•	•			
Oxygen containing compounds											
Furan	493.7	•	•	•				•			
Furan, 2-methyl-	593.5	•	•	•	•	•	•	•			
Furan, tetrahydro-	615.4	•	•	•	•	•	•	•			
Furfural	789.7	•	•	•	•		•	•	•	•	
2-Furanmethanol	811.7				•		•				
2(5H)-Furanone	855.0	•	•	•	•			•	•		
2-Butyl furan	879.1				•		•				
2(3H)-Furanone, dihydro-5-methyl-	909.3	•	•		•	•	•		•		
2(5H)-Furanone, 5,5-dimethyl-	914.5	•	•			•					
2(5H)-Furanone, 3-methyl-	935.6				•		•	•			
Furan, 2-pentyl-	982.3	•	•		•	•	•	•	•		•
Benzofuran	990.3				•						
2(3H)-Furanone, dihydro-5-ethyl-	1014.9	•	•	•	•	•	•	•	•		
2(3H)-Furanone, dihydro-5-propyl-	1119.0	•	•		•	•	•				•
2-Coumaranone	1209.9								•	•	•
2(3H)-Furanone, dihydro-5-butyl-	1227.8	•	•		•	•	•				•
2(3H)-Furanone, dihydro-5-pentyl-	1335.2	•				•	•				•
Chlorinated compounds											
Methylene Chloride	514.5	•		•		•					

Identified compound	RI	Ambient air	*Phaeocystis gl. old*	*Phaeocystis gl. young*	*Ectocarpus sp.*	*E. huxleyi*	*Pseudonitzschia sp.*	Laboratory air	*E. camaldulensis*	Mixed forest	Pine forest
Ethane, 1,1,2-trichloro-1,2,2-trifluoro-	524.3	•			•		•	•			
Chloroform	602.2	•	•	•	•	•	•	•			
Ethane, 1,2-dichloro-	626.5	•					•	•			
Carbon Tetrachloride	657.6	•	•	•			•	•		•	
Oxirane, (chloromethyl)-	691.8		•		•						
Benzene, chloro-	827.3	•				•	•		•		
Benzene, 1,3-dichloro-	1001.5		•		•				•		
Benzene, 1,4-dichloro-	1006.5	•							•		
Benzene, 1,2-dichloro-	1029.2								•		
Sulfur containing compounds											
Dimethyl sulfide	509.4		•	•		•					
Carbon disulfide	529.2	•	•	•	•	•	•				
Disulfide, dimethyl	727.3	•	•		•	•	•	•	•		
Dimethyl trisulfide	962.8	•				•					
Dimethyl Sulfoxide	781.3		•		•						
Dimethyl Sulfone	781.3		•	•	•	•	•				
Benzothiazole	1220.7	•	•		•	•	•	•	•		•

Tab. 3.4: Selection of identified compounds with DB-1 × BPX-50 column configuration

CHAPTER 4

HOHPEX 2004

***H**ohenpeissenberg*

***OH** intercomparison and*

***P**hotochemistry*

***EX**periment*

GC×GC measurements in the
rural continental atmosphere

4.1 Introduction and site description

The focus of the intensive field study HOHPEX 2004 (Hohenpeissenberg OH intercomparison and Photochemistry EXperiment), was to investigate photochemistry in the rural continental atmosphere. For this the quantification of atmospheric volatile organic compounds (VOCs) was important, in particular the characterisation of local emissions and of air masses reaching the Hohenpeissenberg area. An additional goal was to compare VOC measurements from the GC×GC system with those of PTR-MS and routinely conducted GC-MS measurements.
The campaign was conducted in July 2004 at the Meteorological Observatory Hohenpeissenberg (MOHP) in southern Germany. This station is part of the Global Atmospheric Watch network and also functions as meteorological monitoring site for the German Weather Service (Deutscher Wetterdienst, DWD). The station is used for long-term studies [35, 36, 164, 165] and, occasionally for short-term field campaigns [166, 167, 168]. The location of the observatory in Germany is shown in Fig. 4.1, and the large scale map in Fig. 4.2 shows the area around Hohenpeissenberg.

Fig. 4.1: Map of Germany with the location of the Meteorological Observatory Hohenpeissenberg

The measurement site is located on a mountain at an elevation of 980 m asl in a rural agricultural and forested area, approximately 40 km north of the Ammergauer Alps (47°48'N, 11°07'E). The height difference from the circumjacent countryside to the station is approximately 300-400 m. As can be seen in Fig. 4.3, the observatory is surrounded by forest, mostly coniferous trees and beeches, while grassland dominates the submontane region. In close proximity, there are two villages situated to the north and the south. The nearest major city is Munich, at a distance of about 70 km to the northeast. Smaller local cities are Kaufbeuren (northwest, ca. 50 km), and Landsberg/Lech (north, ca. 40 km). The small cities Peissenberg, Schongau and Peiting with about 11.000 inhabitants each are located to the east and west, respectively. The topography of the area is depicted in Fig. 4.4.

The data presented here is a selection of terpenoid, aromatic and aliphatic compounds. The terpenoids are all biogenic while the aromatic and aliphatic compounds are predominately of anthropogenic origin. Biogenically emitted compounds are represented by the terpenes, α- and β-pinene, sabinene, 3-carene, camphene and the oxygenated eucalyptol (1,8-cineol). Representative aromatic compounds are ethylbenzene, o-xylene and the co-eluting p/m-xylene. Benzene and toluene are not included, as the GC×GC chromatogram had a very high background signal or variable interferences in these sections, and therefore could not be reliably integrated. Alkanes

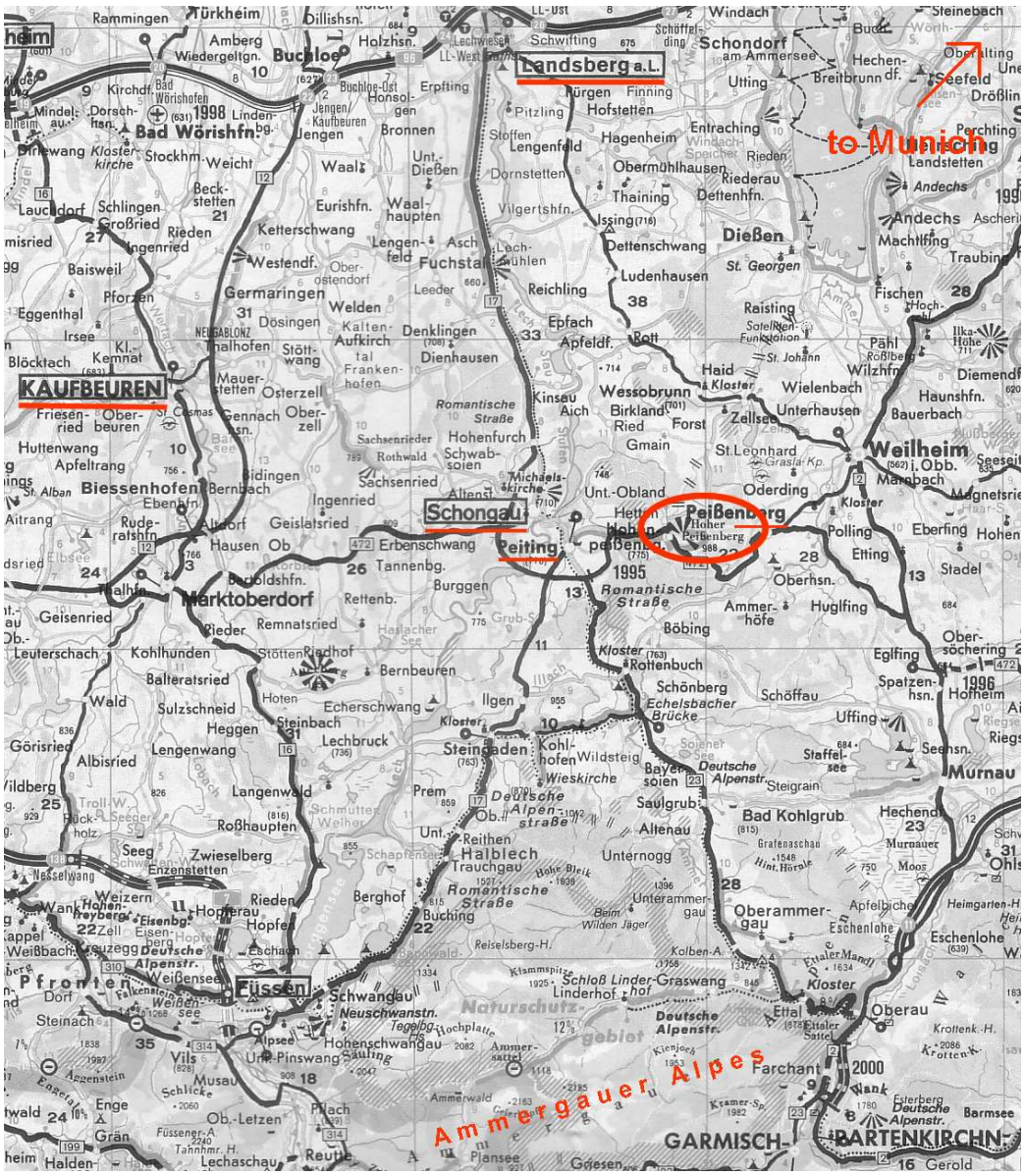

Fig. 4.2: Location of urban centres near Hohenpeissenberg (red circle)

Fig. 4.3: Aerial view of the Meteorological Observatory Hohenpeissenberg

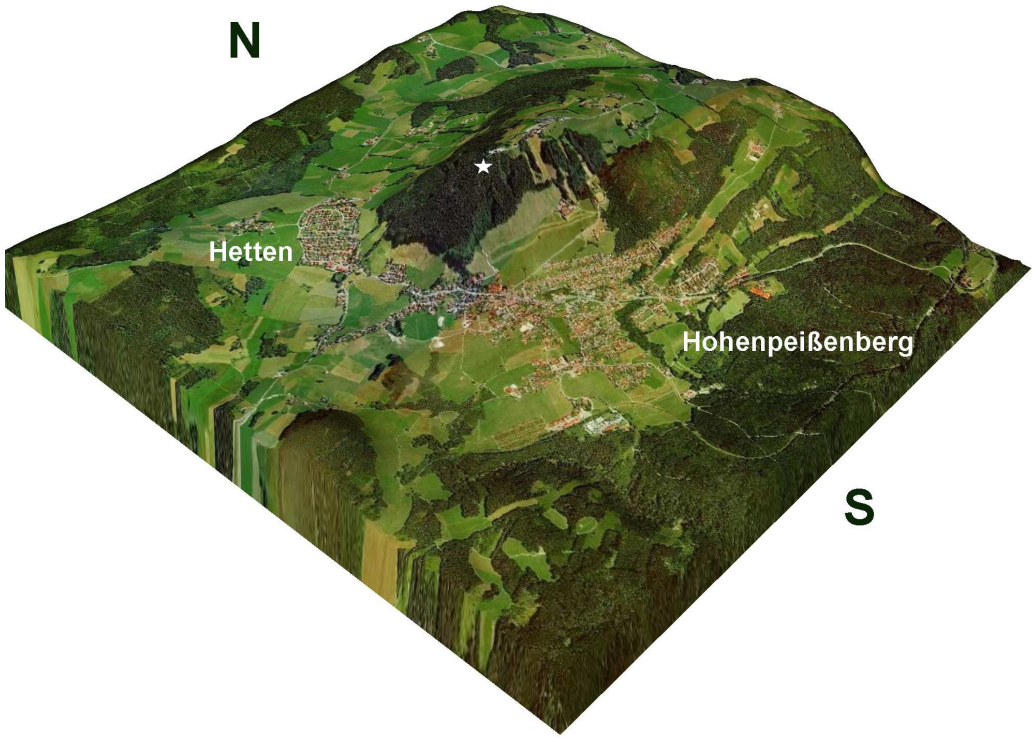

Fig. 4.4: Topography of the area surrounding the Hohenpeissenberg observatory. The station is marked with a white star

are represented by hexane, heptane, octane and nonane. Details about the GC×GC instrumentation used here are given in section 4.4.
The following sections present the meteorological conditions and general air chemistry characteristics as well as the measurement results obtained with the GC×GC-FID in the period between July 7 and July 18, 2004. The VOCs measured in ambient air by GC×GC-FID are compared with measurements of a GC-MS (MOHP) and PTR-MS (MPI for Chemistry, MPI-C). Additionally, the calibration results of a compressed ambient air mixture with the gas chromatographic techniques GC-MS (MOHP), GC-MS (MPI-C) and GC×GC-FID are presented. Diurnal cycles for the aforementioned VOCs are shown and discussed. The influence of the wind direction on detected mixing ratios is examined in combination with the changes between day and night, and the effect of the surface boundary layer. The analysis of the data is extended to a variability lifetime study. This was the first time such a study has been performed on short lived ($\tau < 1$ day) species.

4.2 Site meteorology

The weather in the Hohenpeissenberg region is mainly affected by continental meteorological conditions, with cold and warm frontal systems originating over the Atlantic passing over the site. The area is also occasionally influenced by foehn, a warm dry

wind coming off the northern, leeward slopes of the Alps.
Fig. 4.5 shows the meteorological conditions throughout the course of the campaign.

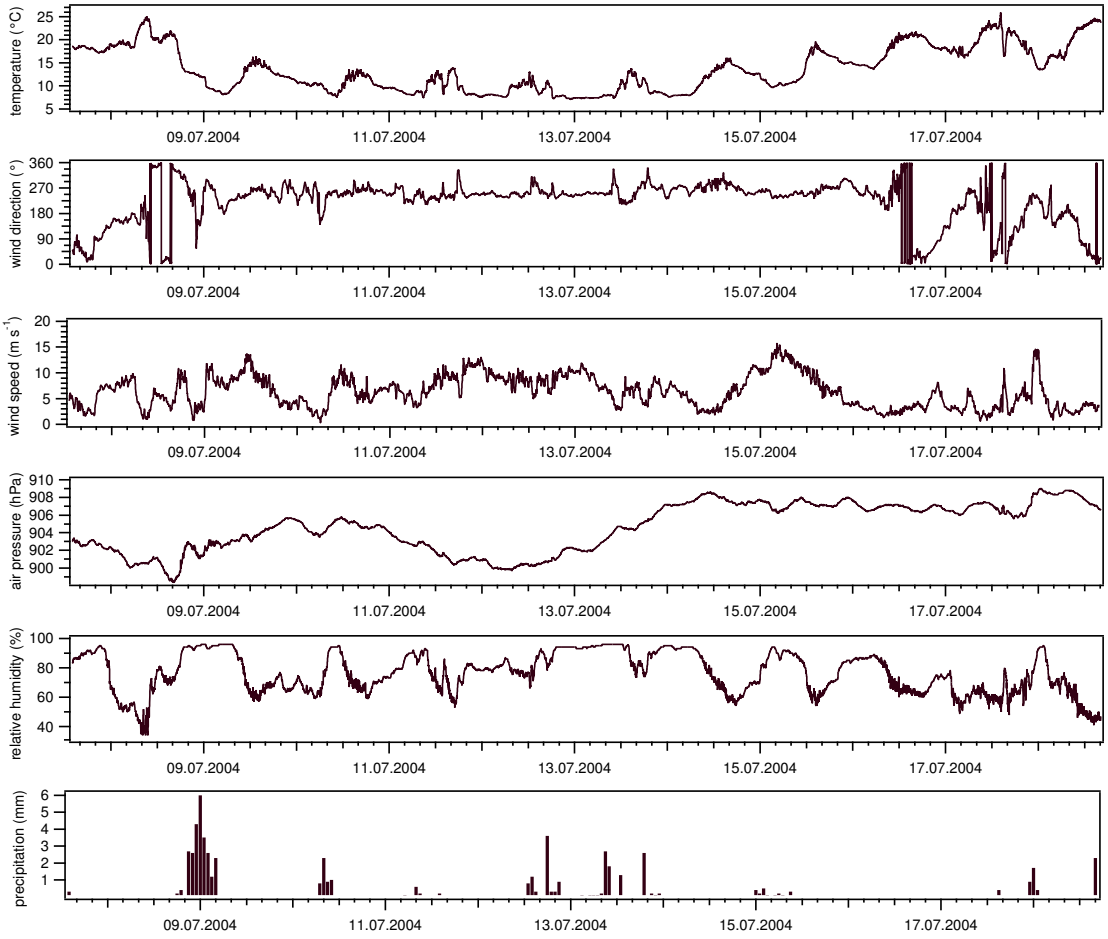

Fig. 4.5: Meteorological data temperature, wind direction, wind speed, air pressure, relative humidity and precipitation between July 7 and 18, 2004

In general the weather during the campaign changed from sunny and warm, to cold and rainy, then back again. The highest temperatures measured were around 25°C, occurring at the beginning and towards the end of the measurements. The lowest temperature of 7°C was reached at night, during the middle section of the campaign. The cooler days between the 11th and 14th of July, showed temperatures mostly below 15°C, and the weather was generally foggy with short rain showers and an overcast sky. The rain showers were associated with a series of warm and cold fronts that passed over the site during the campaign. During the middle part of the campaign, the station was often situated in the clouds or surrounded by fog, which can also be seen in the relative humidity. From the 15th to the 18th of July it was sunny, with scattered clouds and short rain showers. The temperatures were warm, ranging between 14°C at night and more than 20°C during daytime. The strong changes in wind direction at the beginning and the end of the campaign are caused by fast

moving warm, cold and occluded fronts.
Diurnal fluctuations of temperature, global radiation, wind direction and wind speed, averaged over 10 minutes, are shown in Fig. 4.6. The black line represents the mean value, with the maximum and minimum values depicted as upper and lower bars. The red dotted line corresponds to the median of the measured values. The main wind direction from sunset to sunrise was SW, and during daytime S to SW. Interestingly, the wind direction after noon and before evening was highly variable, whereas during the night it stayed mostly between SE to W. Wind speeds ranged from almost windstill to 16 m s^{-1}, with a median of 5.2 m s^{-1}. The highest wind speeds were reached in the early morning hours and around midnight, the lowest speeds were measured between 6:00 and 11:00 and again around 21:00. The sun rose between 5:00 and 5:30 and set again towards 20:00.

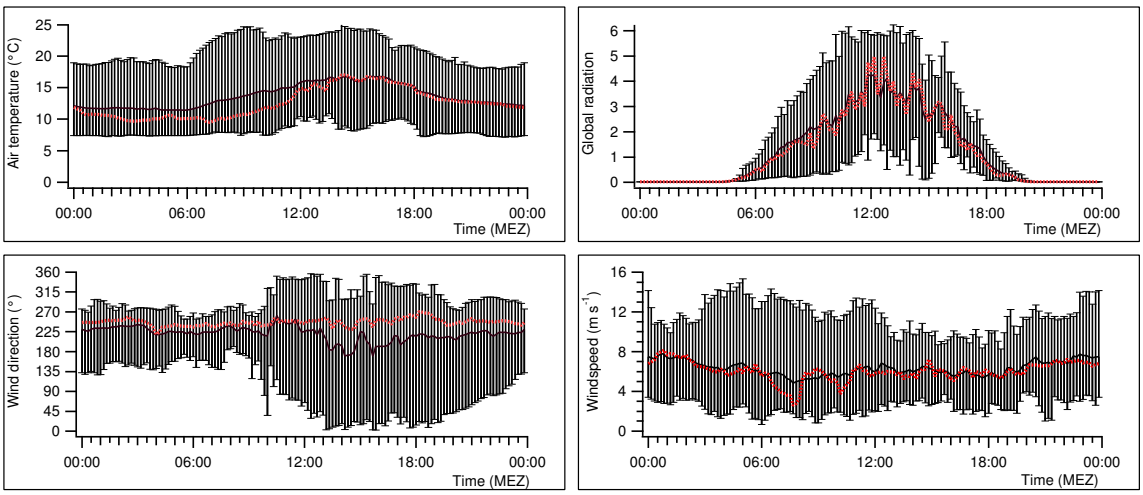

Fig. 4.6: 10-minute averages of diurnal cycles for meteorological parameters in July 2004. Mean measured values: black line, minimum and maximum measured values: error bars, median of measured values: red dotted line

A characteristic and interesting feature of the Hohenpeissenberg mountain is, that during the night the continental boundary layer (BL) is at a few hundred meters altitude and the upper part of the mountain is situated in the free troposphere. This nocturnal surface BL cuts off the station from the continuing anthropogenic or biogenic emissions close to the ground. After sunrise, the surface temperature increases, the BL rises and reaches the station around 9:00, bringing the compounds emitted into the shallow BL during the night and early morning. The further ascent of the BL tends to dilute the surface emissions present into a larger volume, so mixing ratios appear to decrease. Between noon and 16:00, Hohenpeissenberg is situated in the well mixed continental BL, and in this time horizontal transport processes play the dominant role for VOCs measured at the station. The turbulent mixing of the lower atmosphere ceases shortly before sunset [2], the BL subsides again and around midnight the station is situated in the free troposphere. The diurnal cycle in BL height is clearly visible in the diurnal cycles for the VOCs presented in the following sections.

4.3 Supplementary trace gas measurements

The measurements for the trace gases O_3, OH and NO_2 over the period of the field campaign are shown in Fig. 4.7.

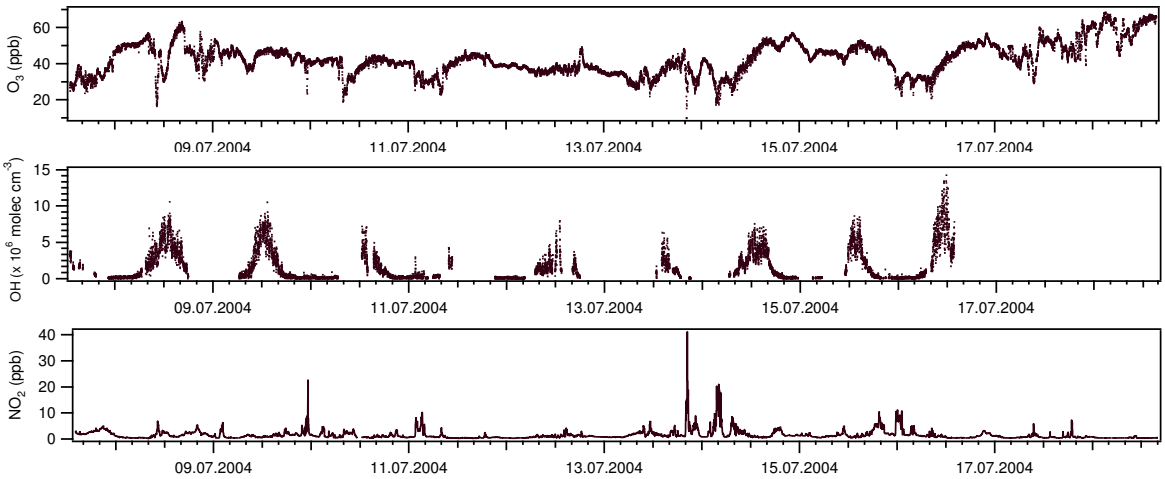

Fig. 4.7: Measurements of O_3, OH and NO_2 from July 7 to 18, 2004

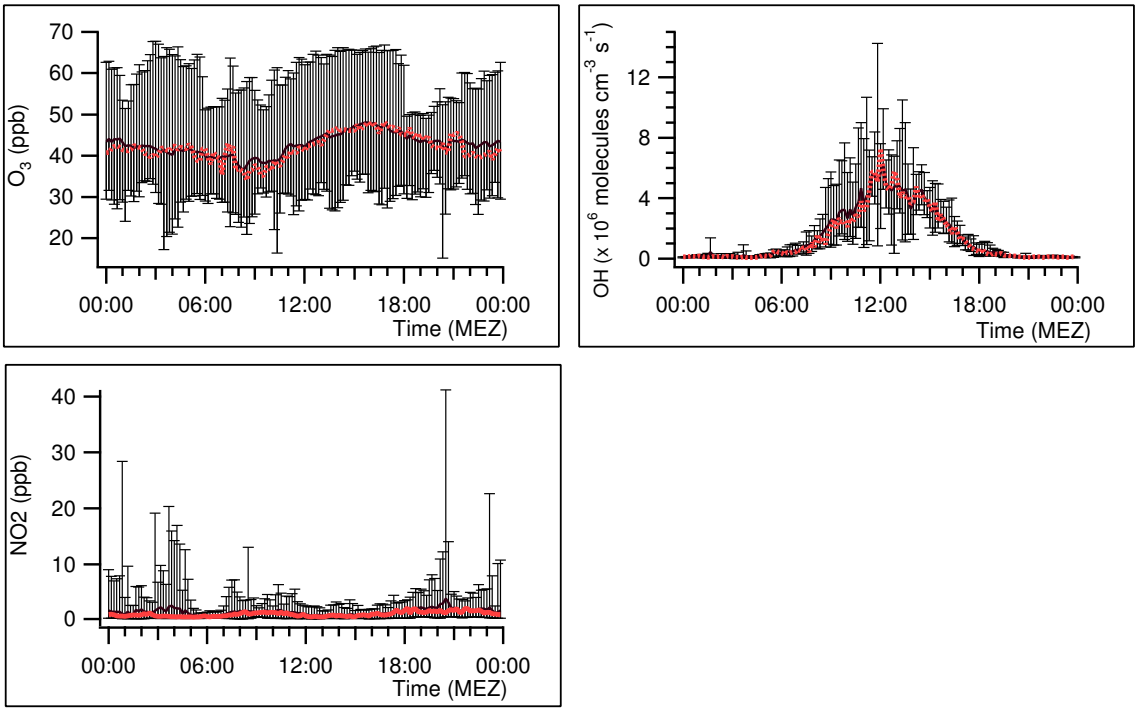

Fig. 4.8: Diurnal cycles of O_3, OH and NO_2 during the field campaign. The black line shows mean values, upper and lower bars the maximum and minimum measured value, the red dotted line shows the median value

The shown trace gas measurements were routinely conducted within the GAW framework. Nitrogen oxides were measured by an NO-O_3 chemiluminescence analyser (ECO Physics CLD). The atmospheric OH was measured using the selected ion/chemical ionisation mass spectrometer (SI/CIMS) described in Berresheim et al. [169]. O_3 was determined with a UV absorption instrument (Thermo Env. Instr.).
Mixing ratios of O_3 range from 20 ppb to 65 ppb, with a median of 42.2 ppb throughout the whole campaign. Nocturnal decreases of O_3 correlate with increased levels of NO_2, the reaction leading to this observation is explained in section 1.2. OH was measured only until July 16, mixing ratios go from 0 ppt to 0.60 ppt (15×10^6 molecules cm^{-3}), the median is at 0.03 ppt (0.63×10^6 molecules cm^{-3}). The days with strong sunlight, high temperatures and higher terpene mixing ratios, at the beginning and the end display higher OH levels as expected. The photochemical production of OH is explained in section 1.3. Measurement gaps were caused by rain, since the instrument is not active during precipitation. The mixing ratios for NO_2 vary between 0.03 ppb to 41 ppb, the median is 1 ppb. Increased levels of NO_2 were usually observed during turbulent atmospheric conditions and increased levels of anthropogenic VOCs.
Fig. 4.8 shows the diurnal cycles for O_3, OH and NO_2, averaged over 10 minutes. The hourly mean O_3 concentration varied between 35 to 48 ppb. A slight decrease in the mean O_3 concentration and an increase in the OH mixing ratios can be observed between 8:00 and 11:00, the time period of the BL transition, marked by sharply increasing levels of VOCs. Mean OH mixing ratios reached their peak around noon with about 0.25 ppt (6×10^6 molecules cm^{-3}) and were close to zero at night, the highest concentration measured was 0.46 ppt (11×10^6 molecules cm^{-3}). NO_2 mean mixing ratios varied from 0.7 ppb to 3.8 ppb without an obvious diurnal cycle although curious high values are seen in the early morning (3:00 to 5:00) and evening (20:00 to 21:00).

4.4 Experimental Setup

During the HOHPEX campaign, the GC×GC sampling system was set up in the automatic on-line measurement mode, combining a flow controller, thermodesorber unit and GC×GC-FID.
An approximately 15 m long, 12.7 mm diameter Teflon line was attached to a metal grid on top of the measurement platform at about 1000 m a.s.l., see Fig. A.6 and A.7 on page 143 in the Appendix. The line itself was shielded from sunlight inside an opaque tube, leading from the platform along the outside wall to the laboratory. The volume flow through the main inlet was set to 3.2 L min^{-1}. The residence time being therefore circa 20 seconds. Air was drawn into the cold trap through a 3.2 mm Teflon line at a rate of 50 ml min^{-1} using a membrane pump.
The pertinent sampling and analysis parameters are given in Table 4.1. Blanks were conducted by focussing helium 6.0 (Messer-Griesheim, Germany) on the cold trap with the same parameters as shown for ambient air. The adsorbent trap temperature was set to 25°C, as the weather was generally humid throughout the campaign and

condensation of water vapour inside the trap had to be strictly avoided. After the sample was accumulated, the trap was purged for 10 minutes with helium to remove traces of water vapour, then heated up to 200°C to inject the focussed compounds onto the column. For complete desorption, this temperature was maintained for 5 minutes. The columns used during the HOHPEX field campaign were a DB-5 (Agilent, Waldbronn, Germany) in the first dimension and a BPX-50 (SGE Deutschland, Darmstadt, Germany) in the second dimension.

Sampling data	Flow:	50 ml min^{-1}
	Duration:	60 min
	Volume:	3L
	Cold trap:	25°C trapping, Tenax TA/Carbograph I
Desorbing Data		
Desorption	Prepurge:	10 min
	Desorption:	200°C, 5 min (Tenax TA/Carbograph I)
	Flow Path:	140°C
Analysis data		
First column	DB-5, 30 m, 0.25 mm I.D., 1μm film 40°C, 100°/min to 50°C, 3°/min to 140°C, 2.5°/min to 170°C, 3.5°/min to 200°C	
Second column	BPX-50, 3 m, 0.1 mm I.D., 0.1μm film 30°C, 3°/min to 120°C, 2.5°/min to 150°C, 3.5°/min to 180°C	
Analysis time	50 min	
Modulation	5 sec, four-jet system (Zoex, USA), nitrogen-cooled 200 ms upstream duration 300 ms downstream duration	

Tab. 4.1: Sampling, desorption and analysis data for the HOHPEX campaign

Fig. A.4 on page 142 in the Appendix shows a GC×GC chromatogram section of an ambient sample taken during the HOHPEX-campaign, the VOCs which are presented in chapter 4 are marked.
Calibration was done using a 74 compound VOC standard (Apel-Riemer, CT, USA). Laboratory multipoint calibrations were accomplished earlier and revealed a good linear dependency of peak area to the respective compound mass. Based on this stability, a one-point calibration of 200 ml standard was carried out every second day throughout the rainy period, whereas the sunny period of four days towards the end of the campaign was only disrupted for blanks. Blanks were taken every third day and showed no high levels for the discussed compounds. Very high blank values were obtained for benzene, which is why it is not included into the study.
The co-eluting p- and m-xylene were calibrated with o-xylene, the C_{10}-terpenes β-pinene, sabinene, 3-carene and camphene with α-pinene. This is reasonable since the FID response is proportional to carbon within a homologous series, as described in section 2.1.3. The mixing ratios were calculated using the following equation:

$$C_{VOC} = C_{Std} \times \frac{PeakArea_{Std}}{PeakArea_{VOC}} \times \frac{V_{Std}}{V_{VOC}} \tag{4.1}$$

where the indices $_{VOC}$ and $_{Std}$ represent the compound in the ambient air and the compound in the standard used for the calibration, respectively. C and $PeakArea$ are concentration/mixing ratio and integrated peak area, respectively, V is the sampling volume. Since no response value was available for the oxygenated eucalyptol, the concept of indirect calibration presented in section 2.1.3 had to be applied. The effective carbon number, ECN, of 9 was determined for eucalyptol (10 × (1.0) for carbon + 1×(-1.0) for the etherlike oxygen), and 10 for α-pinene. To calculate the concentrations for eucalyptol, the following equation was used:

$$C_{VOC} = C_{Std} \times \frac{PeakArea_{Std}}{PeakArea_{VOC}} \times \frac{V_{Std}}{V_{VOC}} \times \frac{ECN_{Std}}{ECN_{VOC}} \tag{4.2}$$

The calibration curves for toluene, ethylbenzene, o-xylene, α-pinene, heptane, octane and nonane are depicted in Fig. A.8 in the Appendix on page 144. Shown are the mean values, the error bars represent $\pm 1\ \sigma$. A positive intercept was found for toluene (0.37 μg) and heptane (0.08 μg), a negative for ethylbenzene (0.05 μg), α-pinene (0.02 μg), o-xylene (0.01 μg), and nonane (0.01 μg). With the exception of toluene, these results show no significant offset. The calibration was linear across the range of concentrations measured. For the calibration curves 100 ml, 200 ml, 300 ml and 400 ml of the standard gas were sampled. The degree of correlation in the calibration curves was good for all VOCs and ranged between R^2 0.94 and 0.98.
The accuracy for the compounds measured by GC×GC-FID was determined by calculating the geometrical mean of the uncertainties discussed below. Influencing the accuracy of all organic compounds is the uncertainty in the calibration gas concentrations, which is given by the manufacturer as 2%. Further uncertainty is caused by the peak integration and volume calculations which are estimated to add at most an additional 5% to the accuracy. The overall accuracy for the measurements of VOC contained in the standard was therefore estimated to be 5%, i.e. hexane, heptane, octane, nonane, toluene, ethylbenzene, o-xylene, p/m-xylene and α-pinene. The same accuracy is valid for all terpenes directly calibrated with α-pinene. The accuracy for the oxygenated eucalyptol is evaluated to be around 11%. This is attributable to the possible inaccuracy of the calculated response factor used for indirect calibration via α-pinene, which adds 10% to the overall accuracy. The accuracy ranges from 5 to 11 % for the individual VOC.
Factors influencing the precision of the GC×GC-FID are the uncertainties in flow and temperature control during sampling and analysis. Contributing as well are the uncertainties in baseline removal, peak integration and peak volume calculation of the individual compounds. To determine the precision of the measurements during the HOHPEX field campaign, the 1σ standard deviation of all 200 ml calibration gas measurements was calculated. The precision for the compounds contained in the calibration standard range from 6.1% for toluene to 10.0% for heptane and are

presented in Table 4.2.
Table 4.2 also shows the limit of detection (LOD) for the VOCs analysed during the field campaign as well as the compounds measured in the standard gas used for the comparison of GC×GC-FID, GC-FID and GC-MS. The LOD was defined as two times the standard deviation (2σ) of the integrated baseline noise in the absence of a peak. It ranges from 0.1 ppt for some terpenes to 6.1 ppt for p/m-xylene.

	LOD (2σ) ppt	Precision (1σ) %
Hexane	2.8	10.0
Heptane	1.9	10.0
Octane	0.6	9.7
Nonane	0.4	8.7
Toluene	2.8	6.1
Ethylbenzene	0.3	6.5
o-Xylene	1.0	7.1
p/m-Xylene	0.4	7.1
α-Pinene	0.4	7.0
β-Pinene	0.9	7.0
Sabinene	0.1	7.0
Camphene	0.1	7.0
Limonene	0.5	7.0
Eucalyptol	1.5	7.0
3-Carene	0.1	7.0
Methylcyclopentane*	4.9	10.0
Methylcyclohexane*	2.4	10.0
2-methylhexane*	4.1	10.0
2-/4-methylheptane*	2.1	9.7
3-methylheptane*	2.0	9.7
Propylbenzene*	1.4	9.1
1-ethyl-(3+4)-methyl-benzene*	1.0	9.1
1,3,5-trimethylbenzene*	1.2	9.1
1,2,3-trimethylbenzene*	1.5	9.1
1,3-diethylbenzene*	2.1	6.5
1,4-diethylbenzene*	2.1	6.5

Tab. 4.2: Limit of detection (2σ) and precision (1σ) of the measured compounds. VOCs measured for the calibration gas comparison with GC-FID and GC-MS are marked with a *

4.5 GC×GC-FID VOC measurements: Results and discussion

4.5.1 VOC measurements over time

The results of the VOC measurements made by GC×GC-FID from July 7 to 18, 2004 are presented in Fig. 4.9 and 4.10. The markers indicate the middle of sampling period, all times are in MEZ. The long measurement gaps during the middle of the campaign are caused by lack of liquid N_2, short gaps were caused by calibration or blank measurements. Diurnal cycles are visible for all biogenically emitted VOCs. More pronounced profiles with higher mixing ratios can be seen for all terpenes during the days with temperatures above 15°C, at the beginning and towards the end of the measurements. At temperatures below 15°C, weaker diurnal cycles with lower mixing ratios are visible. The middle phase with cooler temperatures was mostly overcast, whereas the sun was shining on days with high temperatures. VOC mixing ratios varied as a function of the weather conditions at Hohenpeissenberg as reported in an earlier study [164]. Higher temperatures and increased light intensities have been shown to enhance the emission of biogenic VOCs from different plant species [7]. The predominant biogenic VOCs measured were α- and β-pinene. These compounds also display the highest maximum mixing ratios usually measured between 9:00 and 10:00. α-Pinene shows the highest with 180 ppt, followed by β-pinene, sabinene and eucalyptol (between 80 and 120 ppt), and 3-carene and camphene (30 to 35 ppt). The mean concentrations are between circa 15 ppt for camphene and 3-carene, up to 70 ppt for α-pinene.
For the aromatic and aliphatic VOCs, no distinct light driven recurring cycles can be seen. There is however a tendency to higher mixing ratios around 9:00. An emission temperature dependency, like for the biogenic VOCs, was not found, and higher mixing ratios were also seen during the cold periods. The highest maximum mixing ratios were measured for the co-eluting isomers p- and m-xylene with a summed concentration of 120 ppt. o-Xylene and ethylbenzene were found at 50 and 45 ppt, respectively. Mean values vary from around 30 ppt for p-/m-xylene to 15-20 ppt for the other aromatic compounds. Maximum alkane concentrations were found to be around 35 ppt for hexane, 30 ppt for heptane, 20 ppt for nonane and 10 ppt for octane. Mean concentrations range from 4 ppt for octane to a three times higher value for hexane and heptane.

4.5.2 Comparison of measurement methods

Accurate and precise measurements of organic compounds in the atmosphere are essential for a better understanding of tropospheric processes. To assess the comparability of VOCs measured from different research groups at different locations it is necessary to evaluate the individual instrument performances. To do this, various interlaboratory comparisons of a standard air mixture and ambient air measurements

have been performed to date [170, 171, 30, 172, 173, 174, 175]. Within the HOHPEX field campaign, a comparison of different VOC measurement techniques from the Max-Planck-Institute for Chemistry (MPI-C), Mainz, and the Meteorological Observatory Hohenpeissenberg (MOHP) was completed. This section focusses on the comparison of ambient measurements conducted with GC×GC-FID (MPI-C), PTR-MS (MPI-C) and GC-MS (MOHP) during the HOHPEX field campaign. The following section 4.5.3 investigates the correlation of the ambient air measurements between the instruments. The details of the GC×GC-FID experimental set-up and the measurement site are given in section 4.4.

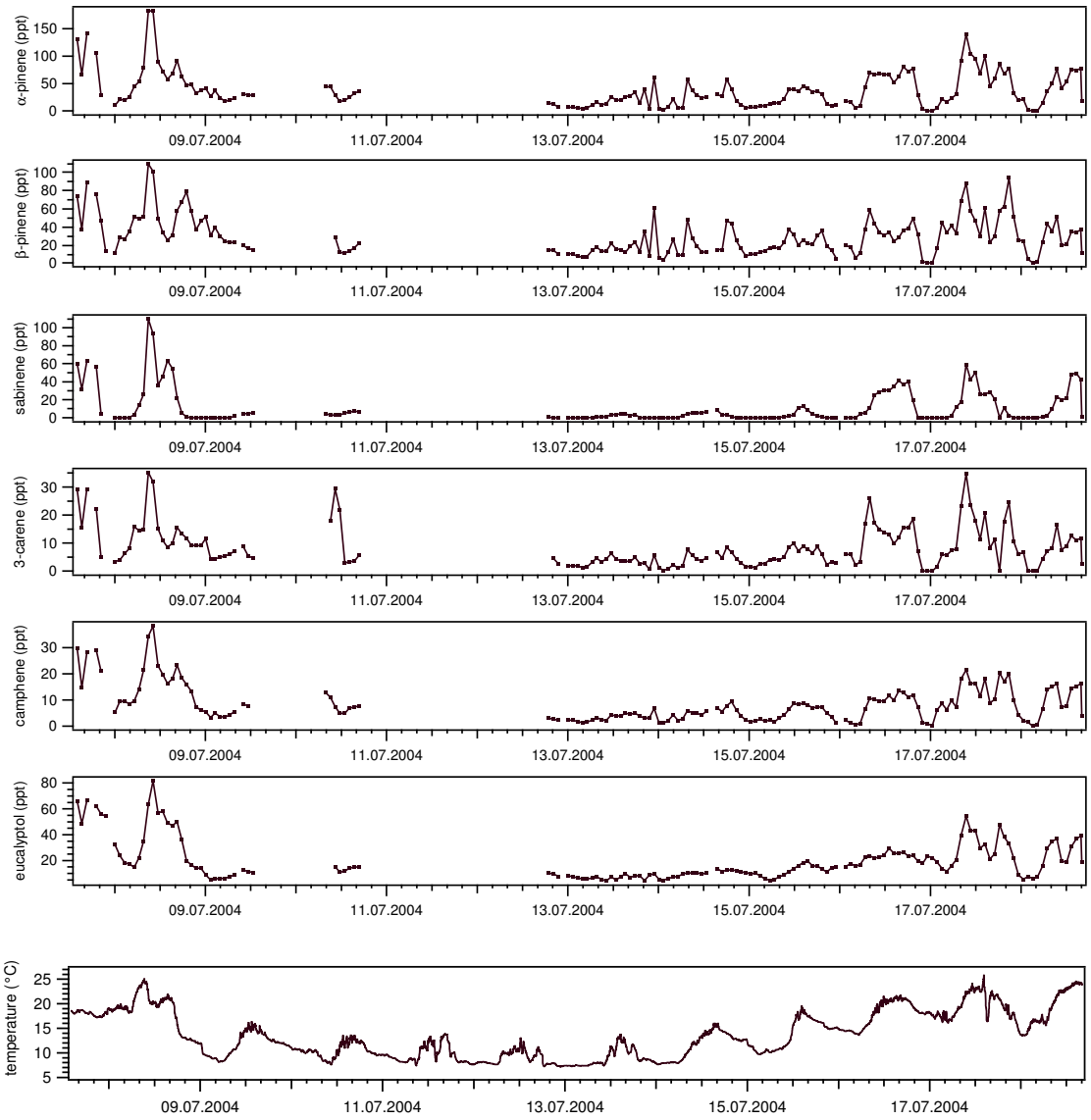

Fig. 4.9: Ambient air temperature and mixing ratios of terpenes measured during the campaign, the markers represent the middle of the sampling. The gaps in the measurements were caused by lack of liq. N_2 or calibration and blank measurements

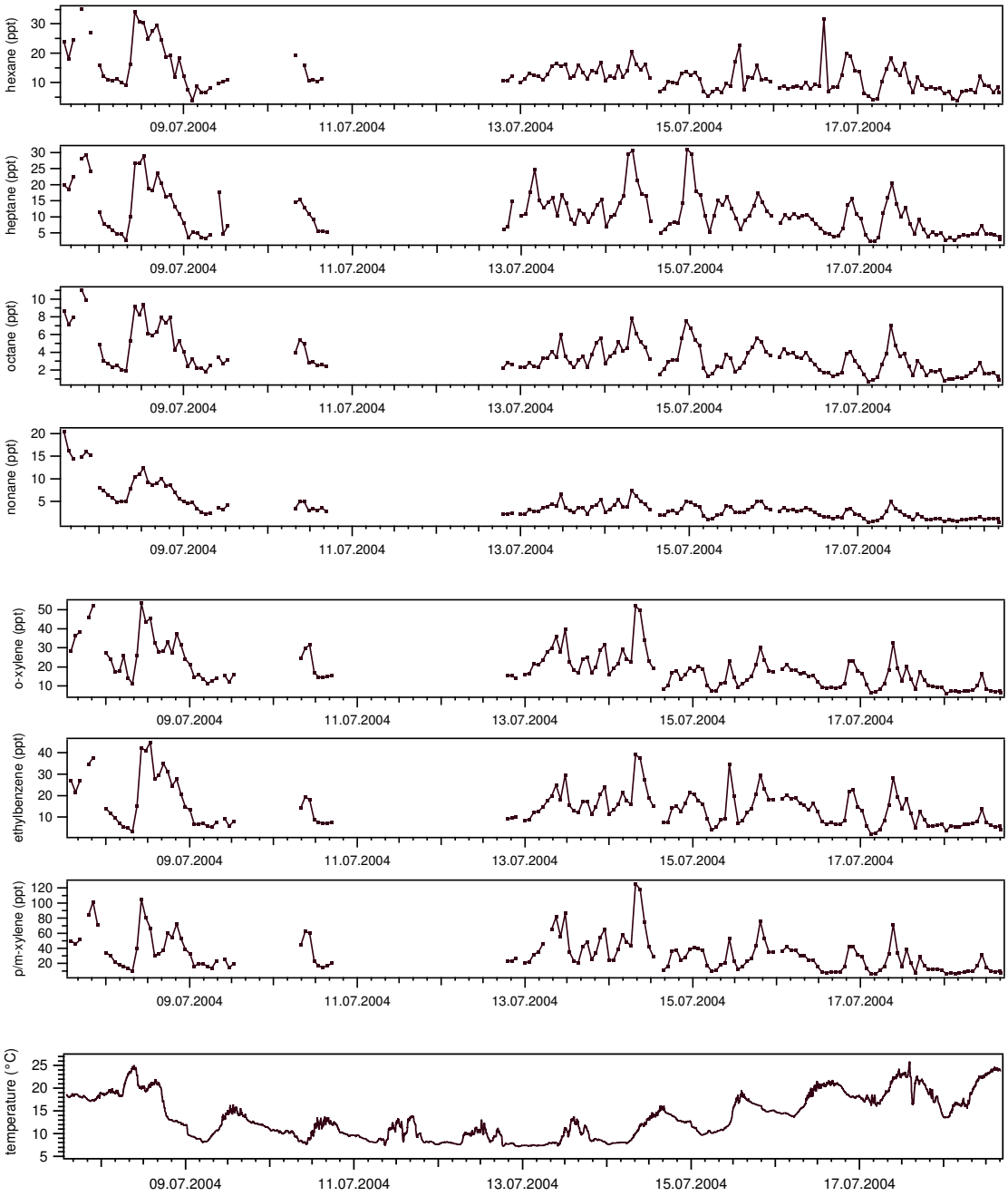

Fig. 4.10: Ambient air temperature and mixing ratios of measured aromatic and aliphatic compounds during the campaign, the markers represent the middle of the sampling. The gaps in the measurements were caused by lack of N_2 or calibration and blank measurements

The sample inlets for the GC-MS and PTR-MS were fixed at a height of 20 m above ground to the same mounting as the GC×GC inlet. The PTR-MS sampling line was an 11 m long 3.2 mm outer diameter Teflon tube. The flow rate of air was set to 270 ml min^{-1} and each mass was scanned for 2 s during a 45 s cycle. More details

about the PTR-MS instrument can be found in [28].
Continuous daily GC-MS measurements were conducted at the observatory within the GAW network. The sampling was done from a permanently installed 10 m × 40 mm I.D. glass tube flushed with ambient air at a rate of 1 m^3 min^{-1}. The sample was accumulated from this glass tube for 20 min at 75 ml min^{-1} and the data points shown here specify the middle of this sampling period. The sampling and analysis details are given in Table 4.3.
The time period relevant for the GC-MS and GC×GC-FID comparison was from July 7 to July 18, 2004. The GC-MS measured during approximately 77% of the 12 days, the GC×GC-FID during 73%. The mixing ratios of the biogenic compounds α-, β-pinene, camphene, 3-carene, and eucalyptol measured by GC-MS and GC×GC-FID are shown in Fig. 4.11. Fig. 4.12 depicts the anthropogenic aliphatic VOCs hexane, heptane, octane, nonane and Fig. 4.13 the aromatics: toluene, the co-eluting p- and m-xylene, o-xylene and ethylbenzene. In the graphs, the red line illustrates the GC×GC-FID measurements and the black line the GC-MS measurements. The markers represent the middle of the sampling time, the upper and lower bars the measurement uncertainty for the depicted VOC. The measurement uncertainty as well as the limit of detection (LOD) for the instruments are shown in Table 4.4.
It can be seen, that the LODs for the anthropogenic VOCs for both gas chromatographic systems are similar. Exceptions are o-xylene, where the GC×GC-FID detection limit is higher and octane, where it is lower than the GC-MS. The GC×GC-FID shows a lower LOD for the biogenic VOCs. The total measurement uncertainties are lower for the GC×GC-FID. The GC measurements will be compared to the PTR-MS data in separate graphs, since the measurement periods are slightly different. Generally, all the VOCs compared show mixing ratios of similar magnitude and degree of variability. Toluene is an exception as it shows not only higher mixing ratios in the GC×GC-FID, but also different diurnal variations.

Sampling data		
Preconcentration	Flow:	75 ml min^{-1}
	Duration:	20 min
	Volume:	1.5L
	Cold trap:	Tenax TA/Carboxen
	Temperature:	30°C
	Desorption:	190°C
Refocussing	Cold trap:	FS Capillara (0.25 mm I.D., 20 cm)
	Temperature:	-196°C (liq. N_2)
	Desorption:	180°C
Analysis data		
Column	BPX-5, 50 m, 0.22 mm I.D., 1μm film (SGE, Germ.)	
	10°C, hold 10 min, 6°/min to 240°C	
Analysis time	48 min	

Tab. 4.3: Sampling, desorption and analysis data for the GC-MS (MOHP)

VOC	Uncertainty (%)		LOD (ppt)	
	GC-MS	GC×GC	GC-MS	GC×GC
Toluene	12	6	2.3	2.8
Ethylbenzene	12	7	0.5	0.3
o-Xylene	14	7	0.5	1.0
p-/m-Xylene	13	7	0.5	0.4
Hexane	12	10	2.6	2.8
Heptane	13	10	1.9	1.9
Octane	14	10	1.2	0.6
Nonane	11	9	0.5	0.4
α-Pinene	15	7	1.3	0.4
β-Pinene	12	7	1.0	0.9
3-Carene	19	7	0.9	0.1
Camphene	23	7	1.1	0.1
Eucalyptol	34	7	2.5	1.5

Tab. 4.4: Measurement uncertainties and limits of detection (LOD) for the GC-MS and GC×GC-FID

During the first half of the campaign between July 7 and 11, the aliphatic VOCs and o-xylene from the GC×GC-FID system appear to be higher. As can be seen in the graphs, high mixing ratios of volatile organic compounds found with the GC-MS are sometimes lower in the GC×GC measurements and vice versa. Slight differences can be caused by differing sampling periods for the individual instruments: the GC-MS sampled for 20 minutes, while the GC×GC collected for 60 minutes. Nonetheless there is generally good agreement for the biogenic VOC measurements. This is in spite of a recent study that showed, that sampling of terpenes on Tenax in presence of O_3 leads to losses, if no O_3 scrubber is used [176]. No scrubber was applied during the GC×GC sampling, but no severe differences to the GC-MS, which had a $Na_2S_2O_3$ impregnated filter as a scrubber, measurements can be observed.
Figure 4.14 shows the on-line measurements for PTR-MS, GC-MS and GC×GC. The blue dots represent the unsmoothed PTR-MS measurements, the black line GC-MS and the red line GC×GC-FID. The PTR-MS and GC-MS measurements were performed simultaneously from July 5 to 14, whereas the PTR-MS and GC×GC can be compared between July 7 and 14. A complicating factor in the comparison with the PTR-MS data is that the mass data can correspond to several species measured separately by GC. In such cases the candidate VOCs measured by GC will be summed prior to comparison with the PTR-MS. The PTR-MS cannot distinguish between the various terpenes but can give us a general idea of the total terpene concentration present. Generally, terpenes tend to fragment after protonation in the PTR-MS, 40% of the signal remaining at the protonated mother mass (mass 137) and 60% as a fragment at mass 81. The sum of the terpenes α- and β-pinene, camphene and 3-carene for GC-MS and GC×GC-FID respectively are also included in the graph. It is apparent, that short-term variations are detected much better with the PTR-MS,

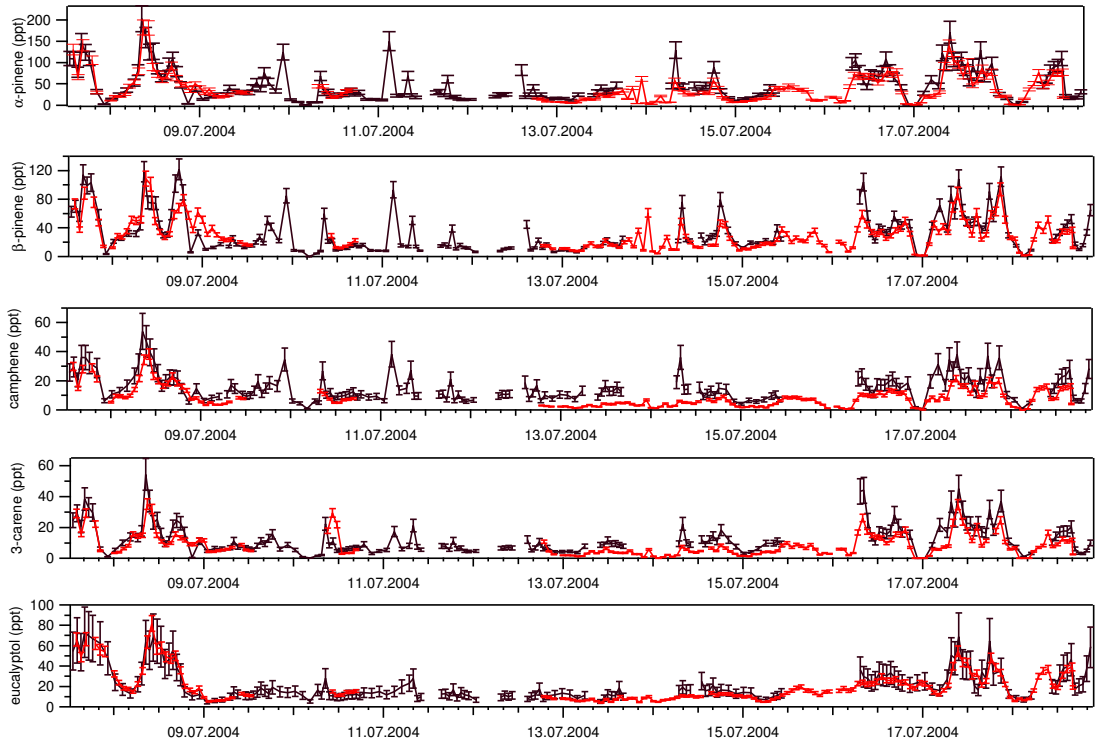

Fig. 4.11: Biogenic VOCs measured from July 7 to 18 during HOHPEX. The black line illustrates GC-MS measurements, the red line GC×GC-FID. The bars represent the measurement uncertainty

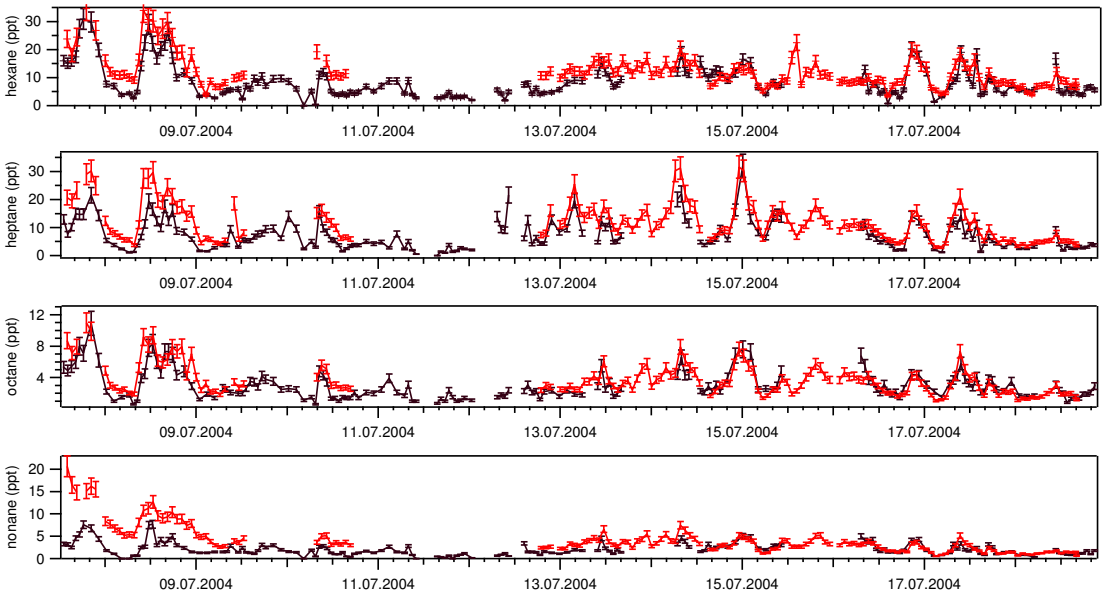

Fig. 4.12: Anthropogenic alkanes measured from July 7 to 18 during HOHPEX. The black line illustrates GC-MS measurements, the red line GC×GC-FID. The bars represent the measurement uncertainty

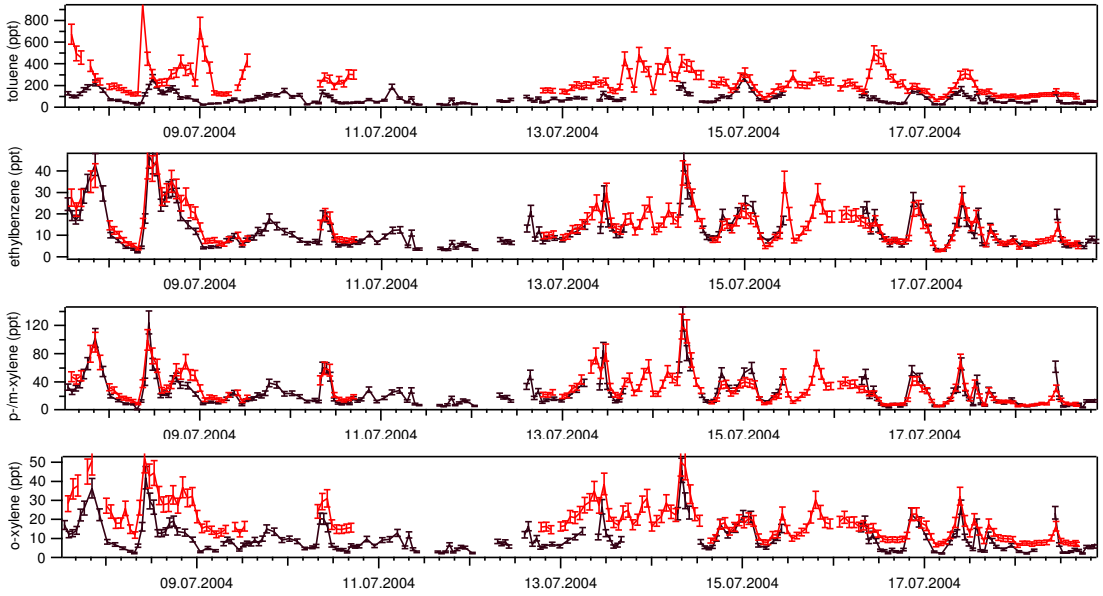

Fig. 4.13: Anthropogenic aromatic VOCs measured from July 7 to 18 during HOHPEX. The black line illustrates GC-MS measurements, the red line GC×GC-FID. The bars represent the measurement uncertainty

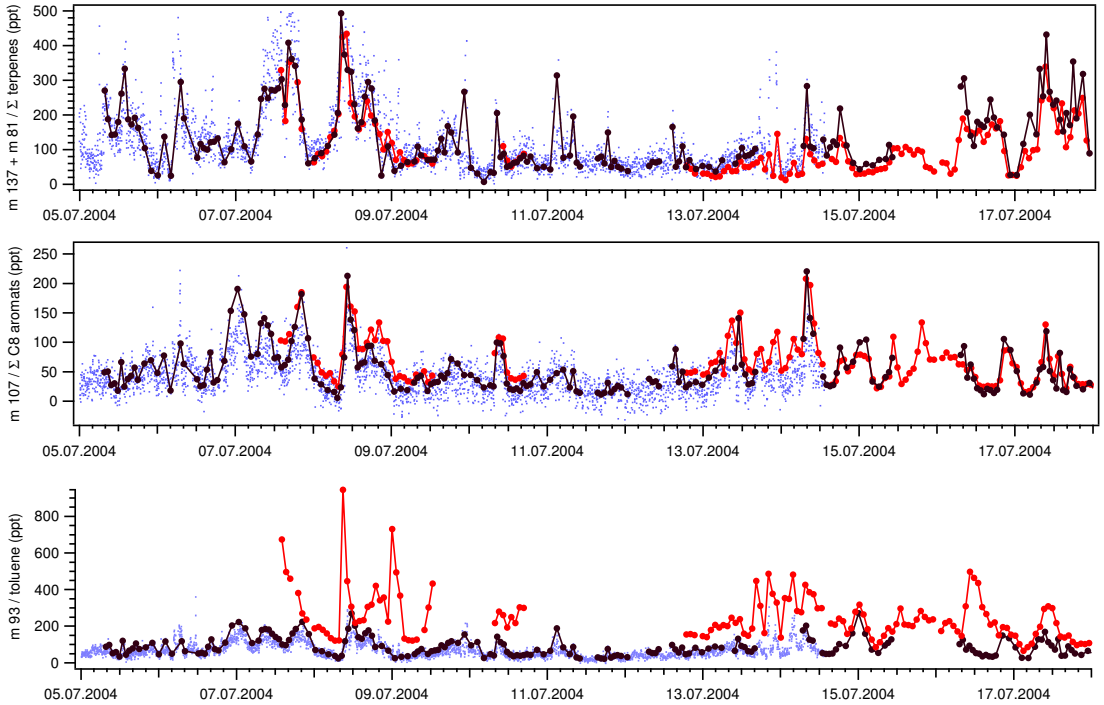

Fig. 4.14: VOCs measured from July 5 to 18 during HOHPEX. The black line illustrates GC-MS measurements, the red line GC×GC-FID, the blue dots PTR-MS

and the measured mixing ratios are similar to the GC-MS and the GC×GC-FID. In the middle graph, the PTR-MS mass 107, i.e. the sum of all protonated C8 aromatic compounds, and the sum of the gas chromatographically measured xylenes and ethylbenzene are depicted. It appears as if the individual measurements agree well, and the PTR-MS again picks up temporary fluctuations much better than both gas chromatographs. The lower graph shows mass 93, assumed to be toluene. As can be seen, the PTR-MS and GC-MS measurements agree well, whereas the GC×GC-FID not only displays higher mixing ratios, but also different diurnal variations. On closer inspection, the GC-MS and GC×GC-FID measurements fit well for short periods during the nights of July 15 and July 17. Systematic errors can thus be excluded. A dependency of the varying mixing ratios on the wind direction could not be found. Nor did days with high O_3 show suspicious differences compared to other days. Although the peak separation achieved with the GC×GC-FID is superior to that of the GC-MS, we suspect an occasionally co-eluting compound for the column configuration applied. Due to this observation, the toluene measurements are not included in the discussion.
To further evaluate the data, the correlation for the measured compounds is investigated in the following section.

4.5.3 Correlation of GC-MS, GC×GC-FID and PTR-MS on-line measurements

This section examines the correlation between the GC-MS and the GC×GC-FID for the ambient measurements presented above. Additionally, the correlation between the individual gas chromatographic techniques and the PTR-MS measurements will be examined.
Since the cycle and sample acquisition times for the two gas chromatographic systems were different, no ambient samples were completely synchronised. Rather than interpolating one dataset, data points from the GC-MS system for which the 20 minutes sampling time fell within the 60 minutes sampling time of the GC×GC-FID are compared. The correlation plots are depicted in Figs. A.9 and A.10 in the Appendix A.6 on pages 145 and 146. The solid line represents the best fit obtained by orthogonal distance regression, the dashed line the 1:1 relationship. The correlation parameters slope, intercept and the square of the correlation coefficient, r^2, are also shown in Table 4.5. The fitted slope and the intercept were determined by orthogonal distance regression (ODR) instead of standard linear regression (SLR). With the ODR method, all data points are assumed to have an equal weight and the orthogonal distance between the fitted line and the individual data points is minimised, whereas in the SLR only the distance in the y-direction is optimised. Since both datasets possess a measurement uncertainty, it is difficult to chose which data to treat as x- and which as y-values, this problem can be avoided with the ODR.
The slope of the fitted line indicates higher measured values of the GC×GC between 8 and 28% for the majority of the anthropogenic compounds. The GC-MS measurements of the biogenic compounds are generally between 4 and 31% higher than the

GC×GC values. R^2 ranges for all compounds between 0.88 for eucalyptol to 0.14 for toluene, the biogenic compounds usually correlate better than the anthropogenic VOCs.
The correlations for the alkanes range between 0.77 and 0.69, only nonane shows a poor correlation with 0.41. A positive offset between 1.5 and 2.4 ppt was found for the GC×GC measurements of hexane, heptane and octane, nonane shows a negative offset of 0.2 ppt. The mixing ratios measured with the GC-MS are generally 9 to 30% lower, except for nonane, which is 97 % lower compared to the GC×GC. If the obviously higher measurements before July 10^{th} are disregarded, the slope decreases and the GC-MS measurements are only 21 % lower than the GC×GC. The aromatic compounds with the exception of toluene display an r^2 between 0.86 and 0.72, the mixing ratios found with the GC-MS are 8 to 62% lower than the GC×GC-FID values. Similarly to the nonane measurements, a correlation of the o-xylene mixing ratios after July 10^{th} result in 37% lower values for the GC-MS. Positive offsets between 1.5 and 4.5 ppt were again found for the GC×GC, except for toluene. The poor r^2 of 0.14 for toluene is attributed to the co-elution of another compound in the GC×GC-FID analysis, as discussed earlier. The biogenic VOCs in Fig. A.10 show an r^2 between 0.74 and 0.88, which is very good considering the high variability of these compounds and the different sampling times. The slope information shows that the GC×GC-FID measures mixing ratios between 4 and 31% lower than the GC-MS, except for eucalyptol. Positive GC×GC offsets of 0.1 and 0.3 ppt were calculated for α- and β-pinene, the other biogenic compounds show negative offsets between 0.1 and 3.1 ppt. Both chromatographic systems show a correlation within 25% for most compounds except toluene and nonane. The offsets of the compounds nonane, ethylbenzene, and the monoterpenes were not significantly different from zero. However, the remaining VOCs, especially toluene, hexane, o-xylene, p/m-xylene show a significant offset.
To correlate the PTR-MS data with the gas chromatographic data, average values were calculated from the PTR-MS measurements over the sampling period for the respective GC, i.e. 20 minutes for the GC-MS and 60 minutes for the GC×GC-FID. A total of 154 and 82 data points have been obtained for the PTR-MS/GC-MS and PTR-MS/GC×GC-FID correlation plots. The PTR-MS detects all C_8 aromatic compounds, i.e. ethylbenzene, o-, m- and p-xylene, at mass 107. Similarly, all terpenes are detected at mass 137 and with partial fragmentation at mass 81. To compare these masses with the GC, the individual compounds were summed prior to correlation.
The correlation parameters for mass 137 + mass 81 (terpenes), mass 107 (xylenes and ethylbenzene) and mass 93 (toluene) measured by PTR-MS versus the relevant compounds measured by GC-MS and GC×GC-FID are shown in Table 4.5. The respective correlation plots are depicted on page 147 in Fig. A.11, see Appendix A.6. The correlation for the biogenic VOCs between the PTR-MS and the gas chromatographic systems is very good, with an r^2 of 0.94 for the PTR-MS/GC×GC-FID and an r^2 of 0.77 for the PTR-MS/GC-MS comparison. Both GC-MS and GC×GC measure more terpenes than the PTR-MS, 16.6 and 11.4 ppt offset can be seen for the PTR-MS compared to the GC-MS and the GC×GC. The C_8 aromatic compounds

correlate well for all instruments with an r^2 of 0.85 and 0.74 for the GC×GC-FID and GC-MS measurements, respectively. The PTR-MS apparently measures lower mixing ratios than the gas chromatographic systems, 37% higher than the GC-MS and 50% higher than the GC×GC-FID. As well as for the terpenes, a positive offset was found for the PTR-MS. For mass 93, the r^2 for the PTR-MS and the GC-MS amounts to 0.74, the values measured with PTR-MS are 30% lower. The toluene mixing ratios determined by GC×GC-FID show, as expected from the earlier findings, a poor correlation coefficient with the PTR-MS as well. All offsets can be considered significant, except for the comparison of mass 107 between the PTR-MS and the GC×GC.

Good correlations were found for the examined compounds, with the exception of nonane for the GC-MS and GC×GC-FID comparison and toluene for the comparison of the GC×GC-FID with the other instruments. The GC-MS measured the highest

VOC	slope	intercept (ppt)	r^2
GC×GC vs GC-MS			
Hexane	1.09±0.05	2.41	0.69
Heptane	1.28±0.05	1.91	0.77
Octane	1.10±0.06	1.46	0.69
Nonane	1.97±0.10	-0.21	0.41
Toluene	5.58±0.49	-95.0	0.14
Ethylbenzene	1.08±0.04	0.92	0.86
o-Xylene	1.62±0.07	4.42	0.72
p-/m-Xylene	1.10±0.03	2.97	0.85
α-Pinene	0.87±0.02	0.13	0.83
β-Pinene	0.96±0.02	0.33	0.74
3-Carene	0.73±0.02	-0.08	0.77
Camphene	0.69±0.03	-0.59	0.81
Eucalyptol	1.20±0.11	-3.09	0.88
mass 107	1.19±0.04	8.66	0.83
mass 137+81	0.96±0.05	-11.40	0.81
PTR-MS vs GC-MS			
mass 137+81	0.80±0.05	16.63	0.77
mass 107	0.63±0.02	11.43	0.74
mass 93	0.66±0.03	5.21	0.81
PTR-MS vs GC×GC			
mass 137+81	0.51±0.04	11.42	0.94
mass 107	0.50±0.05	1.95	0.85
mass 93	0.06±0.01	34.02	0.14

Tab. 4.5: Correlation parameters slope, intercept and coefficient of variation (r^2) of VOCs measured by GC-MS, GC×GC-FID and PTR-MS. Mass 107 represents all C8 aromatics, mass 137+81 the measured terpenes and mass 93 toluene.

anthropogenic mixing ratios, followed by the GC×GC-FID and the PTR-MS. For the terpenes at mass 137+81, the GC-MS found the highest values, followed by the GC×GC-FID and the PTR-MS. The PTR-MS measured generally lower mixing ratios than the gas chromatographic systems. Since a comparison for acetone (mass 59) between the PTR-MS and GC-MS revealed a good agreement, it is suspected that the PTR-MS is less accurate for higher masses. This may be related to changes in the transmission efficiency of ions in the PTR-MS. Although determined at the start of the campaign, the transmission may have changed with time.

4.5.4 Calibration of compressed ambient air with two GC-MS systems and GC×GC-FID

The second part of this instrument comparison was to quantify VOCs in a compressed ambient air sample using the gas chromatographic instruments GC-MS (MOHP and MPI-C) and the GC×GC-FID (MPI-C).
The VOC standard used in this experiment was generated by compressing ambient air in Mainz into a 20 L stainless steel cylinder using a three stage RIX oil-free piston compressor [177]. The compressed gas mixture was assumed to be stable and analysed during the field campaign in July 2004 by the GC-MS systems and in December 2004 for the GC×GC-FID. The results are shown in Fig. 4.15. The blue colour represents mixing ratios measured with the GC-MS from the MOHP, yellow the GC-MS values

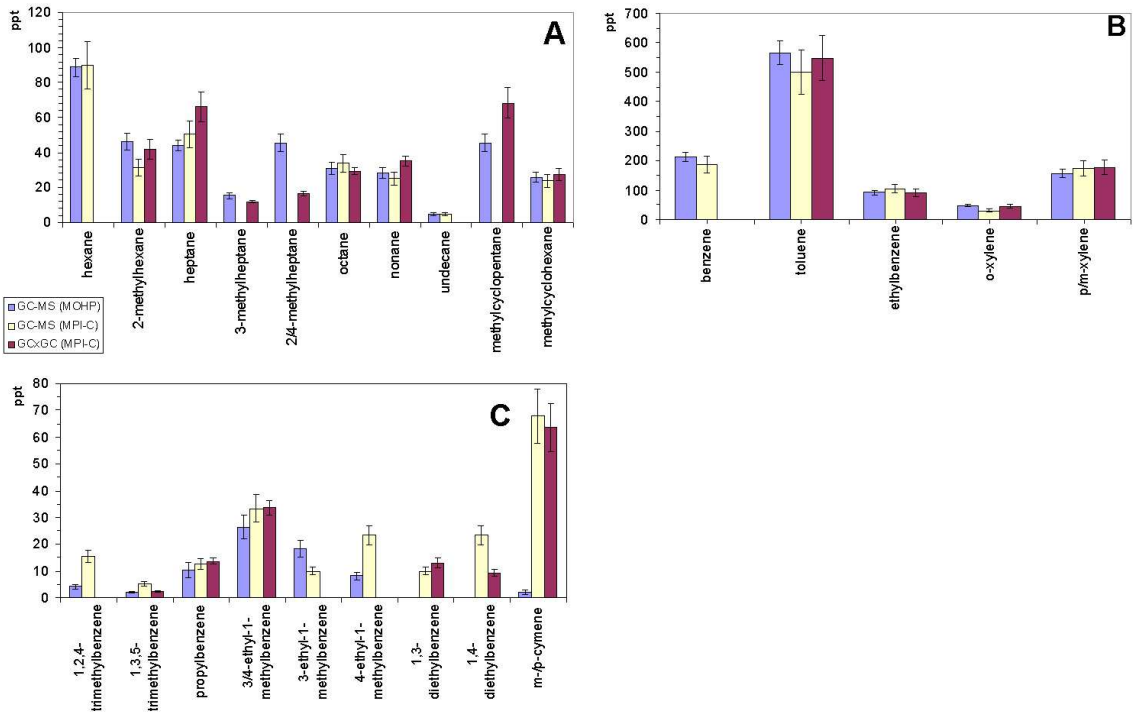

Fig. 4.15: Overview of the measurement results with error bars for the ambient air sample. The blue bar represents the MOHP GC-MS, yellow the GC-MS from the MPI-C and red the GC×GC-FID

Compound	GC-MS (MOHP) (ppt)	Error (%)	GC-MS (MPI-C) (ppt)	Error (%)	GC×GC-FID (MPI-C) (ppt)	Error (%)
Aromatic VOCs						
Benzene	212.9	7.0	186.8.0	10.0	-	
Toluene	566.3	7.0	500.0	12.0	548.3	14.0
Ethylbenzene	92.5	8.0	104.6	12.0	91.2	14.0
o-Xylene	47.6	7.0	30.0	14.0	44.6	15.0
p/m-Xylene	156.5	8.0	173.7	14.0	177.8	15.0
1,2,3-trimethylbenzene					2.4	12.0
1,2,4-trimethylbenzene	4.2	18.0	15.5	14.0	-	12.0
1,3,5-trimethylbenzene	2.0	18.0	5.2	14.0	2.4	12.0
propylbenzene	10.3	27.0	12.5	15.0	13.6	8.0
3/4-ethyl-1-methylbenzene					33.6	8.0
3-ethyl-1-methylbenzene	18.4	17.0	10.0	20.0		
4-ethyl-1-methylbenzene	8.1	18.0	23.4	20.0		
1,3-diethylbenzene	-		10.0	20.0	12.9	14.0
1,4-diethylbenzene	-		23.4	20.0	9.3	14.0
p-Cymene	1.6	22.0	67.8 + m	9.0	43.1	14.0
m-Cymene	0.5	20.0			20.4	14.0
Aliphatic VOCs						
Hexane	88.6	6.0	89.8	6.0	-	14.0
2-methylhexane	46.2	10.0	31.5	6.0	42.0	13.0
Heptane	44.0	7.0	50.4	10.0	66.2	13.0
3-methylheptane	15.4	11.0			11.8	7.0
2/4-methylheptane	45.2	11.0			16.5	7.0
Octane	30.8	12.0	33.7	20.0	29.3	7.0
Nonane	28.2	11.0	25.2	15.0	35.1	8.0

Compound	GC-MS (MOHP) (ppt)	Error (%)	GC-MS (MPI-C) (ppt)	Error (%)	GC×GC-FID (MPI-C) (ppt)	Error (%)
Undecane	4.6	17.0	4.7	10.0		9.0
methylcyclopentane	45.2	11.0			68.1	13.0
methylcyclohexane	25.8	11.0	23.7	10.0	27.0	13.0
Biogenic VOCs						
Camphene	0.8	25.0			0.8	10.0

Tab. 4.6: Mixing ratios and systematic error of the ambient air sample measured by GC-MS (MOHP and MPI-C) and GC×GC-FID

from the MPI-C and red the GC×GC-FID. The black bars indicate the estimated measurement error for the individual compound. Fig. 4.15 A depicts acyclic and cyclic aliphatic VOCs, and Fig. 4.15 B and C aromatic compounds analysed by all three systems. The averages of the measured values including the error are additionally presented in Table 4.6. Terpenes could not be compared as they were below the detection limit in this cylinder for all except camphene which was 0.8 ppt for the GC-MS (MOHP) and GC×GC-FID, respectively.
A good agreement can be observed between all instruments for the aliphatic compounds in Fig. 4.15 A. Exceptions were heptane and methylcyclopentane, where the GC×GC-FID is much higher than the other participating GCs with 50% and 31% compared to GC-MS (MOHP) and GC-MS (MPI-C), respectively. For the co-eluting 2-/4-methylheptane, the GC-MS (MOHP) shows an almost three times higher value than the GC×GC-FID.
The comparison of the aromatic compounds is displayed in Fig. 4.15 B. Very good agreement can be seen for the aromatic compounds measured in the campaign. The good correlation with respect to toluene further supports the earlier assumption of a co-eluting compound in the GC×GC-FID analysis of ambient air.
Fig. 4.15 C shows substituted aromatic compounds which were not compared for the field campaign and which exhibit significant differences between the individual measurement systems. The compounds 3- and 4-Ethyl-1-methylbenzene co-elute only in the GC-MS analyses. The isomers p- and m-cymene are co-eluting for both the GC-MS and the GC×GC-FID. To compare these VOCs, the separately measured compounds were added up. The summed mixing ratios found for 3- and 4-ethyl-1-methylbenzene display excellent agreement between the two GC systems of the MPI, but both agree less with the GC-MS from Hohenpeissenberg. For the individually measured 3- and 4-ethyl-1-methylbenzene, which are resolved in both GC-MS measurements, the mixing ratios curiously display an inversed ratio. The sum of the cymene isomers agrees well for the GC×GC-FID and GC-MS from the MPI, but not for the GC-MS from the MOHP, which shows a 30 times lower value. Significant differences are also visible for the diethylbenzenes measured by the GC-MS and GC×GC-FID from the MPI-C.
Generally, the calibration measurements show with few exceptions a good agreement within the measurement error for the gas chromatographic systems, especially for the VOCs analysed during the field campaign.

4.5.5 Diurnal cycles

The diurnal cycles of the VOCs analysed by GC×GC-FID during the field campaign are shown in Fig. 4.16. The black line illustrates the hourly mean value of the mixing ratios, the lower and upper bars represent the minimum and maximum measured value respectively and the dotted line the median value. To determine the hourly mean mixing ratio, the main sampling time intervals of the individual measurements were assessed (hour± 30 minutes) and the acquired mixing ratios averaged.
The effects of the diurnally changing boundary layer height described in section 4.2

can be observed for all measured VOCs in the late morning around 9:00, when the ascending BL reaches the station. In the night, the usually low BL and the stations' isolation from the ground based sources leads to lower VOC levels.
All biogenically emitted compounds follow a similar trend: a slow increase of mixing ratios beginning at sunrise, a strong increase at the arrival of the BL, then an additional maximum around 14:00, and for some terpenes also later in the afternoon. These observed diurnal cycles are caused by the proximity of the emitting sources (e.g. forest) and the dependence of the emission on meteorological conditions like light and temperature. Resulting from the mixed spruce forest surrounding the station, the most abundant biogenic compounds are α- and β-pinene. These VOCs, along with camphene and 3-carene, are known to be emitted by spruce trees [178, 179]. Continuous elevated mixing ratios for these terpenes have been detected on some of the cooler nights, indicating a constant release from the storage pools in the needles [10]. In contrast, sabinene has been reported to be mainly emitted from beech and deciduous trees [180, 181]. At Hohenpeissenberg, sabinene is almost only observed during daytime, suggesting that the emission is dependent on light. This phenomenon has been observed in earlier studies [182, 183] and was also reported for beech and birch leaves, where emission in the dark gradually decreased for all measured monoterpenes at a constant temperature [181, 184]. Eucalyptol also makes a significant proportion of the total terpenes. Previous studies have indicated that it is emitted from various plants such as rape, birch, spruce, hornbeam and grassland [185, 186, 187]. The emission from grassland is reported to be particularly strong at elevated temperatures and after mowing [185]. Short-term increases in mixing ratios for all terpenes have been detected occasionally during the night, curiously mainly in the cold and rainy phase of the field campaign, see Fig. 4.9. A recent study suggested a positive influence of relative humidity and rainfall on the emission of monoterpenes from pine trees [188], and a further study suggested a connection between contact stimulation and stronger emission of terpenes in Japanese cypresses [189]. Both hypotheses might be relevant for nocturnal emissions originating from the mixed spruce forest around the Hohenpeissenberg, as the observed wind speed at night was mostly higher than 8 m s^{-1}, the humidity was very high and precipitation occurred frequently.
The anthropogenic compounds show a slightly different diurnal cycle to the biogenic VOCs. The mean atmospheric mixing ratios for anthropogenic compounds also peak between 9:00 and 10:00, but remain approximately constant at this level until around noon, when the boundary layer is completely mixed. The fluctuating course of the mixing ratios throughout the rest of the day are probably driven by variations in anthropogenic emissions and/or a changing fetch area. The prolonged elevated mixing ratios in the early evening around 21:00 are likely generated by VOCs from rush hour traffic in all neighbouring conurbations. The lowering of the BL between 22:00 and 1:00 is accompanied by an almost steady or decreasing level of anthropogenic VOCs during the night, until the BL ascends over the station again the following morning. Vacillating anthropogenic nighttime mixing ratios were usually measured, when the nocturnal BL did not develop as a result of a turbulent atmosphere and the station was not situated in the free troposphere but still influenced by surface sources through horizontal transport processes.

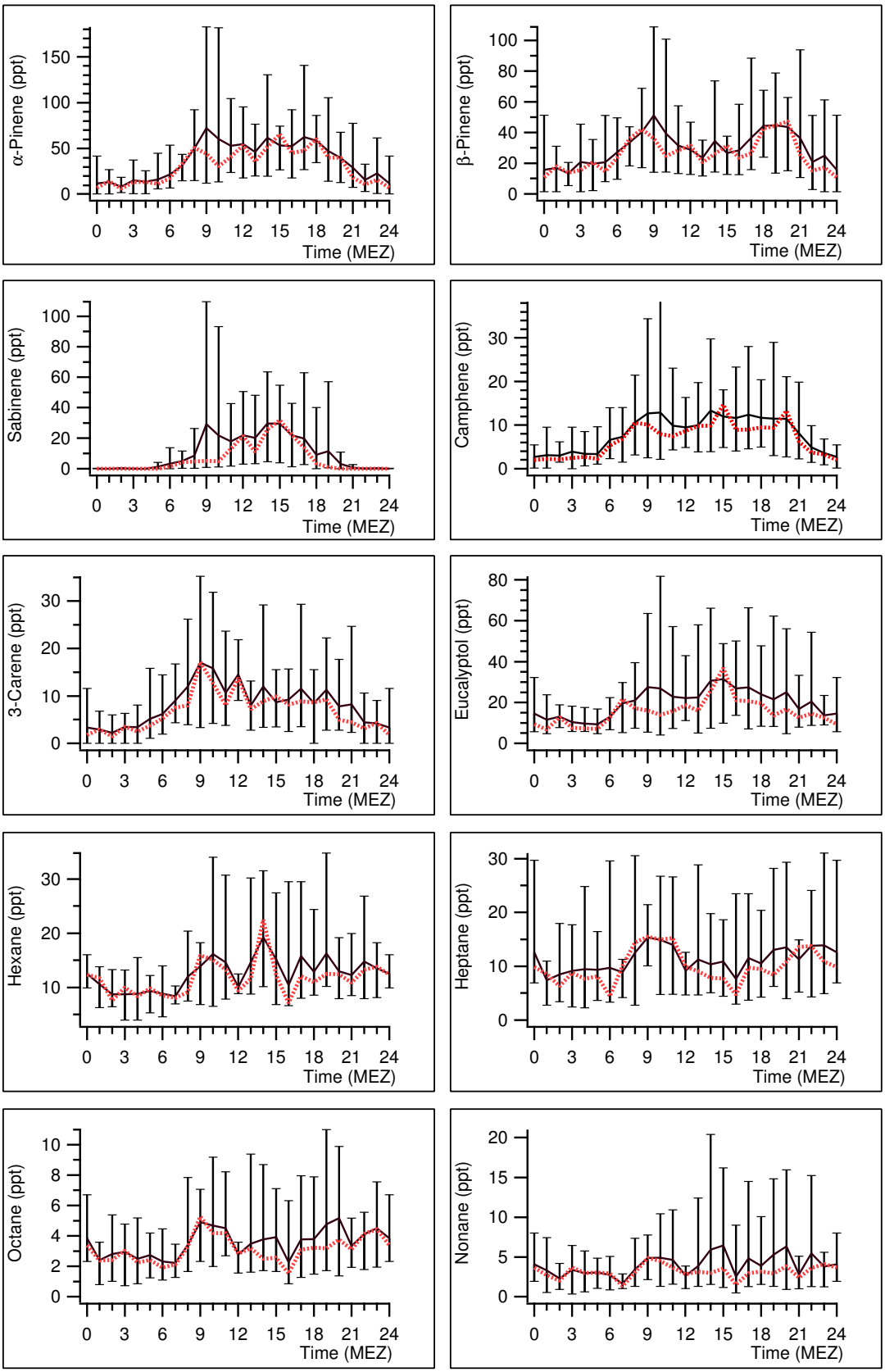

Fig. 4.16: Hourly averaged diurnal cycles of VOCs measured by GC×GC. The black line shows mean values, upper and lower bars the maximum and minimum measured value, the red dotted line shows the median value. All times are MEZ (GMT + 2)

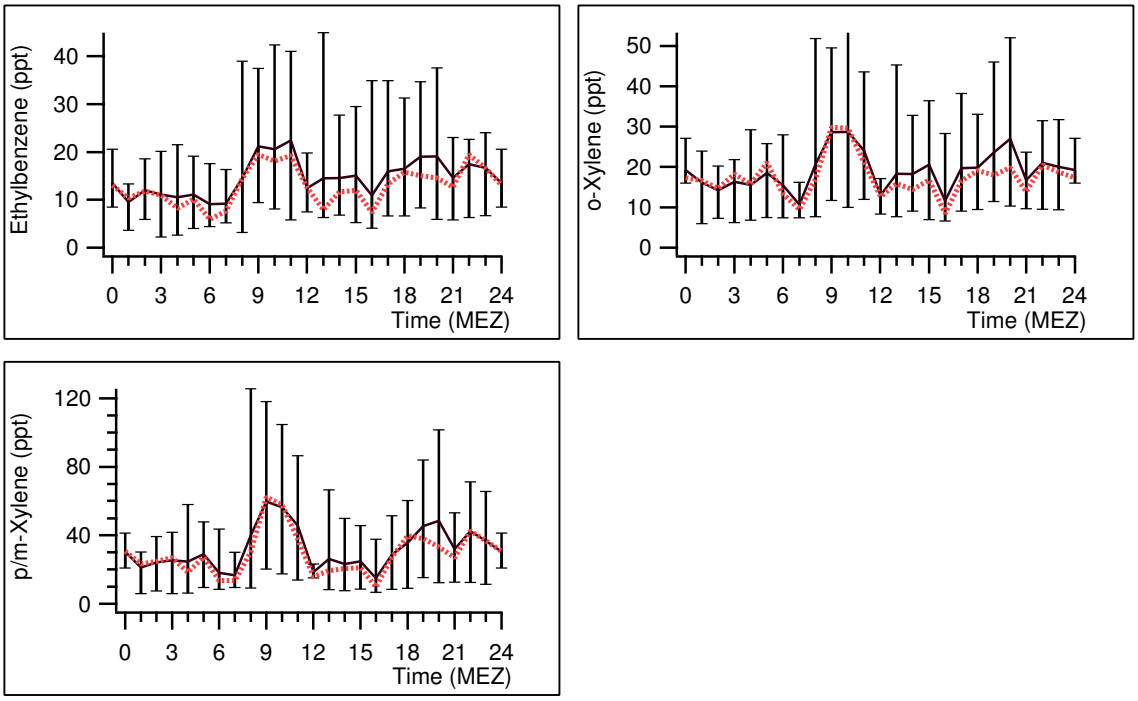

Fig. 4.16: contd.

Fig. 4.17 and 4.18 display the mixing ratios of the biogenic compounds as well as the anthropogenically emitted VOCs as a sum and a fractional contribution. The biogenic species show a smooth threefold increase during the daylight hours with a local minimum around 13:00 and almost constant low mixing ratios at night. The anthropogenic compounds show a much less intense contrast between mixing ratios measured during day and night and are less variable due to their longer lifetimes, although maxima at 9:00 and 20:00 and three minima at noon, 16:00 and 21:00 are visible. Another difference between anthropogenic and biogenic VOCs can be observed in these graphs in the morning: After sunrise, when temperatures first rise and the mixing ratios for terpenes increase again, the anthropogenic compounds continue to stay at a low level. This suggests that the top of the mountain is still in the free troposphere without contact to the plain and the terpenes originate from the vegetation surrounding the station.

4.5.6 Influence of wind direction

The influence of vertical transport processes during the BL transition period has been examined in the previous section. The analysis is now extended to examine the effect of the wind direction and horizontal transport on mixing ratios. The polar plots in Fig. 4.19 show the biogenically emitted compounds, Fig. 4.20 displays the anthropogenic aromatic and aliphatic VOCs. The differently coloured markers represent the time periods *day* (blue, 5:00 -20:00 MEZ), *night* (black, 20:00 - 5:00

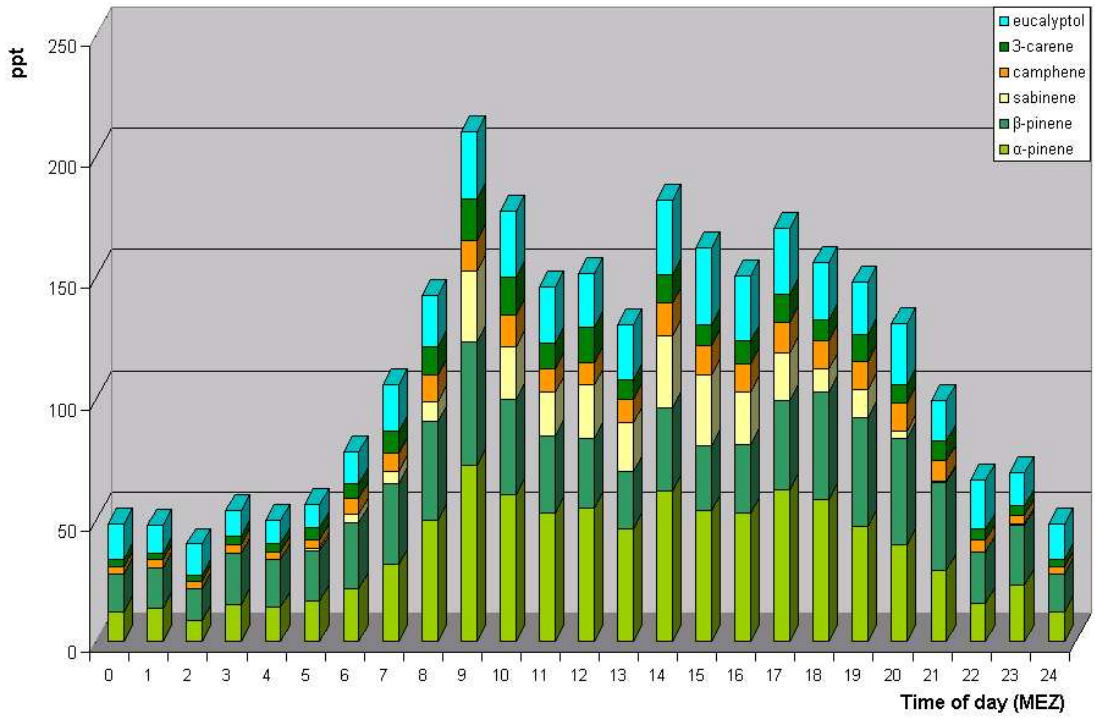

Fig. 4.17: Sum and fractional contribution of the measured biogenic VOCs to the diurnal concentrations

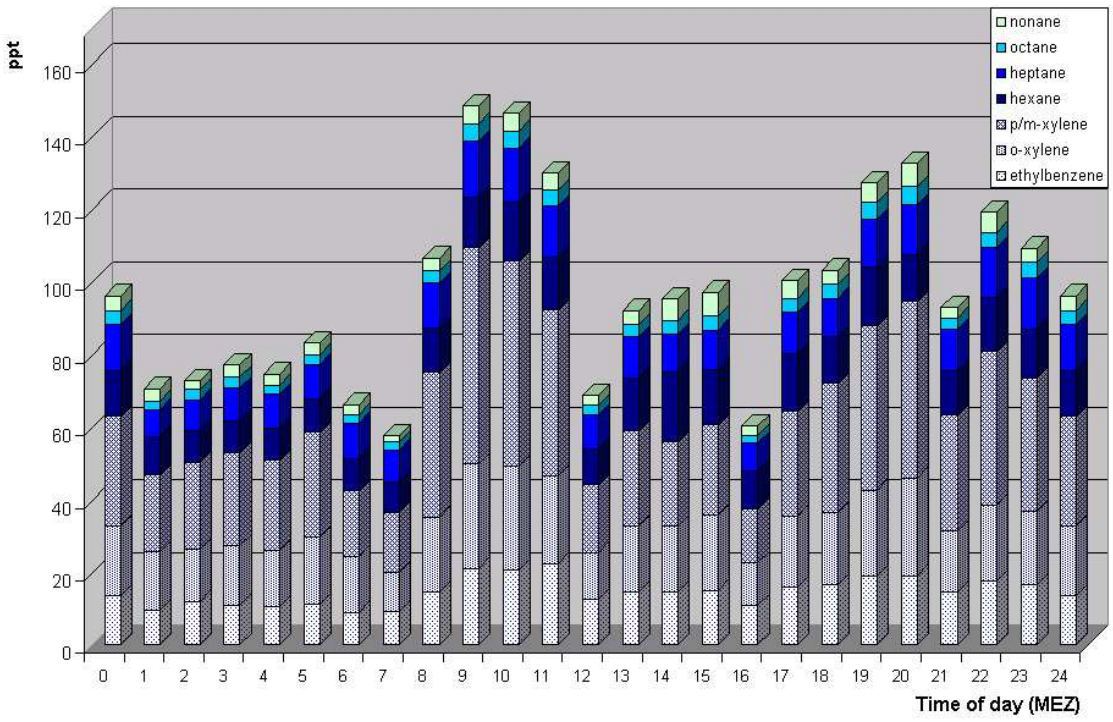

Fig. 4.18: Sum and fractional contribution of the measured alkanes and aromatics to the diurnal concentrations

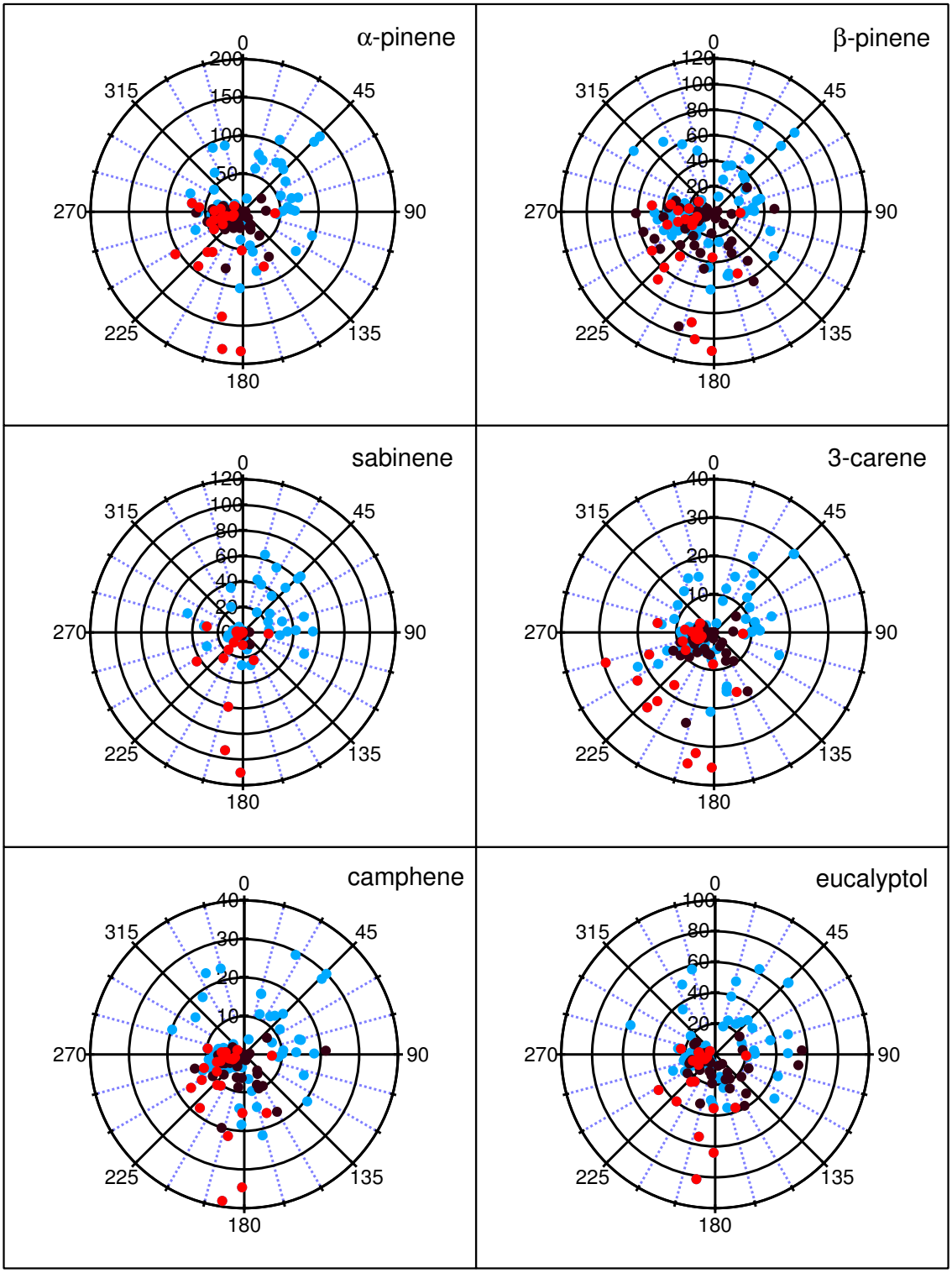

Fig. 4.19: Wind direction dependency of measured biogenic compounds (mixing ratios in ppt). Blue dots represent daytime measurements, black dots nighttime measurements and red dots measurements during boundary layer breakthrough

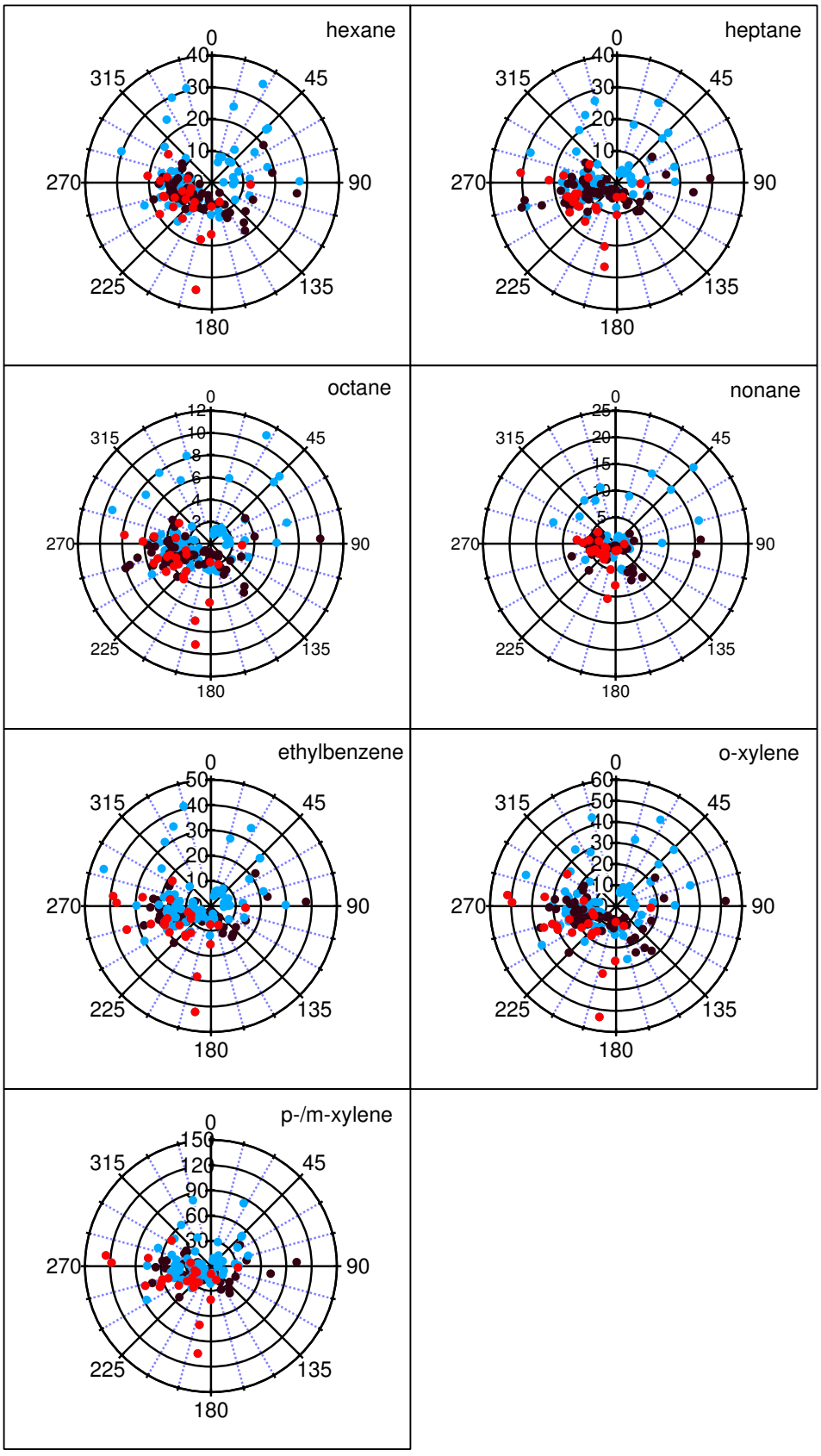

Fig. 4.20: Wind direction dependency of measured anthropogenic VOCs (mixing ratios in ppt). Blue dots represent daytime measurements, black dots nighttime measurements and red dots measurements during boundary layer breakthrough

MEZ) and *BL transition period* (red, 7:30-10:30 MEZ). The graphs illustrate that the main wind direction during the campaign and during the day is from the west. The main wind direction during the transition period ranged between west and south.
In the transition period, the biogenic species show lower mixing ratios in westerly winds than southerly, despite there being a large wooded area to the west (Fig. 4.4). Another forest is situated around 5 km to the south and transport from there only takes 15 to 30 minutes at low to average wind speeds. It should be noted that these suppressed mixing ratios may be attributable to lower sunlight and temperatures on the west facing slope, and consequently lower terpene emissions. A closer look at the topography in Fig. 4.4 reveals a ridge-like area on the mountain slope to the southwest, cutting off the western side from possible warm air flows. There are too few data during hot periods with westerly wind, for these hypotheses to be confirmed in this study. The highest biogenic mixing ratios during transition period and the day were found for the 8th and 17th July 2004, both were hot days with morning temperatures around 24°C and sunshine encouraging the emission of VOCs.
The highest mixing ratios for the aromatic xylenes were measured as the BL first crossed the site, whereas the aliphatic species as well as ethylbenzene show similarly high or higher mixing ratios in the daytime. During the day the main wind direction is west. There are indications, however, that higher levels of all anthropogenic VOCs are transported with air masses coming from the larger settlements to the northwest (Landsberg/Lech, Kaufbeuren) and northeast (Weilheim, Munich) and less from western direction (Schongau, Peiting). Interestingly, anthropogenic emissions seem to be very low between 100° and 180° (east to south). A closer look at the map in Fig. 4.2 reveals no major settlements into this direction. Garmisch-Partenkirchen could be a source for anthropogenic compounds, but it is enclosed between mountains and the valley runs from southwest to northeast, so direct transport of emissions seems unlikely. The mixing ratios during the day are with few exceptions higher than during the night. The high nocturnal values visible to the east occurred in the late evening around 21:00, when the station was still situated in the mixed BL. Higher nighttime levels of anthropogenic VOCs were only found if the station was not in the free troposphere.

4.5.7 Lifetime and variability of VOCs

VOCs are removed from the atmosphere mainly through reaction with the hydroxyl radical (OH), but reactions with O_3 and the nitrate radical (NO_3) also play a role in oxidising the ambient VOCs, see chapter 1.3. Through oxidation, VOCs can be converted into more polar and hydrophilic forms, which makes the photooxidation products more susceptible to wet removal by rain or dry removal at surfaces. The residence time, or lifetime, τ of an organic compound in the atmosphere is chiefly affected by these aforementioned physical processes and reactions. The specific chemical lifetime of a VOC is expressed as the time needed for its initial concentration in the atmosphere to be reduced to *1/e* times the initial concentration [190]. Compounds displaying a high reactivity with the oxidants above (OH, O_3, NO_3) are removed

faster than less reactive ones.
The lifetime is defined as

$$\tau_{VOC} = \frac{1}{rate\,of\,removal} \tag{4.3}$$

The *rate of removal* is the product of the reaction rate coefficient k_{Ox}, which is specific for every compound/oxidant pair, and the concentration of the oxidant in the atmosphere, [Ox]:

$$\tau_{VOC} = \frac{1}{k_{_{Ox}}[Ox]} \tag{4.4}$$

τ_{VOC} represents the lifetime of the VOC with respect to the specified oxidant. The atmospheric removal of the VOCs described here mainly depends on their reactivity with the oxidants O_3 and OH and to a smaller extent NO_3. A detailed description of the oxidation cycle is given in section 1.3.

In Table 4.7 the reaction rate coefficients of selected compounds with their corresponding calculated atmospheric lifetimes with respect to OH and O_3 during the HOHPEX campaign are shown. The concentrations of OH and O_3 were determined by calculating the campaign median from measurements of both species, 1.7×10^6 molecules cm^{-3} (0.071 ppt) and 1×10^{12} molecules cm^{-3} (42.2 ppb) for OH and O_3 respectively. The total lifetime ($\tau_{_{total}}$) of each VOC was calculated using the equation

$$\frac{1}{\tau_{_{total}}} = \frac{1}{\tau_{_{OH}}} + \frac{1}{\tau_{_{O_3}}} \tag{4.5}$$

which is equal to

$$\tau_{total} = \frac{1}{k_{_{OH}}[OH]} + \frac{1}{k_{_{O_3}}[O_3]} \tag{4.6}$$

where k is the rate constant of the oxidant OH or O_3 reacting with the organic compound, [OH] and [O_3] are the concentration of the oxidants OH and O_3, respectively.

The atmospheric lifetimes of the species discussed here vary from approximately 1 hour (sabinene) to 1.2 days (hexane). In general the biogenic species have shorter atmospheric lifetimes than anthropogenic species. This higher reactivity with both OH and O_3 is caused by the unsaturated double bonds contained in most of the biogenic VOCs.
The atmospheric lifetime of a species determines the extent to which it may be transported. As can be seen in Table 4.8, the emitted VOCs can be transported over long distances, depending on their respective lifetime. At high wind speeds, e.g. in fast moving frontal systems, the longer lived species can be transported thousands of kilometers away from their sources within one lifetime. They therefore have an impact not only on the local, but also on the regional, continental or even global scale. The very reactive terpenes with the shorter lifetimes, however, are relevant only in the regional to local scale.

	k(OH) $\times 10^{-12}$ cm^3 molc^{-1} s^{-1}	τ_{OH} in days	k(O_3) $\times 10^{-17}$ cm^3 molc^{-1} s^{-1}	τ_{O_3} in days	τ_{OH+O_3} in days
Biogenic compounds					
Isoprene	101.0	0.07	1.28	0.90	0.063
α-Pinene	53.7	0.13	8.70	0.13	0.065
β-Pinene	78.9	0.09	1.50	0.77	0.078
Sabinene	115.7	0.06	8.70	0.13	0.041
3-Carene	80.0	0.09	3.70	0.31	0.067
Camphene	52.6	0.13	0.09	12.86	0.128
Eucalyptol	5.7	1.19	0.001	1157.41	1.19
Aromatic compounds					
Ethylbenzene	7.10	0.96		n.r	
(p+m)-Xylene	13.70	0.50		n.r	
o-Xylene	18.95	0.36		n.r	
Alkanes					
Hexane	5.61	1.21		n.r	
Heptane	7.08	0.96		n.r	
Octane	8.68	0.78		n.r	
Nonane	10.00	0.68		n.r	

Tab. 4.7: Reaction rate coefficients k and atmospheric lifetimes τ in days of selected compounds in presence of 1.7×10^6 molecules cm^{-3} (0.071 ppt) OH and 1×10^{12} molecules cm^{-3} (42.2 ppb) O_3. (n.r.= not relevant, since atmospheric lifetimes are > 4.5 years)

The variability of a VOC can give valuable information on its sources and sinks. Intuitively, we may expect a high variability from species that are most rapidly removed from the atmosphere. If the transport time from source to measurement location varies with time, then the largest range of concentrations measured (variability) will be seen for the most reactive compound. In contrast, long-lived species will be relatively insensitive to the transport time and hence show smaller ranges in measurement concentration (i.e. variability). The lifetime-variability dependency for atmospheric species was first investigated in the 1970s by Junge [191] for long lived species, who noticed that the relative standard deviation of a data set is inversely proportional to the residence time (or lifetime) in years. Later it was found empirically that for such studies the variability for compounds with shorter atmospheric lifetimes can be better expressed by using the standard deviation of the ln of the mixing ratio [192]. The concept has been applied in many subsequent studies [41, 193, 194, 195, 196, 197]. The equation

$$Sln(X) = A\tau^{-b} \tag{4.7}$$

has been used to define the variability lifetime relationship of VOCs, where Sln(X) represents the standard deviation of the logarithm of the mixing ratios of compound X, τ the chemical lifetime, and A and b empirical fitting parameters. It has been

	τ_{VOC}	Distance, km @ wind speed 5 m s^{-1}	Distance, km @ wind speed 1 m s^{-1}	Distance, km @ wind speed 15 m s^{-1}
Isoprene	1.5 h	27	5	81
α-Pinene	1.6 h	29	6	87
β-Pinene	1.9 h	34	7	102
Sabinene	1.0 h	18	4	54
Camphene	3.1 h	56	11	168
3-Carene	1.6 h	29	6	87
Eucalyptol	1.2 d	518	104	1554
Ethylbenzene	23 h	414	83	1242
p/m-Xylene	12 h	216	43	648
o-Xylene	8.6 h	155	31	465
Hexane	1.2 d	518	104	1554
Heptane	23 h	414	83	1242
Octane	18.7 h	337	67	1011
Nonane	16.3 h	293	59	879

Tab. 4.8: Range of dispersion area corresponding to one lifetime of VOCs at different wind speeds. The values for τ_{VOC} in presence of O_3 and OH are taken from Table 4.7. The wind speed 5 m s^{-1} is the median value during the campaign, 1 and 16 m s^{-1} are approximately the lowest and the highest wind speeds. The distance to Munich for example is around 80 km

shown that the exponent b indicates the proximity of the measurement to the source region. A value of b=0 indicates a nearby source, where the source emissions rather than the chemistry defines the variability, and b=0.5 indicates a remote source, where the variability is strongly influenced by the chemistry and thus the dependency between variability and lifetime can be seen. The coefficient A has been interpreted as defining the range of air mass ages arriving at a measurement site [41]. A low A suggests a narrow distribution of air mass ages, whereas a high A indicates a strong variation in air mass ages. Variability studies for longer-lived VOCs (1 to 500 days) in assorted environments were carried out by Jobson et al. [193] and revealed a b value of 0.18 for measurements conducted over the Harvard forest. This indicates sources close to the measurement site. In comparison, the same study assessed the variability at a remote location on sea ice north of Alert, Canada, to a b value of 0.92. This dependence shows that the variability is dominated by chemical loss. A study of Gros et al. [41] revealed a value of b=0.23 for a site affected by sources between 300 to 700 km away. A similar b was found for the Hohenpeissenberg measurement site. However, since the lifetimes of the VOCs examined in this study are much shorter than in the mentioned work of Gros et al. (an hour to 2 days as compared to one day to 270 years), „remote“ sources are still on a regional scale.
A further possible influence on variability is a source that changes with time. The emissions of biogenic compounds are highly variable, being strongly dependent on the weather conditions, light intensity, source activity and position. This may induce

extra variability on top of that coming from chemistry and transport. In the case of sabinene (as noted previously) there is no emission by night which is in contrast to the other terpenes.

Fig. 4.21 illustrates the variability-lifetime relationship for a selection of VOCs. Lifetimes are calculated based on reactions with OH and O_3. The atmospheric concentrations for the oxidants assumed are derived from the mean values calculated during the campaign, i.e. for OH 1.7×10^6 molecules cm^{-3} (0.071 ppt) and for O_3 1×10^{12} molecules cm^{-3} (42.2 ppb). Circles show the atmospheric lifetime with respect to OH and O_3, squares to O_3 only and triangles with OH only. As was seen in Table 4.7 the lifetime of some VOCs is influenced by the presence of OH, but not O_3. A good example for a slow VOC/O_3 reaction is eucalyptol, leading to an atmospheric lifetime of > 4.5 years, compared with 1 day in presence of OH. Similarly the aromatics and alkanes are unreactive with ozone. A strong influence of O_3 on the total lifetime τ can be observed in the biogenic terpenoid compounds like sabinene or 3-carene, where the reactions with OH and O_3 combine to give a significantly shorter lifetime than with either one alone.

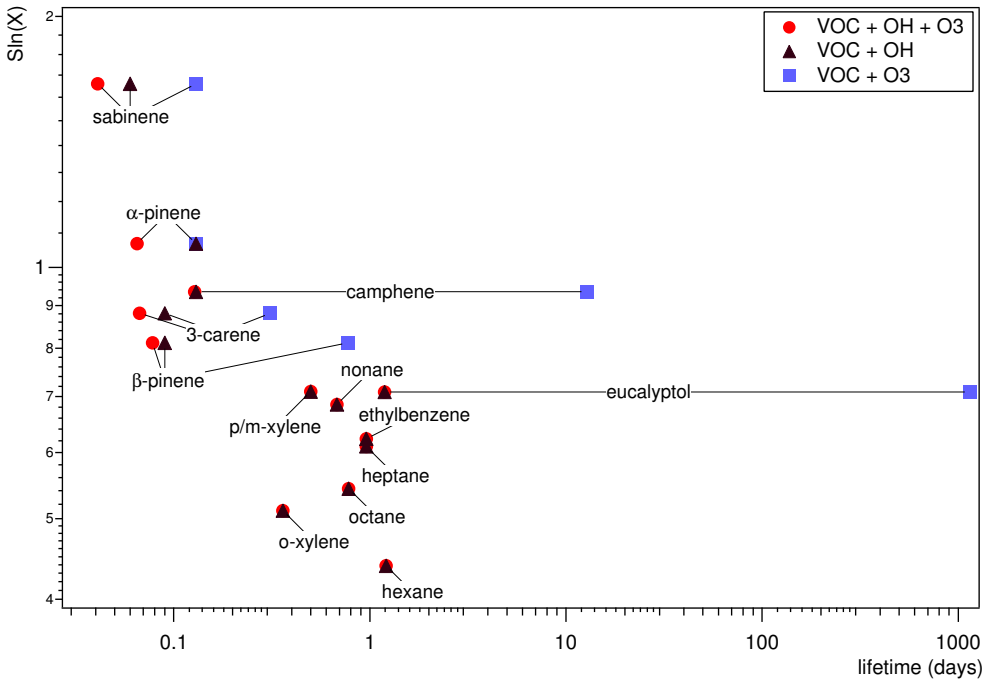

Fig. 4.21: Lifetimes of VOCs in presence of OH and/or O_3

Fig. 4.22 shows the relation between the measured VOC variability and their corresponding lifetimes in the presence of OH and O_3. A relatively high variability can be observed in all biogenic compounds, particularly sabinene. The reason for this high variability is a combination of both the high reactivity and the dependency of emission on factors such as light, temperature, or moisture which varied considerably during the HOHPEX campaign. Also, the distribution of plant species and their respective emission patterns play a major role. Spruce and beech trees are the

predominating tree species surrounding the station. From previous studies spruce trees are known to emit α- and β-Pinene, and 3-carene [178, 179], deciduous trees like beeches primarily emit sabinene [180]. The emission of sabinene from beeches depends strongly on temperature. A decrease from 25° to 10°C leads to a significant reduction in leaf emissions [180, 185].

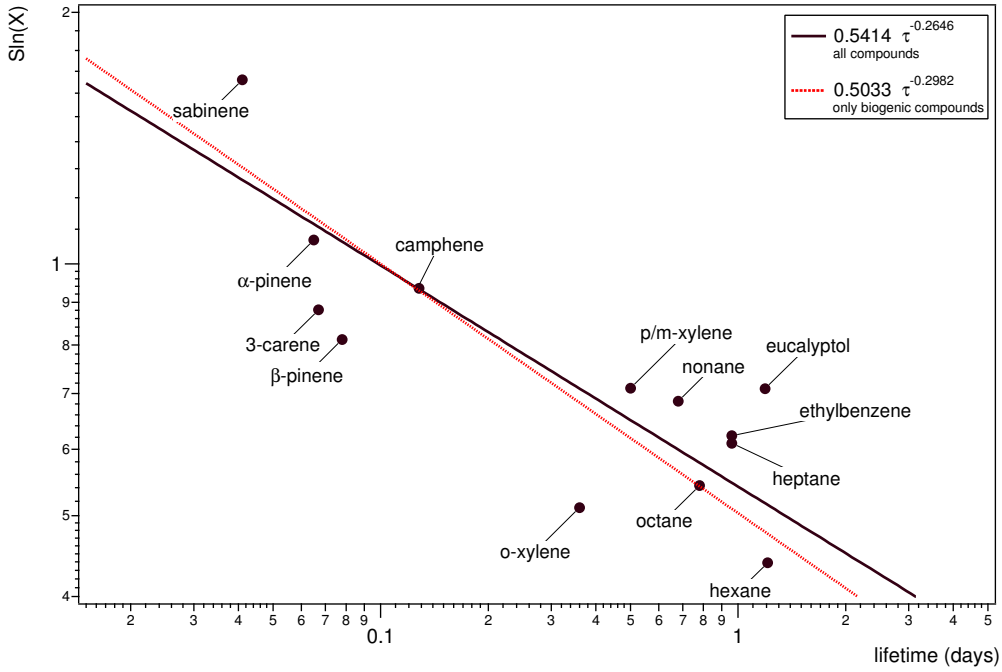

Fig. 4.22: Logarithmically scaled graph showing the variability of measured short-lived VOCs. The black line is a fit through all VOCs, the dotted line is with biogenically emitted compounds only. Assumed concentration for OH is 1.7×10^6 molecules cm^{-3} (0.071 ppt) and for O_3 1×10^{12} molecules cm^{-3} (42.2 ppb)

The VOC variability and lifetime data are fitted to the function Sln(X)=A τ^{-b}. The coefficients derived for all discussed compounds are A=0.5414 ± 0.067 and b=0.2646 ± 0.054. The exponent b=0.2646 indicates that there is a significant dependency of the variability on lifetime of these species and therefore that chemistry is playing an important role in the concentrations measured. If only the biogenically emitted compounds are considered, b amounts to 0.2982 ±0.134, which indicates an even stronger influence of chemistry on these VOCs.
Based on evidence of previous studies this is a surprising finding, since it is clear that Hohenpeissenberg is close to a strong source, see Fig. 4.4. For compounds with lifetimes of 2 day and greater, it has been shown that measurement sites in close proximity to sources show no variability lifetime dependence. In such cases the variability is dominated by the emissions. However in this study, very reactive species have been considered, chemical removal may therefore compete with mixing processes even near to heterogeneous spruce forests surrounding Hohenpeissenberg. It was examined, whether differences between day and night variabilities are observable. To minimise the dynamic effects during the morning BL transition period, only values

measured between 10:00 and 19:30 were considered for the day data. For the nocturnal variability the values measured between sunset and sunrise, 19:30 until 5:30, were chosen. To obtain representable data, the mean concentrations of the atmospheric O_3 and OH were calculated accordingly. The mean OH during the day was 3.05×10^6 molecules cm^{-3} (1.26 ppt) and O_3 1.06×10^{12} molecules cm^{-3} (44.4 ppb). During the night, the OH concentration was much lower with (0.08×10^6 molecules cm^{-3} (0.03 ppt), whereas the O_3 was only slightly higher with 1.01×10^{12} molecules cm^{-3} (42.5 ppb). The obtained coefficient A is higher during the night with a value of 0.8695 $\pm$ 0.020 as compared to 0.5221 $\pm$ 0.089 during the day. The low A for both periods indicates air masses of similar ages arriving in the Hohenpeissenberg area, but with a higher age difference during the night. The day and night b values do not differ significantly. A b of -0.1459 $\pm$ 0.066 was found for the day data and a b of -0.1324 $\pm$ 0.020 for the night. Although b may be expected to be higher for the nighttime case, since the station is cut off from the surface layer and the emitting sources, the OH levels are much lower. After restricting the timeframe to between 22:00 and 5:30, the time around which the BL descends below the station and before the light-induced terpene emission starts, b increased to 0.1837 $\pm$ 0.049. This similarity of the b values to the whole dataset is presumably caused by the instable weather conditions during some nights. The nocturnal BL could not develop and thus surface layer air masses affected the variability of the VOCs. The proximity of the vegetation to the station and their occasional nocturnal emissions also have the effect of decreasing b.

4.5.8 Estimation of OH and NO_3 radical concentration

Several studies have used the variability lifetime relationship to estimate the radical concentration in the atmosphere [193, 194, 198]. If the atmospheric concentrations of one or more VOC oxidants, e.g. O_3 or NO_3, are available, it is in principle possible to estimate the concentration of an unknown reactant, assuming that all reaction rates are known. This is accomplished by keeping the known concentrations constant and only varying the concentration of the unknown oxidant species. This technique gives rise to different distributions of the data points on the variability lifetime plot with differing fits. The assumed concentration of the oxidant that gives the best fit to the data can be interpreted as the average concentration of the said oxidant. The goodness of a fit is expressed by the χ^2 value, which evaluates the correlation of the least squares fit and indicates the discrepancy between the fitting function and the data. The lower χ^2, the better the fit to the data.
This method was applied here for the first time to the short-lived VOCs, to compare the result with the in-situ OH measurements carried out during the HOHPEX field campaign. To do so, the O_3 concentration was kept constant at 1×10^{12} (42.2 ppb) and the OH concentration was varied, thus changing the lifetimes of the VOCs susceptible to OH. The assumed OH concentrations versus χ^2 are shown in Fig. 4.23 A. The best fit for all VOCs with the lowest χ^2 lies at approximately 5.55×10^5 OH molecules cm^{-3} (0.023 ppt). From the in-situ measurements made at the MOHP,

a higher average OH concentration of 1.7 $\times$ 10^6 molecules cm^{-3} (0.071 ppt) was obtained. To understand this difference it must be considered what the OH value derived from the terpene variability represents: It expresses the average OH concentration experienced by the VOCs in the time taken to travel from the point of emission (e.g. in the canopy) to the point of measurement. A fraction of the time will have been spent in the shaded canopy which has lower OH than the more sunlit area where the OH measurement took place. For this reason we may expect that the VOC derived OH value will be lower than the in-situ, and this is indeed the case.

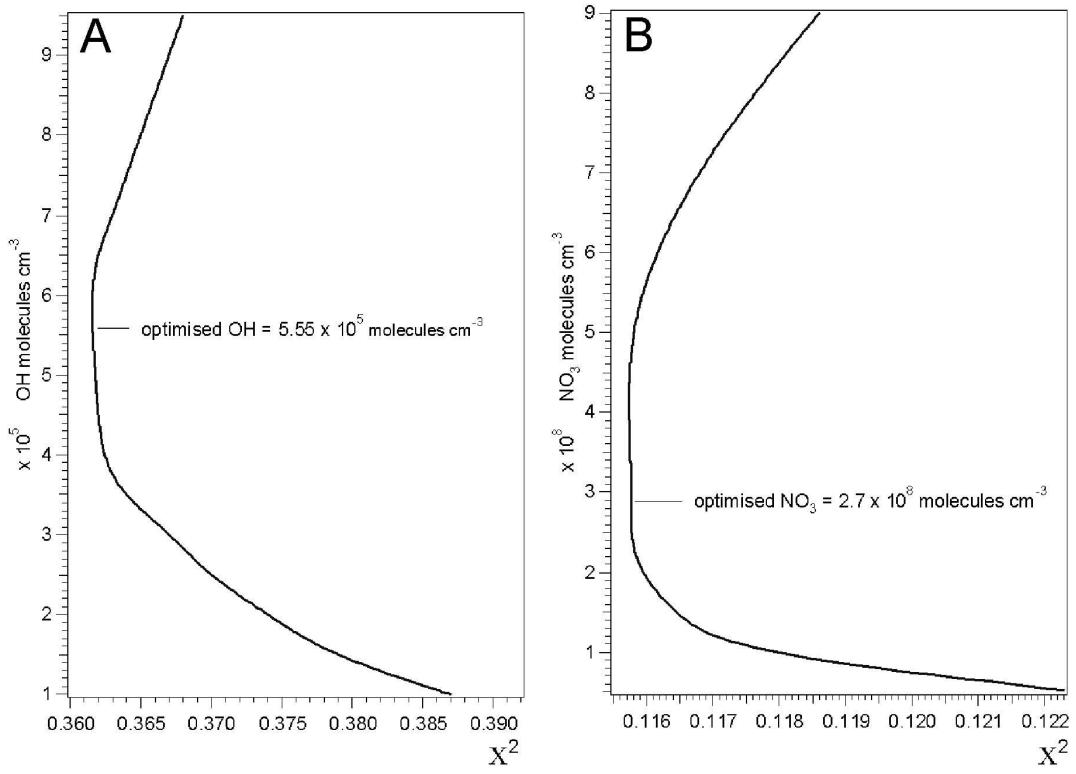

Fig. 4.23: **A**. Variation of the OH concentration versus χ^2 for the HOHPEX data. The optimum is at 5.55 $\times$ 10^5 molecules cm^{-3} (0.023 ppt) **B**. Variation of the NO_3 concentration versus χ^2. The optimum is at 2.7 $\times$ 10^8 molecules cm^{-3} (11.3 ppt)

As described in section 4.3, significant NO_2 concentrations were occasionally observed at night. This can give rise to NO_3 radicals, which can also oxidise VOC species. To investigate the levels of this unmeasured oxidant, the variability analysis was extended to include NO_3. NO_3 is the main atmospheric oxidant for reactive organic species during the night and equally important as OH during the day. The chemistry involved is described in section 1.3. For the calculation, the O_3 and OH concentrations were kept constant at the measured mean values, and the NO_3 concentrations were varied. The reaction rate coefficients used for the calculations are shown in Table 4.9. A broad optimum is obtained, the optimal mean NO_3 mixing ratios calculated for the GC$\times$GC measurements amounted to 2.7 $\times$ 10^8 molecules cm^{-3} (11.3 ppt). The results of the NO_3 variation are shown in Fig. 4.23 B.

This is the first attempt to examine the variability-lifetime dependencies on the local scale and comparable analyses for the very short-lived and reactive compounds has not been reported. It has been proposed by Ehhalt et al. to derive an average OH concentration using the variability lifetime relationship [199]. Williams et al. also determined an OH concentration from VOCs measured over a rain forest [194]. However in both cases, since the compounds used had lifetimes between several days to months, the OH concentration derived had to be interpreted as the radical abundance along the air mass back trajectory. In the case of the reactive compounds measured in HOHPEX, the OH derived represents the local OH.

As shown, the variability concept can be used for an estimate of the atmospheric mixing ratios of OH radicals, if sufficient VOCs with different atmospheric lifetimes as well as O_3 are measured at the site. A broad optimum was obtained for the calculations, ranging from 4.1×10^5 molecules cm^{-3} (0.017 ppt) to 6.5×10^5 molecules cm^{-3} (0.027 ppt), with an optimised value at 5.55×10^5 molecules cm^{-3} (0.023 ppt).

The calculation of the nighttime NO_3 radical concentration throughout the campaign revealed also a broad optimum of 2.2 to 5.0×10^8 molecules cm^{-3} (9.2 ppt to 21 ppt). An atmospheric mean concentration of circa 2.7×10^8 molecules cm^{-3} (11.3 ppt) was the optimised value. This result is in general agreement with several previous in-situ measurements of NO_3. In the marine BL of Rügen Island, Germany, a similar nocturnal average of 6-10 ppt was reported [201]. NO_3 mixing ratios measured in the free troposphere at Izaña, Tenerife, showed a nocturnal average of 8 ppt during early summer [202]. Lower values of 4.5 ppt were determined in the marine BL in the eastern Mediterranean [203], and an average of 4.6 ppt was found in the continental boundary layer near Berlin [204].

	k(NO_3) cm^3 $molc^{-1}$ s^{-1}
Isoprene	6.78×10^{-13}
α-Pinene	6.16×10^{-12}
β-Pinene	2.51×10^{-12}
Sabinene	10.00×10^{-12}
3-Carene	9.10×10^{-12}
Camphene	6.60×10^{-13}
Eucalyptol	1.90×10^{-16}
Ethylbenzene	5.70×10^{-16}
(p+m)-Xylene	4.50×10^{-16}
o-Xylene	3.80×10^{-16}
Hexane	1.05×10^{-16}
Heptane	1.45×10^{-16}
Octane	1.82×10^{-16}
Nonane	2.41×10^{-16}

Tab. 4.9: Atmospheric reaction rate coefficients *k*, for selected VOCs with NO_3. The values are taken from [200]

4.6 Conclusions

During the field campaign HOHPEX at the Meteorological Observatory Hohenpeissenberg (MOHP) in July 2004, anthropogenic and biogenic VOCs were measured applying GC×GC-FID.

To investigate the reliability of the on-line GC×GC-FID measurements, the mixing ratios were compared to PTR-MS (MPI-C) and routinely conducted GC-MS mea-

surements during the same period. All systems show a good correlation for ambient samples. The exception is toluene, where the correlation is significantly worse for the comparison of the GC-MS and the PTR-MS with the GC×GC-FID. We suggest this is caused by a co-eluting compound. The GC-MS measured the highest mixing ratios for the anthropogenic VOCs, followed by the GC×GC-FID, the PTR-MS found in the ambient air up to almost 45% lower values than the GCs. For the biogenic compounds, the GC-MS measured the highest ambient mixing ratios, followed by the GC×GC-FID and the PTR-MS. The detection limits are lowest for the GC×GC-FID, followed by the GC-MS and the PTR-MS.
A compressed ambient air sample was analysed using two different GC-MS systems (MOHP and MPI-C) and the GC×GC-FID. With few exceptions, all gas chromatographic instruments measured VOC concentrations within the instrumental uncertainty. Of the VOCs measured by the GC×GC-FID in the calibration task, only heptane did not agree with the value estimated using the GC-MS. Interestingly, for the GC×GC-FID heptane was found to be higher in the calibration, whereas during the field campaign the measured values were usually lower.
Pronounced diurnal cycles were found for the biogenically emitted compounds α- and β-pinene, camphene, sabinene, 3-carene and eucalyptol. The mixing ratios were strongly influenced by the mixed forest surrounding the station as well as the parameters light and temperature. In agreement with previous studies, cool and cloudy days showed less terpene emission than warm and sunny days. Diurnal cycles for the anthropogenic aromatic and aliphatic compounds were also found, but with different characteristics to those of the biogenics. The highest mixing ratios for all VOCs were measured in the morning when the boundary layer rose over the station.
Several nights deviating from a normal nocturnal cycle with decreasing mixing ratios for biogenic and anthropogenic compounds have been noted. This can in most cases be attributed to frontal systems passing through the area and changing air masses. Relative humidity, precipitation and wind speed appear to have played a role during nocturnal emission of the terpenes [188, 189].
The wind direction is an important factor for the mixing ratio levels of anthropogenic VOCs measured during the day. The highest values were found for west, south and east, where the cities Schongau (west), Kaufbeuren (north), and Munich (northeast) are situated.
The variability-lifetime relationship of the measured short-lived VOCs has been examined for the first time. The weak but significant b dependence of the measured compounds showed, that their respective sources are relatively close but that chemistry is playing a role their concentration variability. This is expected for the anthropogenic VOCs as there are several towns nearby, and for the biogenic terpenes as the site is surrounded by forest. The relationship was also used to estimate the atmospheric mean OH concentration during the GC×GC measurements. The calculated value of 5.55×10^5 molecules cm^{-3} (0.023 ppt) presents an approximation of the average OH concentration acting upon the discussed VOCs from emission to measurement. By extending the analysis, the NO_3 nighttime radical concentration was estimated using the same method to be 2.7×10^8 molecules cm^{-3} (11.3 ppt).

CHAPTER 5

MINATROC 2002

MIN*eral dust*

A*nd*

TRO*pospheric*

C*hemistry*

GC×GC measurements of
hydrocarbons in the atmosphere

5.1 Introduction and site description

The aim of the MINATROC (MINeral dust And TROpospheric Chemistry) campaign held between July 15^{th} and August 15^{st}, 2002 was to investigate the effects of heterogeneous reactions involving mineral aerosol on tropospheric chemistry. The project included field measurements, laboratory experiments and model studies. As part of the field study, GC×GC-FID measurements were carried out to characterise the influence of anthropogenic and biogenic sources during the day, when the station is partly influenced by the boundary layer; and the night, when it is situated in the free troposphere. Additionally, the influence of a Saharan dust storm on the VOC measurements was examined at Izaña, Tenerife.

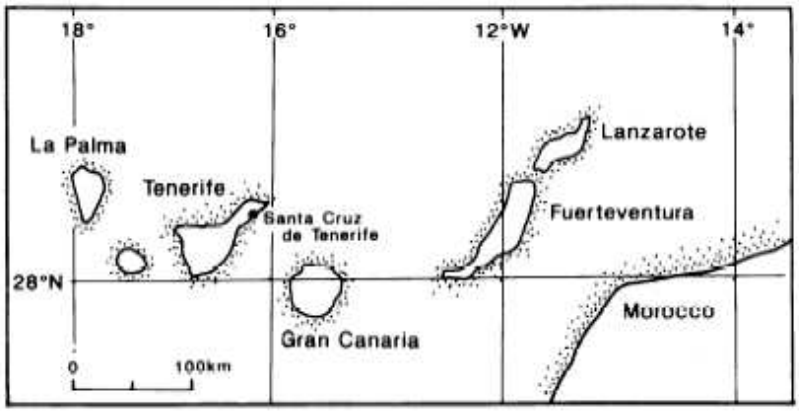

Fig. 5.1: Canary islands location to the west of the north African coast. Tenerife is close to the 16° longitude

The field campaign took place on the island Tenerife (28°18'N, 16°30'W), Spain, circa 400 km west of the coast of Africa in the Atlantic Ocean, see Fig. 5.1. The island is the largest of the Canary islands with an area of 2059 km^2, a length of approximately 100 km, and width of between 16 and 48 km.
The measurement instruments were sited at the meteorological station Izaña, operated by the Instituto Nacional de Meteorología (INM). This station is part of the Global Atmospheric Watch (GAW) network and has been used previously for both long-term and short-term studies of the free troposphere [205, 206, 207, 208, 209, 210]. The observatory is located on a northeastern flank plateau of the volcanic crater Pico del Teide (3700 m), at an elevation of 2360 m asl (above sea level), see Fig. 5.2 and Fig. 5.3. The horizontal distances to the northwest and southeast coast are about 15 km. Located about 1 km away from the meteorological station are the astrophysical observatory of the Instituto de Astrofísica de Canarias (IAC) as well as a television station, the roads leading there are closed to public traffic and only about 10 to 20 employee cars pass the station every day. The main tourist road from La Laguna to the Teide is about 100 m downhill and a few hundred meters to the north; up to 60 cars and buses pass per hour, especially in the mornings and late afternoon. Major

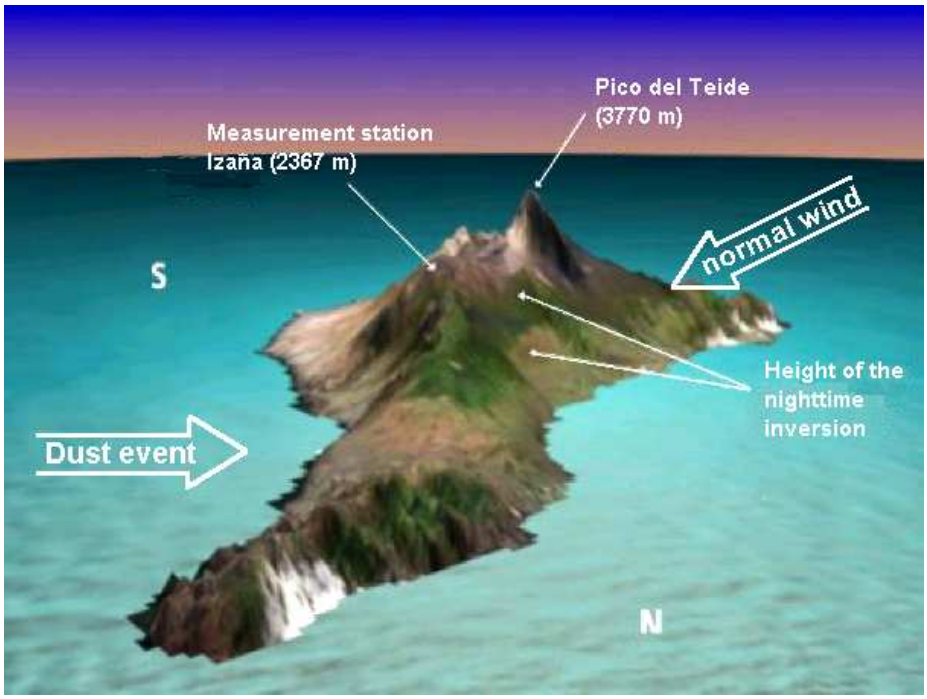

Fig. 5.2: Orography of the island Tenerife, Spain. The Izaña observatory, the mountain Teide and the inversion layer are shown

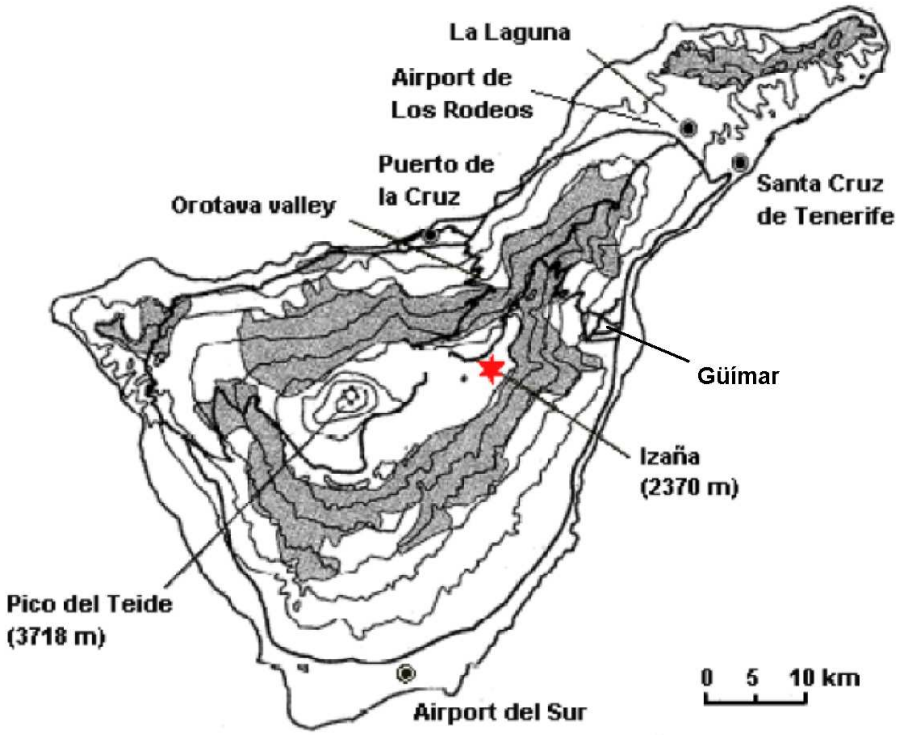

Fig. 5.3: Map of Tenerife, the Izaña observatory in the middle of the island is marked with a red star. Major towns relevant to this study are Puerto de la Cruz, La Laguna, Güímar and Santa Cruz de Tenerife, dark areas illustrate forest

cities on the island are the capital Santa Cruz de Tenerife (population 200 000) and La Laguna (125 000) to the northeast, Puerto de la Cruz (27 000) and La Orotava (36 000) to the north and Los Cristianos to the southwest. Above 1000 m asl the island is almost uninhabitated. Two airports are located on Tenerife, a smaller one mainly for domestic flights is close to Santa Cruz, whereas the major international airport is situated on the southern tip of the island. The major industry is an oil refinery in the vicinity of Santa Cruz, and two oil-fired power plants to the east and south of the station. A busy industrial harbour is also located in Santa Cruz, tankers and freight ships pass the island mainly to the south. High precipitation caused by the northeast trade wind leads to subtropical vegetation on the luff side, whereas the southern side of the island has more characteristics of a semi-desert. An evergreen laurel forest is predominating in the lower regions of the island, covered mainly with trees such as Canary laurel (*Laurus azorica*), tree heath (*Erica arborea*), or bog myrth (*Myrica gale*) [211]. Endemic Canary Pine forests (*Pinus canariensis*) predominate between 1200 m and 2000 m asl all around the island, at higher altitudes, subalpine and alpine flora prevail. The ground surrounding the station itself is loosely covered with light volcanic material, the vegetation is sparse (mostly the broom species *Spartocytisus supranubius* and *Adenocarpus viscosus*).

The GC×GC-FID data presented in this chapter is a selection of biogenic and anthropogenic compounds, instrumentation details are given in section 5.4. The biogenic VOCs include α-pinene, camphene, 3-carene and eucalyptol (1,8-cineol), the anthropogenic VOCs are represented by the aromatic species benzene, toluene, ethylbenzene, o-xylene and the co-eluting p- and m-xylenes as well as the aliphatic compounds heptane, octane, nonane and decane. In the following sections, the meteorological conditions and characteristics as well as measurement results obtained with GC×GC are discussed. Diurnal cycles for the biogenic and anthropogenic compounds are shown, as well as the influence of the wind direction on the measured species. The influence of Saharan dust on the measured VOC is also examined.

5.2 Site meteorology

The weather on the Canary Islands is influenced by marine meteorological conditions. A characteristic feature for subtropical oceanic islands adjacent to the western parts of continents like the Canary Islands, is a distinct temperature inversion layer. This inversion layer separates the dry free troposphere (about 20 % relative humidity) from the moist and cooler marine boundary layer (MBL, circa 55% relative humidity) which is influenced by the tradewinds [212]. On Tenerife, this temperature/trade wind inversion occurs between 1200 m and 1800 m asl throughout most of the year. In summer the upper boundary of this inversion layer lies at about 1400 m asl, which is significantly lower than the altitude of the station. This inversion impedes transport from the ocean and coastal cities to the site. During daytime the local thermal and dynamical upslope surface winds dominate, and marine boundary layer air mixed with local anthropogenic and biogenic emissions reaches the station. These winds cease slowly

in the evening and, because of the inversion, the station is located in the free troposphere during the night. In this time, downslope winds from the upper troposphere generally prevail.

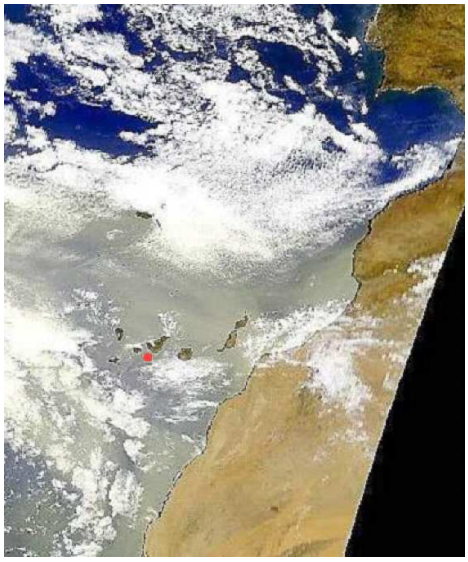

Fig. 5.4: Satellite picture of the Saharan dust event originating from West Africa. The image was taken on July 30^{th}, 2002. Tenerife is marked with a red dot

Air masses reaching the station during the GC×GC measurement phase originated either from over the Atlantic Ocean to the north of the Canary Islands or from the northeastern part of Africa. Several incidences of Saharan dust were detected at the island. Of these events, one was significantly larger than the others and occurred between July 28^{th} and August 1^{st}, 2002 [213]. Aerosol index images from the TOMS satellite show that the origins of the dust particles lay in western Algeria at the border region with Mali and Mauritania. A satellite picture of the main dust event over the Canary Islands originating from the west coast of Africa is shown in Fig. 5.4.

The meteorological parameters temperature, wind direction and speed, air pressure and relative humidity during the GC×GC measurements are shown in Fig. 5.5, the data is shown as 30 minute averages. The period of the main dust event is shaded grey. The temperature ranged from a minimum of 9.6°C in the morning of August 1^{st} to a maximum of 26.2°C in the afternoon of July 22^{nd}. The average temperature was 18.8°C with a median of 18.9°C. Temperatures below the campaign average were measured until July 19^{th}, between July 26^{th} and 28^{th} and again at the beginning of August. The main wind direction was between westnorthwest, with occasional periods of easterly winds. Between July 27^{th} and 31^{st}, the wind varied between east and south. Wind speeds during the measurement period varied between windstill (0.6 m s^{-1}) and 19.5 m s^{-1}. The average wind speed was 8.2 m s^{-1} and the median 7.4 m s^{-1}. Relative humidity was, as expected in the free troposphere, very low. The relative humidity occasionally increased above the mean value of 16.3% during some short periods before July 19^{th} and during a longer period between July 29^{th} and 31^{st}. The minimum relative humidity found was around 1% during the night, the maximum of 63% during the dust event, the median was 12.8%. The air pressure was measured on July 18^{th} and 19^{th}, and continuously after July 23^{rd}. Lower pressure prevailed between July 26^{th} and 29^{th}, the values ranged from a minimum of 769 hPa to a maximum of 780 hPa. Superimposed on this trend are diurnal cycles peaking around noon and midnight. The sun rose around 6:00 and set again shortly after 20:00.

The average diurnal cycles of the meteorological parameters temperature, wind direction, windspeed, relative humidity and air pressure are depicted in Fig. 5.6. The data are 30 minute averages, the graphs on the left show the diurnal variations during the

complete GC×GC measurement period, the middle graphs show the low dust period between July 16^{th} and 27^{th} and the graphs on the right show the meteorological con-

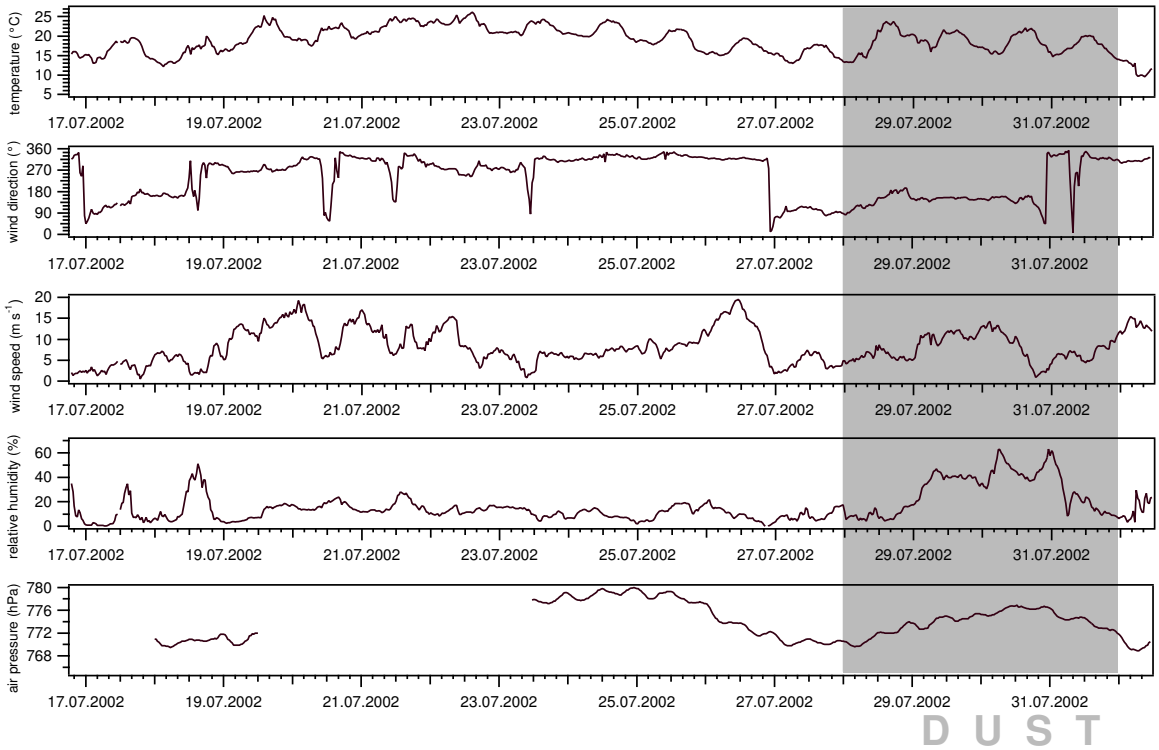

Fig. 5.5: Meteorological parameters temperature, wind direction, wind speed, air pressure and relative humidity, 30 minute averages, between July 16^{th} and August 1^{st}, 2002.

ditions during the dust event from July 28^{th} to August 1^{st}. The black line illustrates the mean measured value, the red dotted line the median value and the upper and lower bars the maximum and minimum measured value, respectively. The term 'low dust' arose from LIDAR measurements which revealed, that Saharan dust was present at low concentrations throughout the course of the campaign [213].
As can be seen in the graphs, the mean daily temperature during the dust event was lower than during the low dust period (17.2°C as compared to 19.1°C). The variations in minimum and maximum temperatures during the nights of the dust event were much smaller. The median wind direction during the dust event was between south and east. The mean calculated values indicate a predominating wind direction of between south and west. This is caused by a strong change of the wind direction from the southeast to the north towards the end of the dust event. During the low dust period the mean and median wind direction was westerly. Wind speeds show a greater diurnal variation and higher average speed during the dust event. Moreover, the mean relative humidity was between 20 to 30% (mean 26%), whereas the atmosphere during the low dust period was drier with 10 to 20% (mean 13%). Surprisingly the dust laden air from the Sahara desert has a higher relative humidity

than average. This may indicate that it has mixed with marine boundary layer air, either during the transport from Africa or more locally at the island.

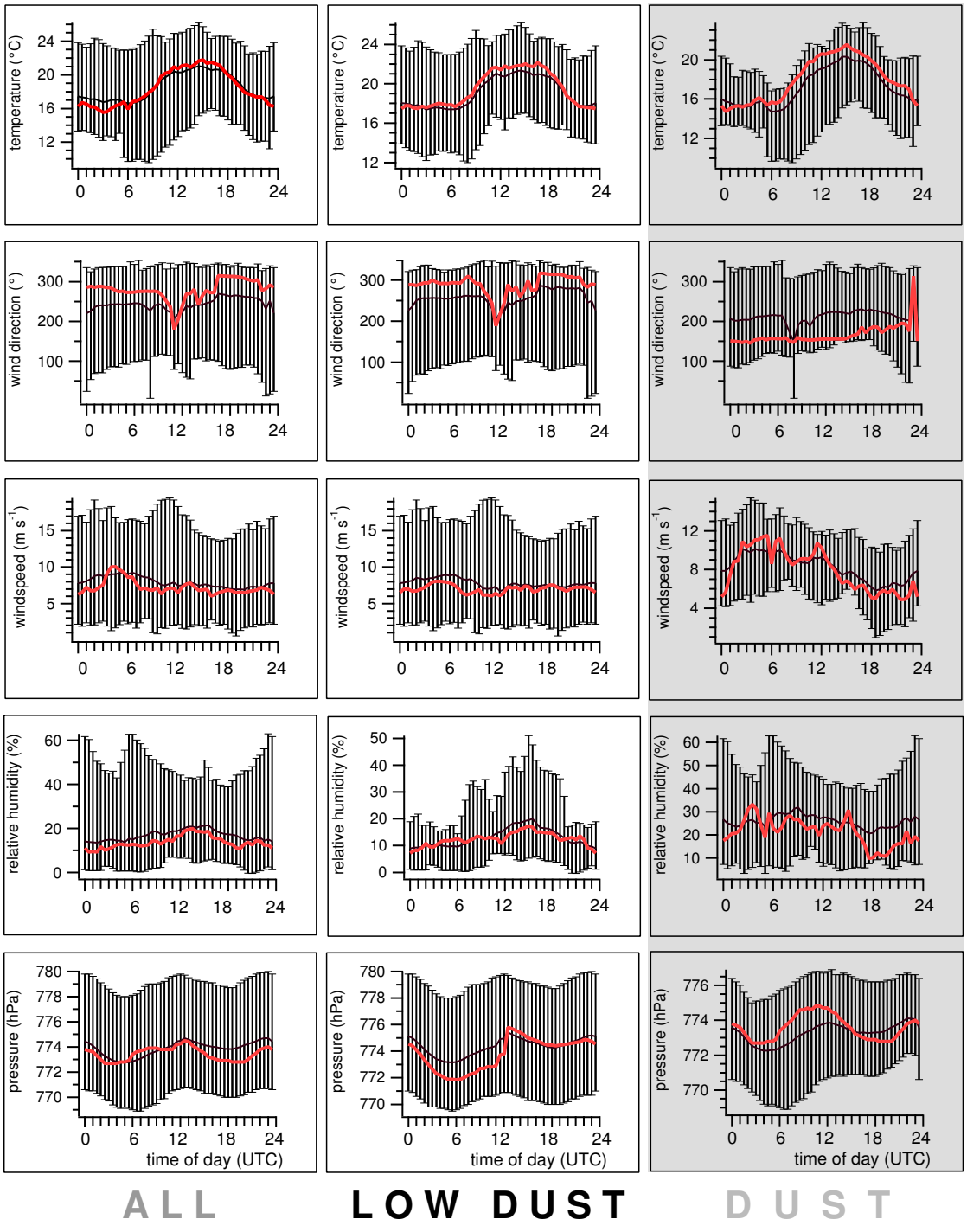

Fig. 5.6: Diurnal cycles of the meteorological parameters. The black line illustrates the mean value, upper and lower bars the maximum and minimum measured value and the red line the median of the hourly data. Graphs on the left: during complete GC×GC measurements, middle: during the low dust period, July 16^{th} to 27^{th}, right: during the dust event, July 28^{th} to August 1^{st}

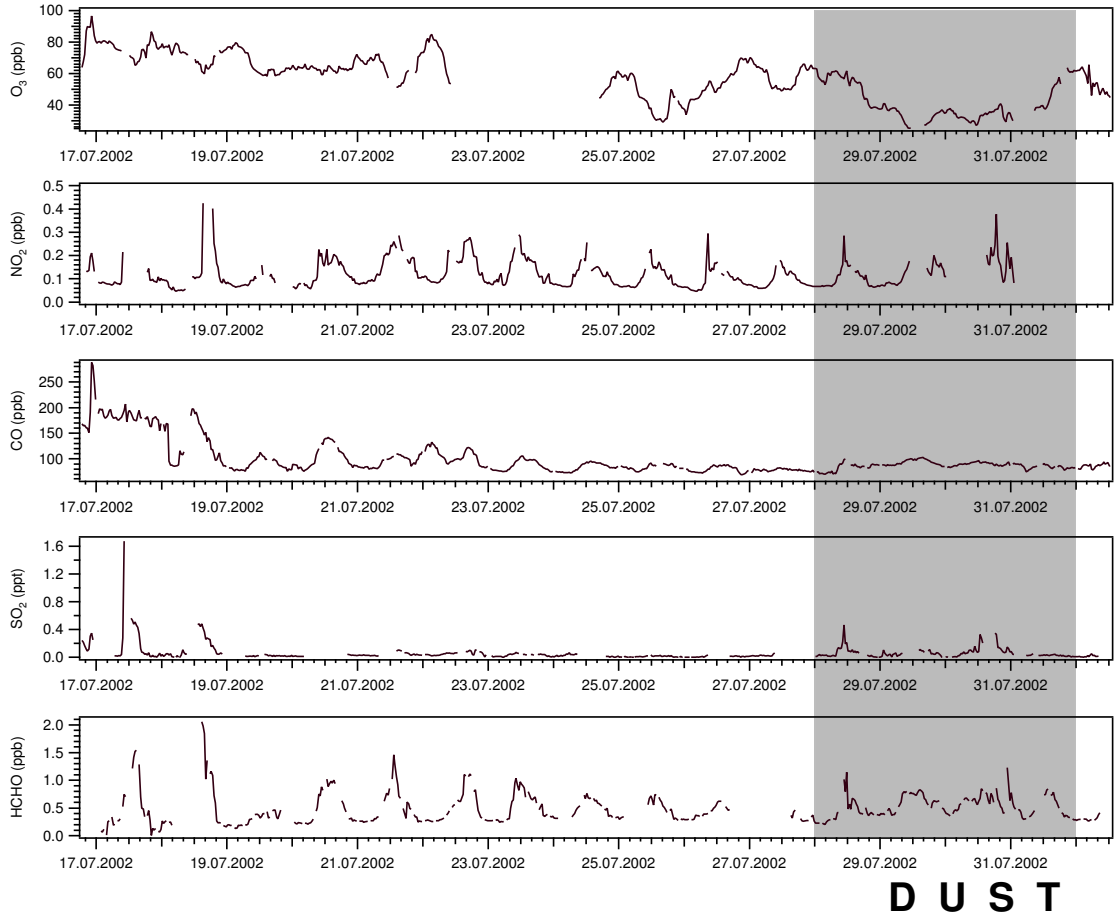

Fig. 5.7: Trace gas measurements during the MINATROC field campaign

5.3 Trace gas measurements

The measurements of the trace gases O_3, NO_2, CO, SO_2 and formaldehyde (HCHO) from July 16^{th} to August 1^{st}, 2002 are displayed in Fig. 5.7.
The instruments for all shown gases, except the CIMS used for SO_2 measurements [214], were operated from a laboratory container by the Max-Planck-Institute for Chemistry, Mainz (MPI-C). O_3 was measured with the UV absorption method (Ansyco 41M). An in-situ GC with a gas reduction (HgO) detector was applied to measure CO. A tunable diode laser absorption spectrometer was used for the measurement of NO_2. These instruments are described in Fischer et al. [215]. For the HCHO measurements, a liquid chemistry fluorescence detector (AERO laser model AL4021) was used. This instrument was previously used for airborne campaigns and is described in detail in [216].
O_3 varies from 25.1 ppb to 96.6 ppb, the average O_3 concentration is 56.6 ppb, the median 62.7 ppb. The data shows higher O_3 levels at the beginning of the field campaign, whereas during the main dust event the values are below the average. This

phenomenon of a lower O_3 concentration in air originating from the Sahara has been observed in several previous studies and attributed to heterogeneous removal of ozone on mineral dust [208]. NO_2 mixing ratios range between 0.05 ppb and 1.2 ppb. The average value is 0.12 ppb, the median 0.11 ppb. A diurnal cycle is visible with NO_2 increasing in the morning to a maximum around 12:00 UTC and decreasing again in the evening, minimum concentrations are measured during the night. CO shows con-

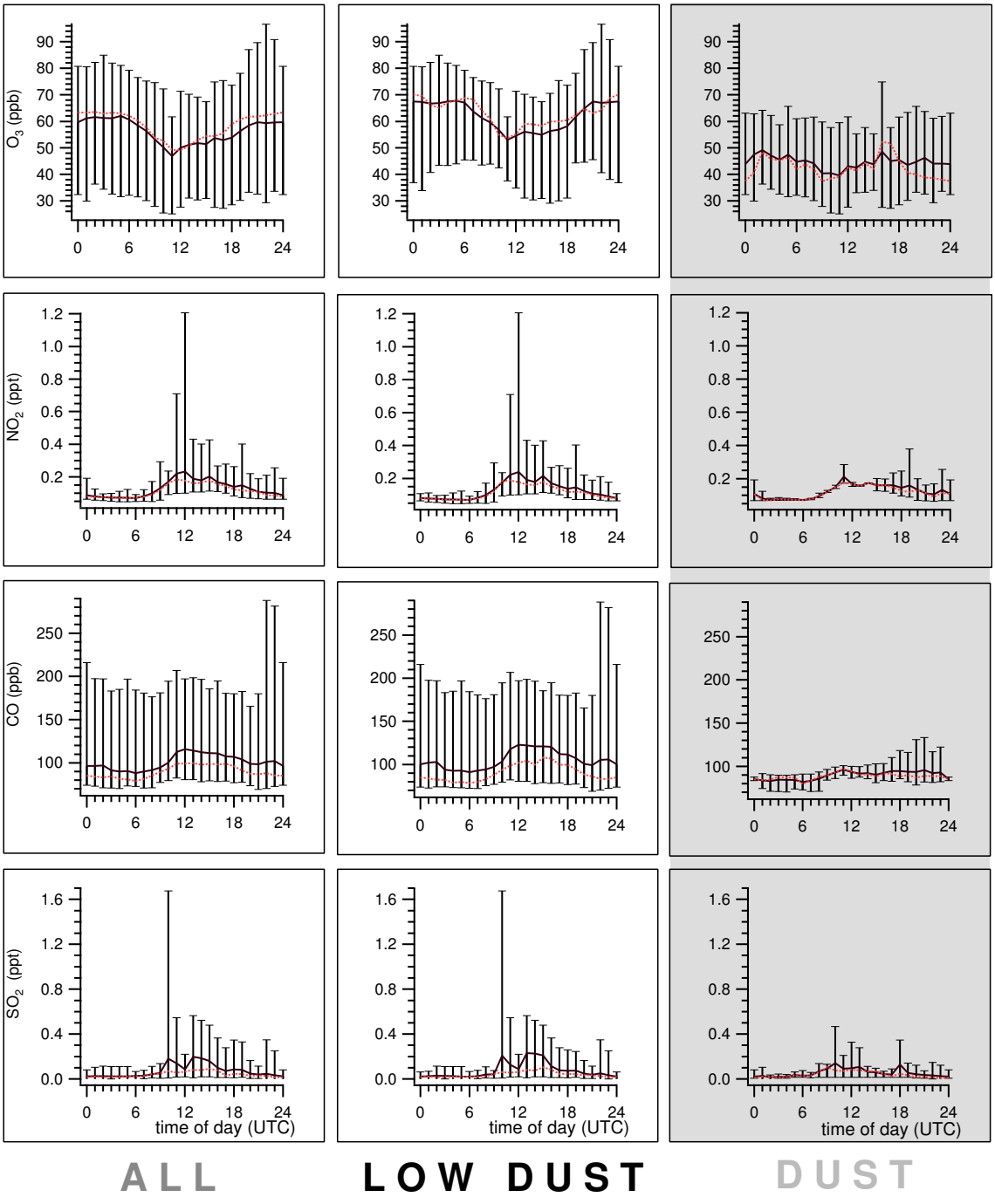

Fig. 5.8: contd.

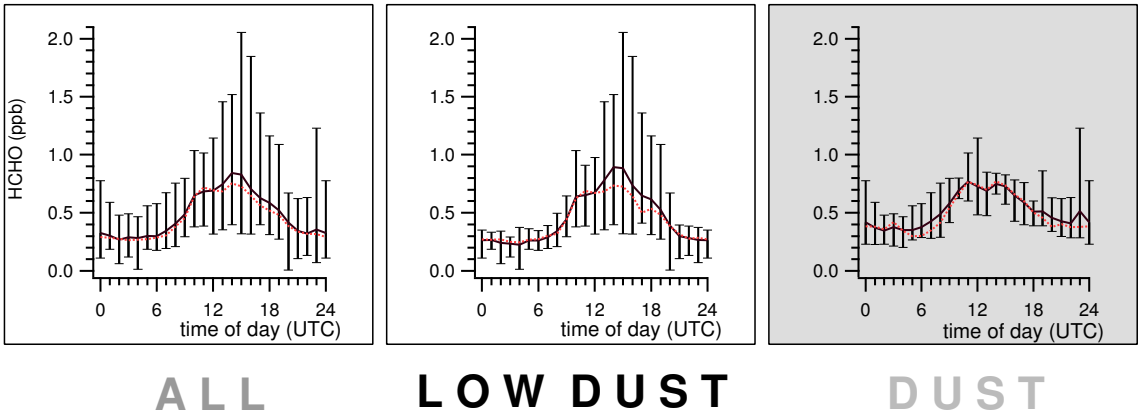

Fig. 5.8: Diurnal cycles of the trace gases. The black line illustrates the mean value, upper and lower bars the maximum and minimum measured value and the red line the median of the hourly data. Graphs on the left: during complete GC×GC measurements, middle: during the low dust period, July 16^{th} to 27^{th}, right: during the dust event, July 28^{th} to August 1^{st}

centrations between 69 ppb and 288 ppb, with an average of 99 ppb and a median of 89 ppb. For the first day, a continuously high CO level was seen during day and night, afterwards regular diurnal cycles occur. However, the daytime CO concentration was decreasing gradually after July 22^{nd} until July 28^{th}. During the dust event, only very weak diurnal cycles could be observed and the CO was higher than the days before. SO_2 ranges from below the detection limit of around 18 ppt to a maximum of 1.7 ppb. For most of the time, the atmospheric concentration was below the detection limit, weak diurnal cycles could be observed. Fig. 5.8 illustrates the diurnal cycles of the trace gases O_3, NO_2, CO, SO_2 and HCHO averaged over 1 hour. Some higher SO_2 levels during the day were measured at the beginning of the campaign and, with a smaller magnitude, during parts of the main dust event. The values for HCHO were between 6 ppt and 2 ppb. Highest mixing ratios were reached around noon, lowest during the night when the site was in the free troposphere. The average mixing ratio is 0.49 ppb, the median is 0.56 ppb. Again, diurnal profiles and higher variability can be seen until the main dust event on July 29^{th}, where the mixing ratios are also elevated during the nights and the diurnal cycles are suppressed. It is apparent, that the mixing ratios for all gases are somewhat lower during the dust event. Diurnal cycles can be observed for all trace gases due to the upslope flows on the mountain during the day (see section 5.2).

The diurnal cycle for O_3 shows a decrease throughout the morning leading to a minimum around 11:00. Higher levels are measured during the night when the station is situated in the free troposphere and O_3 rich air from the upper troposphere is descending. The diurnal cycle during the dust event is much less pronounced and the measured concentrations are lower. NO_2 shows a diurnal profile in which concentrations start rising in the morning as the site is influenced from the boundary layer and decreasing in the evening when the site is in the free troposphere. The maximum

is reached around noon. During the high atmospheric dust content, a similar cycle can be observed, but with lower concentrations. Similarly, the CO concentrations measured at the beginning of the campaign display a diurnal cycle with low values in the early morning hours. The steady high concentration between noon and 17:00 is a marker for anthropogenic influence originating from the marine boundary layer. After 17:00, with the calming of the upslope winds, the CO concentration decreases again. During the dust event, this cycle is only weakly pronounced and the mean concentrations appear to be much lower. However, a comparison of the diurnal median shows, that the values during the dust event as compared to the low dust period are only marginally lower. SO_2 is low during the night, increases quickly in the morning around 10:00, decreases until noon and then increases again throughout the early afternoon. A similar but weaker trend can be seen during the high atmospheric dust load. The medians of both CO and SO_2 are significantly lower than the mean. This indicates that the site has been affected by short-term pollution events. For SO_2, this mainly happens during the day, whereas for CO this can be observed during day and night. Compared to the period with low dust, the measurements of HCHO during the dust event indicate higher nocturnal mixing ratios, but lower mixing ratios during the day. The diurnal cycle shows a first peak in the morning around 8:00 and a second peak in the afternoon, both for low dust and high dust conditions.

5.4 Experimental Setup

The instruments operated by the MPI-C were situated in a container close to the Izaña observatory, see Fig. A.12 and A.13 on page 148 in the Appendix. The sample air inlet was installed on the roof of the container about 4 m above the ground. The main sampling line was a 9 mm i.d. Teflon line through which ambient air was drawn constantly at a flow rate of 75 l min^{-1}. Attached to this line were the GC×GC-FID, a PTR-MS and a canister sampling device, in this order. The GC×GC was connected to the main line via a T-piece 9.5 m from the inlet. The residence time in the main sampling line from the inlet to the GC×GC was calculated to be about 0.5 seconds. During the MINATROC field campaign the GC×GC system described in section 2.6.1 was set up in the on-line measurement mode, with the thermodesorbing unit, the flow controller and the GC×GC-FID. To concentrate the VOCs, a stream of 50 ml min^{-1} air was drawn from the main sampling line, through a 3.2 mm diameter Teflon tube, and into the cold trap of the GC×GC using a membrane pump. The exact details of sampling and analysis are shown in Table 5.1. Before the actual sampling started, ambient air or, in the case of a blank sample helium, was purged through the system without gas flowing into the cold trap, then the stream was directed onto the cold trap for a given time. To avoid the condensation of water, the cold trap temperature was set at 10°C, which was suitable for the target C_6-C_{14} organic compounds. After sampling, the cold trap was purged with helium for 4 minutes to remove any water present, and then heated up to 250°C in less than 5 seconds to inject the focused compounds onto the analytical column. This temperature was held for 5 minutes to ensure complete desorption.

For the gas chromatographic separation, a nonpolar 95% dimethylpoly- siloxane DB-5 column (30 m, 0.25 mm I.D., 1μm film, Agilent, Waldbronn, Germany) was employed in the first dimension and a polar polyethylene glycol Carbowax column (1 m, 0.1 mm I.D., 0.1μm film, Quadrex, Woodbridge, CT, USA) in the second dimension. Blank measurements with helium were carried out every 10 samples (15 hours), calibrations were done once every 2 days with a 74 compound VOC standard (Apel-Riemer, CT, USA) attached directly to the sampling inlet of the cold trap. Laboratory calibrations revealed a good linearity for the discussed VOCs, see also the experimental description of the HOHPEX-campaign (section 4.4). Based on this stability, only 2-point calibrations were carried out during the campaign.
The co-eluting p- and m-xylene were calibrated with o-xylene, the terpenes camphene and 3-carene were calibrated using α-pinene. Eucalyptol was indirectly calibrated with α-pinene. The calculations applied to obtain the atmospheric mixing ratios of the directly and indirectly calibrated compounds are described in the experimental part of the HOHPEX field campaign, see section 4.4.

Sampling data	Flow:	50 ml min^{-1}
	Duration:	60-80 min
	Volume:	3-4L
	Cold trap:	10°C (Tenax TA/Carbograph I)
Desorbing Data		
Desorption	Prepurge:	4 min
	Desorption:	250°C, 5 min (Tenax TA/Carbogr. I)
	Flow Path:	200°C
Analysis data		
First column	DB-5, 30 m, 0.25 mm I.D., 1μm film 40°C, 100°/min to 50°C, 2.5°/min to 200°C,	
Second column	Carbowax, 1 m, 0.1 mm I.D., 0.1μm film 40°C, 2.5°/min to 180°C (until 23.07.2002) 30°C, 2.5°/min to 180°C (from 23.07.2002)	
Analysis time	60 min	
Modulation	6 sec, four-jet system (Zoex, USA), nitrogen-cooled 200 ms upstream duration 300 ms downstream duration	

Tab. 5.1: Sampling, desorption and analysis data during the MINATROC campaign

The limit of detection (LOD) for the VOCs measured during the MINATROC campaign are shown in Table 5.2. The LOD was defined as two times the standard deviation (2σ) of the integrated baseline noise in the absence of a peak. It ranges from 0.1 ppt for camphene to 10.0 ppt for benzene. The high LOD for benzene is a result of a higher baseline at the beginning of the chromatogram.
The precision for the compounds measured during MINATROC ranges from 2.9% for heptane to 11.3% for octane and are also presented in Table 5.2. Factors influencing the precision of the GC×GC-FID are the uncertainties in flow and temperature control during sampling and analysis. Also contributing are the uncertainties in baseline

removal, peak integration and peak volume calculation of the individual compounds. To determine the precision of the measurements during the MINATROC field campaign, the 1σ standard deviation of all 250 ml calibration gas measurements was calculated.
The measurement accuracy for the VOCs discussed was determined from the geometrical mean of the relevant uncertainties. Influencing the accuracy of all organic compound measurements is the uncertainty in the calibration gas concentrations, which is given by the manufacturer as 2%. The peak integration

	LOD (2σ) ppt	Precision (1σ) %
Heptane	2.0	2.9
Octane	0.5	11.3
Nonane	0.5	5.0
Decane	0.7	9.6
Benzene	10.0	10.2
Toluene	2.5	10.2
Ethylbenzene	0.5	8.3
o-Xylene	5.0	9.4
p/m-Xylene	0.5	7.2
α-Pinene	0.3	6.7
Camphene	0.1	6.7
Eucalyptol	0.5	6.7
3-Carene	0.5	6.7

Tab. 5.2: Limit of detection (2σ) and precision (1σ) of the measured compounds for the MINATROC field campaign

and volume calculations also add to the uncertainty with an estimated 5%. The overall accuracy for the measurements of the organic compounds contained in the standard was assessed to be 5%, i.e. heptane, octane, nonane, decane, benzene, toluene, ethylbenzene, o-xylene, p/m-xylene and α-pinene. The same accuracy is valid for the terpenes 3-carene and camphene, which are directly calibrated with α-pinene. The accuracy for the indirectly calibrated oxygenated eucalyptol is evaluated to be around 11%. This is attributable to the possible inaccuracy of the calculated response factor used, which adds an estimated 10% to the overall accuracy. The determined accuracy ranges from 5 to 11 % for the compounds. Since similar compounds were analysed as during the HOHPEX campaign, the accuracy is in agreement with the values shown in chapter 4.
Fig. A.5 on page 142 in the Appendix shows a GC×GC chromatogram section of an ambient sample taken during the MINATROC field campaign, the VOCs which are presented here are marked.

5.5 GC×GC-FID VOC measurements: Results and discussion

5.5.1 VOC measurements over time

The results of the ambient air GC×GC-FID measurements between July 16^{th} and August 1^{st}, 2002 are shown in Fig. 5.10, 5.11 and 5.12. The long interruption in the measurements between July 19^{th} and 23^{rd} was caused by a failed delivery of liquid N_2, the short gaps towards the end of July were caused by a malfunctioning valve. Otherwise the measurements were interrupted only by calibration and blank measurements. The main Saharan dust event between July 28^{th} and August 1^{st} is marked with grey shading. The impact of the dust particles on the visibility during the major dust event is illustrated in Fig. 5.9. The left picture was taken during a low dust period, the Pico del Teide in the background is at a distance of about 10 to 15 km. The right photograph was taken during the major dust event on

Fig. 5.9: View of the Pico del Teide from the measurement site. The left picture was taken during the low dust period in July, the right picture from the same position during the major dust event on July 29^{th}, 2002

July 29^{th}, the visibility being so strongly reduced that the mountain can not be seen.

Shown in this section are the group of biogenic compounds including α-pinene, 3-carene, camphene and eucalyptol. Also shown are the anthropogenic aliphatic compounds heptane, octane, nonane and decane as well as the anthropogenic aromatic compounds benzene, toluene, ethylbenzene, o-xylene and p-/m-xylene, the so-called BTEX compounds. The lowest and the highest measured mixing ratios were found for the biogenically emitted VOCs.
Pronounced diurnal cycles are visible for the biogenically emitted VOCs α-pinene, camphene, 3-carene and eucalyptol in Fig. 5.10. To date there have been only few studies on the VOC emissions of Canary pine trees, but they are known to emit mainly the monoterpenes α- and β-pinene, myrcene and limonene [8, 217]. Investi-

gations of another pine tree species, the Scots pine, revealed amongst other terpenes the emission of all four biogenic compounds discussed in this section [15]. As already mentiond, the vegetation in the lower parts of the island is dominated by the Canary laurel *L. azorica*, which is mainly emitting α-pinene and eucalyptol [218] and tree heath *E. arborea*, which is a strong isoprene emitter. The influence of temperature on terpene emission from conifers has been documented in earlier studies where it was observed, that higher temperatures lead to an enhanced emission [7, 219]. In a recent study it was also noted, that the emission of oxygenated VOCs like eucalyptol

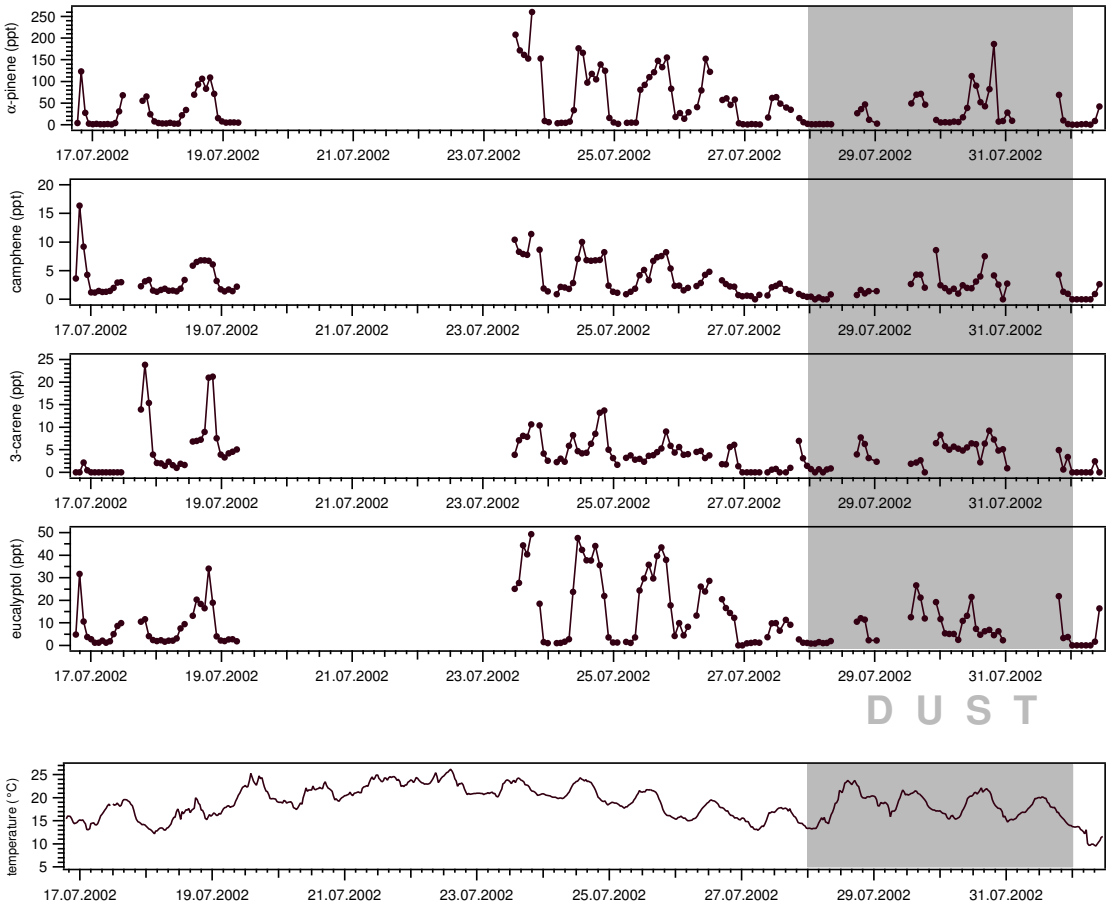

Fig. 5.10: Mixing ratios of measured biogenic VOCs. The markers represent the middle of the sampling, the grey shading indicates the major dust event. The gaps in the sampling between July 19^{th} and 23^{rd} are caused by liquid N_2 delivery failure, the small gaps later by technical problems

from Scots pine is not only temperature, but also light-dependent [15]. A light-dependent emission of the monoterpenes has also been observed in young conifer needles [10]. A strong light dependence for terpene emissions was established in several previous studies on the holm oak (*Quercus ilex)* and other deciduous trees [220, 221, 222, 184, 13]. These findings might also be relevant for the shrub present within the Canary pine forest. In accordance with these aforementioned stud-

ies, the measured mixing ratios of all biogenic compounds start to increase around sunrise with rising temperatures and light intensity and rapidly decrease again after sunset, when temperatures also decline. A general correlation between the magnitude of the presented compounds and temperature can also be observed. However, during the main dust event after July 29^{th}, the mixing ratios are lower for α-pinene, camphene and eucalyptol, even though temperatures during the day are relatively high (above 20°C). In this period, the mixing ratios of 3-carene appear to follow no cycle at all, but instead an almost constant level was observed. It is interesting to note, that during the dust event a two day period of increased relative humidity, with a mean of 42% as compared to 13% during the rest of the field campaign, was observed (July 29^{th} to 31^{st}). In this period, camphene, 3-carene and eucalyptol show higher than normal mixing ratios during the night. Studies carried out on the plant species *Quercus ilex* (evergreen oak) and *Pinus pinea* (Mediterranean pine) showed, that drought and decreased relative humidity inhibit the emission of biogenic VOCs [223, 224]. It can be speculated whether the emission of terpenes was favoured by the increased water content in the atmosphere or alternatively that other factors such as markedly different local meteorology under dust conditions played a more important role. The mixing ratios of the biogenic VOCs measured at Izaña are the result of the light and temperature depending emission and the VOCs individual reactivities and lifetimes in the atmosphere. All biogenic compounds are below the detection limit at least during one night, α-pinene and eucalyptol are detected only rarely during the night, whereas camphene and 3-carene show increased levels on several occasions. The maximum mixing ratio found for the biogenic compounds was α-pinene with 260.6 ppt, followed by eucalyptol with 49.3 ppt, 3-carene with 23.8 ppt and camphene with 16.4 ppt. The mean values are for α-pinene 45.0 ppt, eucalyptol 11.4 ppt, 3-carene 4.1 ppt and camphene 3.1 ppt. The median of the mixing ratios is lower than the mean value, with α-pinene at 33.7 ppt, eucalyptol 9.8 ppt, 3-carene 4.0 ppt and camphene 2.4 ppt.

The measurements of the aliphatic compounds are depicted in Fig. 5.11. The alkanes heptane, octane, nonane and decane discussed in this chapter originate mainly from car exhaust, gasoline spillages and solvents [4]. On close inspection these anthropogenic VOCs exhibit weak diurnal cycles with gently rising and falling gradients. This effect is caused by transport of local pollution with the upslope winds developing during the day as described in section 5.2. At the beginning of the GC×GC measurements, the mixing ratios of the aliphatic as well as the aromatic compounds were slightly higher than during the remaining period. This is accompanied by continuously high concentrations in CO (about 180 ppb) and O_3 (about 80 ppb), indicating the presence of polluted air masses at Izaña. Back-trajectories showed, that the smoke plume from large forest fires in Quebec, Canada, could have been influencing the measurements in that period. Higher levels of CO were occasionally also measured during the dust event, however, these events appear to be associated with local emissions. The highest mixing ratio measured was 23.1 ppt for octane at the beginning of the campaign, followed by 21.3 ppt for heptane, 18.4 ppt for decane and 10.9 ppt for nonane. Minimum measured values were below the detection limit for octane, 0.7 ppt for nonane, 1.3 ppt for decane and 2.3 ppt for heptane. The mean

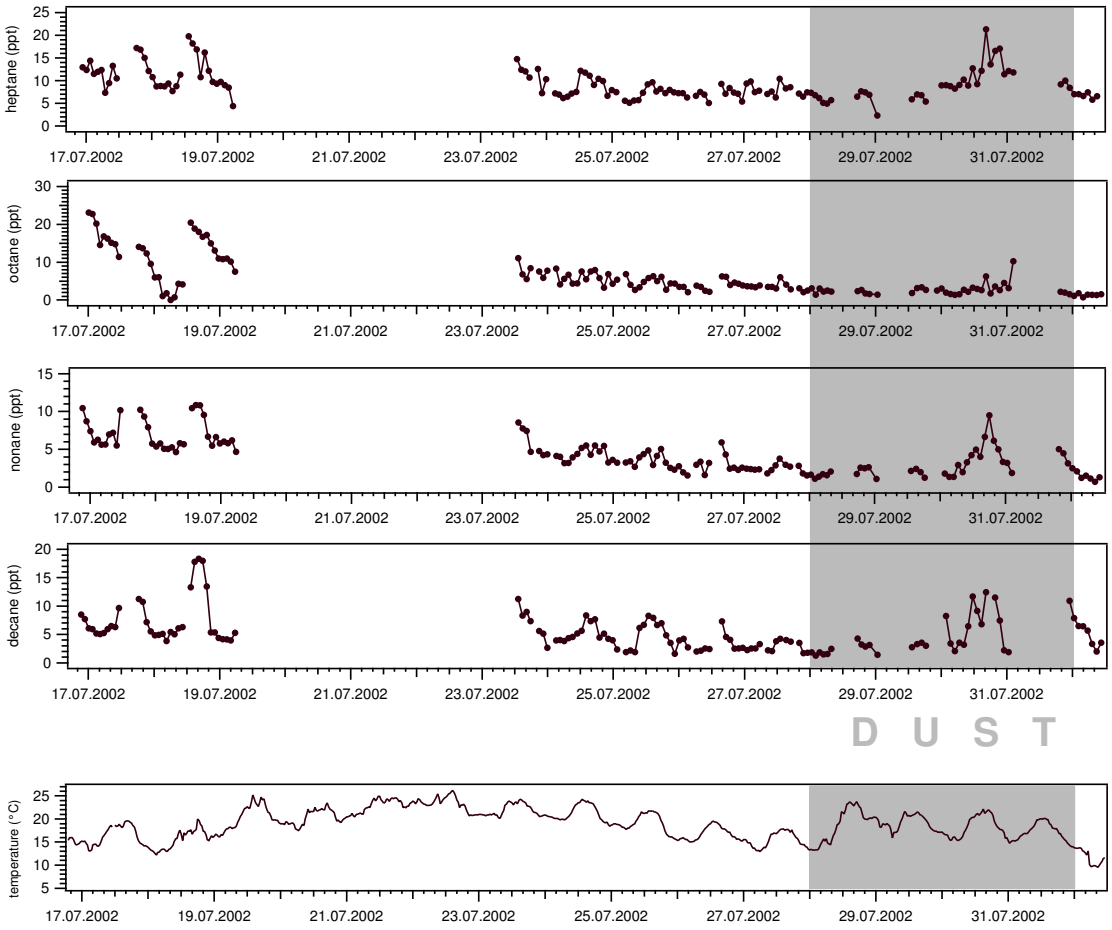

Fig. 5.11: Mixing ratios of measured aliphatic VOCs. The markers represent the middle of the sampling, the grey shading indicates the major dust event. The gaps in the sampling between July 19^{th} and 23^{rd} are caused by liquid N_2 delivery failure, the small gaps later by technical problems

value calculated for the measurement period is 9.2 ppt (median 9.1 ppt) for heptane, 5.9 ppt (median 4.7 ppt) for octane, 4.2 (median 4.4 ppt) for nonane and 5.3 ppt (median 5.3 ppt) for decane.
The aromatic BTEX compounds are illustrated in Fig. 5.12. Benzene, toluene, ethylbenzene and the xylenes are mainly emitted from petroleum, chemical and refining industries as well as car exhaust [4, 225]. Similar to the aliphatic compounds, the BTEX group shows higher mixing ratios during the first 2 days and also display weak diurnal cycles throughout the measurement period. The continuously high level of benzene until July 18^{th} can be attributed to the biomass burning plume mentioned earlier. The maximum measured mixing ratio was found for benzene with 158.2 ppt, o-xylene with 101.3, toluene with 109.7, ethylbenzene with 16.1 ppt and the co-eluting p-/m-xylene with 8.9 ppt. They are therefore mostly at much higher concentrations than the aliphatic compounds that have similar sources. Minimum mixing ratios measured during the campaign were 0.7 ppt, 0.9 ppt, 3.1 ppt, 10.5 ppt and 14.1

ppt for ethylbenzene, p-/m-xylene, toluene, o-xylene and benzene, respectively. The calculated mean values were 3.5 ppt for ethylbenzene (median 3.0 ppt), 3.0 ppt for p-/m-xylene (median 3.0 ppt), 18.5 ppt for toluene (median 14.8 ppt), 35.2 ppt for o-xylene (median 29.8 ppt) and 63.5 ppt for benzene (median 59.4 ppt).
The diurnal cycles of the anthropogenic and biogenic compounds shown here are discussed in the following section.

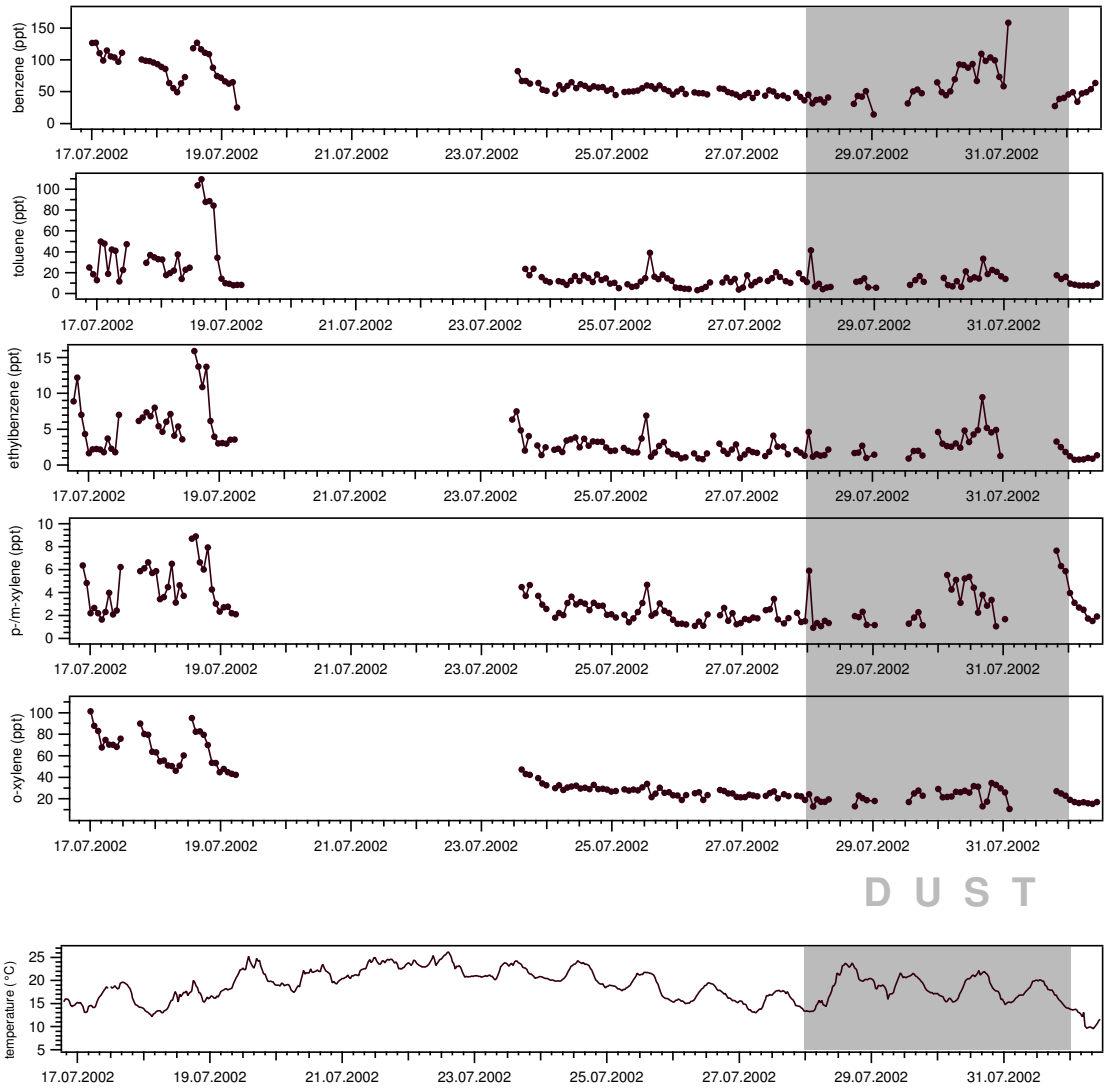

Fig. 5.12: Mixing ratios of measured aromatic VOCs. The markers represent the middle of the sampling, the grey shading indicates the major dust event. The gaps in the sampling between July 19^{th} and 23^{rd} are caused by liquid N_2 delivery failure, the small gaps later by technical problems

5.5.2 Diurnal cycles

The diurnal cycles for the compounds measured with GC×GC-FID during the field campaign are shown in Fig. 5.13, 5.14 and 5.15. The hourly means were obtained by assigning the mean sampling time to the nearest whole hour. In the left column,

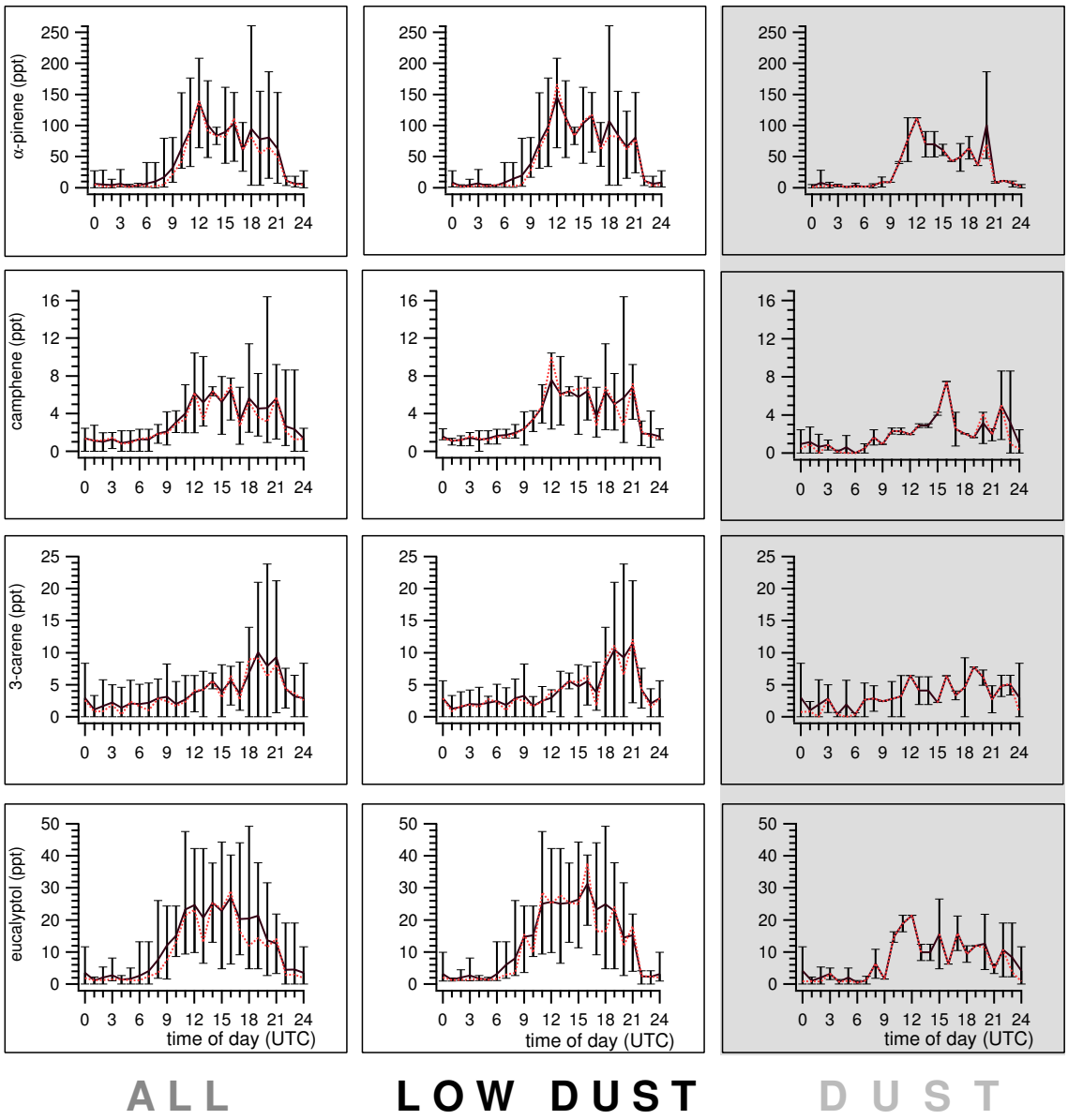

Fig. 5.13: Diurnal cycles of measured biogenic VOCs, averaged over 1 hour. Shown are measurements during different periods. Left column: July 16^{th} to August 1^{st}, 2002, middle: before the main dust event, July 16^{th} to 27^{th}, right column: during the dust event, July 28^{th} to August 1^{st}. The black line shows mean values, upper and lower bars the maximum and minimum measured value, the red dotted line represents the median value. All times are in UTC, which was 1 hour behind local time

hourly means of all analyses during the field campaign from July 16^{th} to August 1^{st}, 2002 are depicted. The graphs in the middle column contain only data from the measurements carried out before the main dust event, i.e. from July 16^{th} to 27^{th}. As already mentioned in section 5.2, Saharan dust was present at low concentrations throughout the course of the campaign [213], and hence this period was termed 'low dust'. The graphs in the right-hand column show the diurnal cycles of the measurements during the main dust event, July 28^{th} to August 1^{st}.

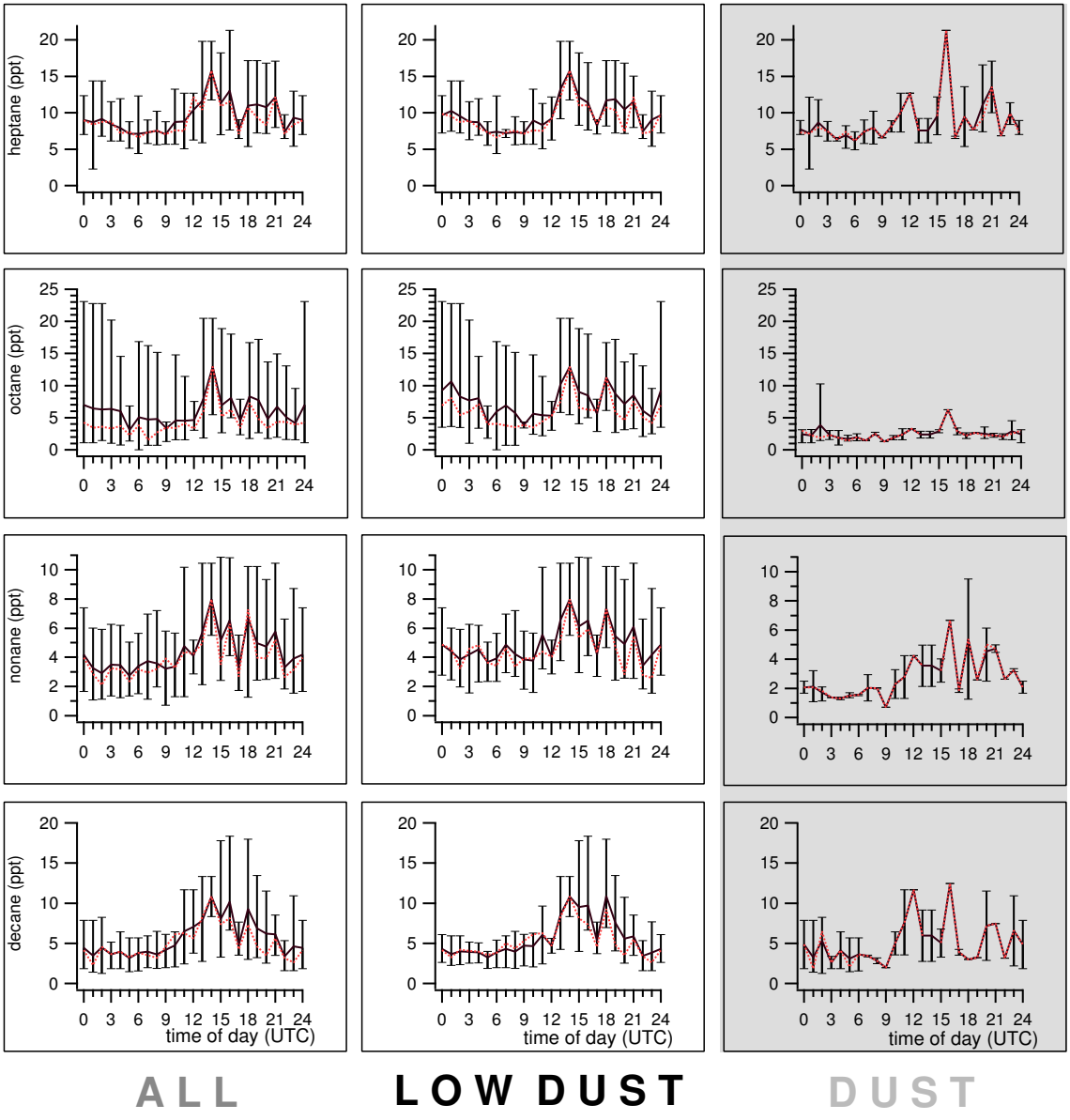

Fig. 5.14: Diurnal cycles of measured aliphatic VOCs, averaged over 1 hour. Shown are measurements during different periods. Left column: July 16^{th} to August 1^{st}, 2002, middle: before the main dust event, July 16^{th} to 27^{th}, right column: during the dust event, July 28^{th} to August 1^{st}. The black line shows mean values, upper and lower bars the maximum and minimum measured value, the red dotted line represents the median value. All times are in UTC as in previous figure

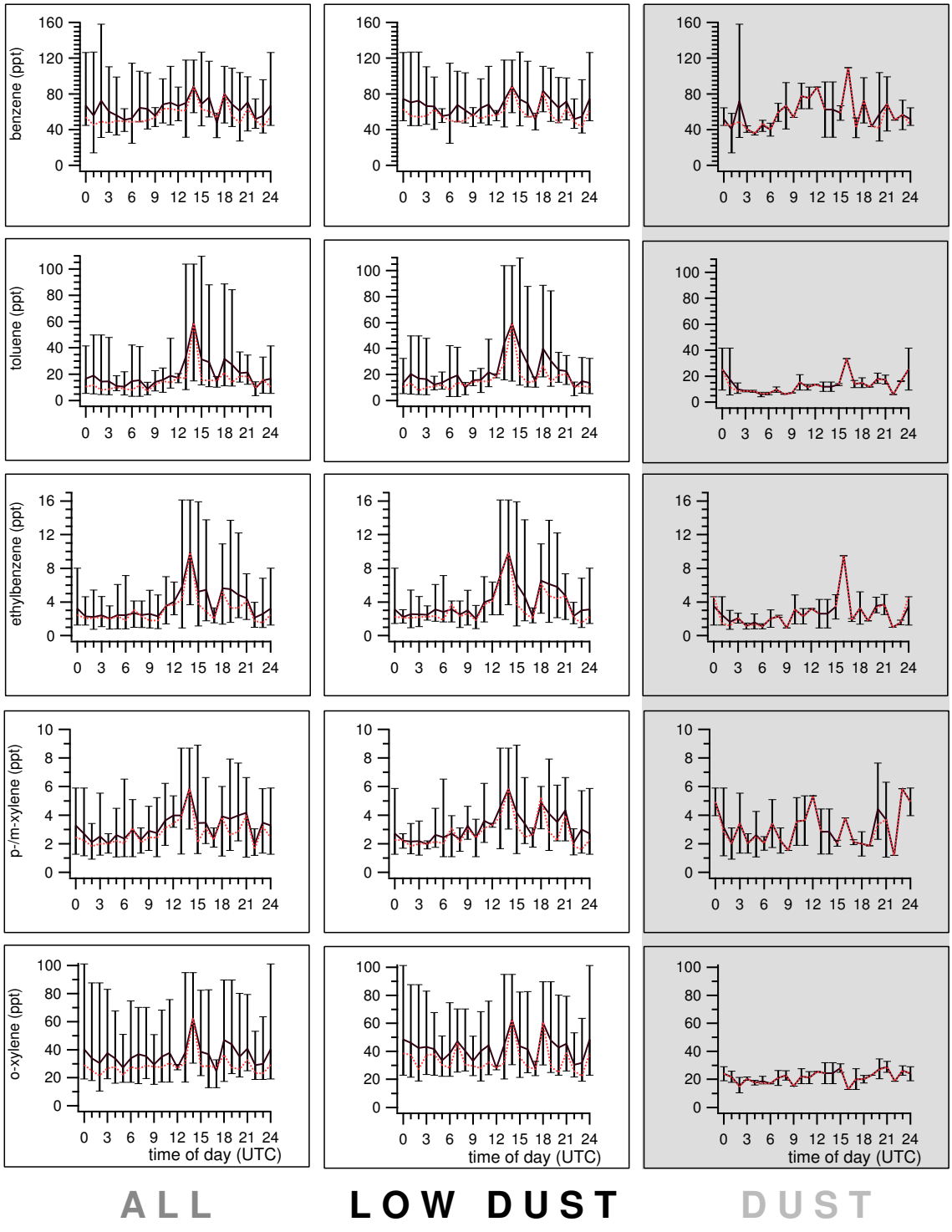

Fig. 5.15: Diurnal cycles of measured aromatic VOCs, averaged over 1 hour. Shown are measurements during different periods. Left column: July 16^{th} to August 1^{st}, 2002, middle: before the main dust event, July 16^{th} to 27^{th}, right column: during the dust event, July 28^{th} to August 1^{st}. The black line shows mean values, upper and lower bars the maximum and minimum measured value, the red dotted line represents the median value. All times are in UTC, as in previous figure

Due to technical problems in this period and the limited duration of the event, only a small dataset is available (two data points per hour). In the graphs, the black lines illustrate the hourly mean value of the measured mixing ratios, the upper and lower bars represent maximum and minimum measured value, respectively and the red dotted line the median value. All graphs have the same scaling on the ordinate to illustrate contrasts between the individual periods.
The biogenically emitted VOCs α-pinene, 3-carene, camphene and eucalyptol in Fig. 5.13 show clear diurnal cycles, albeit with differing patterns. Maximum mean mixing ratios for α-pinene were measured around noon, whereas 3-carene shows the highest mixing ratios in the evening between 19:00 and 21:00. Camphene and eucalyptol display no apparent maximum in the mean mixing ratios throughout the day, but instead a relatively constant high level. Measured mixing ratios of the terpenes are low during the night and increase in the morning with rising temperature and increasing light, as already mentioned in section 5.5. An indication for nocturnal α-pinene emission of the broom vegetation surrounding the station can be taken from the plots. The biogenic compounds eucalyptol, camphene and 3-carene are close to the instruments' detection limits most of the time, whereas α-pinene exhibits mean mixing ratios clearly above the detection limit. Transport of VOCs emitted from vegetation in lower regions can be excluded, since the atmospheric lifetime of α-pinene during the night is as short or shorter than the lifetimes of the other biogenic VOCs (see Tab. 1.1 on page 11). During the dust event, mean mixing ratios are generally lower for all biogenic compounds and the diurnal patterns are less pronounced or absent compared to the remaining measurement period.
The aliphatic compounds heptane, octane, nonane and decane are shown in Fig. 5.14. The highest mean mixing ratios were measured around 14:00 for all alkanes, a daily minimum is visible around 17:00, followed by a second peak. The lowest values were found in the early morning, since mean mixing ratios generally decrease slowly during the night, when the station is isolated from local sources. Mean mixing ratios are lower during the dust event. Octane was mostly close to the detection limit, whereas the other alkanes show strong hourly variations during the day.
The diurnal cycles of the BTEX compounds are illustrated in Fig. 5.15. Similar to the alkanes, the mean mixing ratios peak around 14:00 and 18:00 during the low dust period. Additionally, the mean mixing ratios show the same minimum around 17:00 and lower values during the night. This diurnal pattern was found to be only weakly pronounced for benzene and o-xylene. During the dust event, toluene and o-xylene show almost no difference in mixing ratios between day and night, whereas the remaining aromatic VOCs show similar hourly variations than during low dust conditions.
Generally it can be said, that the increase for the mixing ratios of the anthropogenic compounds observed in the late morning is caused by the upslope transport of pollutants. Presumably, these dynamic vertical winds intensify with continuing solar irradiation and warming of the ground, thus shortening the transport time from the coastal area to the measurement site. For an average vertical wind speed of 1 m s^{-1}, transport takes 4 hours, whereas for an average vertical wind speed of 5 m s^{-1}, the transport time is shortened to 50 minutes. Contributing to the increased levels of

anthropogenic VOCs throughout the day is tourist traffic passing the station to the north in a distance of a few hundred meters. The measurements of biogenic VOCs are already influenced in the morning from emission of surrounding vegetation as well as from the forest above the inversion layer. In the afternoon, the upslope wind additionally carries emitted compounds from below or in the inversion layer. The mean mixing ratios of all measured VOCs are lower during the dust event and weakened or no diurnal cycles can be observed.

5.5.3 Influence of wind direction

The influence of the wind direction on the mixing ratios of the measured VOCs during the low dust period (July 16^{th} to July 27^{th}, 2002) and the dust event (July 28^{th} to August 1^{st}, 2002) is examined in this section. Fig. 5.16, 5.17 and 5.18 illustrate the mixing ratios found, the graphs on the left side show the time period with low dust in the atmosphere whereas the graphs on the right side show the time during the elevated dust load. The black markers represent measurements carried out during the night (22:00 to 6:00 UTC), when the station is assumed to be in the free troposphere [208], the blue markers represent measurements during the day (6:00 to 22:00 UTC). As can be seen in the polar plots, the main wind direction is northwest. This direction prevailed at the beginning of the campaign, but turned to the southeast during the dust event.
Fig. 5.16 shows the wind directional plots of biogenically emitted VOCs. Measurements conducted in the daytime show higher mixing ratios than at night for the low dust period. For air masses arriving from the northwest, the mixing ratios are highest, only 3-carene shows additionally higher levels to the south. Studies show, that the emission of biogenic VOCs depends strongly on factors like climate, vegetative cover, leaf biomass and the emission characteristics of the individual species [7, 226, 8]. A possible explanation for the differences in biogenic compound mixing ratios is therefore provided in the meteorological conditions and the resulting vegetation on the island, see section 5.1 and 5.2. While the southern part of the island is dry with only sparse vegetation, the northern part is subtropical with a greater number and variety of plant species, and presumably stronger VOC emission.
During the main dust event from July 28^{th}, the mixing ratios are lower than during the earlier measurement period, α-pinene for example has a calculated mean mixing ratio of 52.3 ppt for the low dust period as compared to 28.2 ppt during the dust event. However, if only the air masses arriving from the southeastern direction are considered, the mixing ratios during the dust event are higher. As can be seen, the measured mixing ratios in the period of the higher atmospheric dust load are similar during day and night, except for α-pinene. The possible influence on the biogenic mixing ratios caused by the increased atmospheric humidity or changes in the local meteorology has already been described in section 5.5.
The alkanes heptane, octane, nonane and decane are depicted in the polar plots of Fig. 5.17. With the exception of octane, the mixing ratios during the days with low dust are higher than during the respective nights. The highest mixing ratios were

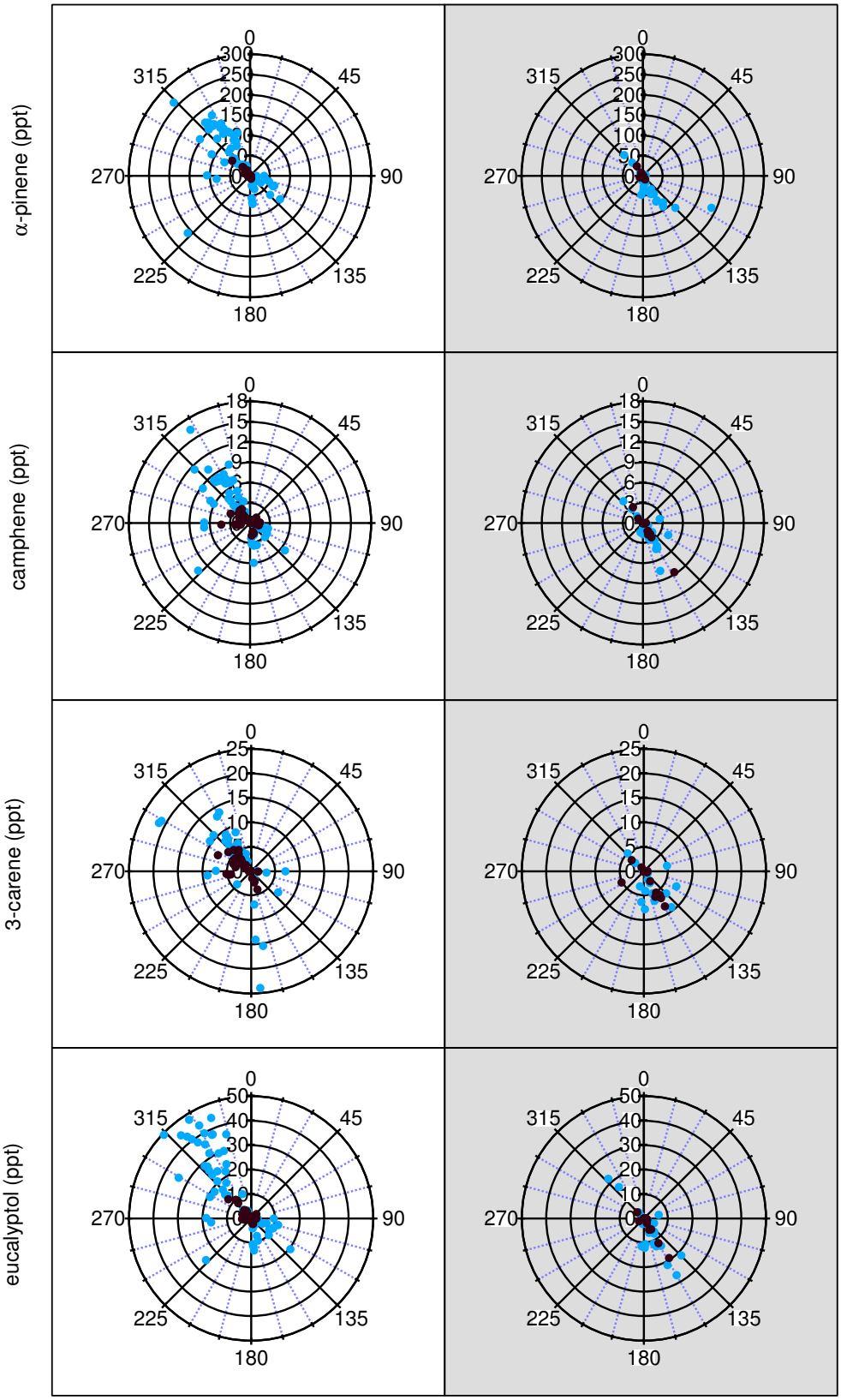

Fig. 5.16: Wind direction plots of measured biogenic VOCs, the mixing ratios are in ppt. Blue markers represent daytime measurements (6:00 to 22:00 UTC), black markers nighttime measurements (22:00 to 6:00 UTC). Graphs on the left show the low atmospheric dust period (July 16^{th} and 27^{th}, 2002), the right graphs the measurements during the dust event (July 28^{th} and August 1^{st}, 2002)

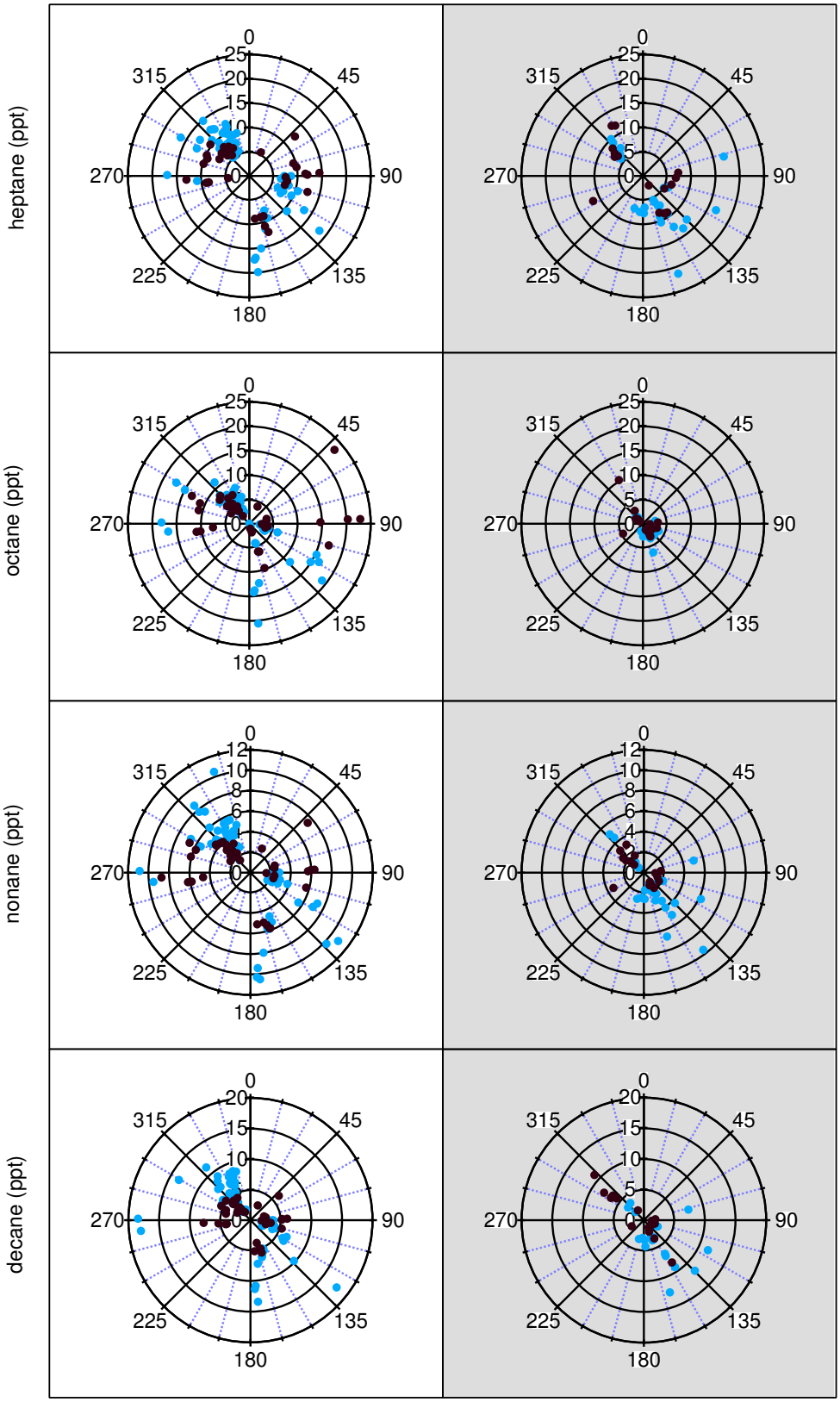

Fig. 5.17: Wind direction plots of measured alkanes, the mixing ratios are in ppt. Blue markers represent daytime measurements (6:00 to 22:00 UTC), black markers nighttime measurements (22:00 to 6:00 UTC). Graphs on the left show the low atmospheric dust period (July 16^{th} and 27^{th}, 2002), the right graphs the measurements during the dust event (July 28^{th} and August 1^{st}, 2002)

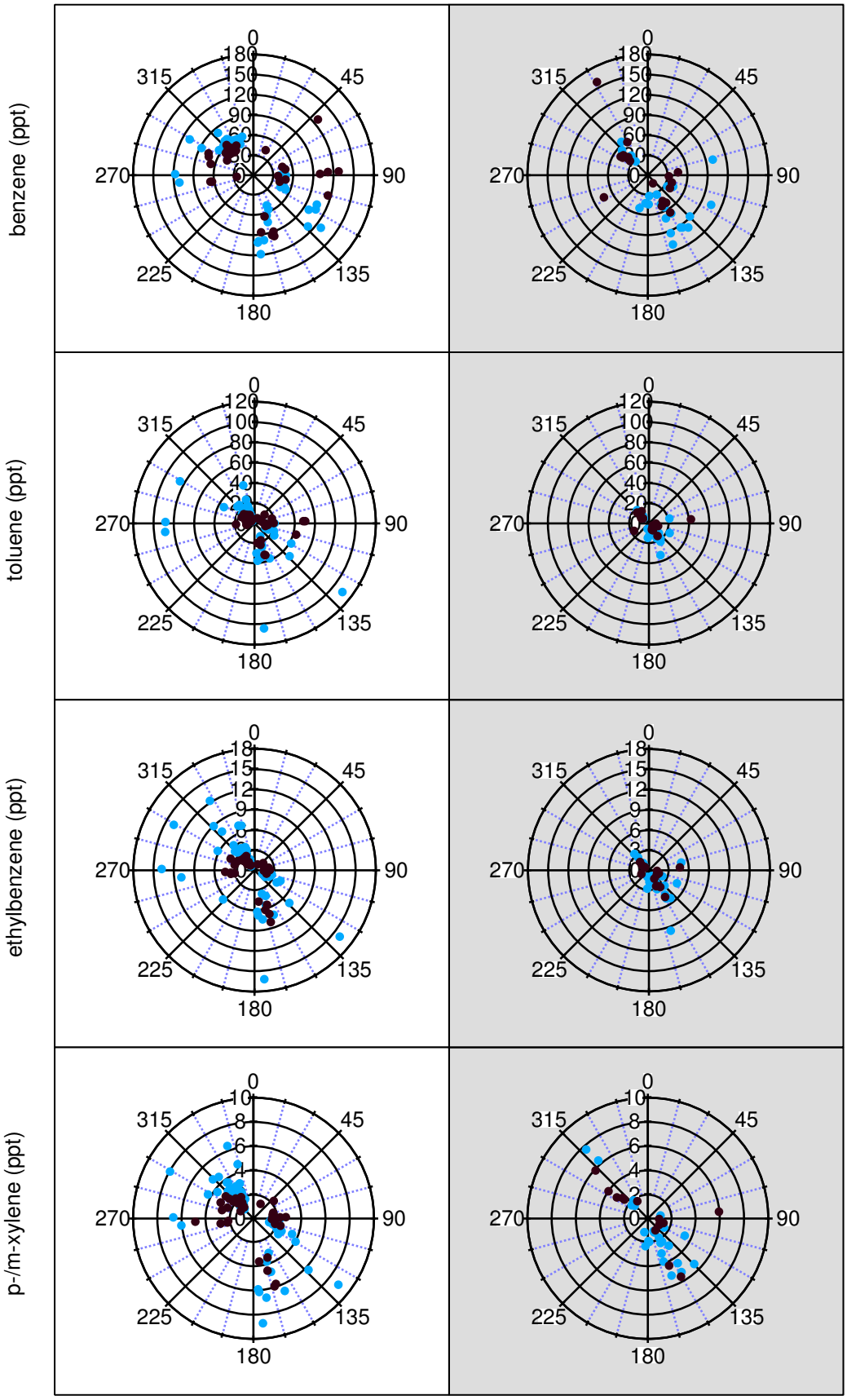

Fig. 5.18: contd.

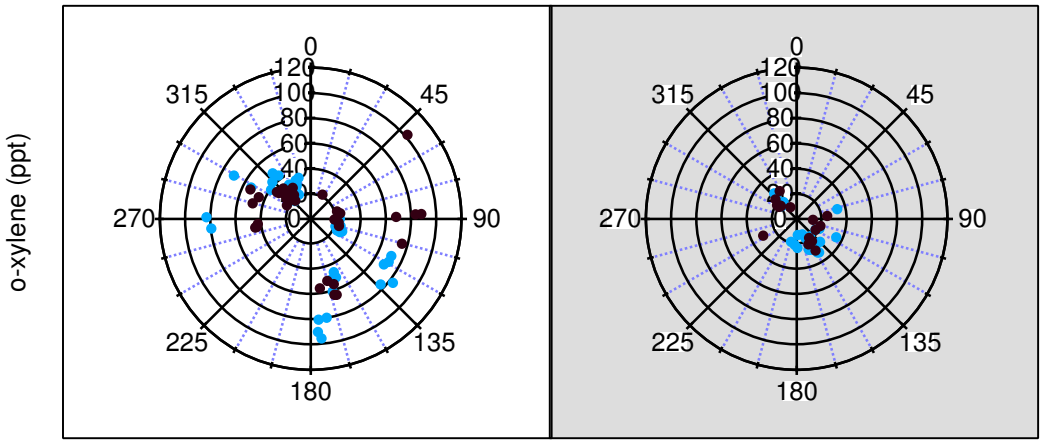

Fig. 5.18: Wind direction plots of measured aromatic compounds, the mixing ratios are in ppt. Blue markers represent daytime measurements (6:00 to 22:00 UTC), black markers nighttime measurements (22:00 to 6:00 UTC). Graphs on the left show the low atmospheric dust period (July 16^{th} and 27^{th}, 2002), the right graphs the measurements during the dust event (July 28^{th} and August 1^{st}, 2002)

found in air masses arriving from the southeast, but elevated levels were also detected from the northwest. Sources of the alkanes examined here include car exhaust, gasoline spillages and solvents [4]. Elevated mixing ratios measured in northerly and westerly wind direction can be explained by the road passing the station close by to the north and the emissions of Puerto de la Cruz (north to the site, see Fig.5.3) that are channeled and transported through the Orotava valley. The coastal road and the power station located downhill to the south and east of the observatory could explain the higher aliphatic mixing ratios observed in these directions. Transport of VOCs from the northern or southern coast to the observatory takes approximately 4 hours at an assumed wind speed of 1 m s^{-1} or 50 minutes at a wind speed of 5 m s^{-1}, since the distance is only 15 km. Generally, the alkane mixing ratios during the dust event were lower than during the low dust period. In the dust event, only octane stayed close to the detection limit, the other alkanes show elevated mixing ratios. The highest levels for aliphatic VOCs were measured for air masses arriving from southeast. Curiously, except for nonane, the nocturnal mixing ratios arriving from northwest were equally high or higher than daytime mixing ratios. This coincides with the observation of elevated SO_2 levels and indicates the presence of an anthropogenically polluted air mass.
The aromatic compounds are shown in Fig. 5.18. In the first few days of the campaign, benzene and o-xylene, maintain high mixing ratios during the nighttime even, when the station is obviously situated in the free troposphere. This observation coincides with the biomass burning plume from Canada reaching the station. The high levels measured during the night are most likely caused by the presence of the fire emissions. Aromatic compounds have similar sources to the alkanes, such as the chemical and refining industry as well as car exhaust [4, 225], which is why they show similar wind direction dependencies for all observed anomalies. During the dust event

the measured mixing ratios were much lower except for benzene and the co-eluting p-/m-xylene.
All measured compounds analysed in this section showed similar differences between the low dust and high dust period. Anthropogenic mixing ratios were generally lower during the dust event at the end of July. Biogenically emitted VOCs show higher mixing ratios with air masses arriving from the northwest, whereas anthropogenic compounds display increased mixing ratios from all prominent wind directions, i.e. between west and northwest as well as between east and south.

5.6 Summary and conclusion

During the MINATROC field campaign at the meteorological observatory Izaña (Tenerife, Spain) in July and August 2002, C_6 to C_{14} organic compounds were measured using a new GC×GC-FID analytical system. The main aim was the characterisation of the measurement site with respect to anthropogenic and biogenic VOCs during the day when the site is influenced by dynamic transport processes originating from the boundary layer, and the night, when the site is situated in the free troposphere. Furthermore, the influence of Saharan dust on the measured mixing ratios was examined.

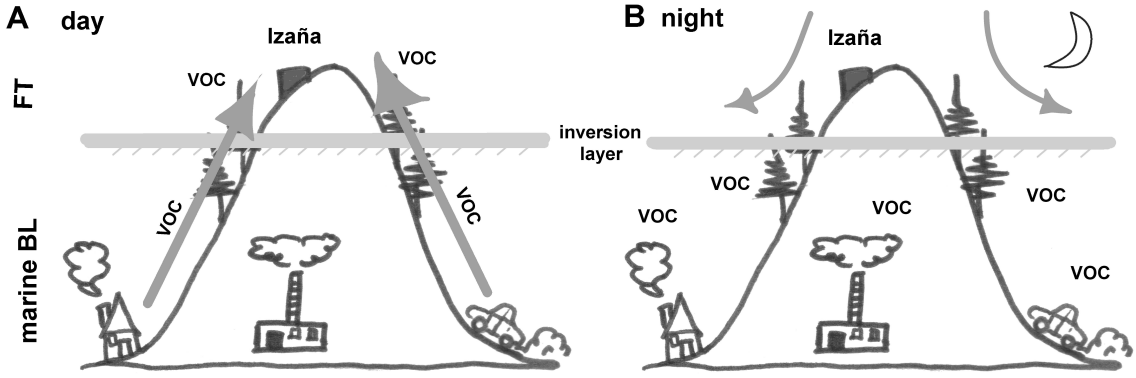

Fig. 5.19: Schematic diagram of the daytime and nighttime function of the inversion layer on Tenerife during the low dust period. A. The left picture shows the upslope winds passing the inversion layer during the day. B. On the right picture during the night, no transport from pollution below the inversion layer to the station occurs

Generally, the measurement site Izaña is influenced by biogenically emitted compounds by both day and night. It was also observed, that locally emitted anthropogenic compounds affect the site mainly during the day, although some evidence of long distance transport of biomass burning pollution was also seen on one occasion. The upslope wind transports the anthropogenic and biogenic emissions from the boundary layer from the early to the late afternoon, see the schematic diagram in Fig. 5.19 A. This can be seen particularly in the diurnal cycles of the anthropogenic compounds, which are mostly emitted at the coast. Mixing ratios start

to increase shortly before noon and decrease again after 18:00. Transport of anthropogenic VOCs from the coastal city Puerto de la Cruz for example would take approximately 50 minutes at assumed wind speed of 5 m s^{-1}. Similar transport times can be expected for pollution originating from the east, where the small industrial town Güímar (population 15 000) and a fuel gas power plant are situated, or the south, with mainly smaller villages, the coastal road and a further power plant. Additionally, the emissions of the traffic passing the observatory on the tourist road can influence the measurements, particularly in the afternoon. Both dynamic processes and varying car emissions during the day cause the observed anthropogenic diurnal cycle. Compared to the day, the nocturnal mixing ratios are low and tend to show almost no fluctuation. The influence of the MBL and the coastal cities is stopped by the inversion layer and background free troposphere concentrations predominate, see Fig. 5.19 B.
In contrast, the biogenic compounds show a different pattern with a slow increase in the early morning beginning at sunrise and rising with temperature, remaining steady at high mixing ratios throughout the daylight period, and a quick decrease at sunset with the onset of cooler temperatures. During the night, the measured mixing ratios were considerably lower as compared to the day. Similar temperature and light intensity dependencies have been also observed in other studies [7, 15, 219, 220] and were discussed earlier in section 5.5. A small fraction of the early morning increases in biogenic VOC emissions can certainly be assigned to the sparse vegetation surrounding the station. However, the major role is played here by the emissions of the pine forest situated above the inversion layer. The inversion is at an approximate altitude of 1400 m during the summer, cutting off the lower part of the forest and the populated areas in the boundary layer. However, since the pine forest extends to approximately 2000 m, VOCs emitted above the inversion can be mixed up quickly to the measurement site. As can be seen in Fig. 5.3, the forested area is at a distance of around 5 km to the north and much closer to the south. The transport from the forest situated in a north/northwesterly direction would take approximately 45 minutes and from the south even less at a wind speed of 1 m s^{-1}. For an assumed wind speed of 5 m s^{-1}, transport would take only 20 minutes.

During the dust event from July 28^{th} to August 1^{st}, 2002, measured mixing ratios in the daytime for both anthropogenic and biogenic compounds were generally lower than in the period before. Interestingly, a few hours after the dust plume arrived at Tenerife, the CO concentration increased to around 80 ppb and remained almost constant at this level throughout day and night, see Fig. 5.7. This suggests anthropogenic pollution in the dust laden air masses arriving at Izaña. A similar effect can not be observed for the aromatic and aliphatic compounds measured, however the atmospheric lifetime of CO is with around 2 months much longer than the lifetimes of the anthropogenic VOCs measured with GC×GC (1 day to 15 days). We therefore assume aged but polluted air affected the site in this time. The relative humidity levels also increased markedly, indicating mixing of the more humid MBL air with the dry, free tropospheric air. Temperature soundings launched from Santa Cruz de Tenerife showed, that the inversion layer was lower down during the night of July 29^{th}. The temperature inversion re-established itself at around

1.5 km on August 1^{st}, 2002. Measurements of the wind direction showed that from sea-level to the observatory air arrived from between south and southeast. On July 30^{th}, however, the wind direction turned east before swinging to the north during the night. LIDAR measurements conducted during the campaign showed that the dust layer extended to about 7 km altitude, and hazy conditions prevailed down to sea level throughout the event [213]. From the observations presented it can be assumed, that the inversion was weakened or did not exist during parts of the dust event. In which case the marine boundary layer was not clearly separated from the free troposphere in this period. Fig. 5.20 shows a schematic diagram of the flow regimes at the onset of the Saharan dust on the left side and for the well mixed dust influenced troposphere, i.e. without the separation in BL and free troposphere during the dust event.

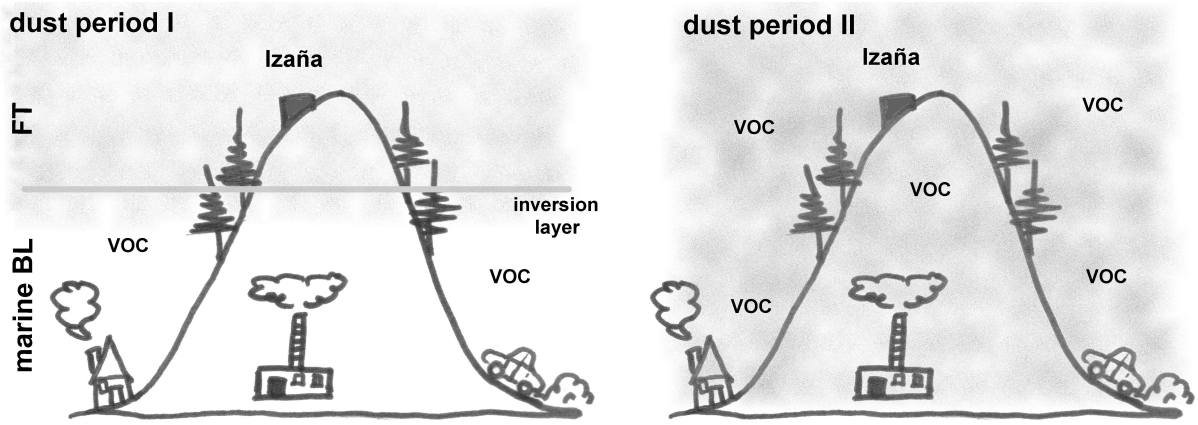

Fig. 5.20: Schematic diagram of inversion layer during the dust event. The left picture shows the beginning of the dust period, the inversion layer is still separating the BL from the free troposphere. The right picture shows the rest of the dust event, where the BL and the free troposphere are well mixed

Weak diurnal cycles can be observed for some of the anthropogenically emitted compounds, but toluene, ethylbenzene, o-xylene and octane display no cycle at all during the dust event. Their mixing ratios remain low in the range of the nocturnal free tropospheric air measurements. This can be either attributed to the less populated area with less industry towards the southeast or to dust related dynamic effects. A comparison of the measurements conducted during the low dust period with the dust event is difficult, since the wind direction changed from northwest to southeasterly. However, the wind direction did change 24 hours prior to the arrival of the dust and a comparison of the measured values from July 27^{th} with the days after shows, that the mixing ratios during the dust event are lower until July 30^{th}. On that particular day, the increase of anthropogenic mixing ratios in the morning is accompanied by higher SO_2 concentrations, suggesting that local anthropogenic pollution is effectively transported from the boundary layer to the station. This effect is possibly caused by the change in wind direction from southeasterly to east. Only small settlements and

no industry can be found in the southerly direction prevailing during the beginning of the dust event. On July 30^{th}, the wind direction changed towards the east, where the industrial area of Güímar and a fuel gas power plant are situated, leading to higher mixing ratios for the anthropogenic species.
Compared to the low dust period, the biogenically emitted compounds α-pinene, camphene, 3-carene and eucalyptol show lower mixing ratios during the days of the dust event. The original diurnal cycle can be observed to a weaker extent for α-pinene, camphene and eucalyptol. The morning emissions start later at around 8:00. This could be attributed to the diffuse light conditions in the morning caused by the dust particles in the air. Although in the dust period the temperature is as high as during other parts of the campaign, biogenic mixing ratios in the daytime are generally lower. As already noted, the wind direction changed shortly before the dust plume arrived, and the lower concentrations might be ascribed to the more arid conditions and associated vegetation prevailing in the southern part of Tenerife. On close inspection it can be seen that the nocturnal mixing ratios of the biogenic compounds only increase in the second night of the dust event simultaneously with the relative humidity. 3-Carene for example shows an almost constant level throughout day and night between July 30^{th} and 31^{st}. Also, the biogenic VOC degradation product HCHO showed higher mixing ratios during the nights of the dust event compared to the low dust period.
As recent studies showed, drought stress constricts the emission of biogenic VOCs from pine trees, whereas an increase in relative humidity increases the emission of for example 3-carene [223, 224, 188]. Similar behaviour with respect to relative humidity is observed in this study not only during the dust event, but also in the night between July 25^{th} and 26^{th}. During that particular night, the humidity was with approximately 20% higher than during other nights (about 10%), and all terpenes showed mixing ratios clearly above the detection limit. It may be hypothesised, whether the increased concentrations in nocturnal terpenes may be driven by higher emissions due to the changes in humidity. Additionally, the impact of mineral dust on the emission of biogenic VOCs has not been studied yet. In a study investigating the effects of contact stimulation on the emission of VOCs, japanese cypress seedlings were rotated inside a chamber with the leaves touching each other. An increased emission of terpenes was observed for these trees as compared to seedlings that remained fixed [189]. It can be further speculated, whether the dust particles hitting the leaves at high wind speeds (circa 10 m s^{-1}) during the dust event also had an increasing effect on the emission. Another possible explanation is that the higher relative humidity lead to enhanced scavenging of the nighttime oxidant NO_3, as various studies have shown this to be an important removal pathway in the marine boundary layer [227, 228]. An increase in the heterogeneous loss reaction of the NO_3 with water vapour in the atmosphere can lead to longer lifetimes of the reactive species, which translates to higher nocturnal mixing ratios, since the reaction with O_3 is much slower, see Tab. 1.1. A mean atmospheric NO_3 concentration of 8 ppt was measured during an earlier field study at Izaña in May [202]. Using this figure, a nocturnal removal rate of 30 ppt/h can be calculated for the highly reactive 3-carene, the less reactive camphene is still removed with about 1 ppt/h. A strong decrease

in NO_3 can thus lead to an effective increase of the biogenically emitted VOCs. On the other hand, eucalyptol is known to react very slowly with NO_3 (removal < 0.01 ppt/h), the higher mixing ratios observed for this compound are thus most likely caused by an increased emission. The observed higher nocturnal mixing ratios of the biogenic compounds are probably the result of increased emission due to higher relative humidity and contact stimulation from the high wind during the dust period together with longer lifetimes.

The VOC measurements in the free troposphere at the meteorological observatory Izaña with the new analytical GC×GC-FID technique revealed a strong influence of local anthropogenic and biogenic compounds on the site. This influence can not only be observed during the day, but also occasionally at night. The highly reactive terpenes are present even at night as a consequence of the emitting vegetation present above the inversion layer. Anthropogenic VOCs were measured during pollution events and during the day, when the dynamic upslope winds originating from the boundary layer reach the station. The measurements during the dust event from July 28^{th} to August 1^{st} showed no apparent direct effect of the mineral dust on the anthropogenic and biogenic species through heterogeneous reactions. The different diurnal cycles of the anthropogenic compounds during the dust event were more likely to be caused by the changing wind direction. For the biogenic compounds, however, changes in the vertical temperature and humidity structure lead to a different emission pattern during the dust event. These effects must be taken account of in future if the Izaña site is used to characterise free tropospheric air.

APPENDIX A

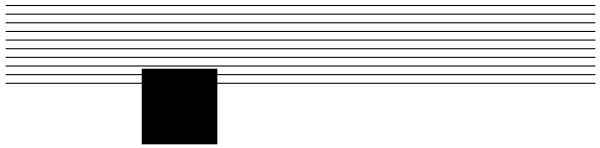

A.1 Data Analysis software

Commercially available software for peak detection and integration was found to be slow and unsuitable. Additionally, the ensuing necessary control for proper integration of the peaks into all directions is a slow task as the borders frequently need to be corrected. An integration procedure was written within IgorPro 4.0 software (WaveMetrics Inc., OR, USA) as part of this work to allow semi-automatic data analysis processing of selected peaks. The data were exported as csv-files to the processing software with the export-function of the ChemStation software (Agilent, DE, USA). Background removal is an important first step for the quantitative analysis. The background subtraction for the HOHPEX campaign was based on the observation, that the background level of the chromatograms is not rising with increasing temperatures towards the end of the analysis. Therefore it was possible to calculate a mean value from the first 15000 pixels of the chromatogram and subtract it from all data points. Baseline removal for the MINATROC campaign had to be performed differently, since the background was rising with increasing temperatures. The mean baseline value was obtained for each individual peak by calculating an average value of the lower part of the chromatogram beneath the peak of interest that does not contain any peaks. The obtained value was then subtracted from the chromatogram prior to peak integration. This step was carried out for every peak. Thorough checks have proven that both methods result in a near zero background surrounding the particular peak. The peaks of interest have to be defined within an upper, lower, left and right border and an identification name. As the retention times in both directions do not change or only vary slightly, i.e. one or two modulation cycles/pixels into the horizontal first dimension retention direction and only a few mseconds/pixels into the vertical second dimension retention direction, the chosen frame almost always encloses the peak.

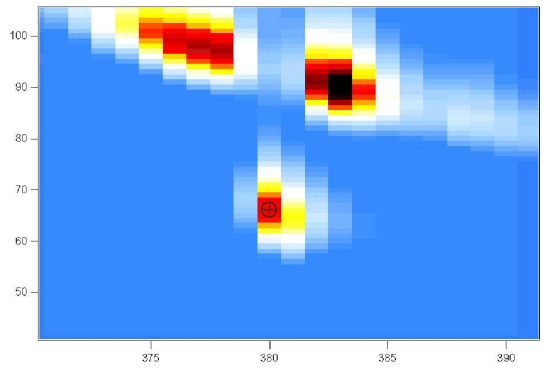

Fig. A.1: Peak maximum as shown with the integration program

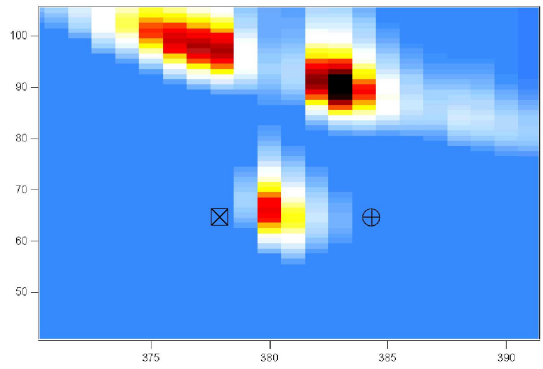

Fig. A.2: Peak borders shown in the integration software

Once the area is defined, the peak maximum is computed and depicted as shown in Fig. A.1. In case of a false indication, the peak maximum can be identified and marked manually by moving the cursor and clicking the ‚continue'-button provided.

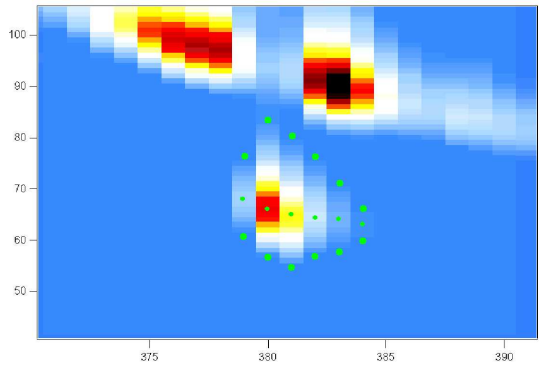

Fig. A.3: Encircled peak

Starting from the maximum, the left and right borders of the peak are calculated. Different criteria can be set for peak border detection. In this study, the beginning and the end of the peaks were reached as soon as the threshold reached 0.08 or the value fraction of pixel A+1 to A (or A-1 to A) was bigger than 0.99, an indication for a very gentle tailing of the peak or the end of the slope. The peak borders can also be changed by moving the beginning or ending cursor in case this algorithm has failed, see Fig. A.2. The peak borders into all directions are shown with marks on top of the displayed peak image, see Fig. A.3. If it is apparent that the peak end or beginning is not properly calculated, the false values can be checked with the cursor and changed manually in a pop-up table.
If the peak identification is finished, the software computes the peak volume by summing up the area calculated underneath every labeled slice of the peak in agreement with [60]. The results are inserted into the table assigned to the name, see Tab. A.1. The table additionally shows the first dimension retention time, the second dimension retention time and the peak maximum.

PeakArea	Peak_ tR1	Peak_ tR2	PeakMax	Filename
114.348	0.53	29.3333	4.88518	HOPE_ 172

Tab. A.1: Output-Table of the integration program

A.2 Compounds identified by GC×GC/TOF-MS

Identified compound	1st R.T (min)	2nd R.T (sec)	Retention Index	Ambient air	*Phaeocyst. gl. young*	*Phaeocyst. gl. old*	*Ectocarpus sp.*	*Emiliania H.*	*Pseudonitzschia sp.*	Laboratory	*E. camaldulensis*	Mixed forest	Pine forest	Calibration
1(3H)-Isobenzofuranone	42.32	0.84	1327.4	•					•				•	
1,3,5-Cycloheptatriene	15.70	0.52	750.0				•		•					
1,3-Dioxolane, 2-methyl-	10.67	0.50	630.9	•	•	•	•	•	•					
1,4-Dioxane	11.64	0.53	687.9		•	•		•	•	•		•		
1-Butanol	10.88	0.52	643.073	•	•	•	•	•	•	•	•			
1-Butene	2.38	0.39	440.3			•								
1-Decene	26.85	0.49	988.3		•			•						
1-Dodecene	44.31	0.56	1390.1	•				•						
1-Heptene	11.64	0.46	687.9	•	•	•	•	•	•		•			
1-Hexanol	21.33	0.54	839.5	•	•	•	•	•	•	•			•	
1-Hexanol, 2-ethyl-	29.53	0.55	1012.8	•	•		•	•	•		•		•	
1-Hexene	8.03	0.44	586.2				•		•		•			
1-Hexene, 4-methyl-	11.69	0.46	691.2				•		•					
1H-Inden-1-one, 2,3-dihydro-	39.73	0.77	1268.0	•	•		•				•			
1-Nonanol	35.91	0.59	1155.1	•	•								•	
1-Nonene	22.51	0.48	887.1	•	•	•	•	•	•	•			•	
1-Octene	16.25	0.47	775.4	•	•	•	•	•	•					
1-Pentanol	15.51	0.52	741.1	•	•	•	•	•	•	•	•			
1-Propanol, 2-methyl-	10.32	0.51	610.3		•		•	•			•			
1-Tetradecene	44.30	0.57	1389.5						•					
2(3H)-Furanone, dihydro-5-butyl-	38.47	0.71	1227.8	•	•		•	•	•				•	
2(3H)-Furanone, dihydro-5-ethyl-	29.59	0.73	1014.9	•	•	•	•	•	•	•	•			

Identified compound	1st R.T (min)	2nd R.T (sec)	Retention Index	Ambient air	*Phaeocyst. gl. young*	*Phaeocyst. gl. old*	*Ectocarpus sp.*	*Emiliania H.*	*Pseudonitzschia sp.*	Laboratory	*E. camaldulensis*	Mixed forest	Pine forest	Calibration
2(3H)-Furanone, dihydro-5-methyl-	24.71	0.71	909.3	•	•		•	•	•		•			
2(3H)-Furanone, dihydro-5-pentyl-	42.58	0.71	1335.2	•				•	•				•	
2(3H)-Furanone, dihydro-5-propyl-	34.77	0.71	1119.0	•	•		•	•	•				•	
2(5H)-Furanone	21.70	0.79	855.0	•	•	•	•			•	•			
2(5H)-Furanone, 3-methyl-	25.43	0.76	935.6				•		•	•				
2(5H)-Furanone, 5,5-dimethyl-	24.85	0.65	914.5	•	•			•						
2,3-Pentanedione	11.31	0.51	668.2	•	•		•		•					
2-Butanone	7.82	0.49	571.1	•	•	•	•	•	•	•	•			
2-Butanone, 3-methyl-	10.79	0.50	638.3		•		•	•	•	•				
2-Butenal	10.54	0.53	623.2	•	•	•	•	•	•	•				
2-Butenal, 3-methyl-	15.67	0.57	747.0	•	•		•	•	•					
2-Butenoic acid, butyl ester	29.71	0.56	1019.3		•			•	•	•				
2-Coumaranone	37.90	0.77	1209.9								•	•	•	
2-Cyclohexen-1-one	24.62	0.64	905.9	•	•	•	•	•	•	•	•			
2-Cyclopenten-1-one	16.48	0.64	786.2	•	•	•	•	•	•	•	•			
2-Cyclopenten-1-one, 2-methyl-	22.24	0.62	876.6		•			•	•					
2-Cyclopentene-1,4-dione	21.20	0.67	835.0				•	•	•					
2-Decanone	36.54	0.59	1175.0	•	•		•	•		•	•		•	
2-Decenal	39.02	0.61	1245.5	•	•		•							
2-Dodecanone	43.98	0.61	1379.7	•				•					•	
2-Ethylacrolein	10.96	0.50	648.1		•	•	•	•						
2-Furanmethanol	20.60	0.60	811.7				•		•					
2-Heptanone	21.92	0.53	863.2	•	•	•	•	•	•					

Identified compound	1st R.T (min)	2nd R.T (sec)	Retention Index	Ambient air	*Phaeocyst. gl. young*	*Phaeocyst. gl. old*	*Ectocarpus sp.*	*Emiliania H.*	*Pseudonitzschia sp.*	Laboratory	*E. camaldulensis*	Mixed forest	Pine forest	Calibration
2-Heptanone, 6-methyl-	25.43	0.53	935.7		•		•	•	•					
2-Heptenal	25.37	0.61	933.9	•			•		•					
2-Hexanone	15.87	0.52	757.4	•	•		•	•	•	•				
2-Hexenal	20.64	0.55	813.6	•			•							
2-Hexene, 5,5-dimethyl-	14.89	0.46	711.0		•	•	•	•		•				
2H-Pyran-2-one, tetrahydro-	29.46	0.80	1009.0	•			•	•	•	•	•			
2-Butyl furan	22.31	0.52	879.1				•		•					
2-Nonanone	31.29	0.56	1073.1	•	•			•	•				•	
2-Nonenal	35.48	0.61	1141.0	•			•		•					
2-Octanone	26.38	0.54	970.9	•	•		•	•	•	•	•		•	
2-Oxepanone	34.36	0.80	1104.9	•			•		•					
2-Pentanone	11.23	0.50	663.7	•	•	•	•	•	•			•		
2-Propenal	2.58	0.44	476.8	•	•	•				•	•			
2-Propenal, 2-methyl-	7.49	0.48	546.8	•	•	•	•		•	•				
2-Propenenitrile	2.69	0.49	497.2		•	•	•							
2-Propenoic acid, butyl ester	22.08	0.53	869.5		•	•	•		•					
2-Pyrrolidinone, 1-methyl-	29.26	0.75	1003.8		•		•		•					
2-Thiophenecarboxaldehyde	26.44	0.71	973.4	•				•						
2-Undecanone	40.01	0.60	1276.8	•	•		•	•	•	•	•		•	
3-Penten-2-one	14.90	0.54	712.0	•	•	•	•	•	•	•	•			
3-Pentenenitrile	15.36	0.57	733.9				•	•						
4-Nonene	22.65	0.48	892.6		•		•	•	•	•	•			
5,9-Undecadien-2-one, 6,6-dimethyl-	46.25	0.64	1424.7	•	•	•	•	•	•	•	•			

Identified compound	1st R.T (min)	2nd R.T (sec)	Retention Index	Ambient air	*Phaeocyst. gl. young*	*Phaeocyst. gl. old*	*Ectocarpus sp.*	*Emiliania H.*	*Pseudonitzschia sp.*	Laboratory	*E. camaldulensis*	Mixed forest	Pine forest	Calibration
5-Hepten-2-one, 6-methyl-	26.20	0.56	964.3		●		●		●			●	●	
Acetic Acid	7.63	0.55	557.1	●	●		●	●	●	●				
Acetone	2.60	0.45	479.2	●	●	●								
Acetonitrile	2.56	0.50	472.2	●		●				●	●			
Azulene	37.04	0.69	1191.4	●	●									
Benzaldehyde	25.56	0.67	940.6	●	●		●	●	●		●		●	
Benzaldehyde, 3-methyl-	30.69	0.66	1055.8		●		●							
Benzaldehyde, 4-methoxy-	38.66	0.75	1233.9	●	●		●	●	●	●	●		●	
Benzaldehyde, 4-methyl-	30.67	0.64	1053.2	●				●		●	●			
Benzene	11.03	0.49	652.2	●	●	●	●	●	●	●	●	●	●	●
Benzene, 1,2,3-trimethyl-	29.80	0.55	1022.0	●	●			●	●		●			●
Benzene, 1,2,4-trimethyl-	26.94	0.54	991.6	●			●		●	●	●			●
Benzene, 1,2-dichloro-	30.00	0.61	1029.2								●			
Benzene, 1,3,5-trimethyl-	26.22	0.54	965.0	●	●	●				●	●			●
Benzene, 1,3-bis(1-methylethenyl)-	39.80	0.63	1270.1					●	●	●				
Benzene, 1,3-dichloro-	29.19	0.58	1001.5		●		●				●			
Benzene, 1,3-dimethyl-	21.85	0.54	859.2	●	●					●	●		●	●
Benzene, 1,4-bis(1-methylethenyl)-	41.57	0.64	1303.7					●	●					
Benzene, 1,4-dichloro-	29.34	0.60	1006.5	●							●			
Benzene, 1,4-dimethyl-	21.73	0.53	856.3	●			●	●	●					●
Benzene, 1-ethyl-2-methyl-	26.55	0.55	977.3	●	●		●	●			●		●	●
Benzene, 1-ethyl-3-methyl-	26.02	0.54	957.5	●	●						●		●	●
Benzene, 1-ethyl-4-methyl-	26.14	0.54	961.3		●									●

Identified compound	1st R.T (min)	2nd R.T (sec)	Retention Index	Ambient air	*Phaeocyst. gl. young*	*Phaeocyst. gl. old*	*Ectocarpus sp.*	*Emiliania H.*	*Pseudonitzschia sp.*	Laboratory	*E. camaldulensis*	Mixed forest	Pine forest	Calibration
Benzene, 1-methyl-2-(1-methylethyl)-	29.80	0.54	1022.4	•			•				•		•	
Benzene, 1-methyl-3-(1-methylethyl)-	31.31	0.55	1074.1				•				•			
Benzene, chloro-	20.97	0.55	827.3	•				•	•		•			
Benzene, propyl-	25.83	0.53	950.7	•							•			•
Benzeneacetaldehyde	29.74	0.66	1020.1	•	•		•		•	•	•		•	
Benzenepropanenitrile	37.79	0.77	1206.0		•		•	•	•		•			
Benzofuran	26.90	0.61	990.3				•							
Benzonitrile	26.02	0.66	957.6	•	•		•	•	•	•	•	•	•	
Benzothiazole	38.25	0.77	1220.7	•	•		•	•	•	•	•		•	
Benzyl Alcohol	29.46	0.68	1010.4	•	•		•	•	•	•	•		•	
Benzyl nitrile	34.32	0.76	1102.9		•		•		•	•				
Bicyclo[2.2.1]heptan-2-one, 1,7,7-trimethyl- [1]	35.68	0.60	1147.6	•	•			•	•		•	•	•	
Bicyclo[2.2.1]heptane, 2,2-dimethyl-3-methylene- [2]	26.09	0.51	960.4	•	•		•	•	•			•	•	
Bicyclo[3.1.0]hexane, 4-methylene-1-(1-methylethyl)- [3]	24.50	0.51	978.0									•		
Bicyclo[3.1.1]hept-2-ene, 2,6,6-trimethyl- [4]	25.65	0.50	944.1	•	•	•	•	•	•	•		•	•	•
Bicyclo[3.1.1]hept-3-en-2-one, 4,6,6-trimethyl- [5]	37.76	0.67	1205.4	•	•		•	•	•		•	•	•	
Bicyclo[3.1.1]heptan-2-one, 6,6-dimethyl- [6]	35.17	0.64	1131.2	•			•		•			•	•	
Bicyclo[3.1.1]heptane, 6,6-dimethyl-2-methylene- [7]	26.83	0.52	987.6				•					•	•	
Bicyclo[4.2.0]octa-1,3,5-triene [8]	22.34	0.55	879.9		•		•			•	•			
Biphenyl	44.14	0.72	1384.6	•				•					•	
Butanal, 2-methyl-	10.88	0.49	643.3				•							

[1] Camphor [2] Camphene [3] Sabinene [4] α-Pinene [5] Verbenone [6] Norinone [7] β-Pinene [8] Cardene

Identified compound	1st R.T (min)	2nd R.T (sec)	Retention Index	Ambient air	*Phaeocyst. gl. young*	*Phaeocyst. gl. old*	*Ectocarpus sp.*	*Emiliania H.*	*Pseudonitzschia sp.*	Laboratory	*E. camaldulensis*	Mixed forest	Pine forest	Calibration
Butanal, 3-methyl-	10.72	0.49	633.4	•	•	•	•	•	•					
Butane, 1-bromo-	14.95	0.50	714.5		•				•	•	•			
Butane, 2,2,3-trimethyl-	10.56	0.44	623.1			•			•	•		•		
Butane, 2,2-dimethyl-	7.29	0.42	532.0	•	•	•	•	•	•	•		•		
Butanenitrile	10.73	0.55	634.4				•	•						
Butanenitrile, 2-methyl-	11.70	0.54	691.3			•	•	•						
Butanenitrile, 3-methyl-	11.78	0.56	696.2				•	•	•	•				
Caprolactam	38.14	0.82	1216.9	•			•	•	•	•				
Carbon disulfide	7.25	0.46	529.2	•	•	•	•	•	•					
Carbon Tetrachloride	11.13	0.47	657.6	•	•	•			•	•		•		
Chloroform	10.19	0.48	602.2	•	•	•	•	•	•	•				
Cinnamaldehyde	39.23	0.74	1252.0	•	•		•	•	•	•		•	•	
Cyclohexane	11.20	0.46	662.3		•	•	•		•	•				•
Cyclohexane, isocyanato-	26.82	0.56	987.2	•	•				•	•				
Cyclohexane, methyl-	15.13	0.46	723.1	•	•	•	•	•	•	•		•	•	•
Cyclohexanone	22.02	0.60	867.3	•	•	•	•	•	•	•			•	
Cyclohexene	11.48	0.47	678.1	•	•	•	•	•	•	•		•		•
Cyclohexene, 1-methyl-	15.91	0.49	760.0				•	•						
Cyclohexene, 1-methyl-4-(1-methylethenyl)- [8]	30.14	0.52	1033.8	•	•		•	•	•	•	•	•	•	
Cyclopentane, methyl-	10.62	0.45	628.3	•					•	•				
Cyclopentanone	15.79	0.58	753.9	•	•	•	•	•	•	•	•			
Cyclopropane, ethylidene-	6.91	0.43	504.1		•	•					•			

[8] Limonene

Identified compound	1st R.T (min)	2nd R.T (sec)	Retention Index	Ambient air	*Phaeocyst. gl. young*	*Phaeocyst. gl. old*	*Ectocarpus sp.*	*Emiliania H.*	*Pseudonitzschia sp.*	Laboratory	*E. camaldulensis*	Mixed forest	Pine forest	Calibration
Decanal	36.98	0.59	1189.4	•	•		•		•	•	•		•	
Decane	29.15	0.49	1000.0	•	•		•	•	•	•	•	•	•	•
Diazene, dimethyl-	2.61	0.44	481.8							•	•			
Dimethyl sulfide	6.98	0.47	509.4		•	•		•						
Dimethyl sulfone	21.42	0.86	843.1		•	•	•	•	•					
Dimethyl Sulfoxide	16.35	0.76	781.3		•		•							
Dimethyl trisulfide	26.16	0.62	962.8	•				•						
Disulfide, dimethyl	15.22	0.54	727.3	•	•		•	•	•	•	•			
Dodecanal	44.45	0.61	1394.4	•				•					•	
Dodecane	37.60	0.52	1200.0	•	•		•	•	•	•	•	•	•	
Ethane, 1,1,2-trichloro-1,2,2-trifluoro-	7.18	0.42	524.3	•			•		•	•				
Ethane, 1,2-dichloro-	10.60	0.52	626.5	•					•	•				
Ethanol	2.48	0.46	462.5	•	•	•				•				
Ethanol, 2-butoxy-	22.50	0.56	887.2			•							•	
Ethanol, 2-phenoxy-	37.25	0.71	1198.2		•		•				•		•	
Ethanone, 1-(4-methylphenyl)-	36.43	0.68	1171.6				•	•						
Ethyl Acetate	8.18	0.48	596.8		•		•		•	•				
Ethylbenzene	21.52	0.53	847.886	•		•	•	•	•	•	•	•	•	•
Eucalyptol	30.14	0.54	1035.535								•	•		
Formamide, N,N-diethyl-	24.55	0.62	903.0	•	•		•	•	•	•	•			
Formamide, N,N-dimethyl-	15.51	0.66	742.3	•	•		•		•		•			
Furan	2.67	0.43	493.7	•	•	•				•				
Furan, 2-methyl-	8.13	0.47	593.5	•	•	•	•	•	•	•				

Identified compound	1st R.T (min)	2nd R.T (sec)	Retention Index	Ambient air	*Phaeocyst. gl. young*	*Phaeocyst. gl. old*	*Ectocarpus sp.*	*Emiliania H.*	*Pseudonitzschia sp.*	Laboratory	*E. camaldulensis*	Mixed forest	Pine forest	Calibration
Furan, 2-pentyl-	26.69	0.53	982.3	•	•		•	•	•	•	•		•	
Furan, tetrahydro-	10.41	0.49	615.4	•	•	•	•	•	•	•				
Furfural	16.52	0.62	789.7	•	•	•	•		•	•	•	•		
Heptanal	22.27	0.54	877.5	•	•	•	•	•	•	•	•		•	
Heptane	14.65	0.45	700.0	•	•	•	•	•	•	•	•	•		•
Hexanal	16.06	0.53	766.4	•	•		•	•	•	•	•			•
Hexanal, 2-ethyl-	25.54	0.53	940.0		•		•	•	•	•	•			
Hexane	10.15	0.43	600.0	•	•		•	•	•	•		•		•
Hexane, 2,3-dimethyl-	16.23	0.46	785.7	•	•		•	•						
Hexane, 2,5-dimethyl-	15.24	0.45	727.9	•	•		•		•		•			
Hexane, 2-methyl-	11.25	0.45	665.5	•	•	•		•	•	•			•	•
Hexane, 3-methyl-	11.42	0.45	675.3	•	•	•	•	•	•	•			•	•
Hexanenitrile	21.11	0.58	832.1				•	•						
Indane	30.25	0.59	1037.9		•									•
Isopropyl Alcohol	2.63	0.46	486.8		•	•								
Methane, bromo-	2.44	0.41	454.1	•	•	•				•	•			
Methanethioamide, N,N-dimethyl-	26.56	0.81	977.7	•				•						
Methyl Isobutyl Ketone	15.02	0.50	717.8	•	•		•	•	•		•	•		
Methylene Chloride	7.05	0.46	514.5	•		•		•						
Methylstyrene	26.48	0.56	974.6	•	•		•	•	•		•			
Naphthalene	37.03	0.69	1191.0	•			•	•	•	•	•	•	•	
Naphthalene, 1-methyl-	41.63	0.70	1305.5	•				•			•			
N-Formylmorpholine	31.39	0.81	1081.4	•				•	•					

Identified compound	1st R.T (min)	2nd R.T (sec)	Retention Index	Ambient air	*Phaeocyst. gl. young*	*Phaeocyst. gl. old*	*Ectocarpus sp.*	*Emiliania H.*	*Pseudonitzschia sp.*	Laboratory	*E. camaldulensis*	Mixed forest	Pine forest	Calibration
Nonanal	31.66	0.58	1086.3	•	•	•	•	•	•	•			•	
Nonane	24.45	0.48	900.0	•	•		•	•	•	•	•	•	•	•
Octanal	26.72	0.56	983.7	•	•		•	•	•	•	•		•	
Octane, 1-chloro-	30.73	0.53	1054.1	•	•					•				
Octane, 4-methyl-	21.80	0.48	859.1								•			
Oxirane, (chloromethyl)-	11.70	0.56	691.8		•		•							
Pentanal	11.39	0.51	673.5	•	•	•	•	•	•	•	•		•	
Pentane	6.85	0.41	500.0	•	•	•	•	•	•	•				•
Pentane, 1-chloro-	15.41	0.49	736.2								•			
Pentane, 2,3-dimethyl-	11.32	0.45	669.2	•	•		•		•	•		•	•	•
Pentane, 2-methyl-	7.74	0.43	565.1	•	•		•	•	•		•			•
Pentane, 3,3-dimethyl-	11.09	0.45	655.6		•		•		•	•			•	
Pentane, 3-methyl-	7.96	0.43	581.0	•	•	•	•		•	•	•			•
Pentanenitrile, 4-methyl-	16.59	0.56	792.7				•	•	•		•			
Phenol	25.80	0.64	949.7	•	•		•	•	•		•	•	•	
Phenylethyne	21.76	0.56	857.6	•				•					•	
Propanal, 2-methyl-	7.34	0.47	536.0		•		•							
Propanenitrile	7.39	0.53	538.8		•	•	•	•	•	•				
Propanenitrile, 2-methyl-	8.11	0.53	592.1		•	•	•	•						
Pyrazine	14.82	0.59	708.7	•	•		•		•					
Pyrrole	15.16	0.57	724.8	•	•		•	•	•	•	•			
Styrene	22.33	0.55	879.7	•	•		•	•	•	•				•
Tetradecane	43.42	0.57	1400.0	•				•					•	

Identified compound	1st R.T (min)	2nd R.T (sec)	Retention Index	Ambient air	*Phaeocyst. gl. young*	*Phaeocyst. gl. old*	*Ectocarpus sp.*	*Emiliania H.*	*Pseudonitzschia sp.*	Laboratory	*E. camaldulensis*	Mixed forest	Pine forest	Calibration
Thiocyanic acid, methyl ester	11.32	0.65	669.4		•		•							
Thiophene, tetrahydro-, 1,1-dioxide	35.91	0.93	1154.2	•	•		•	•	•					
Toluene	15.75	0.51	752.3	•	•	•	•	•		•	•	•	•	•
Tridecane	41.45	0.54	1300.0	•	•				•	•	•		•	
Undecanal	40.48	0.60	1292.0	•	•			•	•	•	•	•	•	
Undecane	34.20	0.50	1100.0	•					•			•	•	•

Tab. A.2: Identified compounds on a DB-1 × BPX-50 column configuration

A.3 Example chromatograms

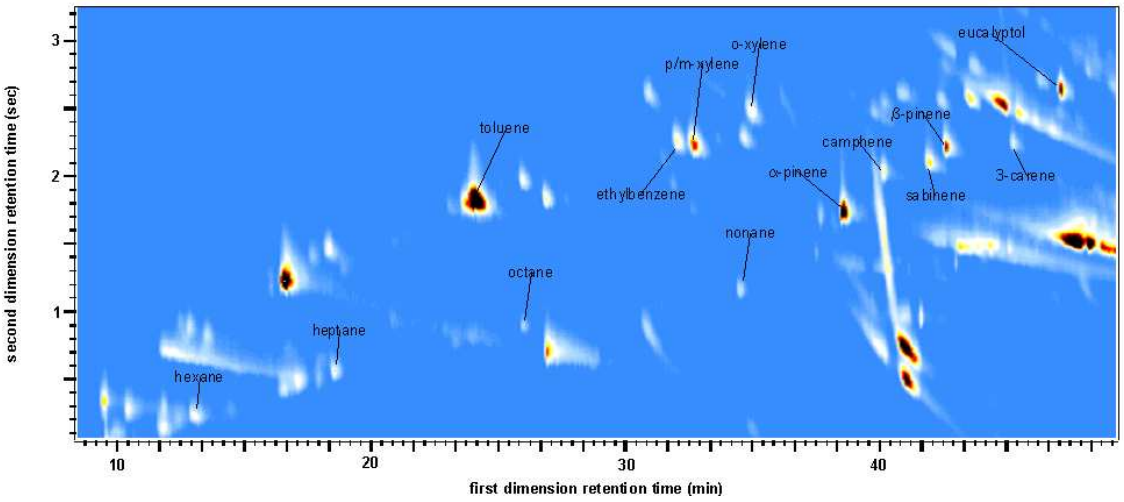

Fig. A.4: HOHPEX ambient air sample taken on July 8, 2004, between 11:00 and noon. The compounds discussed for the HOHPEX field campaign are marked

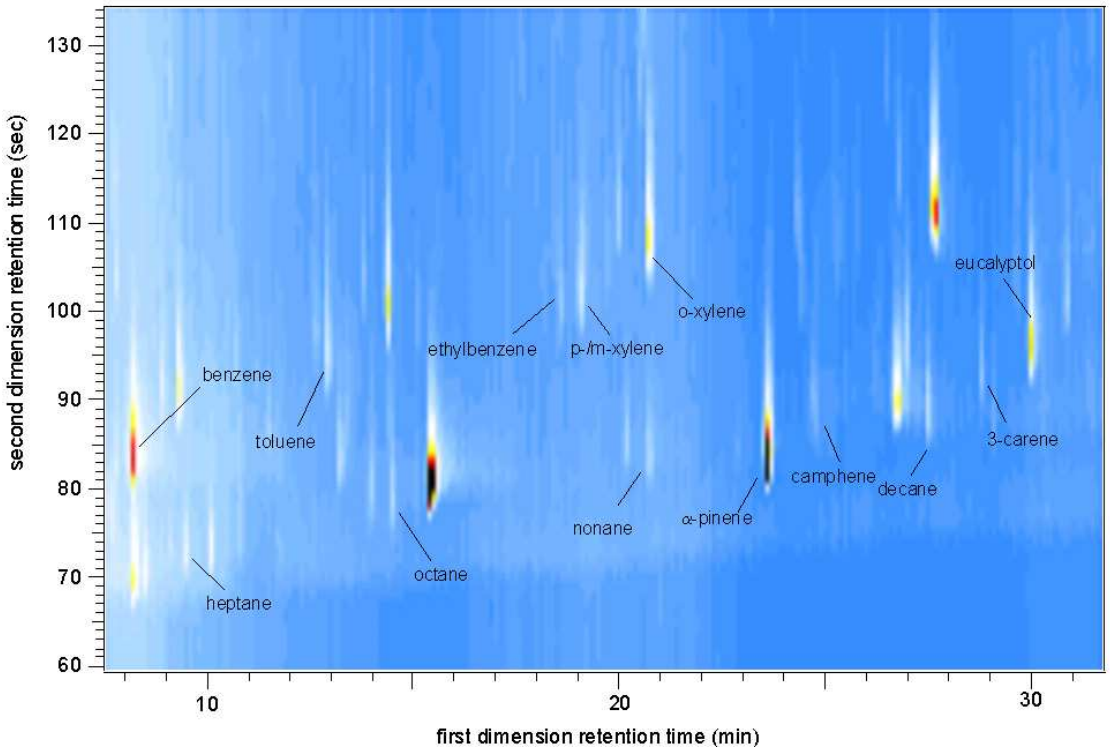

Fig. A.5: MINATROC ambient air sample collected on July 24, 2002, between 13:30 and 14:40. The compounds discussed for the MINATROC field campaign are marked

A.4 Photographs of HOHPEX measurement site

Fig. A.6: View of the Meteorological Observatory Hohenpeissenberg

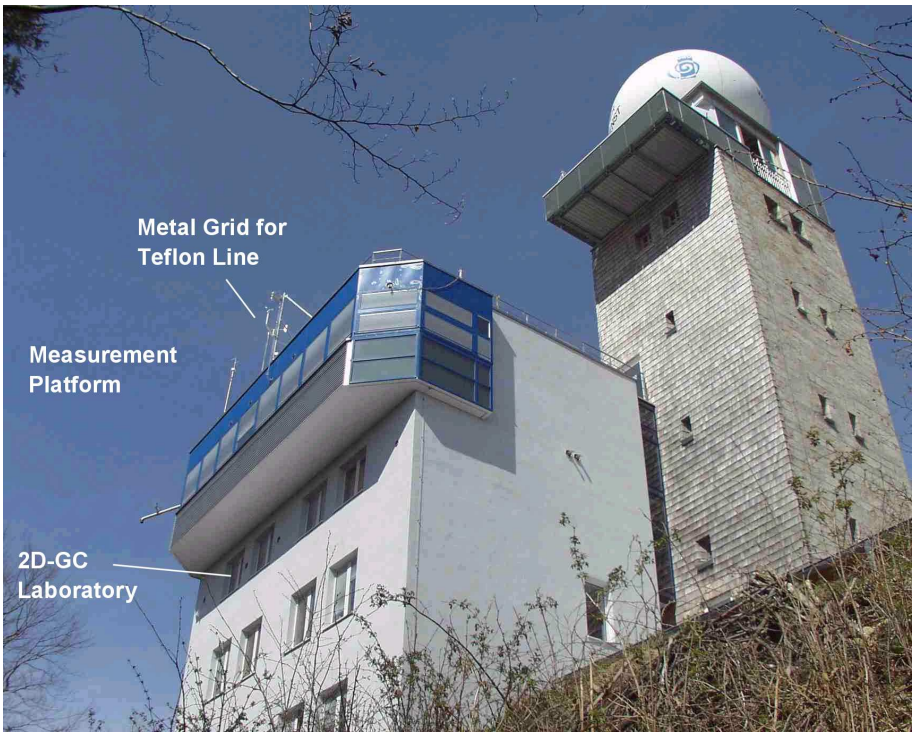

Fig. A.7: View of the measurement platform

A.5 Calibration curves

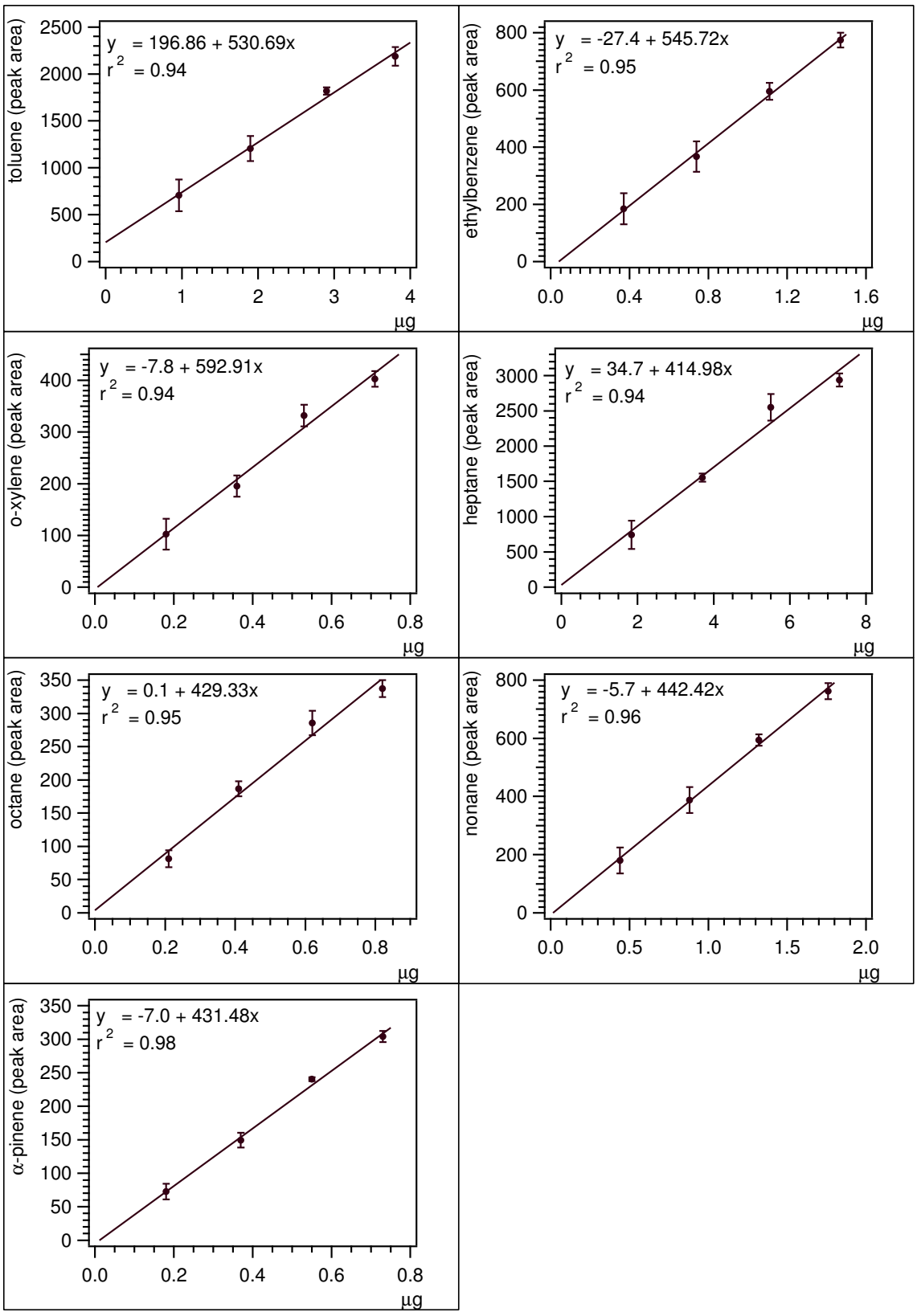

Fig. A.8: Calibration curves for the HOHPEX field campaign

A.6 Correlation plots HOHPEX 2004

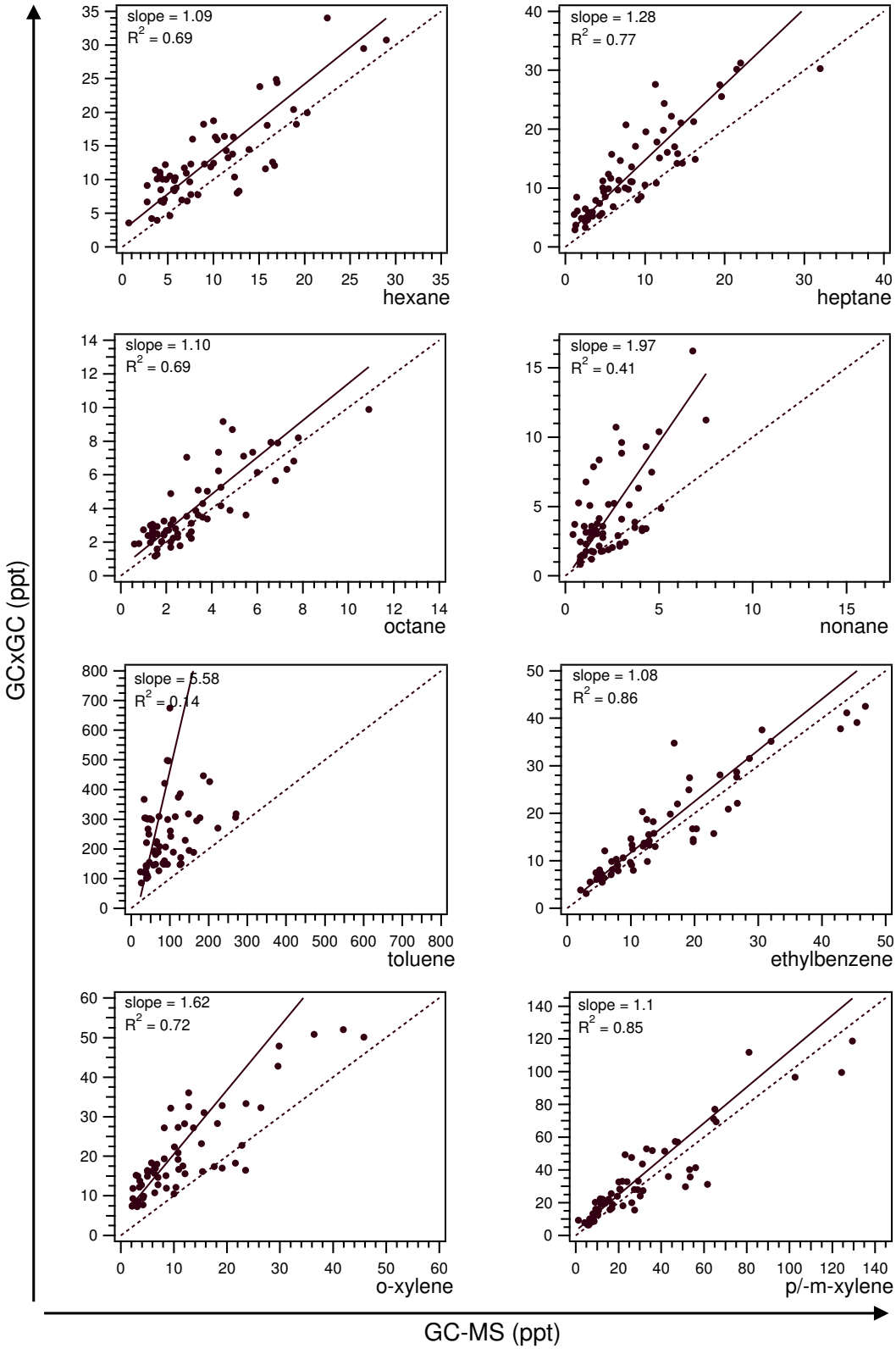

Fig. A.9: Linear correlation plots of the alkanes and aromatic VOCs for GC×GC vs GC-MS. The mixing ratios are in ppt, the solid lines show the fitting results of the ODR analyses, the dashed lines the 1:1-relationship

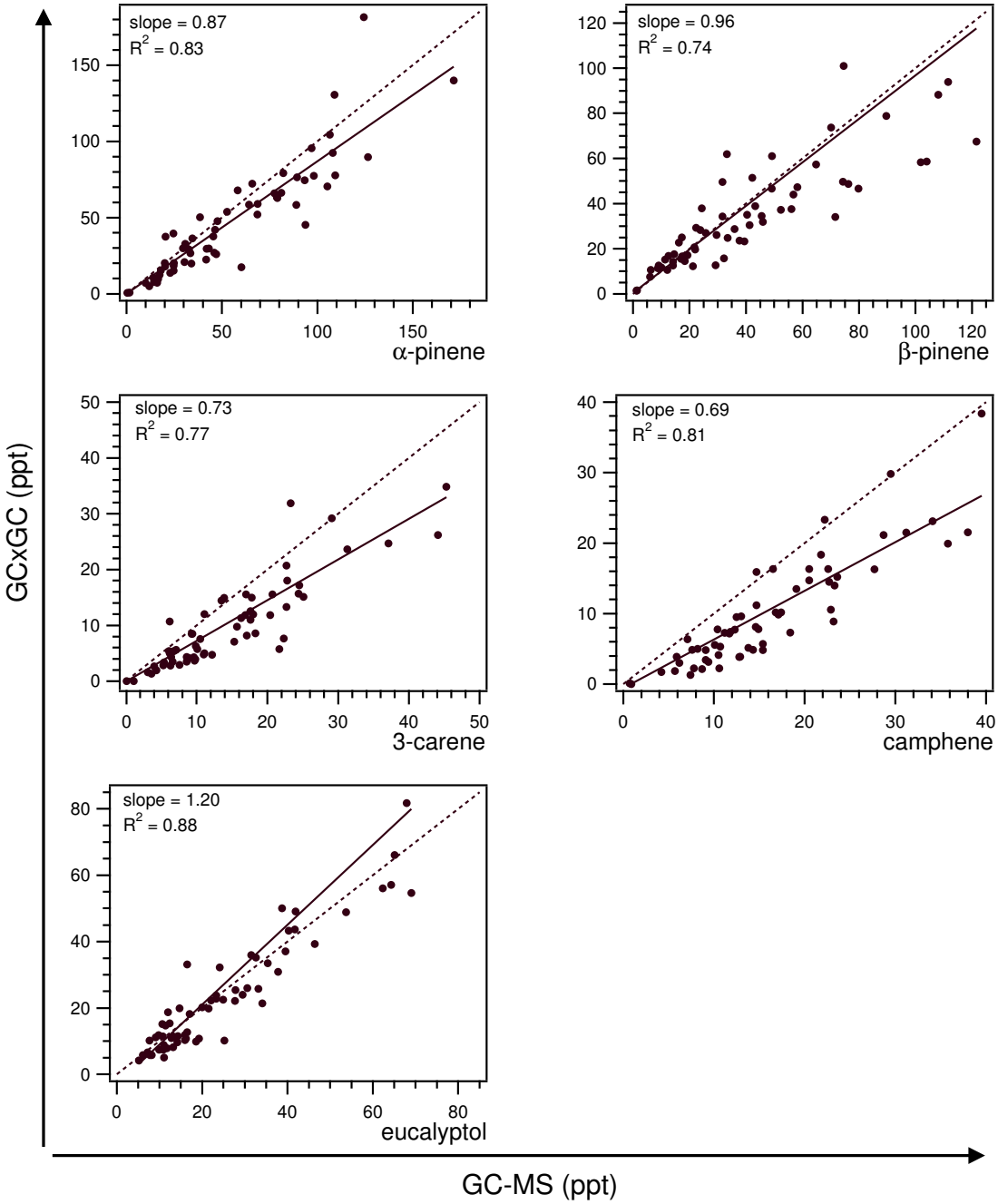

Fig. A.10: Linear correlation plots of the terpenes measured by GC×GC vs GC-MS. The mixing ratios are in ppt, the solid lines show the fitting results of the ODR analyses, the dashed lines the 1:1-relationship

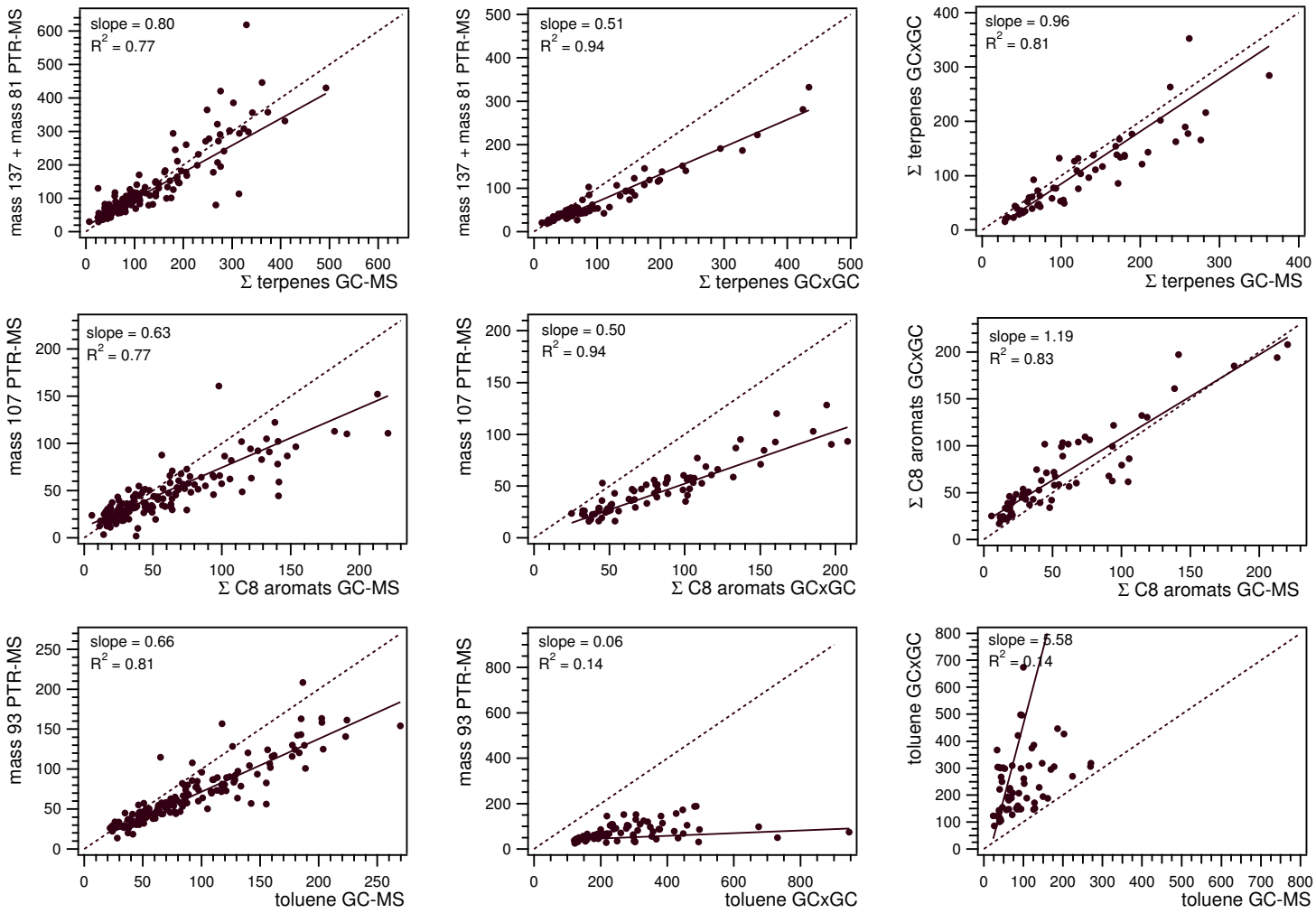

Fig. A.11: Correlation plots of PTR-MS vs GC-MS and GC×GC-FID. The mixing ratios are in ppt, the solid lines show the fitting results of the ODR analyses, the dashed lines the 1:1-relationship

A.7 Photographs of MINATROC measurement site

Fig. A.12: View of the Izaña measurement station, Tenerife, Spain. The buildings in the background belong to the observatory, the containers in the foreground contain the measurement instrument for the intensive field campaign

Fig. A.13: View of the Max-Planck-Institute containers. The GC×GC instrument was set up in the blue container to the right

BIBLIOGRAPHY

[1] G.P. Brasseur, J.J. Orlando, and G.S. Tyndall. *Atmospheric chemistry and global change*. Oxford University Press, Inc., 1999.

[2] R.B. Stull. *An introduction to boundary layer meteorology*. Kluwer Academic Publishers, 1988.

[3] M.Z. Jacobson. *Atmospheric pollution. History, science and regulation*. Cambridge University Press, Inc., 2000.

[4] P. Warneck. *Chemistry of the natural atmosphere*. Academic Press, 2000.

[5] H.B. Singh and P. Zimmermann. *Atmospheric distribution and sources of nonmethane hydrocarbons*. John Wiley and Sons, 1992.

[6] S.D. Piccot, J.J. Watson, and J.W. Jones. A global inventory of volatile organic compound emissions from anthropogenic sources. *J. Geophys. Res.*, 97:9897–9912, 1992.

[7] A. Guenther, C.N. Hewitt, D. Erickson, R. Fall, C. Geron, T. Grädel, P. Harley, L. Klinger, M. Lerdau, W. A. McKay, T. Pierce, B. Scholes, R. Steinbrecher, R. Tallamraju, J. Taylor, and P. Zimmermann. A global model of natural volatile organic compound emissions. *J. Geophys. Res.*, 100:8873–8892, 1995.

[8] J. Kesselmeier and M. Staudt. Biogenic volatile organic compounds (VOC): An overview on emission, physiology and ecology. *J. Atmos. Chem.*, 33:23–88, 1999.

[9] R. Atkinson. Atmospheric chemistry of VOCs and NOx. *Atmos. Env.*, 34:2063–2101, 2000.

[10] J.D. Fuentes, M. Lerdau, R. Atkinson, D. Baldocchi, J.W. Bottenheim, P. Ciccioli, B. Lamb, C. Geron, L. Gu, A. Guenther, T.D. Sharkey, and W. Stockwell. Biogenic hydrocarbons in the atmospheric boundary layer: A review. *Bull. Am. Met. Soc.*, 81:1537–1575, 2000.

[11] A. Guenther, C. Geron, T. Pierce, B. Lamb, P. Harley, and R. Fall. Natural emissions of non-methane volatile organic compounds; carbon monoxide, and oxides of nitrogen from North America. *Atmos. Env.*, 34:2205–2230, 2000.

[12] BEMA: A European commision project on biogenic emissions in the Mediterranean area. *Atmos. Env. Suppl.*, 31, 1997.

[13] U. Kuhn, S. Rottenberger, T. Biesenthal, W. Wolf, G. Schebeske, P. Ciccioli, E. Brancaleoni, M. Frattoni, T.M Tavarel, and J. Kesselmeier. Seasonal differences in isoprene and light-dependent monoterpene emission by Amazonian tree species. *Glob. Change Biol.*, 10:663–682, 2004.

[14] G. Schuh, A.C. Heiden, T. Hoffmann, J. Kahl, P. Rockel, J. Rudolph, and J. Wildt. Emission of volatile organic compounds from sunflower and beech: Dependence on temperature and light intensity. *J. Atmos. Chem.*, 27:291–318, 1997.

[15] V. Tarvainen, H. Hakola, H. Hellén, J. Bäck, P. Hari, and M. Kulmala. Temperature and light dependence of the VOC emissions of Scots pine. *Atmos. Chem. Phys.*, 5:989–998, 2005.

[16] J.E. Andrews, P. Brimblecombe, T.D Jickells, P.S. Liss, and B.J. Reid. *An introduction to environmental chemistry.* Blackwell Science Ltd., 2004.

[17] J.E. Lovelock. Natural halocarbons in air and in sea. *Nature*, 256:193–194, 1975.

[18] M.E. Jenkin and K.C. Clemitshaw. Ozone and other secondary photochemical pollutants: Chemical processes governing their formation in the planetary boundary layer. *Atmos. Env.*, 34:2499–2527, 2000.

[19] M.V. Migeotte. Methane in the Earths atmosphere. *Astrophys. J.*, 107:400–403, 1948.

[20] E.R. Stephens, P.L. Hanst, R.C. Doerr, and W.E. Scott. Reactions of nitrogen dioxide and organic compounds in air. *Ind. Eng. Chem.*, 48:1498–1504, 1956.

[21] E.R. Stephens. Long-path infrared spectroscopy for air pollution research. *Infrared Phys.*, 1:187–, 1961.

[22] D. Brocco, R. Fratarcangeli, L. Lepore, M. Petricca, and I. Ventrone. Determination of aromatic hydrocarbons in urban air of Rome. *Atmos. Environ.*, 31:557–566, 1997.

[23] R. Volkamer, T. Etzkorn, A. Geyer, and U. Platt. Correction of the oxygen interference with UV spectroscopic (DOAS) measurements of monocyclic aromatic hydrocarbons in the atmosphere. *Atmos. Environ.*, 32:3731–3747, 1998.

[24] H.K. Roscoe and K.C. Clemitshaw. Measurement techniques in gas-phase tropospheric chemistry: A selective view of the past, present, and future. *Science*, 276:1065–1072, 1997.

[25] D. D. Parrish and F. C. Fehsenfeld. Methods for gas-phase measurements of ozone, ozone precursors and aerosol precursors. *Atmos. Env.*, 34:1921–1957, 2000.

[26] C. Warneke, J. A. de Gouw, P. D. Goldan, W. C. Kuster, E. J. Williams, B. M. Lerner, R. Jakoubek, S. S. Brown, H. Stark, M. Aldener, A. R. Ravishankara, J. M. Roberts, M. Marchewka, S. Bertman, D. T. Sueper, S. A. Mckeen, J. F. Meagher, and F. C. Fehsenfeld. Comparison of daytime and nighttime oxidation of biogenic and anthropogenic VOCs along the New England coast in summer during New England Air Quality Study 2002. *J. Geophys. Res.*, 109:10309, 2004.

[27] J. Williams, U. Pöschl, P.J. Crutzen, A. Hansel, R. Holzinger, C. Warneke, W. Lindinger, and J. Lelieveld. An atmospheric chemistry interpretation of mass scans obtained from a Proton Transfer Mass Spectrometer flown over the tropical rainforest of Surinam. *J. Atmos. Chem.*, 38:133–166, 2001.

[28] G. Salisbury, J. Williams, R. Holzinger, V. Gros, N. Mihalopoulos, M. Vrekoussis, R. Sarda-Estève, H. Berresheim, R. von Kuhlmann, M. Lawrence, and J. Lelieveld. Ground-based PTR-MS measurements of reactive organic compounds during the MINOS campaign in Crete, Juli-August 2001. *Atmos. Phys. Chem*, 3:925–940, 2003.

[29] P. J. Crutzen, J. Williams, U. Pöschl, P. Hoor, H. Fischer, C. Warneke, R. Holzinger, A. Hansel, W. Lindinger, B. Scheeren, and J. Lelieveld. High spatial and temporal resolution measurements of primary organics and their oxidation products over the tropical forests of Surinam. *Atmos. Env.*, 34:1161–1165, 2000.

[30] W.C. Kuster, B.T. Jobson, T. Karl, D. Riemer, E. Apel, P.D. Goldan, and F.C. Fehsenfeld. Intercomparison of volatile organic carbon measurement techniques and data at La Porte during the TexAQS2000 air quality study. *Environ. Sci. Technol.*, 38:221–228, 2004.

[31] M.F. Sipin, S.A. Guazzotti, and K.A. Prather. Recent advances and some remaining challenges in analytical chemistry of the atmosphere. *Anal. Chem.*, 75:2929–2940, 2003.

[32] F. Mühlberger, R. Zimmermann, and A. Kettrup. A mobile mass spectrometer for comprehensive on-line analysis of trace and bulk components of complex gas mixtures: Parallel application of the laser-based ionization methods VUV single-photon ionization, resonant multiphoton ionization, and laser-induced electron impact ionization. *Anal. Chem.*, 73:3590–3604, 2001.

[33] F. Mühlberger, J. Wieser, A. Ulrich, and R. Zimmermann. Single photon ionization (SPI) via incoherent VUV-Excimer light: Robust and compact time-of-flight mass spectrometer for on-line, real-time process gas analysis. *Anal. Chem.*, 74:3790–3801, 2002.

[34] S. Konrad and A. Volz-Thomas. Characterization of a commercial gas chromatography-flame ionization detection system for the in situ determination of C_5 - C_{10} hydrocarbons in ambient air. *J. Chromatogr. A*, 878:215–234, 2000.

[35] C. Plass-Dülmer, K. Michl, R. Ruf, and H. Berresheim. C_2 - C_8 hydrocarbon measurement and quality control procedures at the Global Atmosphere Watch Observatory Hohenpeissenberg. *J. Chromatogr. A*, 953:175–197, 2002.

[36] G.M. Handisides, C. Plass-Dülmer, S. Gilge, H. Bingemer, and H. Berresheim. Hohenpeissenberg Photochemical Experiment (HOPE 2000): Measurements and photostationary state calculations of OH and peroxy radicals. *Atmos. Chem. Phys.*, 3:1565–1588, 2003.

[37] C. Badol, A. Borbon, N. Locoge, T. Leonardis, and J.C. Galloo. An automated monitoring system for VOC ozone precursors in ambient air: Development, implementation and data analysis. *Anal. Bioanal. Chem.*, 378:1815–1827, 2004.

[38] J. Kesselmeier, U. Kuhn, S. Rottenberger, T. Biesenthal, A. Wolf, G. Schebeske, M.O. Andreae, P. Ciccioli, E. Brancaleoni, M. Frattonie, S.T. Oliva, M.L. Botelho, C.M.A. Silva, and T.M. Tavares. Concentrations and species composition of atmospheric volatile organic compounds (VOCs) as observed during the wet and dry season in Rondônia (Amazonia). *J. Geophys. Res.*, 107:DOI 8053, 2002.

[39] S. Kato, P. Pochanart, and Y. Kajii. Measurements of ozone and nonmethane hydrocarbons at Chichi-jima island, a remote island in the western Pacific: Long-range transport of polluted air from the Pacific rim region. *Atmos. Env.*, 35:6021–6029, 2001.

[40] V.L. Young, B.N. Kieser, S.P. Chen, and H. Niki. Seasonal trends and local influences on nonmethane hydrocarbon concentrations in the Canadian boreal forest. *J. Geophys. Res.*, 102:5913–5918, 1997.

[41] V. Gros, J. Williams, J.A. van Aardenne, G. Salisbury, R. Hofmann, M.G. Lawrence, R. von Kuhlmann, J. Lelieveld, M. Krol, H. Berresheim, J.M. Lobert, and E. Atlas. Origin of anthropogenic hydrocarbons and halocarbons measured in the summertime european outflow (on Crete in 2001). *Atmos. Chem. Phys.*, 3:1223–1235, 2003.

[42] F. C. Fehsenfeld, P. Daum, W. R. Leaitch, M. Trainer, D.D. Parrish, and G. Hubler. Transport and processing of O-3 and O-3 precursors over the North Atlantic: An overview of the 1993 North Atlantic Regional Experiment (NARE) summer intensive. *J. Geophys. Res.*, 101:28877–28891, 1996.

[43] J.P. Greenberg, D. Helmig, and P.R. Zimmerman. Seasonal measurements of nonmethane hydrocarbons and carbon monoxide at the Mauna Loa Observatory during the Mauna Loa Observatory Photochemistry Experiment 2. *J. Geophys. Res.*, 101:14581–14598, 1996.

[44] A. Colomb, J. Williams, J. Crowley, H. Fischer, V. Gros, R. Hofmann, G. Salisbury, T. Klüpfel, R. Kormann, and A. Stickler. The impact of deep convection on organic trace gases and the consequences for the upper troposphere over continental Europe. in prep.

[45] J. Mühle, A. Zahn, C. A. M. Brenninkmeijer, V. Gros, and P.J. Crutzen. Air mass classification during the INDOEX R/V Ronald Brown cruise using measurements of nonmethane hydrocarbons, CH_4, CO_2, CO, (CO)-C-14, and delta O-18(CO). *J. Geophys. Res.*, 107:Art. No. 8021, 2002.

[46] E. C. Apel, A.J. Hills, R. Lueb, S. Zindel, S. Eisele, and D.D. Riemer. A fast-GC/MS system to measure C-2 to C-4 carbonyls and methanol aboard aircraft. *J. Geophys. Res.*, 108:8794, 2003.

[47] J.W. Elkins, D.W. Fahey, J.M. Gilligan, G.S. Dutton, T.J. Barind, C.M. Volk, R.E. Dunn, R.C. Myers, S.A Montzka, P.R. Wamsley, A.H. Hayden, J.H. Butler, T.M. Thompson, T.H. Swanson, E.J. Dlugokencky, P.C. Novelli, D.F. Hurst, J.M. Lobert, S.J. Ciciora, R.J. McLaughlin, T.L. Thompson, R.H. Winkler, P.J. Fraser, L.P. Steele, and P.M. Lucarelli. Airborne gas chromatograph for in situ measurements of long-lived species in the upper troposphere and lower stratosphere. *Geophys. Res. Lett.*, 23:347–350, 1996.

[48] A.C. Lewis, N. Carslaw, P.J. Marriott, R.M. Kinghorn, P.D. Morrison, A.L. Lee, K.D. Bartle, and M.J. Pilling. A larger pool of ozone-forming carbon compounds in urban atmospheres. *Nature*, 405:778–781, 2000.

[49] J.F. Hamilton and A.C. Lewis. Monoaromatic complexity in urban air and gasoline assessed using comprehensive GC and fast GC-TOF/MS. *Atmos. Env.*, 37:589–602, 2003.

[50] X. Xu, J. Williams, C. Plass-Dülmer, H. Berresheim, G. Salisbury, L. Lange, and J. Lelieveld. GC×GC measurements of C_7-C_{11} aromatic and n-alkane hydrocarbons on Crete, in air from Eastern Europe during the MINOS campaign. *Atmos. Chem. Phys.*, 3:1461–1475, 2003.

[51] H.M. McNair and J.M. Miller. *Basic Gas Chromatography.* John Wiley and Sons, Inc., 1997.

[52] D.A. Skoog, F.J. Holler, and T.A. Nieman. Principles of instrumental analysis. *Harcourt Brace and Company*, 5:100, 1998.

[53] T. Holm and J.Ø. Madsen. Methane formation by flame-generated hydrogen atoms in the flame ionization detector. *Anal. Chem.*, 68:3607–3611, 1996.

[54] T. Holm. Aspects of the mechanism of the flame ionization detector. *J. Chromatogr. A*, 842:221–227, 1999.

[55] L.S. Ettre. The development of chromatography. *Anal. Chem.*, 43:20A–31A, 1971.

[56] L.S. Ettre. M.S. Tswett and the invention of chromatography. *LC GC North America*, 21:458–467, 2003.

[57] W. Bertsch. Two-dimensional gas chromatography. Concepts, instrumentation, and applications - Part 1: Fundamentals, conventional two-dimensional gas

chromatography, selected applications. *J. High Resol. Chromatogr.*, 22:647–665, 1999.

[58] J.V. Hinshaw. Comprehensive two-dimensional gas chromatography. *LC GC North America*, 22:32–40, 2004.

[59] J. Blomberg and U. A. T. Brinkman. Practical and theoretical aspects of designing a flame-ionization detector mass spectrometer Deans' switch - Pressure-flow relations in gas chromatography detector interfaces using vacuum-outlet conditions. *J. Chromatogr. A*, 831:257–265, 1999.

[60] P.J. Marriott, P.D. Morrison, R.A. Shellie, M.S. Dunn, E. Sari, and D. Ryan. Multidimensional and comprehensive two-dimensional gas chromatography. *LC GC Europe*, 16:23–31, 2003.

[61] P.J. Marriott, M. Dunn, R. Shellie, and P.D. Morrison. Targeted multidimensional gas chromatography using microswitching and cryogenic modulation. *Anal. Chem.*, 75:5532–5538, 2003.

[62] B.M. Gordon, M. Uhrig, M.F. Borgerding, H.L. Chung, W.M. Coleman, J.F. Elder, J.A. Giles, D.S. Moore, C.E. Rix, and E.L. White. Analysis of flue-cured tobacco essential oil by hyphenated analytical techniques. *J. Chromatogr. Sci.*, 26:174–180, 198.

[63] N. Ragunathan, K.A. Krock, C. Klawun, T.A. Sasaki, and C.L. Wilkins. Multispectral detection for gas chromatography. *J. Chromatogr. A*, 703:335–382, 1995.

[64] G. Schomburg. Multidimensional capillary gas chromatography. *LC GC North America*, 5:304, 1987.

[65] K.A. Krock, N. Ragunathan, and C.L. Wilkins. Parallel cryogenic trapping multidimensional gas chromatography with directly linked infrared and mass spectral detection. *J. Chromatogr. A*, 645:153–159, 1993.

[66] B.J. Prazen, C.A. Bruckner, R.E. Synovec, and B.R. Kowalski. Enhanced chemical analysis using parallel column gas chromatography with single-detector time-of-flight mass spectrometry and chemometric analysis. *Anal. Chem.*, 71:1093–1099, 1999.

[67] G. Schomburg, H. Husmann, and E. Hubinger. Multidimensional separation of isomeric species of chlorinated hydrocarbons such as PCB, PCDD, and PCDF. *J. High Res. Chrom. Comm.*, 8:395–400, 1985.

[68] M. Dunn, R.A. Shellie, P.D. Morrison, and P.J. Marriott. Rapid sequential heart-cut multidimensional gas chromatographic analysis. *J. Chromatogr. A*, 1056:163–169, 2004.

[69] W.A. König, A. Krüger, D. Icheln, and T. Runge. Enantiomeric composition of the chiral constituents in essential oils. 1. Monoterpene hydrocarbons. *J. High Res. Chrom.*, 15:184–189, 1992.

[70] C. Watanabe, A. Hosaka, Y. Kawahara, P. Tobias, H. Ohtani, and S. Tsuge. GC-MS analysis of heart-cut fractions during evolved gas analysis of polymeric materials. *LC GC North America*, 20:374–378, 2002.

[71] L.F. de Alencastro, D. Grandjean, and J. Tarradellas. Application of multidimensional (heart-cut) gas chromatography to the analysis of complex mixtures of organic pollutants in environmental samples. *Chimia*, 57:499–504, 2003.

[72] J.C. Medina, J. Griffith, K.R. Houston, and B. Winniford. Detectability enhancement of spectrophotometric detectors by the use of multidimensional gas chromatography. *J. Sep. Sci.*, 25:1317–1324, 2002.

[73] P.J. Marriott, P. Haglund, and R.C.Y. Ong. A review of environmental toxicant analysis by using multidimensional gas chromatography and comprehensive GC. *Clinica Chimica Acta*, 328:1–19, 2003.

[74] J.C. Giddings. Two-dimensional separation: Concept and promise. *Anal. Chem.*, 56:1258A–1270A, 1984.

[75] J. Dallüge, J. Beens, and U.A.Th. Brinkman. Comprehensive two-dimensional gas chromatography: A powerful and versatile analytical tool. *J. Chromatogr. A*, 1000:69–108, 2003.

[76] R.E. Murphy, M.R. Schure, and J.P. Foley. Effect of sampling rate on resolution in comprehensive two-dimensional liquid chromatography. *Anal. Chem.*, 70:1585–1594, 1998.

[77] C.J. Venkatramani and J.B. Phillips. Comprehensive 2-dimensional gas-chromatography applied to the analysis of complex mixtures. *J. Micro. Sep.*, 5:511–516, 1993.

[78] Z.Y. Liu and J.B. Phillips. Comprehensive two-dimensional gas-chromatography using an on-column thermal modulator interface. *J. Chrom. Sci.*, 29:227–231, 1991.

[79] Z. Liu, S.R. Sirlmanne, D.G. Patterson Jr., and L.L. Needham. Comprehensive two-dimensional gas chromatography for the fast separation and determination of pesticides extracted from human serum. *Anal. Chem.*, 66:3086–3092, 1994.

[80] H.-J. de Geus, J. de Boer, and U.A.Th. Brinkman. Development of a thermal desorption modulator for gas chromatography. *J. Chromatogr. A*, 767:137–151, 1997.

[81] J. Harynuk and T. Górecki. Design considerations for a GC×GC system. *J. Sep. Sci.*, 25:304–310, 2002.

[82] B.V. Burger, T. Snyman, W.J.G. Burger, and W.F. van Rooyen. Thermal modulator array for analyte modulation and comprehensive two-dimensional gas chromatography. *J. Sep. Sci.*, 26:123–128, 2003.

[83] J.B. Phillips and E.B. Ledford. Thermal modulation: A chemical instrumenta-

tion component of potential value in improving portability. *Field Anal. Chem. Technol.*, 1:23–29, 1996.

[84] J. Blomberg, P.J. Schoenmakers, J. Beens, and R. Tijssen. Comprehensive two-dimensional gas chromatography (GC×GC) and its applicability to the characterization of complex (petrochemical) mixtures. *J. High. Resol. Chromatogr.*, 20:539–544, 1997.

[85] J.B. Phillips, R.B. Gaines, J. Blomberg, F.W.M. van der Wielen, J.M. Dimandja, V. Green, J. Granger, D. Patterson, L. Racovalis, H.J. de Geus, J. de Boer, P. Haglund, J. Lipsky, V. Sinha, and E.B. Ledford. A robust thermal modulator for comprehensive two-dimensional gas chromatography. *J. High Resol. Chromatogr.*, 22:3–10, 1999.

[86] C.A. Bruckner, B.J. Prazen, and R.E. Synovec. Comprehensive two-dimensional high-speed gas chromatography with chemometric analysis. *Anal. Chem.*, 70:2796–2804, 1998.

[87] J.V. Seeley, F.J. Kramp, and K.S. Sharpe. A dual-secondary column comprehensive two-dimensional gas chromatograph for the analysis of volatile organic compound mixtures. *J. Sep. Sci.*, 24:444–450, 2001.

[88] P.A. Bueno Jr. and J.V. Seeley. Flow switching device for comprehensive two-dimensional gas chromatography. *J. Chromatogr. A*, 1027:3–10, 2004.

[89] J.V. Seeley, F.J. Kramp, and C.J. Hicks. Comprehensive two-dimensional gas chromatography via differential flow modulation. *Anal. Chem.*, 72:4346–4352, 2000.

[90] A.E. Sinha, K.J. Johnson, B.J. Prazen, S.V. Lucas, C.G. Fraga, and R.E. Synovec. Comprehensive two-dimensional gas chromatography of volatile and semivolatile components using a diaphragm valve-base instrument. *J. Chromatogr. A*, 983:195–204, 2003.

[91] P.J. Marriott and R.M. Kinghorn. Longitudinally modulated cryogenic system. A generally applicable approach to solute trapping and mobilization in gas chromatography. *Anal. Chem.*, 69:2582–2588, 1997.

[92] R.M. Kinghorn and P.J. Marriott. Comprehensive two-dimensional gas chromatography using a modulation cryogenic trap. *J.High Resol. Chromatogr.*, 21:620–622, 1998.

[93] T. Hyötyläinen, M. Kallio, K. Hartonen, M. Jussila, S. Palonen, and M.-L. Riekkola. Modulator design for comprehensive two-dimensional gas chromatography: Quantitative analysis of polyaromatic hydrocarbons and polychlorinated biphenyls. *Anal. Chem.*, 74:4441–4446, 2002.

[94] J. Beens, M. Adahchour, R.J.J. Vreuls, K. van Altena, and U.A.Th. Brinkman. Simple, non-moving modulation interface for comprehensive two-dimensional gas chromatography. *J. Chromatogr. A*, 919:127–132, 2001.

[95] E.B. Ledford Jr. and C.A. Billesbach. Jet-cooled thermal modulator for comprehensive multidimensional gas chromatography. *J. High Resol. Chromatogr.*, 23:202–204, 2000.

[96] E.M. Kristenson, P. Korýtar, C. Danielsson, M. Kallio, M. Brandt, J. Mäkelä, R.J.J. Vreuls, J. Beens, and U.A.Th. Brinkman. Evaluation of modulators and electron-capture detectors for comprehensive two-dimensional GC of halogenated organic compounds. *J. Chromatogr. A*, 1019:65–77, 2003.

[97] M. Pursch, P. Eckerle, J. Biel, R. Streck, H. Cortes, K. Sun, and B. Winniford. Comprehensive two-dimensional gas chromatography using liquid nitrogen modulation: Set-up and applications. *J. Chromatogr. A*, 1019:43–51, 2003.

[98] J. Harynuk and T. Górecki. New liquid nitrogen cryogenic modulator for comprehensive two-dimensional gas chromatography. *J. Chromatogr. A*, 1019:53–63, 2003.

[99] E.B. Ledford Jr., J.R. TerMaat, and C.A. Billesbach. What is loop modulation? *Technical Note KT030606-1*, 2004.

[100] J. Harynuk, T. Górecki, and C. Campbell. On the interpretation of GC×GC data. *LC GC North America*, 20:876–892, 2002.

[101] R.A. Shellie, L.-L-Xie, and P.J. Marriott. Retention time reproducibility in comprehensive two-dimensional gas chromatography using cryogenic modulation. An intralaboratory study. *J. Chromatogr. A*, 968:161–170, 2002.

[102] R.B. Gaines, G.S. Frysinger, M.S. Hendrick-Smith, and J.D. Stuart. Oil spill source identification by comprehensive two-dimensional gas chromatography. *Environ. Sci. Technol.*, 33:2106–2112, 1999.

[103] P.J. Schoenmakers, J.L.M.M. Oomen, J. Blomberg, W. Genuit, and G. van Velzen. Comparison of comprehensive two-dimensional gas chromatography and gas chromatography-mass spectrometry for the characterization of complex hydrocarbon mixture. *J. Chromatogr. A*, 892:29–46, 2000.

[104] J. Beens, J. Blomberg, and P.J. Schoenmakers. Proper tuning of comprehensive two-dimensional gas chromatography (GC×GC) to optimize the separation of complex oil fractions. *J. High Resol. Chromatogr.*, 23:182–188, 2000.

[105] C.G. Fraga, B.J. Prazen, and R.E. Synovec. Comprehensive two-dimensional gas chromatography and chemometrics for the high-speed quantitative analysis of aromatic isomers in a jet fuel using the standard addition method and an objective retention time alignment algorithm. *Anal. Chem.*, 72:4154–4162, 2000.

[106] K.J. Johnson and R.E. Synovec. Pattern recognition of jet fuels: Comprehensive GC×GC with ANOVA-based feature selection and principal component analysis. *Chemom. Intell. Lab. Syst.*, 60:225–237, 2002.

[107] C. Vendeuvre, F. Bertoncini, L. Duval, J.-L. Duplan, D. Thiébaut, and M.-C. Hennion. Comparison of conventional gas chromatography and comprehensive

two-dimensional gas chromatography for the detailed analysis of petrochemical samples. *J. Chromatogr. A*, 1056:155–162, 2004.

[108] G.S. Frysinger and R.B. Gaines. Separation and identification of petroleum biomarkers by comprehensive two-dimensional gas chromatography. *J. Sep. Sci.*, 24:87–96, 2001.

[109] M. van Deursen, J. Beens, J. Reijenga, P. Lipman, and C. Cramers. Group-type identification of oil samples using comprehensive two-dimensional gas chromatography coupled to a time-of-flight mass spectrometer (GC×GC-TOF). *J. High Resol. Chromatogr.*, 23:507–510, 2000.

[110] G.S. Frysinger and R.B. Gaines. Determination of oxygenates in gasoline by GC×GC. *J. High. Resol. Chromatogr.*, 23:197–201, 2000.

[111] G.S. Frysinger and R.B. Gaines. Quantitative determination of BTEX and total aromatic compounds in gasoline by comprehensive two-dimensional gas chromatography (GC×GC). *J. High. Resol. Chromatogr.*, 22:195–200, 1999.

[112] M.T. Roberts, J.-P. Dufour, and A.C. Lewis. Application of comprehensive multidimensional gas chromatography combined with time-of-flight mass spectrometry (GC×GC-TOF/MS) for high resolution analysis of hop essential oil. *J. Sep. Sci.*, 27:473–478, 2004.

[113] X. Die, R.A. Shellie, P.J. Marriott, and C.W. Huie. Application of headspace solid-phase microextraction (SPME) and comprehensive two-dimensional gas chromatography (GC×GC) for the chemical profiling of volatile oils in complex herbal mixtures. *J. Sep. Sci.*, 27:451–458, 2004.

[114] P.J. Marriott, R.A. Shellie, J. Fergeus, R.C.Y. Ong, and P.D. Morrison. High resolution essential oil analysis by using comprehensive gas chromatographic methology. *Flavour Fragr. J.*, 15:225–239, 2000.

[115] R.A. Shellie and P.J. Marriott. Characterization and comparison of tea tree and lavender oils by using comprehensive gas chromatography. *J. High Resol. Chromatogr.*, 23:554–560, 2000.

[116] J.-M.D. Dimandja, S.B. Stanfill, J. Grainger, and D.G. Patterson Jr. Application of comprehensive two-dimensional gas chromatography (GC×GC) to the qualitative analysis of essential oils. *J. High Resol. Chromatogr.*, 23:208–214, 2000.

[117] R.A. Shellie, L. Mondello, P.J. Marriott, and G. Dugo. Characterization of lavender essential oils by using gas chromatography - mass spectrometry with correlation of linear retention indices and comparison with comprehensive two-dimensional gas chromatography. *J. Chromatogr. A*, 970:225–234, 2002.

[118] H.F. Wu, X. Lu, W.Y. Tang, H.W. Kong, S.F. Zhou, and G.W. Xu. Analytical characteristics of zedoary volatile oil by comprehensive two-dimensional gas chromatography/time-of-flight mass spectrometry. *Chin. J. Anal. Chem.*, 32:582–586, 2004.

[119] H.F. Wu, X. Lu, W.Y. Tang, H.W. Kong, S.F. Zhou, and G.W. Xu. Application of comprehensive two-dimensional gas chromatography-time-of-flight mass spectrometry in the analysis of volatile oil of traditional Chinese medicines. *J. Chromatogr. A*, 1034:199–205, 2004.

[120] M.Z. Ozel, F. Gogus, J.F. Hamilton, and A.C. Lewis. The essential oil of Pistacia, vera L. at various temperatures of direct thermal desorption using comprehensive gas chromatography coupled with time-of-flight mass spectrometry. *Chromatographia*, 60:79–83, 2004.

[121] M. Z. Ozel and H. Kaymaz. Superheated water extraction, steam distillation and Soxhlet extraction of essential oils of *origanum onites*. *Chromatographia*, 60:79–83, 2004.

[122] L. Mondello, A. Casilli, P.Q. Tranchida, G. Dugo, and P. Dugo. Comprehensive two-dimensional gas chromatography in combination with rapid scanning quadrupole mass spectrometry in perfume analysis. *J. Chromatogr. A*, 1067:235–243, 2005.

[123] C. Debonneville and A. Chaintreau. Quantitation of suspected allergens in fragrances. Part II. Evaluation of comprehensive gas chromatography-conventional mass spectrometry. *J. Chromatogr. A*, 1027:109–115, 2004.

[124] M. Adahchour, L.L.P. van Stee, J. Beens, R.J.J. Vreels, M.A. Batenburg, and U.A.Th. Brinkman. Comprehensive two-dimensional gas chromatography with time-of-flight mass spectrometric detection for the trace analysis of flavour compounds in food. *J. Chromatogr. A*, 1019:157–172, 2003.

[125] J.V. Seeley, F.J. Kramp, K.S. Sharpe, and S.K. Seeley. Characterization of gaseous mixtures of organic compounds with dual-secondary column comprehensive two-dimensional gas chromatography (GC×2GC). *J. Sep. Sci.*, 25:53–59, 2002.

[126] A.L. Lee, K.D. Bartle, and A.C. Lewis. A model of peak amplitude enhancement in orthogonal two-dimensional gas chromatography. *Anal. Chem.*, 73:1330–1335, 2001.

[127] M. Harju and P. Haglund. Comprehensive two-dimensional gas chromatography (GC×GC) of atropisomeric PCBs, combining a narrow bore β-cyclodextrin column and a liquid crystal column. *J. Microcol. Sep.*, 13:300–305, 2001.

[128] M. Harju, C. Danielsson, and P. Haglund. Comprehensive two-dimensional gas chromatography of the 209 polychlorinated biphenyls. *J. Chromatogr. A*, 1019:111–126, 2003.

[129] D. Cavagnino, P. Magni, G. Zilioli, and S. Trestianu. Comprehensive two-dimensional gas chromatography using large sample volume injection for the determination of polynuclear aromatic hydrocarbons in complex matrices. *J. Chromatogr. A*, 1019:211–220, 2003.

[130] R.C.Y. Ong, S. Lundstedt, P. Haglund, and P.J. Marriott. Pressurized liquid extraction - comprehensive two-dimensional gas chromatography for fast-screening of polycyclic aromatic hydrocarbons in soil. *J. Chromatogr. A*, 1019:221–232, 2003.

[131] P. Korýtar, P.E.G. Leonards, J. de Boer, and U.A.Th. Brinkman. High-resolution separation of polychlorinated biphenyls by comprehensive two-dimensional gas chromatography. *J. Chromatogr. A*, 958:203–218, 2002.

[132] P. Haglund, M. Harju, R.C.Y. Ong, and P. J. Marriott. Shape selectivity: A key factor in comprehensive two-dimensional gas chromatographic analysis of toxic PCBs. *J. Microcol. Sep.*, 13:306–311, 2001.

[133] J.F. Focant, A. Sjodin, and D.G. Patterson. Qualitative evaluation of thermal desorption-programmable temperature vaporization-comprehensive two-dimensional gas chromatography-time-of-flight mass spectrometry for the analysis of selected halogenated contaminants. *J. Chromatogr. A*, 1019:143–156, 2003.

[134] T.T. Truong, P.J. Marriott, N.A. Porter, and R. Leeming. Application of comprehensive two-dimensional gas chromatography to the quantification of overlapping faecal sterols. *J. Chromatogr. A*, 1019:197–210, 2003.

[135] W. Welthagen, J. Schnelle-Kreis, and R. Zimmermann. Search criteria and rules for comprehensive two-dimensional gas chromatography-time-of-flight mass spectrometry analysis of airborne particulate matter. *J. Chromatogr. A*, 1019:233–250, 2003.

[136] M. Kallio, T. Hyötyläinen, M. Lehtonen, M. Jussila, K. Hartonen, M. Shimmo, and M.-L. Riekkola. Comprehensive two-dimensional gas chromatography in the analysis of urban aerosols. *J. Chromatogr. A*, 1019:251–260, 2003.

[137] J. de Boer, H.-J. de Geus, and U.A.Th. Brinkman. Multidimensional gas chromatographic analysis of toxaphene. *Environ. Sci. Technol.*, 31:873–879, 1997.

[138] J. Dallüge, M. van Rijn, J. Beens, R.J.J Vreuls, and U.A.Th. Brinkman. Comprehensive two-dimensional gas chromatography with time-of-flight mass spectrometric detection applied to the determination of pesticides in food extracts. *J. Chromatogr. A*, 965:207–217, 2002.

[139] J. Zrostlíková, J. Hajslová, and T. Cajka. Evaluation of two-dimensional gas-chromatography-time-of-flight mass spectrometry for the determination of multiple pesticide residues in fruit. *J. Chromatogr. A*, 1019:173–186, 2003.

[140] T. Hyötyläinen, M. Kallio, M. Lehtonen, S. Lintonen, P. Peräjoki, M. Jussila, and M.-L. Riekkola. Comprehensive two-dimensional gas chromatography in the analysis of dietary fatty acids. *J. Sep. Sci.*, 27:459–467, 2004.

[141] H.-J. de Geus, I. Aidos, J. de Boer, J.B. Luten, and U.A.Th. Brinkman. Characterization of fatty acids in biological oil samples using comprehensive multidimensional gas chromatography. *J. Chromatogr. A*, 910:95–103, 2001.

[142] L. Mondello, A. Casilli, P.Q. Tranchida, P. Dugo, R. Costa, S. Festa, and G. Dugo. Comprehensive multidimensional GC for the characterization of roasted coffee beans. *J. Sep. Sci.*, 27:442–450, 2004.

[143] J. Dallüge, L.L.P. van Stee, X. Xu, J. Williams, J. Beens, R.J.J. Vreuls, and U.A.Th. Brinkman. Unravelling the composition of very complex samples by comprehensive gas chromatography coupled to time-of-flight mass spectrometry - Cigarette smoke. *J. Chromatogr. A*, 974:169–184, 2002.

[144] X. Lu, J. Cai, H. Kong, M. Wu, R. Hua, M. Zhao, J. Liu, and G. Xu. Analysis of cigarette smoke condensates by comprehensive two-dimensional gas chromatography/time-of-flight mass spectrometry. Part I: Acidic fraction. *Anal. Chem.*, 75:4441–4451, 2003.

[145] X. Lu, M. Zhao, J. Cai, J. Wu, M. Wu, R. Hua, J. Liu, and G. Xu. Characterization of cigarette smoke condensates by comprehensive two-dimensional gas chromatography/time-of-flight mass spectrometry. *J. Sep. Sci.*, 27:101–109, 2004.

[146] A.J. Kueh, P.J. Marriott, P.M. Wynne, and J.H. Vine. Application of comprehensive two-dimensional gas chromatography to drugs analysis in doping control. *J. Chromatogr. A*, 1000:109–124, 2003.

[147] S.M. Song, P.J. Marriott, A. Kotsos, O.H. Drummer, and P. Wynne. Comprehensive two-dimensional gas chromatography with time-of-flight mass spectrometry (GC×GC-TOF/MS) for drug screening and confirmation. *Forensic Science International*, 143:87–101, 2004.

[148] J. Dallüge, R.J.J. Vreuls, J. Beens, and U.A.Th. Brinkman. Optimization and characterization of comprehensive two-dimensional gas chromatography with time-of-flight mass spectrometric detection (GC×GC-TOF/MS). *J. Sep. Sci.*, 25:201–214, 2002.

[149] A.E. Sinha, B.J. Prazen, C.G. Fraga, and R.E. Synovec. Valve-based comprehensive two-dimensional gas chromatography with time-of-flight mass spectrometric detection: Instrumentation and figures of merit. *J. Chromatogr. A*, 1019:79–87, 2003.

[150] X. Xu, L. L. P. van Stee, J. Williams, J. Beens, M. Adahchour, R. J. J. Vreuls, U. A. T. Brinkman, and J. Lelieveld. Comprehensive two-dimensional gas chromatography GC×GC measurements of volatile organic compounds in the atmosphere. *Atmos. Chem. Phys.*, 3:665–682, 2003.

[151] R.J. Western and P.J. Marriott. Retention correlation maps in comprehensive two-dimensional gas chromatography. *J. Sep. Sci.*, 25:832–838, 2002.

[152] R.J. Western and P.J. Marriott. Methods for generating second dimension retention index data in comprehensive two-dimensional gas chromatography. *J. Chromatogr. A*, 1019:3–14, 2003.

[153] P. Fruekilde, J. Hjorth, N.R. Jensen, D. Kotzias, and B. Larsen. Ozonolysis at vegetation surfaces: A source of acetone, 4-oxopentanal, 6-methyl-5-hepten-2-one, and geranyl acetone in the troposphere. *Atmos. Env.*, 32:1893–1902, 1998.

[154] J. Williams, R. Holzinger, V. Gros, X. Xu, E. Atlas, and D.W.R. Wallace. Measurements of organic species in air and seawater from the tropical Atlantic. *Geophys. Res. Lett.*, 31:L23S06, 2004.

[155] H.W. Bange and J. Williams. New perspectives on the role of acetonitrile in atmospheric and biogeochemical cycles. *Atmos. Environm.*, 34:4959–4960, 2000.

[156] M.O. Andreae. Ocean-atmosphere interaction in the global biogeochemical sulfur cycle. *Marine Chem.*, 30:1–29, 1990.

[157] L.J. Rose, R.B. Simmons, S.A. Crow, and D.G. Ahearn. Volatile organic compounds associated with microbial growth in automobile air conditioning systems. *Curr. Microbiol.*, 41:206–209, 2000.

[158] D.C. Frank, C.M. Owen, and J. Patterson. Solid phase microextraction (SPME) combined with gas-chromatography and olfactometry-mass spectrometry for characterization of cheese aroma compounds. *Food Sci. Technol.*, 37:139–154, 2004.

[159] E.A. O'Gara Z.M. Ross, D.J. Hill, H.V. Sleightholme, and D.J. Maslin. Antimicrobial properties of garlic oil against human enteric bacteria: Evaluation of methodologies and comparisons with garlic oil sulfides and garlic powder. *App. Environ. Microbiol.*, 67:475–480, 2001.

[160] R.D.M. Prentice, G. McKernan, and J.H. Bryce. A source of dimethyl disulfide and dimethyl trisulfide in grain spirit produced with a Coffey still. *J. Am. Soc. Brewing Chem.*, 56:99–103, 1998.

[161] H.M. Burbank and M.C. Qian. Volatile sulfur compounds in cheddar cheese determined by headspace solid-phase microextraction and gas-chromatograph-pulsed flame photometric detection. *J. Chromatogr. A*, 1066:149–157, 2005.

[162] A.C. Heiden, K. Kobel, M. Komenda, R. Koppmann, M. Shao, and J. Wildt. Toluene emission from plants. *Geophys. Res. Lett.*, 26:1283–1286, 1999.

[163] N. Yassaa, B.Y. Meklati, E. Brancaleoni, M. Frattoni, and P. Ciccioli. Polar and non-polar volatile organic compounds (VOCs) in urban Algiers and saharian sites of Algeria. *Atmos. Env.*, 35:787–801, 2001.

[164] W. Birmili, H. Berresheim, C. Plass-Dülmer, T. Elste, S. Gilge, A. Wiedensohler, and U. Uhrner. The Hohenpeissenberg aerosol formation experiment (HAFEX): a long-term study including size-resolved aerosol, H_2SO_4, OH, and monoterpenes measurements. *Atmos. Chem. Phys.*, 3:361–376, 2002.

[165] W. Birmili, A. Wiedensohler, C. Plass-Dülmer, and H. Berresheim. Evolution of

newly formed aerosol particles in the continental boundary layer: A case study including OH and H_2SO_4 measurements. *J. Geophys. Res.*, 27:2205–2208, 2000.

[166] K. Mannschreck, S. Gilge, C. Plass-Dülmer, W. Fricke, and H. Berresheim. Assessment of the applicability of NO-NO_2-O_3 photostationary state long-term measurements at the Hohenpeissenberg GAW Station, Germany. *Atmos. Chem. Phys.*, 4:1265–1277, 2004.

[167] S. Trepte and P. Winkler. Reconstruction of erythemal UV irradiance and dose at Hohenpeissenberg (1968-2001) considering trends of total ozone, cloudiness and turbidity. *Theoret. Appl. Climatol.*, 77:159–171, 2004.

[168] L. Gantner, P. Winkler, and U. Kohler. A method to derive long-term time series and trends of UV-B radiation (1968-1997) from observations at Hohenpeissenberg, (Bavaria). *J. Geophys. Res.*, 27:2205–2208, 2000.

[169] H. Berresheim, T. Elste, C.Plass-Dülmer, F.L. Eisele, and D.J. Tanner. Chemical ionization mass spectrometer for long-term measurements of atmospheric OH and H_2SO_4. *Int. J. of Mass Spect.*, 202:91–109, 2000.

[170] D. D. Parrish, M. Trainer, V. Young, P. D. Goldan, W. C. Kuster, B. T. Jobson, F. C. Fehsenfeld, W. A. Lonneman, R. D. Zika, C. T. Farmer, D. D. Riemer, and M.O. Rodgers. Internal consistency tests for evaluation of measurements of anthropogenic hydrocarbons in the troposphere. *J. Geophys. Res.*, 103:22339–22359, 1998.

[171] J. Slemr, F. Slemr, R. Partridge, H. D'Souza, and N. Schmidbauer. Accurate Measurements of Hydrocarbons in the Atmosphere (AMOHA): Three European intercomparisons. *J. Geophys. Res.*, 107:Art. No. 4409 SEP–OCT 2002, 2002.

[172] E. C. Apel, J. G. Calvert, and F. C. Fehsenfeld. The nonmethane hydrocarbon intercomparison experiment (NOMHICE) - task-1 and task-2. *J. Geophys. Res.*, 99:16651–16664, 1994.

[173] E. C. Apel, J. G. Calvert, T. M. Gilpin, F. C. Fehsenfeld, D. D. Parrish, and W. A. Lonneman. The Nonmethane Hydrocarbon Intercomparison Experiment (NOMHICE): Task 3. *J. Geophys. Res.*, 104:26069–26086, 1999.

[174] E. C. Apel, J. G. Calvert, T. M. Gilpin, F. Fehsenfeld, and W. A. Lonneman. Nonmethane Hydrocarbon Intercomparison Experiment (NOMHICE): Task 4, ambient air. *J. Geophys. Res.*, 108:4300, 2003.

[175] B. Larsen, T. Bomboi-Mingarro, E. Brancaleoni, A. Calogirou, A. Cecinato, C. Coeur, I. Chatzianestis, M. Duane, M. Frattoni, J.-L. Fugit, U. Hansen, V. Jakob, N. Mimikos, T. Hoffmann, S. Owen, R. Perez-Pastor, A. Reichmann, G. Seufert, M. Staudt, and R. Steinbrecher. Sampling and analysis of terpenes in air. An intralaboratory comparison. *Atmos. Env.*, 31:35–49, 1997.

[176] A. Calogirou, B.R. Larsen, C. Brussol, M. Duana, and D. Kotzias. Decomposition of terpenes by ozone during sampling on Tenax. *Anal. Chem.*, 68:1499–1506, 1996.

[177] J.E. Mak and C.A.M. Brenninkmeijer. Compressed air sample technology for isotopic analysis of atmospheric carbon monoxide. *J. Atmos. Ocean Tech.*, 11:425–431, 1994.

[178] R.A. Street, S.C. Duckham, and C.N. Hewitt. Laboratory and field studies of biogenic volatile organic compound emissions from Sitka spruce (*Picea sitchensis* Bong) in the United Kingdom. *J. Geophys. Res.*, 101:22799–22806, 1996.

[179] D. Fulton, T. Gillespie, J. Fuentes, and D. Wang. Volatile organic compound emissions from young black spruce trees. *Agric. Forest Met.*, 90:247–255, 1998.

[180] L. Tollsten and P.M. Müller. Volatile organic compounds emitted from beech leaves. *Phytochemistry*, 43:759–762, 1996.

[181] T. Dindorf, U. Kuhn, L. Ganzeveld, G. Schebeske, P. Ciccioli, C. Holzke, R. Köble, G. Seufert, and J. Kesselmeier. Emission of monoterpenes from European beech (*Fagus sylvatica* L.) as a function of light and temperature. *Biogeosci. Disc.*, 2:137–182, 2005.

[182] M. Staudt, N. Bertin, U. Hansen, G. Seufert, P. Ciccioli, P. Foster, B. Frenzel, and J.-L. Fugit. Seasonal and diurnal patterns of monoterpene emissions from *Pinus Pinea* (L.) under field conditions. *Atmos. Env.*, 31:145–156, 1997.

[183] N. Bertin, M. Staudt, U. Hansen, G. Seufert, P. Ciccioli, P. Foster, J.L. Fugit, and L. Torres. Diurnal and seasonal course of monoterpene emissions from *Quercus ilex* (L.) under natural conditions- Application of light and temperature algorithms. *Atmos. Env.*, 31:135–144, 1997.

[184] H. Hakola, T. Laurila, V. Lindfors, H. Hellén, A. Gaman, and J. Rinne. Variation of the VOC emission rates of birch species during the growing season. *Boreal Env. Res.*, 6:237–249, 2001.

[185] G. König, M. Brunda, H. Puxbaum, C.N. Hewitt, S.C. Duckham, and J. Rudolph. Relative contribution of oxygenated hydrocarbons to the total biogenic VOC emissions of selected mid-european agricultural and natural plant species. *Atmos. Env.*, 29:861–874, 1995.

[186] H. Hakola, V. Tervainen, T. Laurila, V. Hiltunen, H. Hellén, and P. Keronen. Seasonal variation of VOC concentrations above a boreal coniferous forest. *Atmos. Env.*, 37:1623–1634, 2003.

[187] W. Kirstine, I. Galbally, Y. Ye, and M. Hooper. Emissions of volatile organic compounds (primarily oxygenated species) from pasture. *J. Geophys. Res.*, 103:10605–10619, 1998.

[188] G.W. Schade, A.H. Goldstein, and M.S Lamanna. Are monoterpene emissions influenced by humidity? *Geophys. Res. Lett.*, 14:2187–2190, 1999.

[189] M. Yatagai, M. Ohira, T. Ohira, and S. Nagai. Seasonal-variations of terpene emission from trees and influence of temperature, light and contact stimulation on terpene emission. *Chemosphere*, 30:1137–1149, 1995.

[190] B.J. Finlayson-Pitts and J.N. Pitts Jr. *Chemistry of the upper and lower atmosphere*. Academic Press, 2000.

[191] C.E. Junge. Residence time and variability of tropospheric trace gases. *Tellus*, 26:477–488, 1974.

[192] B.T. Jobson, D.D. Parrish, P. Goldan, W. Kuster, and F.C. Fehsenfeld. Spatial and temporal variability of nonmethane hydrocarbon mixing ratios and their relation to photochemical lifetime. *J. Geophys. Res.*, 103:13557–13567, 1998.

[193] B.T. Jobson, S.A. McKeen, D.D. Parrish, F.C. Fehsenfeld, D.R. Blake, A.H. Goldstein, S.M. Schauffler, and J.W. Elkins. Trace gas mixing ratio variability versus lifetime in the troposphere and stratosphere: Observations. *J. Geophys. Res.*, 104:16091–16113, 1999.

[194] J. Williams, H. Fischer, G.W. Harris, P.J. Crutzen, and P. Hoor. Variability-lifetime relationship for organic trace gases: A novel aid to compound identification and estimation of HO concentrations. *J. Geophys. Res.*, 105:20473–20486, 2000.

[195] T. Karl, P.J. Crutzen, M. Mandl, M. Staudinger, A. Guenther, A. Jordan, R. Fall, and W. Lindinger. Variability-lifetime relationship of VOCs observed at the Sonnblick Observatory 1999 - estimation of HO-densities. *Atmos. Env.*, 35:5287–5300, 2001.

[196] T. Karl and A. Guenther. Atmospheric variability of biogenic VOCs in the surface layer measured by proton-transfer-reaction mass spectrometry. *Int. J. Mass. Spectr.*, 239:77–86, 2004.

[197] D.B. Millet, A.H. Goldstein, J.D. Allan, T.S. Bates, H. Boudries, K.N. Bower, H. Coe, Y. Ma, M. McKay, P.K. Quinn, A. Sullivan, R.J. Weber, and D.R. Worsnop. Volatile organic compound measurements at Trinidad Head, California, during ITCT 2K2: Analysis of sources, atmospheric composition, aerosol residence times. *J. Geophys. Res.*, 109:D23S16, 2004.

[198] T. Karl, R. Fall, P. J. Crutzen, A. Jordan, and W. Lindinger. High concentrations of reactive biogenic VOCs at a high altitude site in late autumn. *Geophys. Res. Lett.*, 28:507–510, 2001.

[199] D.H. Ehhalt, F. Rohrer, and A. Wahner. On the use of hydrocarbons for the determination of tropospheric OH concentrations. *J. Geophys. Res.*, 103:18981–18997, 1998.

[200] R. Atkinson. Gas phase tropospheric chemistry of organic compounds. *J. Phys. Chem. Ref. Data*, 2:1–216, 1994.

[201] F. Heintz, U. Platt, H. Flentje, and R. Dubois. Long term observation of nitrate radicals at the Tor Station, Kap Arkona (Rügen). *J. Geophys. Res.*, 101:22891–22910, 1996.

[202] N. Carslaw, J.M.C. Plane, and H. Coe. Observations of the nitrate radical in the free troposphere at Izaña de Tenerife. *J. Atmos. Chem.*, 27:291–318, 1997.

[203] M. Vrekoussis, M. Kanakidou, N. Mihalopoulos, P.J. Crutzen, J. Lelieveld, D. Perner, H. Berresheim, and V. Baboukas. Role of NO_3 radicals in oxidation processes in the eastern Mediterranean troposphere during the MINOS campaign. *Atmos. Chem. Phys.*, 4:169–182, 2004.

[204] A. Geyer, R. Ackermann, R. Dubois, B. Lohrmann, T. Müller, and U. Platt. Long-term observation of nitrate radicals in the continental boundary layer near Berlin. *Atmos. Env.*, 35:3619–3631, 2001.

[205] S. Rodriguez, C. Torres, J.-C. Guerra, and E. Cuevas. Transport pathways of ozone to marine and free-troposphere sites in Tenerife, Canary Islands. *Atmos. Env.*, 38:4733–4747, 2004.

[206] M. Schneider, T. Blumenstock, M.P. Chipperfield, F. Hase, W. Kouker, T. Reddmann, R. Ruhnke, E. Cuevas, and H. Fischer. Subtropical trace gas profiles determined by ground-base FTIR spectroscopy at Izaña (28 degrees N, 16 degrees W): Five-year record, error analysis, and comparison with 3-D CTMs. *Atmos. Chem. Phys.*, 5:153–167, 2005.

[207] W. Armerding, F.J. Comes, H.J. Crawack, O. Forberich, G. Gold, C. Ruger, M. Spiekermann, J. Walter, E. Cuevas, A. Redondas, R. Schmitt, and P. Matuska. Testing the daytime oxidizing capacity of the troposphere: 1994 OH field campaign at the Izaña Observatory, Tenerife. *J. Geophys. Res.*, 102:10603–10611, 1997.

[208] R. Schmitt and A. Volz-Thomas. Climatology of ozone, PAN, CO, and NMHC in the free troposphere over the southern North Atlantic. *J. Atmos. Chem.*, 28:245–262, 1997.

[209] B.L.Van Drooge, J.O. Grimalt, C.J.T. Garcia, and E. Cuevas. Semivolatile organochlorine compounds in the free troposphere of the Northeastern Atlantic. *Enc. Sci. Technol.*, 36:1155–1161, 2002.

[210] H. Fischer, C. Nikitas, U. Parchatka, T. Zenker, G.W. Harris, P. Matuska, R. Schmitt, D. Mihelcic, P. Muesgen, H.W. Paetz, M. Schultz, and A. Volz-Thomas. Trace gas measurements during the Oxidizing Capacity of the Tropospheric Atmosphere campaign 1993 at Izaña. *J. Geophys. Res.*, 103:13505–13518, 1998.

[211] J.R. Arévalo and J.M. Fernández-Palacios. Spatial patterns of trees and juveniles in a laurel forest of Tenerife, Canary Islands. *Plant Ecol.*, 165:1–10, 2003.

[212] H. Maring, D.L. Savoie, M.A. Izaguirre, C. McCormick, R. Arimoto, J.M. Prospero, and C. Pilinis. Aerosol physical and optical properties and their relationship to aerosol composition in the free troposphere at Izaña, Tenerife, Canary Islands, during July 1995. *J. Atmos. Chem.*, 27:291–318, 1997.

[213] G.P. Gobbi, F. Barnaba, A. Conidi, L. Ammannato, and F. Belardinelly. Lidar and photometric measurements at Izaña (Tenerife) during the MINATROC 2002 field campaign, 2003.

[214] M. Hanke, B. Umann, J. Uecker, F. Arnold, and H. Bunz. Atmospheric measurements of gas-phase HNO_3 and SO_2 using chemical ionization mass spectrometry during the MINATROC field campaign 2000 on Monte Cimone. *Atmos. Chem. Phys.*, 3:417–436, 2003.

[215] H. Fischer, R. Kormann, T. Klüpfel, C. Gurk, R. Königstedt, U. Parchatka, J. Mühle, T.S. Rhee, C.A.M. Brenninkmeijer, P. Bonasoni, and A. Stohl. Ozone production and trace gas correlations during the June 2000 MINATROC intensive measurement campaign at Mt. Cimone. *Atmos. Chem. Phys.*, 3:725–738, 2003.

[216] R. Kormann, H. Fischer, M. de Reus, M. Lawrence, C. Brühl, R. von Kuhlmann, R. Holzinger, J. Williams, J. Lelieveld, C. Warneke, J. de Gouw, J. Heland, H. Ziereis, and H. Schlager. Formaldehyde over the eastern Mediterranean during MINOS: Comparison of airborne in-situ measurements with 3D-model results. *Atmos. Chem. Phys.*, 3:851–861, 2003.

[217] H.W. Pfeifhofer. Composition of the essential oil of *Pinus canariensis* Sweet ex Sprengel. *Flav. Frag. J.*, 15:266–270, 2000.

[218] L.G. Pedro, P.A.G. Santos, J.A. da Silva, A.C. Figueiredo, J.G. Barroso, S.G. Deans, A. Looman, and J.J.C. Scheffer. Essential oils from Azorean *Laurus azorica*. *Phytochem.*, 57:245–250, 2001.

[219] M. Komenda, K. Kobel, R. Koppmann, and J. Wildt. Comparability of biogenic VOC emission rate measurements under laboratory and ambient conditions at the example of monoterpene emissions from Scots Pine *(Pinus sylvestris)*. *J. Atmos. Chem.*, 45:1–23, 2003.

[220] J. Kesselmeier, L. Schäfer, P. Ciccioli, E. Brancaleoni, A. Cecinato, M. Frattoni, P. Foster, V. Jacob, J. Denis, J.L. Fugit, L. Dutaur, and L. Torres. Emission of monoterpenes and isoprene from a Mediterranean oak species *Quercus ilex* L. measured within the BEMA (biogenic emissions in the Mediterranean area) project. *Atmos. Env.*, 30:1841–1850, 1996.

[221] J. Kesselmeier, K. Bode, U. Hofmann, H. Müller, L. Schäfer, A. Wolf, P. Ciccioli, E. Brancaleoni, A. Cecinato, M. Frattoni, P. Foster, C. Ferrari, V. Jacob, J.L. Fugit, L. Dutaur, V. Simon, and L. Torres. Emission of short chained organic acids, aldehydes and monoterpenes from *Quercus ilex* L. and *Pinus pinea* L. in relation to physiological activities, carbon budget and emission algorithms. *Atmos. Env.*, 31:119–133, 1997.

[222] F. Loreto, P.Ciccioli, A. Cecinato, E. Brancaleoni, M. Frattoni, and D. Tricoli. Influence of environmental factors and air composition on the emission of α-pinene from *Quercus ilex* leaves. *Plant Physiol.*, 110:267–275, 1996.

[223] M. Staudt, S. Rambal, R. Joffre, and J. Kesselmeier. Impact of drought on seasonal monoterpene emissions from *Quercus ilex* in southern France. *J. Geophys. Res.*, 107:Art. No. 4602, 2002.

[224] L. Núñez, J. Plaza, R. Pérez-Pastor, M. Pujadas, B.S. Gimeno, V. Bermejo, and S. García-Alonso. High water vapour pressure deficit influence on *Quercus ilex* and *Pinus pinea* field monoterpene emission in the central Iberian Peninsula (Spain). *Atmos. Env.*, 36:4441–4452, 2002.

[225] W. Zhao, P.K. Hopke, and T. Karl. Source identification of volatile organic compounds in Houston, Texas. *Environ. Sci. Technol.*, 38:1338–1347, 2004.

[226] L. Otter, A. Guenther, C. Wiedinmyer, G. Fleming, P. Harley, and J. Greenberg. Spatial and temporal variation in biogenic volatile organic compound emissions for Africa south of the equator. *J. Geophys. Res.*, 108:Art. No. 8505, 2003.

[227] Y.Rudich, R.K. Talukdar, R.W. Fox, and A.R. Ravishankara. Reactive uptake of NO_3 on pure water and ionic solutions. *J. Geophys. Res.*, 101:A21023–21031, 1996.

[228] F.J. Dentener and P.J. Crutzen. Reaction of N_2O_5 on tropospheric aerosols - Impact on the global distribution of NO_x, O_3, and OH. *J. Geophys. Res.*, 98:7149–7163, 1993.